DEVELOPMENT OF NOVEL PEPTIDE BASED GENE DELIVERY VECTOR AND SUPRAMOLECULAR ASSEMBLY

Dissertation

zur Erlangung des akademischen Grades eines Doktors der Naturwissenschaften

- Dr. rer. nat.-

vorgelegt von

Mao Li

geboren in Hebei, China

Institut für Organische Chemie

der

Universität Duisburg-Essen

2016

This work was performed during the period from October 2012 to October 2015 at the Institute of Organic Chemistry, Department of Chemistry, University of Duisburg-Essen, under the supervision of Prof. Dr. Carsten Schmuck.

Date of oral examination: 18.10.2016

Chair: Prof. Dr. Torsten Schmidt

Advisor: Prof. Dr. Carsten Schmuck

Reviewer: Prof. Dr. Shirley Knauer

I declare that this dissertation represents my own work, except where due acknowledgement is made.

Essen, January 2016

.....

Acknowledgement

The three years' pursuing of PhD is now finally coming to the end. Looking back to the three years, my feelings are quite mixed. To quote *Dickens*, "*…it was the age of wisdom, it was the age of foolishness; it was the epoch of belief, it was the epoch of incredulity…*" I have never been so frustrated, and I have never been so satisfied. In the end, I can proudly say that I dedicated every part of me into the work I presented here. The experience of being a PhD student is truly an amazing adventure of life and will become my most treasured memory.

At the very first, I would like to express my sincere gratitude to my supervisor, Prof. Dr. Carsten Schmuck, for his supervision and support over the three years. Thank you for providing me the opportunity of studying in the field of bioorganic chemistry and supramolecular chemistry under your guidance. Without your knowledges and wisdoms, I could never accomplish any scientific research I have done here. Thank you for the feedbacks and suggestions for all my questions, and the freedoms for working in the most appealing world of chemistry.

I would like to express my great thanks to my previous supervisor, Prof. Dr. Zhen Xi for his kind recommendation and suggestions. Also, thanks to CSC (China Scholarship Council) for providing me the scholarship to support my PhD study in Germany.

I am also very grateful to the cooperation from Prof. Dr. Shirley Knauer in biology department. Thanks for providing me the materials and helpful suggestions in biological aspects. Thanks Stefanie Schlesiger for the conduction of cell experiments.

I would like to thank Prof. Dr. Ivo Piantanida in Zagreb for the cooperation studies of CD experiments. Thanks Marija and Marijana in the DNA binding and peptide conformation measurements.

I would like to thank Martin Ehlers for the molecular modelling experiments and Elio Zellermann for the TEM measurements. Thanks Christian for the synthesis of terpyridine molecule.

In the end, I would like to say thanks to all the current and former group members in AK Schmuck. Thanks Christine for the organization of lab activities. Special thanks to Dr. Qianqian Jiang for her supports and warm concerns when I first came here. Thanks Alba for

the joyfully moments we had together and the friendship we built. Thanks Elio, Lina and Martin for the happy hours we had in the office. Also thanks Jule and Sandra for helping me start in the lab and all the suggestions I got. Jincheng, Hao, Xi, Qian, Dongshi, Miao and Ruiyong are thanked for the friendship, support and happy times we had.

At last, I would love to express my special thanks to my parents for their support and understanding during my entire studies. Best thanks and loves are given to my fiancee Dejing, for everything she did, for her being presence in my life.

2016-01-13

Essen

使生如夏花般绚烂，死如秋叶之静美。

Let life be beautiful like summer flowers, and Death like autumn leaves.

Rabindranath Tagore

Table of content

1. INTRODUCTION

1.1 Gene delivery

In recent years, gene therapy has emerged as a promising strategy for the treatment of several diseases such as Prakinson´s disease, Alymphocytosis and cancers.[1-3] However, genetic materials cannot enter intact cells by simple diffusion due to their anionic nature and the hydrophobicity of the membrane lipid bilayer as well the negative charges on cell surface.[4,5] Therefore, efficient gene delivery vectors are required to realize the efforts of gene therapy. The main functions of vectors are DNA/RNA condensation, cellular uptake of the resulting complexes and subsequently release from endosome to cytosol or nucleus.[6-8] Additionally, the condensation of genetic materials with vectors can provide protection against enzymatic degradations.[9]

Generally, gene delivery vectors can be classified into two categories: virus-based and non-viral vectors. Although recombinant viruses have been demonstrated as the most efficient vectors in the delivery of genetic materials, their medical applications are limited due to their toxicity and immunogenicity etc.[10,11] On the other hand, non-viral delivery systems have attracted more and more interests in the field of gene therapy. Cationic lipid Lipofectamine and polymers polyethylenimine (PEI) are widely accepted as standard reagents in gene transfection experiments.[12]

In particularly, peptide based gene transfection vectors have attracted increasing interests in recent years due to their ease of synthesis, lower toxicity at least compared to polymeric transfection vectors and versatility of functionalization.[13] Of the most often used peptidic vectors, arginine rich cell penetrating peptides have been identified as being highly efficient in cellular uptake and thus are widely tested as gene delivery vectors. However, a minimum of 6 positive charges is usually required for cellular uptake and even more charges are necessary for efficient gene delivery.[14,15] Even with the current prevailing strategy of adding a hydrophobic aliphatic chain onto the peptide sequence to increase their endosomal release ability, at least 8 to 9 arginines were still necessary for decent gene transfection.[16,17] The transfection efficacy as well cytotoxicity of these peptides requires further improvement, with regard to future applications. Although other cationic peptides such as lysine oligomers have

been used for gene transfection, their efficacies are usually even worse than arginine rich peptides.[18] A new modification strategy for CPPs is therefore in high demand to develop efficient gene delivery vector.

1.2 Peptide assembly

Supramolecular chemistry has developed several strategies to achieve efficient and also controlled peptide assembly. Various nanostructures such as fibers, tape-like aggregates, nanotubes and helix assemblies can be obtained by rationally design of peptide based building blocks.[19] For example, amphiphilic peptides can readily form peptide fibers and nanobelts in aqueous solutions.[20] Also naturally occurring peptides such as amyloid and coiled-coil peptide are interesting building blocks in constructing nanotube structures.[21,22] These peptide assemblies can be applied to variety of applications such as stimuli-responsive materials, tissue engineering and regenerative medicines etc.[23,24]

On the other hand, short peptides that adopt helical and sheet structures under physiological conditions have profound impact on biological systems. One current goal of supramolecular chemistry is to design artificial self-assembling systems that could mimic these structures under biomimetic conditions.[25] This could not only largely enhance our understandings of its functions in biological process but also provide alternatives for the development of biomaterials.

In summary, short peptides have demonstrated to be very promising in the development of gene delivery vectors. However, the efficiency of such peptides in gene delivery still needs to be optimized for future clinical application. The purpose of this thesis is thus to develop new peptide based gene delivery vectors with improved transfection efficiency. We hypothesized that the introduction of tailor made anion binding receptors in the side chains of peptides could enhance their interactions either with cell membrane or with DNA. This property could eventually lead to a better performing peptide in cellular uptake and gene delivery. The same strategy, i.e. modification of peptide with anion receptor could also be applied to provide novel peptide based supramolecular nanomaterials.

2. BACKGROUND INFORMATION

2.1 GCP-oxoanion recognition

2.1.1 GCP-oxoanion binding interactions

In biological systems, the majority of macromolecules such as protein and DNA which sustain body functions are anionic in nature. Even cell membrane which provides a stable and suitable environment for the basic need of cells is highly negatively charged. Development of artificial receptors which can bind anions such as sulfate, phosphate and carboxylate could enormously benefit the discovery of drugs and drug carriers.[26-29]

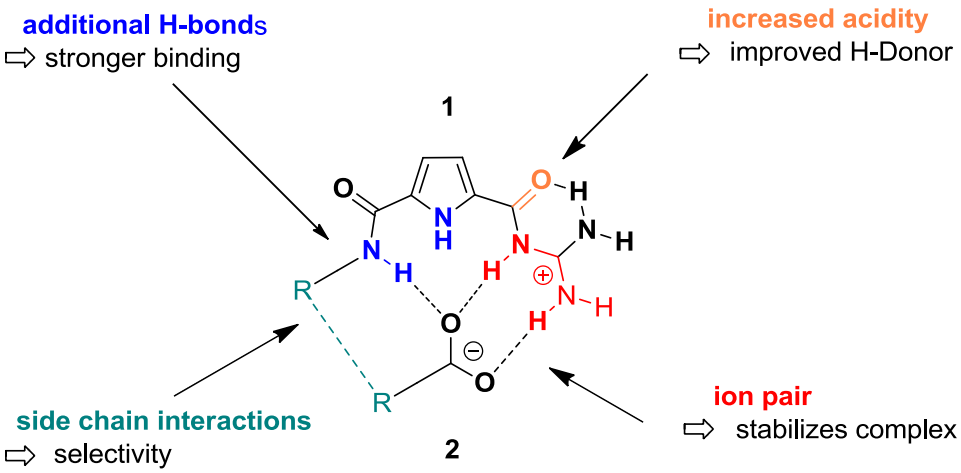

Figure 1. Schematic representation of the binding between GCP and carboxylate

Guanidinium group has been known as a relatively strong binding moiety with oxoanions because of the electrostatic interactions and additional hydrogen bonds.[30] However, the complexes formed between guanidinium cations and carboxylates are normally easy to dissociate in polar solvents such as DMSO and water.[31] Guanidiniocarboxylpyrrole (abbreviated as GCP), a rigid and planar moiety, was thus introduced by *Schmuck* et al. to improve the anion binding ability of guanidinium group (Figure 1).[32,33] This moiety possesses several advantages compared to simple guanidines, which makes it an attractive candidate for the binding of carboxylates even in aqueous solvents:

• the pKa of acyl guanidino is around 7–8 which increases the acidity and favors the formation of hydrogen bonded ion pairs.

• Additional hydrogen bond donors such as the amide NH can further enhance the stability

of the complex.

• GCP motif is planar and rather rigid and therefore ideally pre-organized for the binding of planar anions such as carboxylates.

• Additional secondary interactions between the side chain of GCP and carboxylate can be easily introduced to achieve selectivity.

As consequence, the binding constants between GCP and carboxylates can reach the magnitude of 10^5 M^{-1} in DMSO.[34] Even in aqueous media the anion binding ability of GCP is still sufficiently strong (10^3 M^{-1}).[35] Considering the difficulty to achieve strong binding interactions in water, a highly competitive solvent, the GCP moiety then represents a unique and useful tool to study anion related interactions in biological systems.

2.1.2 GCP recognition of amino acids and short peptides

In biological world the guanidinium moiety is widely applied as a mediator of specific non-covalent binding such as the substrate binding of enzyme, DNA and protein interactions etc.[36-39] Naturally, GCP moiety, an improved guanidinium binding moiety, has been thoroughly examined as artificial receptors for biomolecules owing to its superior binding ability towards anions.

2.1.2.1 Amino acids recognition

The design of artificial receptors which bind amino acids under physiological conditions is still challenging. Most amino acid receptors either required hydrophobic or metal–ligand interactions to achieve efficient substrate binding in water. However, *Schmuck* et al. were able to develop efficient amino acid receptors in high competitive solvents through the utilization of GCP binding moiety.

In 1999, *Schmuck* et al. reported that molecule **3** bound N-acetyl amino acids with binding constants ranging from K = 360 to 1700 mol^{-1} in 40% H_2O–DMSO solution (Figure 2).[40] The recognition process of **3** was selective for the chemical structures of amino acid side chain. The binding with phenylalanine was much stronger than that of alanine or lysine. Molecular modelling suggested that the aromatic ring stacked with the acylguanidinium unit and thus provided extra stabilization.

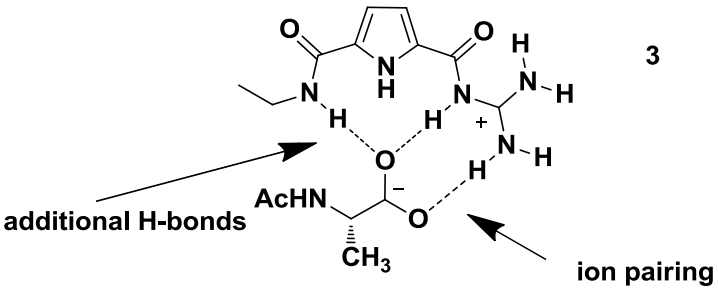

Figure 2. Side chain selective binding of N-acetyl-amino acid carboxylates by **3**

Later, *Schmuck* et al. determined the energetic contributions of the individual interactions in **3** through systematic variations of its structure. A series of GCP based receptors were thus designed and synthesized.[41] Studying their binding properties with carboxylates revealed that not all the hydrogen bonds in **3** contributed equally to the stabilization of the final complex. The results demonstrated that the amide NH next to the pyrrole ring was critical for stronger binding whereas the pyrrole NH and the terminal carbamoyl group contributed less to the overall binding affinity. Additionally, replacement of the pyrrole moiety with pyridine weakened the binding ability with carboxylate due to unfavorable electrostatic and steric effects in pyridine.[42] The electrostatic repulsions between the lone pair in the pyridine nitrogen and the bound carboxylates destabilized the resulting complex.

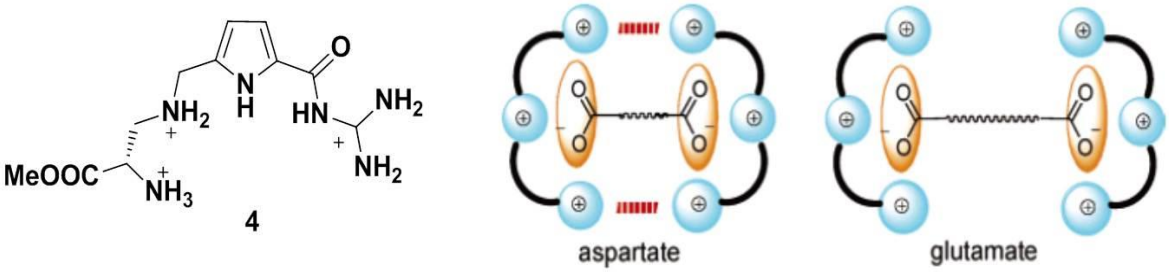

Figure 3. Side chain selective binding of N-acetyl-amino acid carboxylates by **4.** Adapted with permission from Reference 35 .Copyright (2016) American Chemical Society."

Introduction of additional positive charges into **3** can further stabilize the final complex. Tri-cation **4,** with two extra positive charges relative to **3,** showed efficient binding with amino acid carboxylates in water at millimolar salt concentrations (Figure 3).[35] The binding constant was increased up to the range of 10^3. Furthermore, **4** exhibited cooperative 2:1 complex formation with N-acetyl glutamates but not aspartate. This differentiation ability is

rather impressive considering the structural similarity of both amino acids. On the other hand, additional interactions can also be introduced on the backside of molecule **3**. N'-substituted **5**, which was obtained by the activation of a Boc-protected guanidiniocarbonyl pyrrole with triflic anhydride, showed efficient complexation with amino acid carboxylates in water (Figure 4).[43]

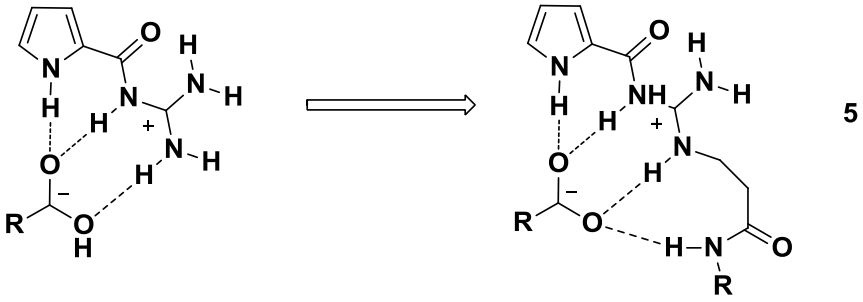

Figure 4. Binding of N'-substituted guanidiniocarbonyl pyrrole **5** with carboxylic acid

2.1.2.2 Short peptides

While recognition of negatively charged amino acids such as aspartic acid and glutamic acid has been achieved, *Schmuck* et al. further applied the GCP moiety in the recognition of short peptides. Short peptides have various important functions in biological systems such as amyloid formation, cell signaling and modulators of many regulatory processes etc. Development of artificial receptors for short peptides could largely benefit the understanding of biological phenomenon and also drug discovery.

In 2004, *Schmuck* et al. designed and synthesized a cationic prototype receptor **6** which showed efficient binding ability towards dipeptide in water (Figure 5).[44] The binding constant between **6** and Val-Val can be up to 54,300 M^{-1} which was 10 fold larger compared with the binding of other GCP-based carboxylate receptors with simple amino acids ($K = 10^3\ M^{-1}$). Obviously the H-bonds between the backbone amides and interactions with the imidazol group played an important role in the stabilization of resulting complex. Further introduction of a hydrophobic group such as naphthyl and additional amino acid residues showed preferential complexation of N-acetyl dipeptide carboxylates containing alanine at the C-terminus.[45,46] *Schmuck* et al. also attached a cyclo-tribenzylene substituted alanine onto the GCP based receptor. The hydrophobic bowl-shaped cavity was just spacious enough to bind a methyl group but not any larger alkyl chain. This property led to a binding preference of

alanine over valine. As consequence, Ac-D-Ala-D-Ala-OH can bind 10 fold stronger with this receptor than Ac-D-Val-D-Val-OH.

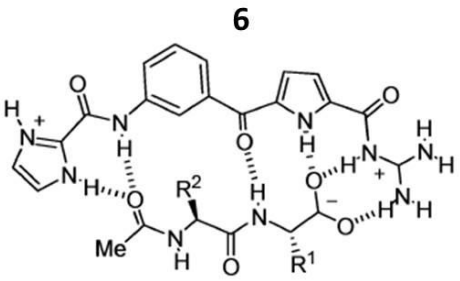

carboxylate	K_{ass}[a]
Gly-Gly (**11**)	15.900
Ala-Ala (**10**)	30.600
Val-Ala (**12**)	43.800
Val-Val (**13**)	54.300
Ala (**14**)	7.400
Gly (**15**)	5.200

Figure 5. Binding of **6** with dipeptide and respective binding constants. Reprinted with permission from Reference 44. Copyright (2016) American Chemical Society."

Moreover, *Schmuck* et al. demonstrated the GCP moiety can be applied to achieve tetra-peptide and amyloid beta peptide recognition.[47,48] Tetra-peptide Ac-Val-Val-Ile-Ala-OH, a segment sequence of amyloid-β-peptide responsible for the formation of protein plaques in the brains of patients suffering from Alzheimer's disease, was used as anionic model peptide. This short tetra peptide forms insoluble, fibril-like aggregates upon prolonged incubation in solution underlining its high tendency to self-aggregate. Thus it is a suitable model to study the self-aggregation process of amyloid-β-peptide. In this work, they established a combinatorial library of receptors on solid support featured with the modification of GCP in N-terminus (Figure 6). Their binding properties were determined directly on bead using a quantitative fluorescence assay. To accomplish this assay, model tetra peptide Ac-Val-Val-Ile-Ala-OH was modified with dansyl group through different linkers. A schematic representation of the screening methods is shown in below:

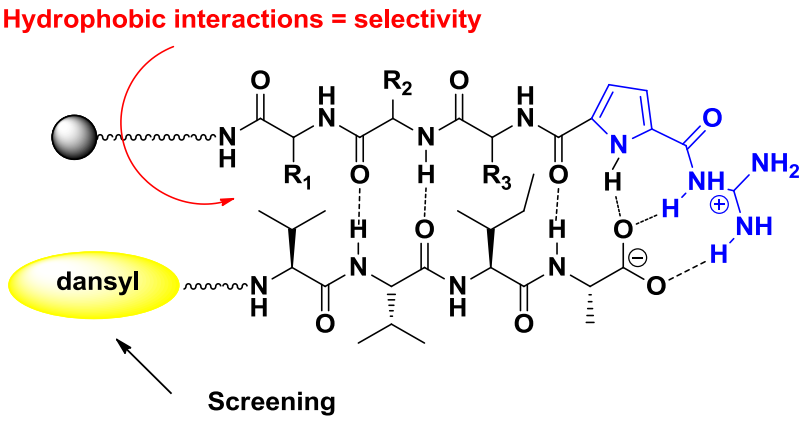

Figure 6. A peptide based library of cationic GCP receptors designed for binding

Comparison of the binding data revealed that the recognition of model tetra peptide with these receptors required both electrostatic and hydrophobic interactions. The binding ability of these receptors was very efficient with binding constants around 10^3 M^{-1} in water. Also it was shown that all the good binding receptors were featured with the use of Lys(Boc) group in the position next to GCP moiety. Molecular dynamic simulation suggested that the favorable hydrophobic interactions between bulky t-Boc group and the first (Val) and third (Ile) amino acid residues of model tetra-peptide were mainly responsible for this preference. By studying their effect on the fibrillogenesis process of Aβ(1–42) in comparison to Aβ(1–40), these receptors indeed inhibited the fibril formation *in vitro* through the selectively binding to the C-terminus.[49]

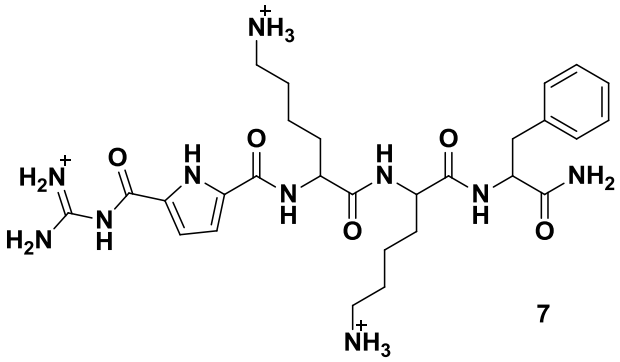

7

Figure 7. Chemical structure of peptide receptor **7**

Besides hydrophobic tetra-peptides, polar tetra-peptide was also selected as target to study the binding with GCP based receptors. With the same principle as described above, they established another medium-sized but focused combinatorial receptor library.[50,51] Quantitative experimental screening and statistical QSAR (quantitative structure–activity relationship) analysis demonstrated that artificial receptor **7** can bind with polar tetra-peptide without additional hydrophobic and metal-ligand interactions in water (Figure 7). The binding constant can reach 15,400 M^{-1} with tetra-peptide N-Ac-EKAA-OH as model. However, when the sequence of target peptide was inversed (N-Ac-AAKE-OH), the binding constant decreased 2-3 folds (6000 M^{-1}) which underlined the importance of amino acid sequence in the design of artificial peptide receptor.

2.1.2 GCP recognition of nucleotides and DNA

In biological systems, peptides and proteins are not the only negatively charged

macromolecules. DNA and RNA are also anionic in nature due to the phosphodiester linkages between each nucleotide. Therefore, the superior anion binding ability of GCP moiety makes it very suitable to be applied to develop efficient DNA and RNA receptors. *Schmuck* et al. thus reported a series of GCP containing compounds which showed interesting properties in DNA binding and gene transfection studies.

In 2008, they demonstrated that a novel pyrene-GCP cation **8** exhibited DNA binding ability in aqueous condition (Figure 8).[52] Pyrene, a well-known polarity-sensitive fluorescence probe, was covalently linked to a GCP cation via a flexible alkyl chain. The length of linker was rational designed so that the pyrene moiety can intercalate into the nucleic acid double strands and meanwhile GCP moiety can still ion-pairing with the sugar phosphate backbone in the grooves. Also four carbon length of linker was not too flexible to lose too much binding energy in entropy. They tested the binding property of **8** at pH 5 and 7 as GCP moiety was only protonated at pH 5.

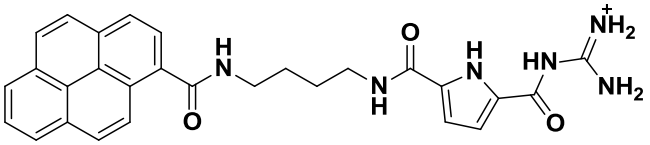

8

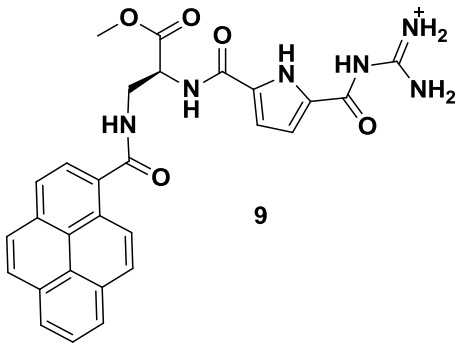

9

Figure 8. Chemical structure of molecules **8** and **9**

Preliminary study showed that molecule **8** exhibited strong affinity (log K_s = 5.1-6.0) with either DNA or RNA at pH 7 even though it was not protonated. Moreover, molecule **8** was able to differentiate dsDNA from dsRNA when it was protonated. At pH 5, the addition of **8** to all ds-DNA studied resulted in a significant decrease of the circular dichroism (CD) bands and induced a new strong CD (ICD) band. The changes in the CD bands, however, were completely different when ds-RNA was added. No ICD bands in the region of 300 - 360 nm

were observed in the CD spectra with the addition of ds-RNA. Instead, an excimer fluorescence emission was appeared exclusively upon the addition of RNA. Replacement of the four carbon linker in **8** to a shorter, rigid two carbon linker resulted in totally different spectroscopic responses.[53] Molecule **9** (Figure 8) equipped with a neutral carboxylic-ester side chain interacted strongly with ds-DNA but only negligibly with ds-RNA. The CD spectrum of ds-RNA upon addition of **9** did not change significantly and no ICD bands were observed. In contrast to this, the addition of **9** to ds-DNA at either pH 5 or pH 7 resulted in pronounced changes. Further study revealed that **9** showed strong selectivity toward AT-DNA with respect to GC-DNA.

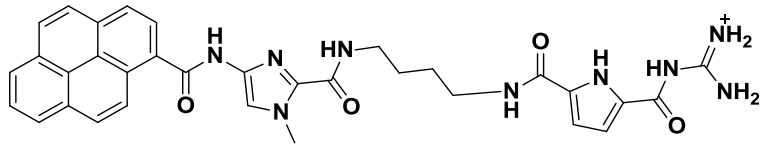

10

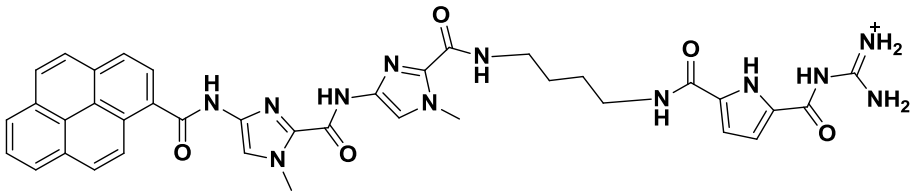

11

Figure 9. Chemical structures of molecules **10** and **11**

Introduction of additional binding sites in the linker resulted in a different series of GCP derived receptors **10** and **11** (Figure 9).[54] Titration studies suggested that these two compounds interacted strongly with ds-DNA, but only weakly with ds-RNA. The changes of fluorescence emission of **10** and **11** were remarkably dependent on the secondary structure of the polynucleotide added. Additionally, the heterocyclic moieties within the central part of linker switched the binding mode from intercalative (as described above for **8** and **9**) to minor groove binding. For example, a negative ICD band at >330 nm was observed when **8** was added to ds-DNA due to the intercalation of the pyrene. On the contrary, addition of **10** and **11** to ds-DNAs resulted in a positive ICD band at 330–350 nm, strongly indicated the positioning of pyrene within the minor groove of the double helix. Molecular modelling suggested that the heterocyclic moiety controlled the alignment of the molecules within DNA minor grooves by steric and hydrogen bonding effect.

Afterwards, *Schmuck* et al. reported a systematic study of the nucleic acid binding property of GCP - aryl derivatives.[55] Three parameters were thoroughly examined: 1, the size of the aromatic ring conjugates (benzene, naphthalene, pyrene and acridine); 2, the length, flexibility and polarity of the linker in between; 3, the number of positive charges at different pH values. A series of compounds were thus designed and synthesized (Figure 10).

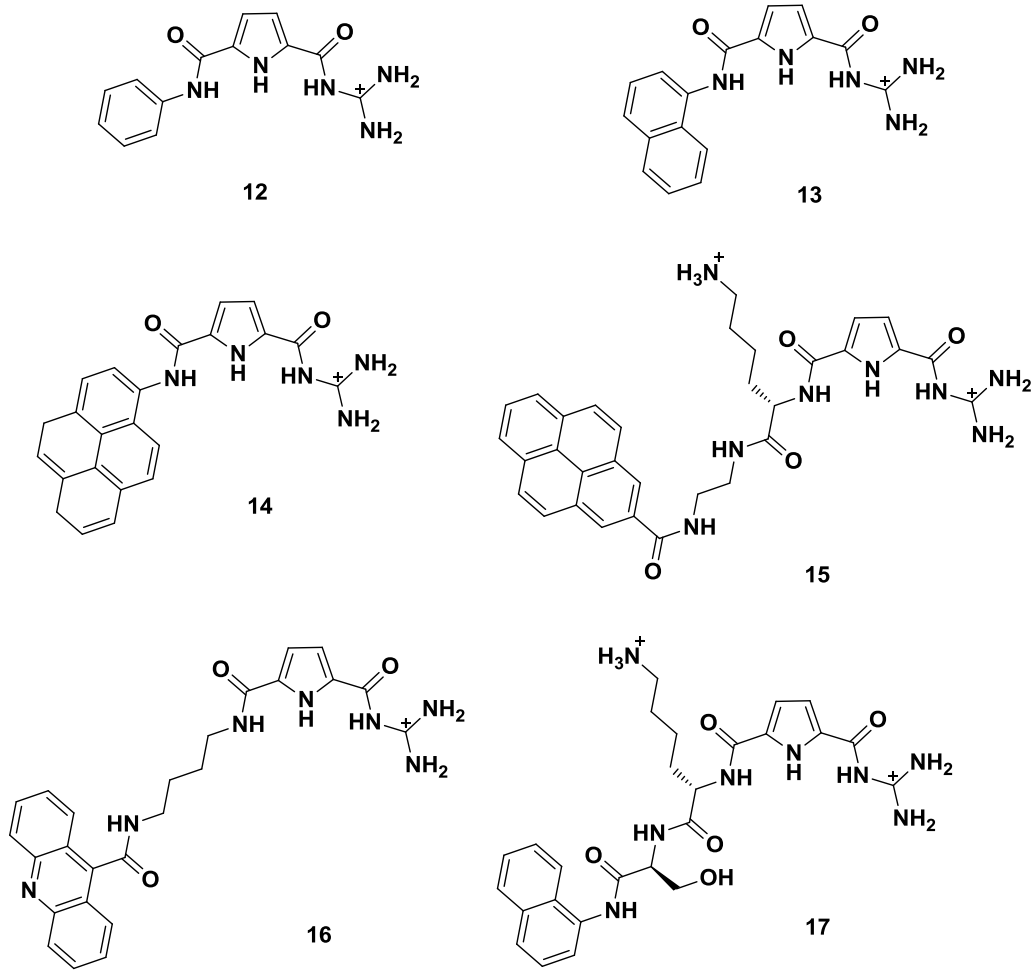

Figure 10. Chemical structure of molecules **12** – **17**

Spectroscopic results showed that **12** and **13** did not significantly interact with DNA/RNA while compound **16** was able to intercalate with DNA which suggested a minimal requirement of aromatic surface area for nucleic acid binding. Introduction of more flexibility and additional positive charges in the linker enhanced the stabilization effect as compared by **8**, **14** and **15**. At pH 5, the fluorescence of **15** was strongly quenched by G–C base pairs, whereas A-T or A-U base pairs induced a strong fluorescence increase. The quenching was probably caused either through aromatic stacking interaction or by electron-transfer through the stacked DNA helix. Molecule **15** was even able to produce a strong positive ICD band at 310 nm upon

the addition of ds-DNA at pH 7 owing to its additional charge. This property was not observed with other GCP derivatives. However, **15** did not show any specific fluorimetric response with ds-RNA. Most probably the steric hindrance and/or charge repulsion in **15** prevented dimer formation within the ds-RNA major groove.

Furthermore, *Schmuck* et al. also determined the biological activity of these compounds for their potential antiproliferative applications. Molecule **15**, with its suitable size of aromatic ring and additional charges in the linker region, exhibited significantly better activity compared to other similar compounds.

Schmuck et al. also prepared nucleic acid receptors with two GCP moiety modifications (Figure 11).[56] The two GCPs were connected with oligo-amide linkers differing in the number of positive charges. The results again underlined the importance of charge interactions as all three compounds **18** - **20** showed significant better binding affinity at pH 5 than 7. Without the aromatic ring such as pyrene and acridine, those molecules exclusively bind to the minor grove of DNA and major grove of RNA. AFM experiments revealed a condensation process of DNA upon the addition of **19**.

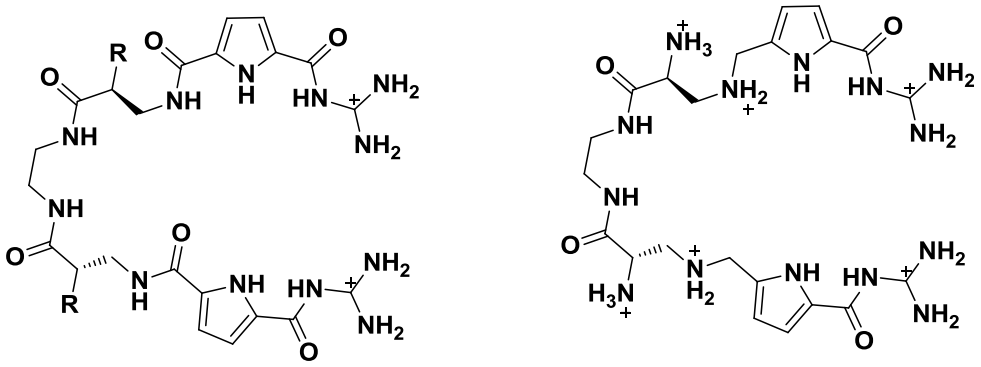

18: (R = NHCbz)
19: (R = $NH3^{+}$)

20

Figure 11. Chemical structure of molecules **18** – **20**

Inspired by the di-GCP receptors, *Schmuck* et al. designed a tweezer like GCP containing peptide based receptor **21**.[57] The new receptor was well soluble in water owing to the peptide scaffold. All nucleotides tested in this work (ADP, ATP, AMP etc.) bound strongly with **21** in pure water with binding constants varying from 10^4 to 10^5 M^{-1}. Intriguingly, **21** favored the binding of adenosine monophosphate (AMP) over adenosine diphosphate (ADP) and adenosine triphosphate (ATP). This property was unprecedented since ATP has more negative

charges than AMP. The tweezer shape of molecule **21** provided a cavity within itself which obviously played an important role in the recognition process of the nucleotide. Molecular modelling suggested π-π stacking interactions facilitated the differentiation of nucleotides from phosphate or pyrophosphate.

Besides oligonucleotides recognition, this kind of GCP containing receptor also showed astonishing ability in gene transfection. Green fluorescence protein (GFP) plasmid, a typically used reporter DNA in gene delivery studies, can bind with artificial peptide based receptor **21** and **22** (Figure 14).[58] The binding ability of both molecules was examined with an ethidium bromide (EB) displacement assay and isothermal titration calorimetry (ITC). Both receptors showed strong binding affinity with DNA with binding constants ranging from 10^6 - 10^7. Thus, they were able to condense DNA into tightly packed aggregated. However, only receptor **22** with three armed binding sites successfully transferred GFP plasmid into cells and led to the expression of the protein. Further studies suggested that although both receptors transported plasmid into cells, only the plasmid transported by **22** escaped from endosome and reached the cell nucleus. The low pKa value of GCP moiety, around 7, may facilitate the release of plasmid DNA from endosome through a proton sponge effect. Nevertheless, peptidic receptor **22** is among the smallest peptide based gene transfection vectors that was reported so far since these types of vector normally require at least eight positive charges to achieve decent transfection.

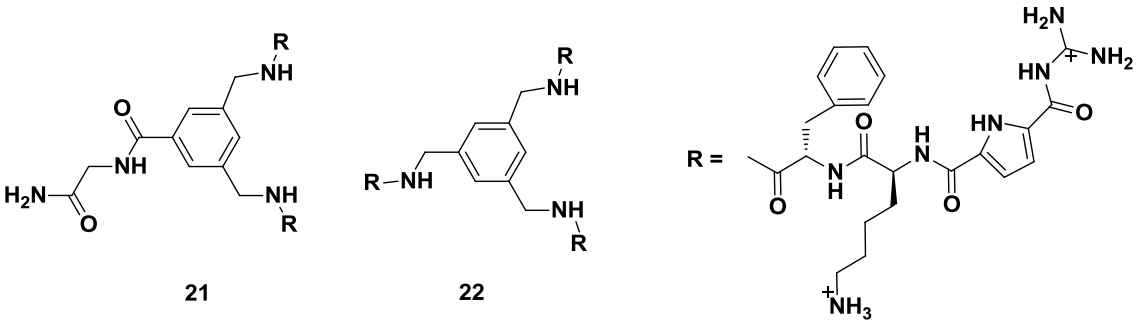

Figure 12. Chemical structures of molecules **21** and **22**

Later, *Schmuck* et al. further extended the applications of GCP moiety in gene transfection. A combinatorial library was established to optimize the binding affinity with DNA.[59] By screening a small but focused combinatorial library of 259 molecular tweezers equipped with GCP binding moieties, receptors with three orders of magnitude enhanced binding affinity

compared to original receptor **21** was identified. However, the significantly improved binding property with DNA did not guarantee a successful gene transfection as the best DNA receptors remained ineffective. Therefore, a lipophilic tail was added to those DNA receptors to facilitate the endosomal escape of DNA inside cells. A new class of artificial transfection vectors was thus obtained, which was comparable in efficiency to the current gold standard Lipofectamine 2000. Notably, the new vectors did not require additional helper lipid which is necessary for Lipofectamie 2000.

2.2 Gene delivery

2.2.1 Gene therapy.

Nucleic acids are the basic and central macromolecules regulating the necessary functions of life. The central dogma of molecular biology points out that any abnormal phenomenon regarding to nucleic acids such as incorrect splicing, mutation and abruption in the transcription and translation process have significant influences in body functions.

A gene is a region of DNA that encodes a functional RNA or protein. Advances in molecular biology and biotechnology as well as the completion of the Human Genome Project in 2000 greatly improved our understanding of genetic diseases. Reports (WHO) suggested that more than 10,000 single gene disorders are related to diseases such as cystic fibrosis, cardiovascular and infectious diseases, Huntington's disease, hemophilia, and sickle cell anemia. Therefore, it has long fascinated scientists to develop therapeutic strategies to treat these kinds of diseases at their genetic root. Moreover, the discovery of RNA interference in 1998 highlighted the potentials of using genetic materials to treat disease which is now known as gene therapy.[60]

Gene therapy can thus be defined as the utilization of genetic materials for the treatment of diseases. Most gene therapy utilized DNA that encodes a functional, therapeutic gene to replace a mutated gene. Other approaches include swapping/repairing an abnormal gene and regulating the degree to which a gene is turned on or off. The first attempt at gene therapy was performed by *Martin Cline* in 1980. However, it was until 1989 that the first clinical trial of gene therapy was conducted.[61] Afterwards, the interests in developing successful methods for gene therapy grew rapidly as can be seen by the increase of the numbers of clinical trials (Figure 13).[62]

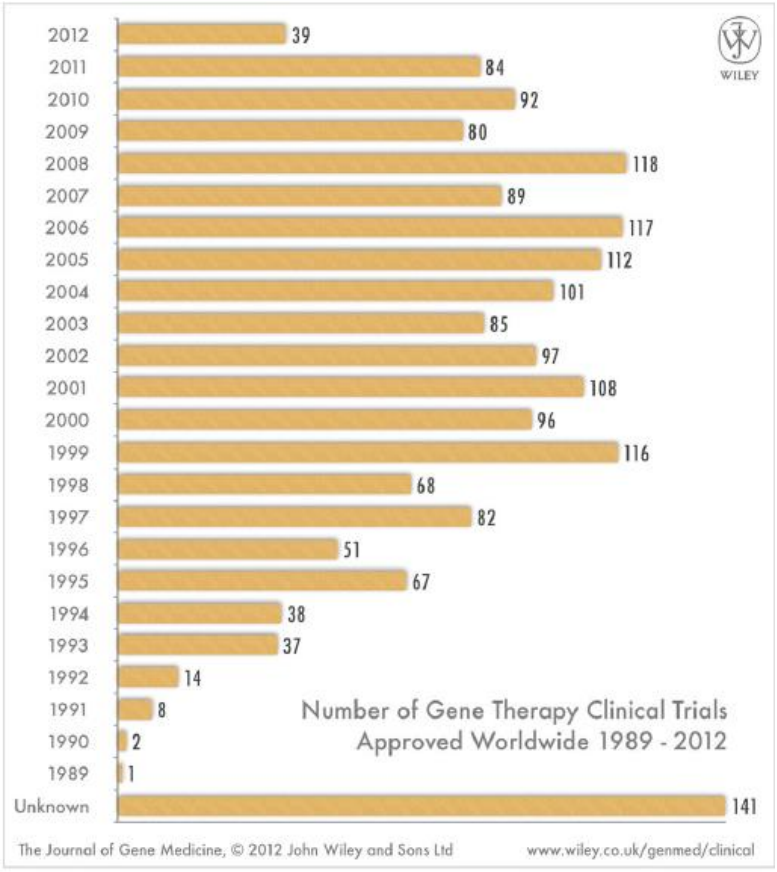

Figure 13. Numbers of clinical trials in gene therapy approved worldwide 1989-2012. Reference 62, copyright (2016) Wiley. Used with permission from John Wiley and Sons.

The main advantage of gene therapy is that it has the potential to serve as a platform technology for treating various diseases since the concept of gene therapy is rather straightforward and adaptable. A variety of diseases such as cancer, cardiovascular and infectious diseases have been tested in clinical trials for gene therapy which makes it a very promising strategy in clinical applications.[11,63,64] However, genetic materials such as DNA and RNA cannot penetrate into cells on their own and they are usually not stable for storage and application. Therefore, it is necessary to develop methods to deliver these genetic materials to desired target cells for the treatment of diseases.

2.2.2 Gene delivery process

A typical gene delivery process is mainly composed of three stages (Figure 14).[7] The first step is the complexation and condensation of genetic materials by vectors which are usually positively charged. The resulting complexes or aggregates are taken up by cell which represents the second step. The crucial step is however the release of genetic materials from

endosome and lysosome before they are degraded by enzymes.

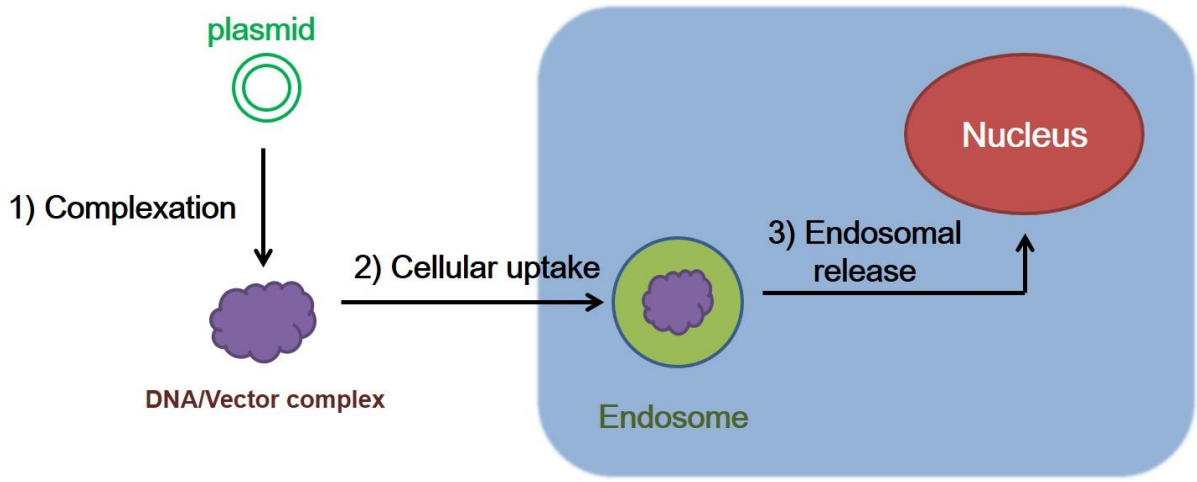

Figure 14. Gene delivery process. 1) Complexation of plasmid DNA with vectors. 2) Cellular uptake of the DNA/vector complex.3) Endosomal release of DNA into cytosol and nucleus

2.2.2.1 Complexation of genes

Genetic materials such as DNA and RNA are subject to constant degradation. Due to the existence of electrostatic repulsions, they are not able to passively translocate through cell membranes. Condensation and complexation of genetic materials prior to transfection is thus the first step and perhaps also the most important step in gene delivery as it determines the fate of genes once entered into cell.

Most transfection vectors bind to DNA by electrostatic interactions between cationic moieties on the vectors and anionic phosphate backbone in DNA. However, it is still not possible so far to determine the best formulation strategy for gene delivery as the complexation and transportation strategy largely vary between different kinds of vectors. The morphology and property of the resulting DNA-vector complexes, referred either as polyplexes, nanoplexes or lipoplexes, depend heavily on the type of transfection vector employed. For example, the condensation of DNA with cationic polymers leads to complexes with sizes proportional to the length and molecular weight of the polymer used.[9] In the case of lipophilic vectors, the head group and hydrophobic domain both significantly influence the binding and condensation process of DNA.[65,66] Furthermore, this process is also dependent on external conditions such as pH and ionic strength of the solutions.[67,68] As consequence, it is necessary to investigate this process for each type of vectors respectively.

2.2.2.2 Cellular Uptake

The main mechanism for the uptake of DNA/vector complexes and other polar macromolecules is endocytosis although other pathways such as membrane fusion have also been reported.[69,70] During this process, the complexes are taken up by cell membrane and delivered into cells through vesicle structures.[71] Therefore, these DNA complexes first need to approach the negatively charged phospholipid bilayer of the cell membrane, which is why it is usually important for a transfection vector to compensate the negative charge of the DNA-backbone.

Endocytosis can be induced not only by unspecific charge interactions, but also by specific receptors located on cell membrane.[72] Such process, i.e. receptor mediated endocytosis, is responsible for the internalization of growth factors, antibodies etc. The receptor mediated endocytosis usually involves clathrin, a protein crucial in the formation of coated vesicles which fuse into endosomes. This strategy can thus be applied for targeting DNA-vector complexes to a specific tissue. The complexes formed with specific targeting ligands such as folate can enter target cells through receptor mediated endocytosis.

2.2.2.3 Endosomal Escape

The normal fate of molecules in endosomes is rapid degradation for cell nutrition.[73] This process starts almost immediately after the endosome is formed, as an ATP driven proton pump in the endosomal membrane decreases the pH from neutral to around 6. Due to the activity of V-ATPase, the pH of the vesicular media is further decreased to ca. 5. Those late endosomes can fuse with intracellular acidic vesicles (lysosomes) that contain a number of enzymes while the pH is continually decreased to ca. 4.5.[74]

Several strategies have been reported for the release of genetic materials entrapped in endosome after endocytosis. One of the widely explored mechanisms is pH sponge effect. In polyplexes of DNA and a vector (e.g. PEI), which contains many primary, secondary and tertiary amine moieties in close proximity, it is likely that a large proportions of these amines are not protonated under physiological conditions. These free but still basic moieties can buffer the decreasing pH within the endosome, which will further promote V-ATPase activity. As more protons are pumped into the endosomal lumen, more counter ions (mainly chloride)

will influx as well. This process increases the osmotic pressure, and water will passively diffuse into the endosome which eventually leads to membrane rupture and release of the genetic materials.

2.2.3 Non-viral gene transfection vector

Two strategies have been developed so far to transport genetic materials into cells: physical methods and non-physical method.[75,7] Physical methods such as gene-gun, electroporation are in most cases limited in lab studies.[76] Non-physical methods then represent a more promising strategy in the application of gene therapy in clinical trials. .

Gene transfection vectors can be classified into two categories: viruses based vector and non-viral based vector. Viruses are by far the most efficient delivery vectors in gene therapy.[77] In fact, most clinical trials conducted with gene therapy rely on retroviruses or adenoviruses to deliver the genetic materials as shown in Figure 15.[62] Other viruses based vectors include adeno-associated viruses, vaccinia virus, lentiviruses, poxviruses and herpes viruses which differ in how well they transfer genes to the cells. Despite the overall high efficiency of virus based vector, their safety has been questioned the first day since their application. Problems and risks such as immune responses and virus transmission exist in the utilization of virus which prevents their further applications in gene therapy.

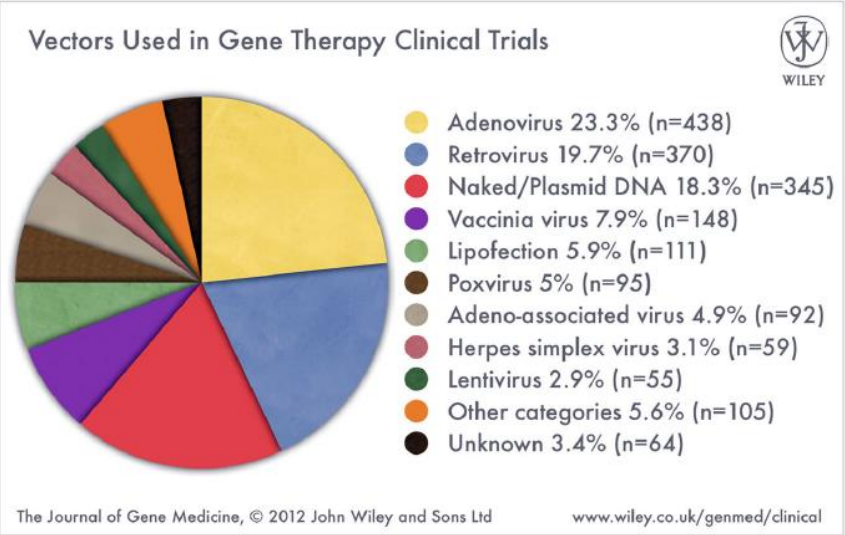

Figure 15. Vectors used in gene therapy clinical trials. Reference 62, copyright (2016) Wiley. Used with permission from John Wiley and Sons.

As consequence, there is more and more interest in the development of non-viral based

gene transfection vectors. It is now becoming a rather active area in the field of chemistry. Chemists have developed several kinds of non-viral gene transfection vectors such as cationic polymers, cationic lipids, cell penetrating peptides and nanoparticles over recent years. Among them, several systems have successfully been applied in molecular biology as a powerful tool to study the functions of various proteins and enzymes. For examples, commercially available cationic polymer polyethylenimine (PEI) and the cationic lipid Lipofectamine are both currently the standard reagents used in gene transfection studies. This will largely benefit the transition of gene therapy from lab studies to clinical trials and finally become a feasible method in the treatment of various diseases.

2.2.3.1 Cationic polymer

DNA molecule is highly negatively charged. Positively charged polymers were naturally considered first in the development of gene delivery vectors. In fact, most of early gene delivery studies utilized cationic polymers, such as poly-lysine (PLL), polyethylenimine (PEI) and polyamidoamine dendrimers (PAMAM) as vectors.[78]

Polylysine

Polylysine can be obtained in a large variety of molecular weights. It was previously used as delivery vector for small drugs due to its polypeptide nature which can be easily degraded by cells.[79] As a poly-cation, its DNA condensation property has also been extensively studied even before the concept of gene therapy was introduced.[80,81]

In 1991, *Xiaohui Zhuo* et al. reported that low molecular weight polylysine conjugated with phospholipid group was very effective in the transfection of mammalian cell lines.[82] The unmodified polylysine, however, exhibited little activity. In 1996, *Gottschalk S.* et al. constructed DNA complexes with short synthetic peptides with a lysine rich peptide sequence and a pH-dependent endosomal releasing agent.[83] Transfection with these complexes resulted in high-levels of gene expression in a variety of cell lines. However, it should be noted that in order to prepare homogenous, small and soluble DNA complexes, parameters such as salt concentration, charge ratio and size of polylysine must be thoroughly examined.

Additional advantage of polylysine based polymers is that the epsilon amino group is a good target site to covalently attach ligands to realize receptor mediated gene delivery.[84]

Ligands such as folate, insulin and proteins have been covalently linked to the side chain of lysine. These systems have been tested not only *in vitro*, but also showed promising results in *in vivo* studies.

Polyethylenimine (PEI)

The application of polyethylenimine (PEI) in gene therapy is a landmark in the development of gene transfection vectors.[85] Among the various poly-cations used for gene delivery, PEI is exceptional attractive due to its superior ability of DNA condensation and its potential in endosomal escape.

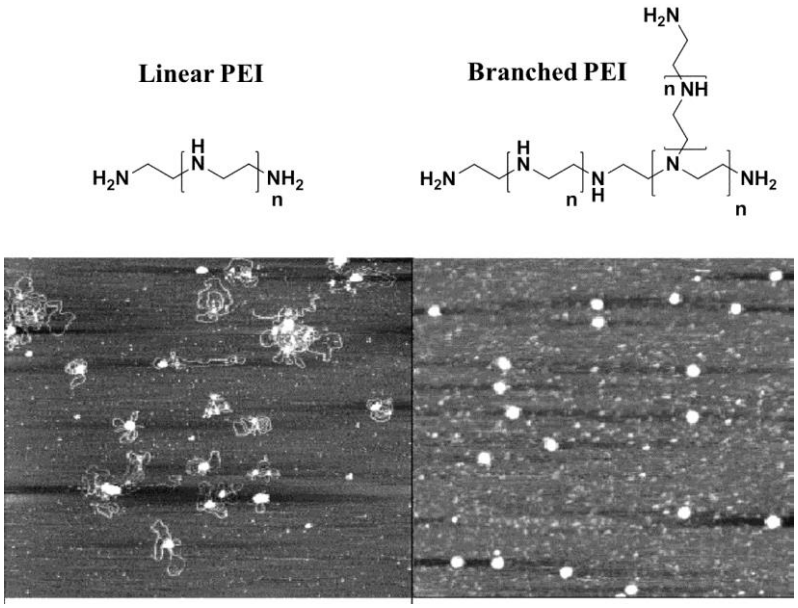

Figure 16. Loosely condensed polymer/plasmid complexes consisting of linear PEI 22 kDa (left) compared to complexes with branched PEI 25 kDa (right). Reference 87, Copyright (2016) Wiley. Used with permission from John Wiley and Sons.

PEI exists both in linear and branched forms as shown in Figure 16. Studies suggested that the secondary structures of PEI played an important role in the physicochemical and biological properties of the complexes with DNA.[86] AFM studies showed that branched PEI can condense DNA more densely than linear PEI (Figure 16).[87] The condensation process between PEI and DNA is mostly driven by electrostatic interactions. The release of counter ions from the backbone of DNA upon binding is considered to be the main driving force for the formation of PEI/DNA complex.

It is now well known that endocytosis is the major cellular uptake pathway for PEI mediated gene delivery. The size of the complexes formed between PEI and DNA are

normally below 200 nm which is ideal for endocytosis. Consequently, most of the DNA transfected with PEI stay entrapped in endosomes. Incubation of cells with bafilomycin, an endosomal escape inhibitor, completely abolished the transfection ability of PEI which further confirmed the importance of endocytosis in PEI mediated gene delivery. Recent study showed that there were two kinds of PEI in DNA/PEI complex, the bound chains and the free chains.[88] The bound PEI was mainly responsible for the condensing of DNA to form DNA/PEI complex. As the N/P ratio increased, most of PEI chains existed as free chains in DNA complex which not only accelerated the cellular uptake process, but also facilitated the endosomal release of DNA by preventing the development of late endosomes. This might be the reason that long chains PEI are more effective than short ones in gene transfection.

In general, the transfection efficiency of PEI is quite high which makes it suitably to be applied as a standard in gene transfection experiment. However, the severe toxicity of PEI hindered its further application in clinical trials. It has been shown that even in *in vitro* experiments, 70% of cells died because of the transfection with PEI. The toxicity of PEI is closely related to its molecular weight and structure.[89] Low molecular weight PEI has lower toxicity in cell studies. Increasing the degrees of branches of PEI leads to higher toxicity.

As consequence, several strategies have been developed to improve the gene delivery property of PEI. The most common used method is the conjugation of biocompatible polymer polyethylenglycol (PEG) to PEI which is the so-called "PEGylation".[90,91] Depending on the nature of the chemical bond in the conjugation, PEG-PEI copolymers can be classified into non-biodegradable and biodegradable polymers.[92] Non-biodegradable polymers, which are usually constructed with urethane and urea, are naturally more stable and easier to synthesis. However, their pharmaceutical behavior after cellular uptake would become a severe issue. On the other hand, biodegradable PEG-PEI copolymers have attracted more interests recently. *Thomas Kissel* et al. reported that by linking several low molecular weight PEI blocks with oligo (L-lactic acid-co-succinic acid), a water-soluble PEG-PEI copolymer was constructed which could be degraded via base-catalyzed amide bond cleavage.[93] Besides the lower toxicity, the new polymer showed significant enhancement in the transfection efficiency compared to unmodified PEI. PEGylation also increased the solubility of PEI in water and its biocompatibility. Moreover, the application of PEG has been reported to reduce the

immunogenicity of drug delivery systems. The interaction of cationic polymer PEI with proteins can be inhibited with the shield from PEG shell.[91] This strategy is thus very promising in the long term application of PEI based gene delivery vectors.

Besides the modification with PEG, disulfide linkage has also been introduced to construct redox responsive PEI based gene delivery vectors. The application of disulfide bond provides an outstanding method to utilize the redox environment inside cells (Figure 17).[94] DNA, which was condensed with PEI prior to cellular uptake, can be easily released into cytosol through the redox reaction of disulfide bond with glutathione (GSH). *Qi Peng* et al. reported that by utilization of ring opening reactions, thiol group was introduced into low molecular weight PEI to obtain PEI-SH.[95] Subsequently oxidation gave rise to disulfide linked cationic polymer PEI-SS-PEI. The resulting biodegradable polymer showed a lower toxicity and enhanced transfection efficiency even compared to high molecular weight PEI. Moreover, PEGylation often resulted in the decease of transfection efficiency of cationic polymers. Introduction of disulfide bond into PEGylated polymers can thus increase their transfection efficiency. Copolymers constructed with polylysine, PEG and PEI through disulfide bond showed successfully delivery of small interfering RNA (siRNA) into cells.[96]

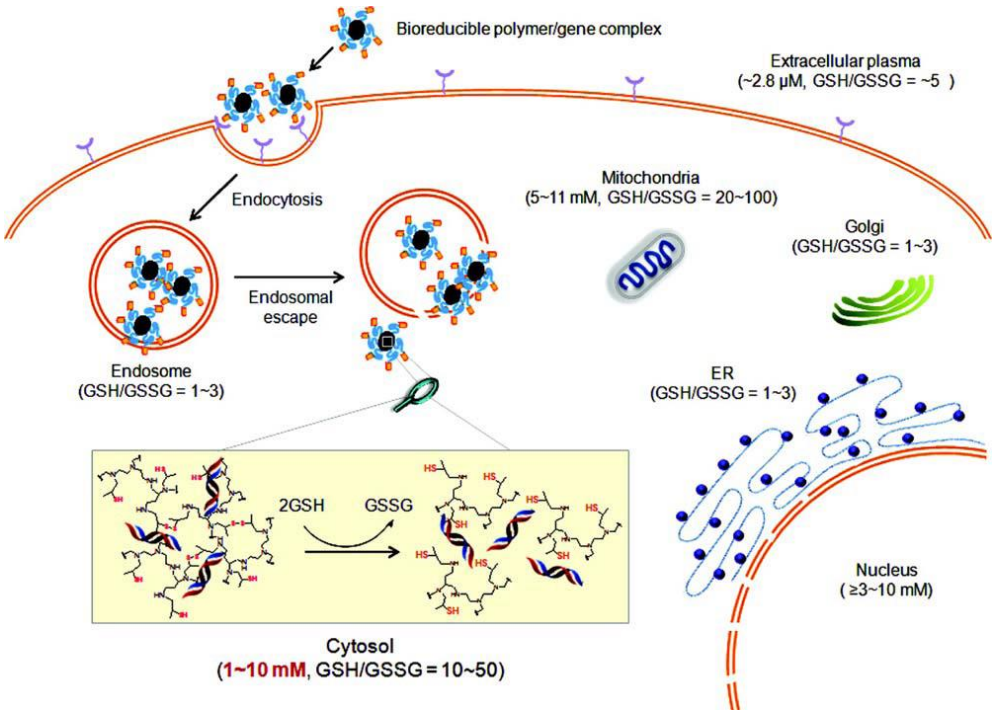

Figure 17. Schematic illustrations of the gene delivery by bio-reducible polymeric vector. Reference 94, Copyright (2016) Wiley. Used with permission from John Wiley and Sons.

Mallory A. Cortez et al. recently reported another interesting strategy to improve the gene delivery property of PEI.[97] A set of cyclic PEIs and its exact linear analogues with same molecular weight were designed and synthesized. Transfection experiments showed that the cyclic PEIs exhibited significantly better efficiency with lower cytotoxicity compared to linear PEIs. This result highlighted the importance of secondary structure of polymer in the efficiency of PEI mediated gene transfection.

Other polymers

Besides polylysine and PEI, other types of cationic polymers such as carbohydrate based polymers,[98] linear poly (amidoamine)[99] and dendrimer based vectors[100] have also been applied for gene delivery. Utilization of the unique property of different polymers can provide interesting functions in gene delivery system. Introduction of targeting ligands after the complexation of polymer with DNA can also be achieved. For example, *M. E. Davis* et al. firstly introduced linear cationic cyclodextrin polymers in the development of gene delivery vectors.[101] The new polymers were able to bind DNA through electrostatic interactions and formed nanoparticles around 100 nm in size. This system showed comparable transfection efficiency to PEI and Lipofectamine and also exhibited significant less cytotoxicity in several cell lines.

Later, they further extended this system to siRNA delivery as a result of the discovery of RNAi therapy (Figure 18).[102] The formulation for siRNA delivery is featured with three components: the key is cationic cycoldextrin polymers which provide multiple functions such as complexation with RNA and protection against nuclease degradation. Cyclodextrins are incorporated in the backbone of the polymer which is linear and water soluble. Other two components are adamantane functionalized PEG (PEG-AD) and Transferrin (Tf-PEG-AD). The inclusion of adamantane with cyclodextrins decorates PEG chains on the surface of cyclodertein-RNA nanoparticles. PEGylation then provides steric protection for systematic delivery of RNA. The addition of transferrin could target these nanoparticles to cancer cells which are known to overexpress transferrin receptors. Notably, the sizes of the nanoparticles formed between polymer and siRNA are important. By using a two vial formulation strategy (Figure 18b), nanoparticles around 70 nm in size were obtained which proved to be best in delivery. In 2008, they demonstrated the first targeted delivery of siRNA in human trials with

this system. Experimental therapeutic drug was initiated in phase I trial and the first patient was treated in May of 2008.

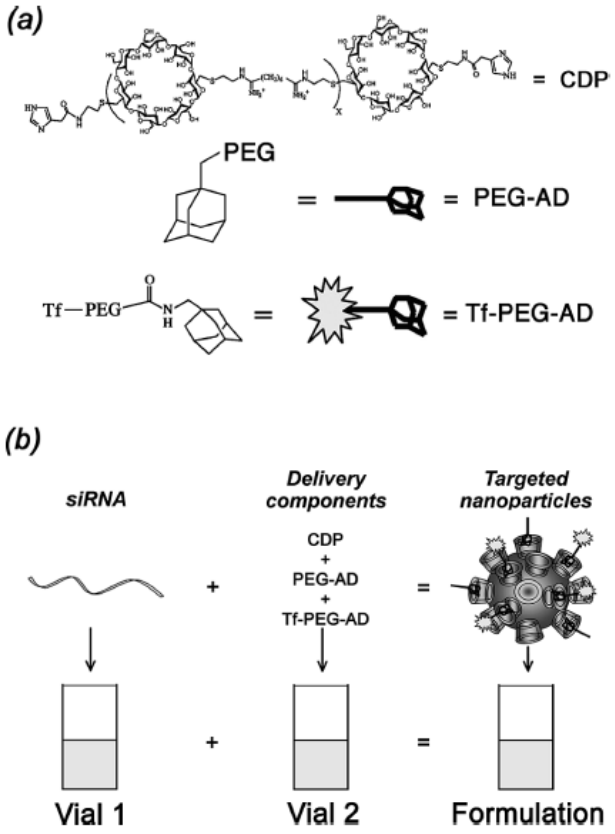

Figure 18. (a) The delivery components: cyclodextrin-containing polymer (CDP), adamantane (AD)-PEG conjugate, human transferrin (Tf) conjugated adamantane (Tf-PEG-AD). (b) The formulation contains two vials, one with siRNA and the other with the delivery components. Reprinted with permission from Reference 102. Copyright (2016) American Chemical Society."

2.2.3.2 Cationic lipids

Cationic lipids are arguably the most widely used non-viral vectors in the field of gene delivery.[103] They normally contain a cationic head group and one or several hydrophobic tails (Figure 19).[69] The amphiphilic nature of such cationic lipids results in the formation of structures such as micelle and vesicle in water solutions. The head group is mainly responsible for the binding with DNA and the hydrophobic tails can also facilitate the condensation of DNA. Genetic materials can thus be entrapped into this compartment and be transferred into cells.

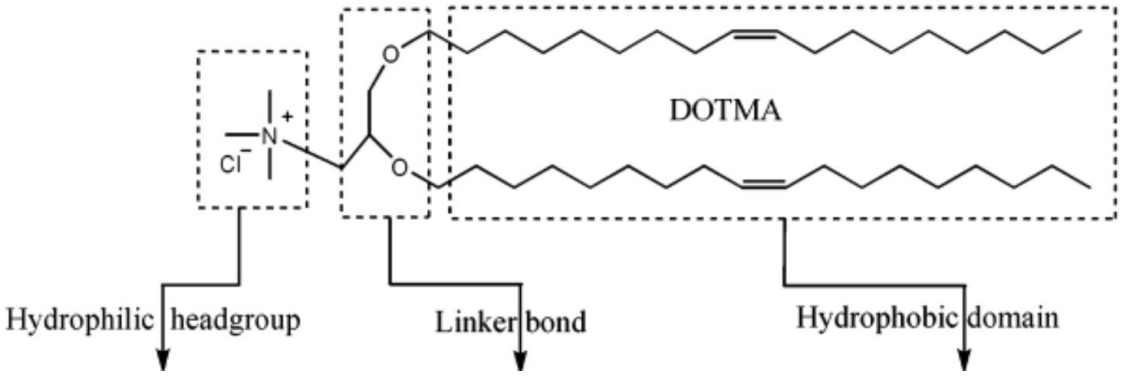

Figure 19. Schematic illustrations of cationic lipid gene delivery vector. Adopted with permission from Reference 65. Copyright (2016) American Chemical Society."

Utilization of these carrier systems for gene delivery can date back to the early 1980s. *Claude Nicolau* et al. reported that a fragment of plasmid DNA was isolated and entrapped in liposomes of different phospholipid compositions.[104] The incubation of DNA-liposome with synchronized cells resulted in the uptake of DNA with efficiency around 2000 molecule per cell. In 1987, *Philip Felgner* et al. firstly reported a synthetic unsaturated cationic lipid that can successfully transfer plasmid DNA into a variety of cells with high efficiency.[105] Cationic lipid N-[1-(2, 3-dioleyloxy) propyl]-N,N,N-trimethylammonium chloride (DOTMA, Figure 19) interacted strongly with DNA and 100 % DNA entrapment was realized. This discovery inspired many researchers to extend the scope of cationic lipids for gene delivery. A variety of cationic lipids with different chemical structures and physical properties has been reported.

However, most cationic lipids reported so far require a “helper lipid” to fulfill their function in gene delivery experiments. Neutral lipids such as cholesterol[106], dioleoylphosphatidylethanolamine (DOPE)[107] and dioleoylphosphatidylcholine (DOPC)[108] are often additionally added to the complexes formed between cationic lipids and DNA. It is the appropriate combination of cationic lipid, DNA and helper lipid that determines the final formula for cationic lipid mediated gene delivery.

The role of helper lipid in transfection is however in debate. Some evidence suggested that the addition of DOPE determined the structural transition pH of the final complexes when the pH decreased from 7 to 5 inside cells.[109] Others pointed out that the presence of helper lipid such as cholesterol and DOPE facilitated the DNA complexes to adopt a fusogenic, inverted hexagonal phase which promoted the release of DNA from endosome to cytosol.[110,111]

Nevertheless, it is clear without doubt that helper lipids are in most cases necessary for the gene transfection mediated by cationic lipids. Therefore, all the cationic lipid systems used in gene transfection experiments mentioned in this context are performed with the addition of helper lipids unless otherwise noted.

The positively charged head groups are crucial in the DNA complexation process. Depending on the structure of the hydrophilic head groups, cationic lipids can be roughly classified as quaternary ammoniums, guanidiniums and other head groups based.[65]

Quaternary ammoniums

Quaternary ammoniums are by far the most often used head groups in cationic lipid mediated gene delivery. A number of elegant cationic lipid transfection systems are equipped with quaternary ammoniums such as DOTAP, DDAB and CTAB (Figure 20).[112] The positively charged head groups provide sufficiently strong binding ability with negatively charged DNA. However, it has been demonstrated that the transfection efficiency of these types of cationic lipids is closely related to the hydration ability and charge density of the ammonium head group region. Therefore, two strategies have been developed to improve their efficiency: addition of hydroxyl groups and introduction of more than one charged groups.

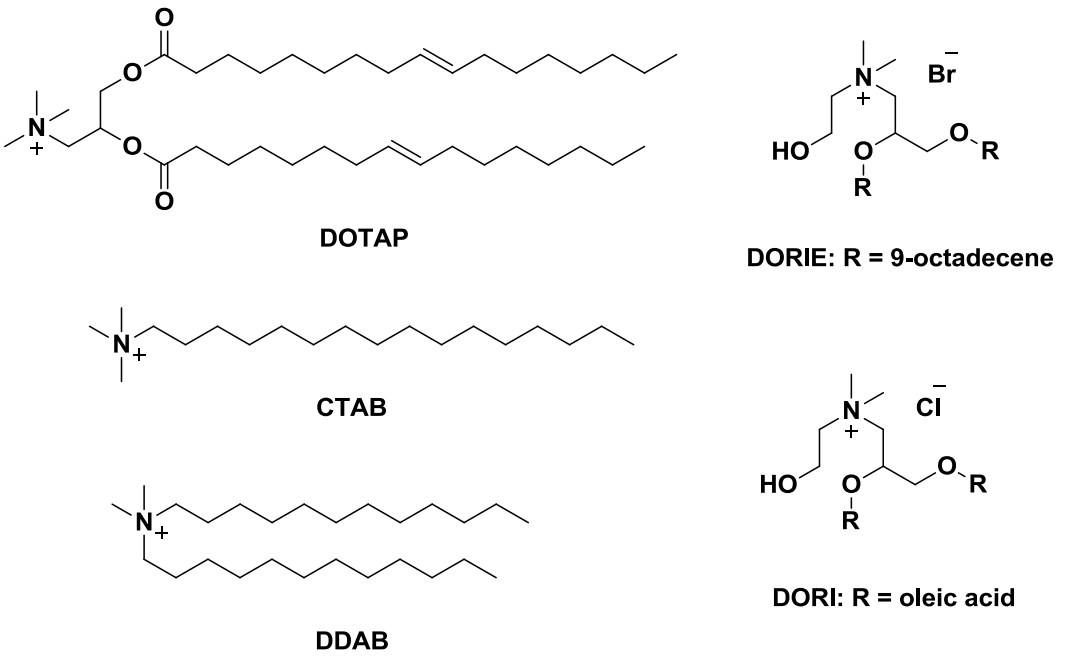

Figure 20. Chemical structures of cationic lipid gene delivery vector

The addition of hydroxyl groups on the hydrophilic domains of cationic lipids could

increase their performance in gene delivery. DORIE and DORI (Figure 20), with additional hydroxyl group on the head groups demonstrated better transfection ability in HeLa cell lines.[69,113] It was proposed that the hydroxyl group could hydrogen-bond with cell membrane or simply enhancing the electrostatic interactions to achieve better affinity. Also the bilayer structures of these cationic lipids benefited from the intermolecular hydrogen bonding between each molecules and the interaction with aqueous phase. The hydroxyl groups might also involve in the binding with DNA through hydrogen bonds. As consequence, cationic lipids bearing more hydroxyl groups in the head groups were designed and synthesized. For example, *Rajkumar Banerjee* et al. reported a series of non-glycerol-based transfection lipids containing two hydroxyethyl groups in the head groups.[114] The transfection efficiency of these cationic lipids was even better than Lipofectamine, the current golden standard in transfection experiment. They further studied the possibility of using sugar molecules as a source of hydroxyl groups in the head groups.[115] The complexation behaviors with DNA were indeed different from other cationic lipids without hydroxyl groups. Compared to cationic lipids with two hydroxyl groups, these newly developed lipids showed an improvement in the transfection efficiency and also exhibited lower cytotoxicity.

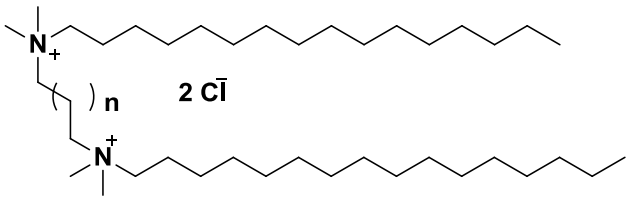

23

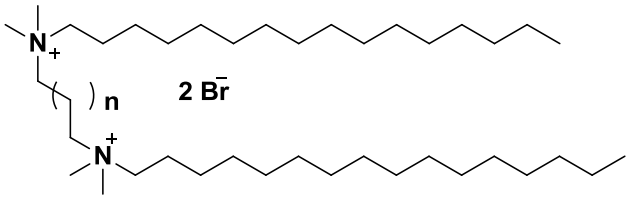

24

Figure 21. Chemical structures of cationic lipid **23** and **24**

Another often used strategy is to introduce more positive charges in the head group which lead to the formation of dimeric lipids. Introduction of additional charges could increase their binding affinity with DNA. *Howard Rosenzweig* et al. reported a new class of cationic lipids

23 and **24** for mediating transfection of DNA in mammalian cell lines (Figure 21).[116] The advantage of these reagents is that they do not need helper lipids in transfection process. Their transfection efficiency was comparable to commercial available transfection reagents such as Lipofectin, Lipofectace and Lipofectamine. The spacer between the two ammonium groups in **23** and **24** significantly influenced the physiochemical property of the resulting complexes. Additionally, head groups bearing three or four positive charges are also very promising in the application of gene delivery vectors.[117] For example, the low micellar sizes and high critical micellar concentration endowed by the higher charge density are very attractive for the development of cationic lipid based gene delivery system.

Guanidiniums

The amino acid sequences of natural DNA-binding proteins and peptides such as protamines are featured with their exclusive use of arginine.[118,119] Protamines are small, highly positively charged peptides used by cells to package DNA at very high densities in sperm nuclei. Of the 32 amino acids of salmon protamine, 21 are arginines. Bovine protamine has 26 arginines of its 50 total amino acids and human protamines also consist half of arginine residues in their sequences. The guanidinium cation in the side chain of arginine, with pKa around 12, is prominently positively charged under physiological conditions. Moreover, guanidinium cations could form bidentate hydrogen bonds with oxoanions such as the phosphodiester linkage in DNA backbone. Therefore, cationic lipids with guanidinium head groups often possess high DNA binding affinity and result in highly condensed DNA complexes compared to that of ammonium head group based cationic lipids. A number of guanidinium head group based cationic lipids thus have been explored in gene delivery experiments.[120]

25, R1 = R2 = n-C13H27
26, R1 = R2 = n-C15H31
27, R1 = R2 = n-C17H35

28, R1 = R2 = n-C13H27
29, R1 = R2 = n-C15H31
30, R1 = R2 = n-C17H35

Figure 22. Chemical structures of guanidinium based cationic lipids

In 2004, *Jean Herscovici* et al. reported the synthesis of new cationic lipids with a

hydrophobic tails connected to guanidinium moiety by an unsaturated glycoside scaffold. These lipids can efficiently compact DNA to form stable lipoplexes.[121] *Joyeeta Sen* et al. then demonstrated that guanidinium containing lipids were rather effective in gene transfection experiments (Figure 22).[122] The efficiencies of cationic lipids **25 - 27**, in particular, were better than that of Lipofectamine in the transfection of several cell lines. In comparison, lipids **28 - 30** were less effective due to the absence of additional positive charges in the head groups. Further introduction of tertiary amine center in the head groups allowed more efficient siRNA binding compared to other cationic lipids.

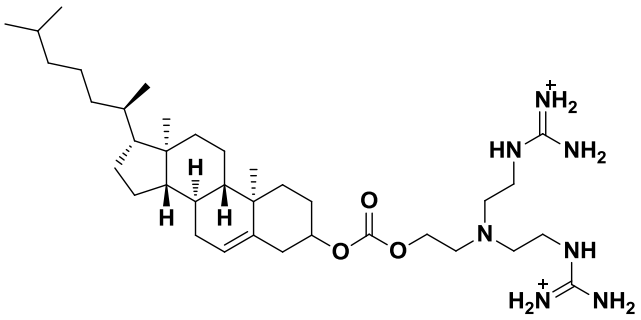

31 (BGTC)

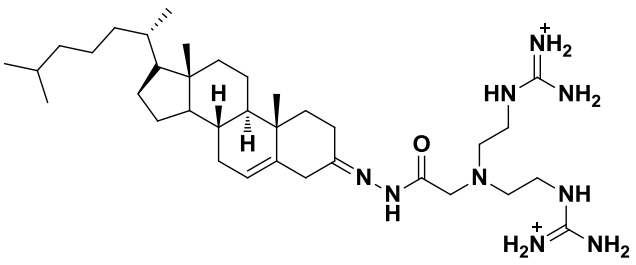

32

Figure 23. Chemical structures of guanidinium based cationic lipid **31** and **32**

T-shaped head groups with two guanidinium cations were first designed and synthesized by *Lehn* et al. in 1996 (Figure 23).[123] The utilization of cholesterol as hydrophobic domain provided their unique property in the interaction with cell membranes. Bis-guanidinium-tren-cholesterol (**31**, BGTC) was very efficient in gene transfection when it was applied as micellar solution. When it was formulated with neutral helper lipid to form liposome, it was able to efficiently transfect airway epithelial cells *in vivo*. They also incorporated an acid sensitive acylhydrazone linkage to connect the bis-guanidinium head group to an unsaturated cholest-4-enone (**32**).[124] Acid catalyzed hydrolysis was confirmed for

32 which implied their potential application in acidic environment such as tumor tissue. The new series of T-shaped bis-guanidinium cationic lipids displayed significant less cytotoxicity and were able to transfect cells both *in vitro* and *in vivo*.

Recently, *Charlotte Gehin* et al. demonstrated a dynamic cationic lipids library to screen for the delivery of siRNA in HeLa cell lines and human primary fibroblasts.[125] This method provided a rapid access to fairly large libraries of complex structures and possible ways to assist uptake and minimize toxicity. Both guanidinium and ammonium cation head groups were applied in the library. The best structure found in this study knocked out 60% of target gene compared to 30% from Lipofectamine. More importantly, the best hit was not predictable from literature reports and thus underlined the importance of conceptually innovative screening approaches.

Other head groups

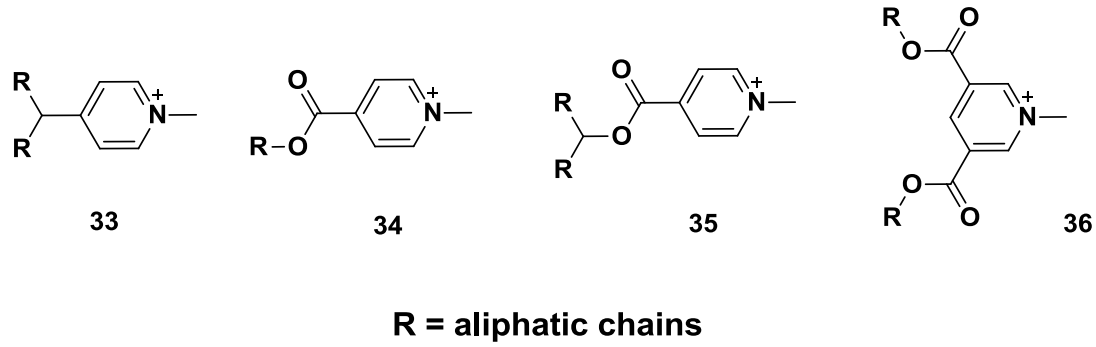

Figure 24. Chemical structures of pyridinium based cationic lipid **33**-**36**

Besides ammonium and guanidinium head groups, there are also several other types of positively charged head groups. For example, pyridine and pyridinium are among the most frequently used hetercyclic polar head groups in the design of cationic lipids.[65] In 2000, *Engberts* and colleagues reported the synthesis of a series of pyridinium based cationic lipid amphiphiles (**33** – **36**) to examine the influence of structural parameters on transfection experiments (Figure 24).[126] The report showed that all the studied compounds can form stable and well-defined complexes with DNA. The introduction of additional charges in the head group and unsaturation of the hydrophobic domain significantly affected the transfection efficiency in eukaryotic cells. They further introduced bio-degradable ester bond to connect the pyridinium and hydrophobic tails.[127] The new lipids demonstrated better transfection

efficiency than their parent lipids through influencing both the overall morphology and DNA releasing ability of the formed lipoplexes. Other kinds of linkage have also been tested such as ether, amide, urethane, or phosphonate ester groups.[128]

Imidazole contains an amine with pKa within the physiological range of 4.5 to 8. Thus, *Vladimir Budker* et al. designed a class of pH sensitive cationic lipids with imidazole as head group.[129] Despite that there were no permanent positive charges in the head groups, these lipids were able to condense and incorporate DNA into liposomes. Transfection efficiency was naturally dependent on the acidification process of endosome. Interestingly, lipids bearing imidazole head groups can also be used as helper lipid to replace DOPE in cationic lipid mediated gene transfection. *Mathieu Mevel* et al. demonstrated that these new helper lipids can improve the transfection by a factor of up to 100 compared to the usage of DOPE as co-lipid.[130]

Neutral or low cationic surface charged head groups represent another interesting class of cationic lipids. Ammonium, guanidinium and other fully positively charged head groups are mostly suitable for DNA binding. However, they also lost their protonation abilities once inside cells which could hinder the release of DNA to cytosol. Therefore, primary, secondary and/or tertiary amine head groups have been developed which process better buffering property to facilitate endosomal release. The well-known and commercially available transfection reagent DC-Chol with a tertiary amine head group is a typical example.[131] It was reported by *Huang Leaf* et al. in 1991 and showed remarkable transfection efficiency in a variety of cell lines. This reagent was rather easy to synthesize and proved to be stable for several weeks.

2.2.3.3 Cell penetrating peptides

Cell penetrating peptides were first discovered in 1988 when it was observed that HIV-Tat regulatory protein could efficiently penetrate into cells.[132] *Bernard Lebleu* et al. then successfully identified that a short truncated HIV-1 Tat protein basic domain rapidly translocated through cell membrane and accumulated in nucleus.[133] The result was very inspiring because they demonstrated that all peptides containing this basic domain can penetrate cell membrane within 5 minutes with concentration as low as 100 nM. A secondary

structure such as a full α-helix was not required in cellular uptake. In the meantime, parallel studies revealed another class of peptides originating from the homeodomain of Antennapedia (a *Drosophila* homeoprotein) which was able to penetrate cells in a receptor-independent manner.[134] In 1994, *Alain Prochiantz* et al. found that the third helix of the homeodomain of Antennapedia was necessary and sufficient for the translocation through cell membrane.[135] A 16 amino acids peptide was thus discovered and later named "penetratin".

Several families of cell penetrating peptides derived from natural occurring proteins are known today such as transportan[136], signal sequence based peptides[137] and arginine nonamer[138] (Figure 25). The discovery of cell penetrating peptides is particular interesting in the field of gene delivery. Most gene delivery systems (polymer, lipid etc.) suffered from severe toxicity either *in vitro* or *in vivo*. Peptides such as arginine oligomers then provide a useful tool to transfer genetic materials into cells due to the cationic nature of most cell penetrating peptides. Their compatibility with cells is in most cases significantly better than other transfection systems. Additionally, these peptides can penetrate cells even at 4°C and other conditions which prevent normal endocytosis. Their penetration process is in most cases not receptor mediated thus it is cell type unspecific. This advantage makes cell penetrating peptides interesting as universal vectors for a variety of genetic materials.

Penetratin:	RQIKIWFQNRRMKWKK
Tat (48-60):	GRKKRRQRRRPPQC
Siganl sequences based peptides:	GALFLGWLGAAGSTMGAWSQPKKKRKV
Tranportan:	GWTLNSAGYLLKINLKALAKALAKKIL
Amphiphilic model peptides:	KLALKLALKALKAALKLA
Arg_9:	RRRRRRRRR

Figure 25. Typical cell penetrating peptides

HIV-Tat peptide

One of the earliest utilization of Tat peptide for gene delivery experiment was demonstrated by *Anna Astriab Fisher* et al. through the conjugation of antisense oligonucleotide in 2000.[139] The antisense oligonucleotide was designed to inhibit the cell surface expression of P-glycoprotein. Effective inhibition was realized with submicromolar concentrations of Tat-antisense conjugates in the presence of serum, in contrast with other approach of nucleic acid delivery. *Akiko Eguchi* et al. later extended the application of Tat peptide to DNA

delivery.[140] Recombinant phage particles displaying Tat peptide on their surfaces were constructed and mammalian genes were incorporated as reporter. Significant expression of phage marker genes was induced when the cells were exposed to Tat-phage. Additionally, *Carsten Rudolph* and coworkers constructed several oligomers of Tat peptide for gene delivery.[141] The oligomers showed excellent ability to compact plasmid DNA to particles with sizes ranging from 70 to 90 nm depending on the charge ratio. Transfection efficiency was 6 fold higher than polyarginine. Remarkably, when DNA was pre-compacted with Tat peptides and PEI, the transfection efficiency was 390 fold higher than commercial vectors.

Despite the initial success, gene transfection mediated by Tat peptide alone remained low effective. Therefore, *Vladimir P. Torchilin* et al. prepared a series of liposomes with different composition of Tat peptides on their surfaces.[142] The modification with Tat peptides resulted in the cellular uptake of relatively large liposomes (200 nm). Further decoration with PEG-2000 abolished the internalization of liposomes which underlined the importance of direct contact between Tat peptides with cell membrane. These liposomes can transfect mouse NIH cell lines and rat H9C2 cardiomyocytes with a high efficiency *in vitro*. Moreover, intra-tumoral injection of TAT-liposome–DNA complexes into the Lewis lung carcinoma tumor of mice resulted in the expression of gene *in situ*.[143]

The application of Tat peptide in gene delivery is mostly limited by its poor endosomal releasing ability and the instability of peptide/DNA complexes. *Shu Wang* et al. thus modified Tat peptides with histidine and cysteine residues which could promote endosomal escape of DNA.[144] Up to 7000 fold enhancement in the transfection efficiency of Tat peptide fused with 10 histidine residues was observed compared to original Tat peptide. Further introduction of cysteine led to disulfide bond formation after air oxidation upon binding to DNA. This property improved the stability of the resulting complex which eventually resulted in an even better transfection. Recently, *Erlei Jin* et al. modified the lysine residue in Tat peptide with succinyl amides (^{a}Tat) to inhibit its nonspecific interactions in the blood compartment (Figure 26).[145] The function of Tat peptide was thus deactivated in normal conditions. Once ^{a}Tat peptide reached the acidic tumor interstitium or internalized into cell endo/lysosomes, a quick hydrolysis from the succinyl amides were triggered due to the low pH and thus reactivated Tat peptides.

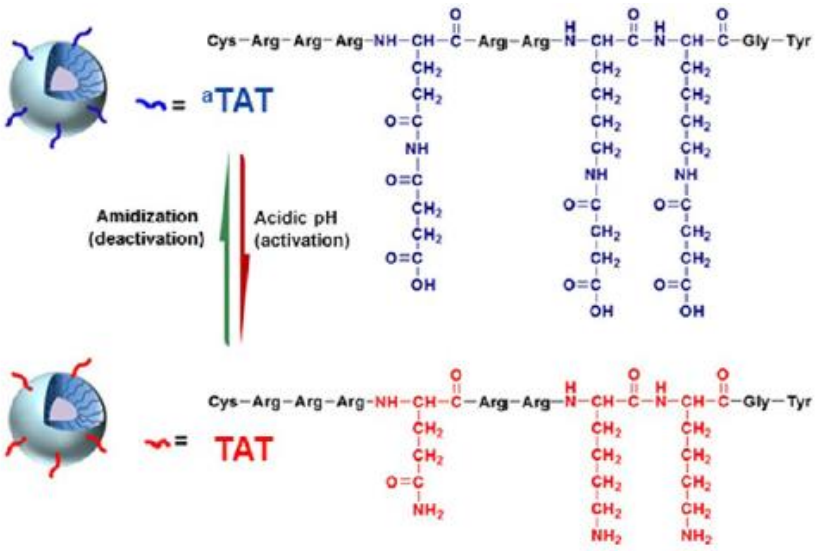

Figure 26. Amidization of TAT's primary amines and their acid-triggered hydrolysis. Adopted with permission from Reference 145. Copyright (2016) American Chemical Society."

Seiichi Yamano et al. combined the advantages of cationic polymers and Tat peptide to develop a novel gene transfection vector.[146] Polyethylenimine (see chapter 2.2.3.1), a cationic polymer widely studied as an efficient gene delivery vector, was formulated with mTat peptide modified with histidine and cysteine residues. The sizes of the particles formed between mTat/PEI/DNA complex and DNA were significantly smaller than that of mTat or PEI alone. As consequences, mTat/PEI produced 5-fold improvement in transfection efficiency through caveolae-mediated endocytosis. Experiments *in vivo* showed that animals administered with mTat/PEI/DNA intramuscularly exhibited a rather long luciferase expression about seven months without any associated toxicity.

Arginine oligomers

Inspired by the discovery of HIV Tat peptides, chemists also developed arginine oligomers which showed excellent cell penetration ability in a variety of cell lines. Studies suggested that at least six positive charges are required for arginine oligomers to penetrated cell membrane.[14] Despite the controversies as how these extremely polar peptides successfully translocate through cell membrane, their gene transfection abilities were tested to be comparable to other peptides. Moreover, the rather simple peptide sequences of arginine oligomers make them attractive in the hybridization with other type of transfection vectors such as polymers and inorganic nanoparticles.

Arginine oligomers previously proved to be very effective in cellular uptake. However,

their DNA transfection efficiency was far less than commercial reagents such as Lipofecamine. In 2001, *Shiroh Futaki* et al. modified a series of arginine oligomers with different hydrophobic groups on the N-terminus (Figure 27).[16] It was found that stearyl-R_8 formed significantly larger complexes with DNA than polyarginine and Lipofectamine. Transfection mediated with stearyl-R_8 was increased approximately 100 times to reach the same order of magnitude as that of Lipofectamine. The differences in the efficiency of transfection between modifications with stearyl, lauryl and cholesteryl were however negligible. Later, it was discovered that stearyl-R_8 could also be used to achieve efficient siRNA delivery into primary hippocampal neurons via endosomal pathway.[147] The transfection efficiency was comparable with cationic liposome while being less cytotoxic in primary neurons.

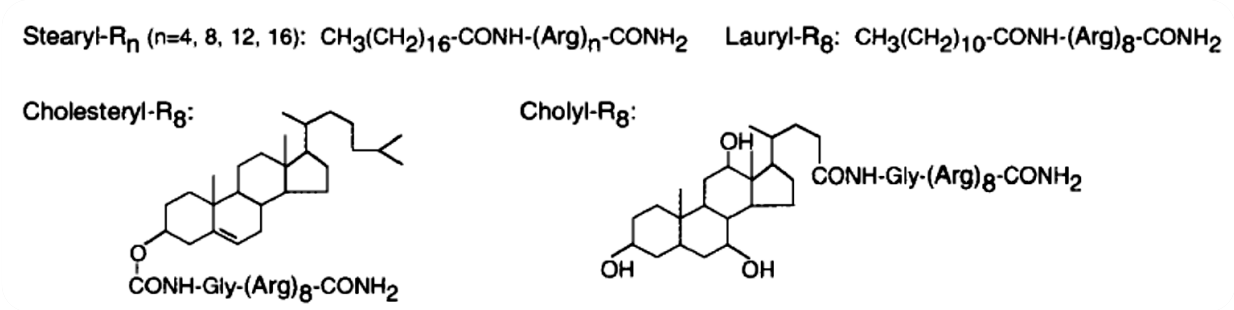

Figure 27. Modification of arginine oligomers with hydrophobic groups. Adopted with permission from Reference 16. Copyright (2016) American Chemical Society."

Another interesting application of arginine octamer (R_8) is to decorate multifunctional envelop nano-device (MEND) as shown in Figure 28.[148] MEND device was prepared with a programmed packaging approach. Firstly, DNA was condensed with polycation such as polylysine. Afterwards, a lipid film hydration process was performed for the electrostatic binding of condensed DNA. Final sonication to package the condensed DNA with lipids resulted in the multifunctional envelop nano device. R_8 peptide was incorporated into MEND to enhance the transfection ability. The resulting R_8-MEND then produced a high transfection activity without cytotoxicity.[149] Its transfection mechanism was found to be dependent on micropinocytosis. Furthermore, the condensation ability of polylysine, stearyl-R_8 and protamine was examined in order to deliver siRNA into cells. Only stearyl-R_8 was able to condense siRNA to form nanoparticles around 100 nm.

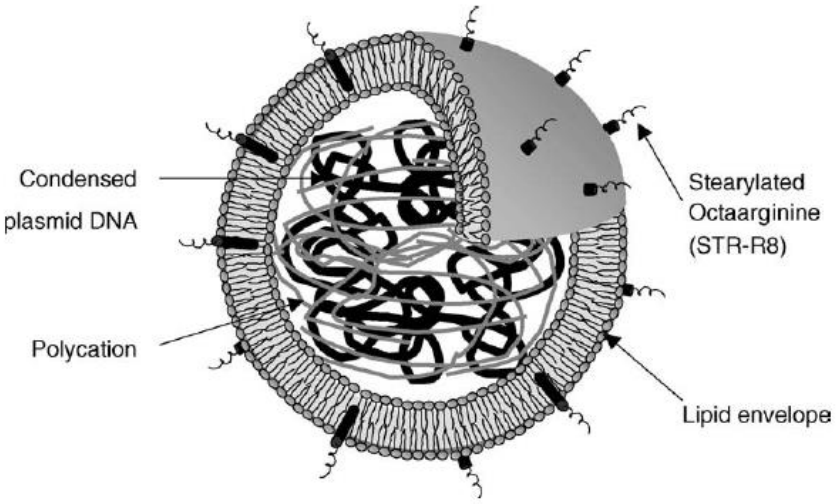

Figure 28. Multifunctional envelope-type nano-device (MEND) modified with stearyl-R8.

Reprinted from Reference 148, Copyright (2016), with permission from Elsevier

Besides arginine octamer, another representative arginine rich cell penetrating peptide, arginine nonamer (R_9), proved to be effective in the delivery of siRNA. *Won Jong Kim* et al. conjugated cholesteryl group on the N-terminus of R_9.[150] Simple complexation of siRNA with Chol-R_9 efficiently delivered siRNA into cells *in vitro*. Local administration of Chol-R_9/siRNA complex in a mouse model led to the regression of tumor. Interestingly, *Priti Kumar* et al. demonstrated a transvascular delivery of small interfering RNA to central nervous system with a hybrid R_9 peptide.[151] R_9 was fused to the C-terminus of RVG, a short peptide derived from rabies virus glycoprotein (RVG) that could specifically bind to the acetylcholine receptor expressed by neuronal cells, to enable siRNA binding. After intravenous injection into mice, the chimeric peptide RVG-R_9 could delivery siRNA across blood brain barrier to neuronal cells. Moreover, repeated injection of RVG-R_9/siRNA complex did not induce any inflammatory responses which implied its potential application in clinical trials.

Other types of peptides

Other types of cell penetrating peptides such as penetratin, KALA peptides and transportan have also been applied in gene delivery experiments. For examples, *B. Allinquant* et al. first demonstrated the application of penetratin peptide, originated from the third helix of the homeodomain of Antennapedia, in the delivery of antisense oligonucleotide designed to block the expression of amyloid precursor protein.[152] Additionally, antisense oligonucleotide aiming

at luciferase reporter gene was also covalently conjugated to penetratin peptide.[153] The antisense-penetratin conjugate entered into cells over a period of hours in a dose-dependent manner. Interestingly, the conjugate displayed similar binding affinity and selectivity compared to those of unmodified oligonucleotides.

David R. Corey et al. conjugated penetratin with a novel type of DNA analogue, peptide nucleic acid (PNA).[154] Peptide nucleic acids are featured with their backbones composed of repeating N-(2-aminoethyl)-glycine units linked by peptide bonds. About 99% of cells were transfected with PNA-penetratin conjugate at a concentration as low as 500 nM, an efficiency rarely observed with other transfection techniques. *Jingsong Ou* et al. reported that penetratin could be applied to increase the transfection efficiency of Lipofectamine 2000 when it was linked with a water soluble amphiphilic helical peptide.[155] However, the new conjugate must be directly associated with liposomes prior to transfection for optimal transfection of endothelial cells. In 2008, *Helene L. Åmand* et al. demonstrated that when all the lysine residues of penetratin were replaced with arginine residues, cellular uptake was increased. The internalization occurred predominantly through micropinocytosis.[156]

Tara B. Wyman et al. designed and prepared a cationic amphipathic peptide KALA (WEAKLAKALAKALAKHLAKALAKALKACEA) which exhibited DNA binding ability.[157] A conformation transformation from random coil to amphipathic α-helical of KALA was identified when the pH was increased from 5.0 to 7.5. Thus, it has a strong propensity for α-helix conformation that positions seven lysine residues on one face to mediate a reversible association with DNA. Once the DNA was compacted, it was able to cross the cell membrane to enter the cytoplasm. This peptide could also induce membrane leakage as evidenced by the fully release of entrapped dyes from neutral liposomes.

Antonio Bernad et al. later prepared another cell penetrating peptide RAWA (RAWARALARALRALARALRALAR) in analogue to KALA peptide.[158] Given the favorable structural and pKa properties of the guanidinium group for DNA interaction, the lysine residues were replaced with arginine. Tryptophan was introduced in the third position due to the finding that a tryptophan residue near N-terminus appeared to enhance gene transfection property. RAWA exhibited an improved DNA condensation effect and weaker membrane destabilization ability compared to KALA. The diminished membrane perturbation

property resulted in a less cytotoxicity which makes it suitable for gene transfection experiment. Transfection efficiency with RAWA was comparable to a number of commercial reagents such as Lipofectamine Plus and Superfect.

2.2.3.4 Inorganic nanoparticles

Inorganic nanoparticles are generally suitable to carry drug molecule into cells due to their tunable sizes, facile modification, and easy preparation.[159] The chemistry of inorganic nanoparticle is well established and thus provides an abundant choice of particles with different properties. Another advantage of inorganic nanoparticles is their inherent physical property. Most inorganic particles have rather rigid and stable framework which is more resistant to environmental stimulus like pH, heat and mechanic stress.[160] The high surface area could also improve the loading amount of drug molecules. More importantly, the unique physical properties of inorganic nanoparticles which cannot be obtained by other kinds of vectors provide several additional benefits. For example, gold nanoparticles can be used in imaging related areas such as computed tomography and surface enhanced Raman spectroscopy.[161] Magnetic nanoparticles such as iron oxide provide further manipulation through magnetic field which could benefit clinical applications.[162]

Inorganic nanoparticles usually cannot work as gene transfection vector by itself due to the lack of condensation ability of genetic materials. Therefore, chemical and/or biological modification is necessary in order to achieve efficient condensation. Cationic moieties are thus decorated onto the surface of inorganic nanoparticles. The modification strategy usually depends on the nature of nanoparticles. Gold nanoparticles generally utilize thiol chemistry to conjugate cationic species onto its surface while charged nanoparticles such as silica nanoparticles prefer co-condensation or grafting.[163,164] Inorganic nanoparticle provides an ideal platform for the hybridization of different kinds of transfection vectors. Cationic polymer, liposome and cell penetrating peptides have all been successfully applied.

Inorganic nanoparticle – Polymer hybrids

Nanoparticles decorated with cationic polymers are well studied in gene transfection experiments and easy to obtain. Such a system has a very good condensing ability towards genetic materials and is usually water soluble. Among them, magnetic nanoparticle has

become the most appealing strategy to achieve efficient and target transfection. Transfection mediated by magnetic nanoparticle was pioneered by *Planck* and coworkers who also coined the term 'magnetofection'.[165] Magnetofection (MNP) is usually rather fast with high efficiency and low cytotoxicity. As shown in Figure 29, superparamagnetic nanoparticles are applied as the core and cationic polymer is decorated to their surfaces. During the transfection process, magnetic nanoparticles can be manipulated by the application of magnetic gradient fields.[166] This unique property offers the possibility for this method to treat local diseases.

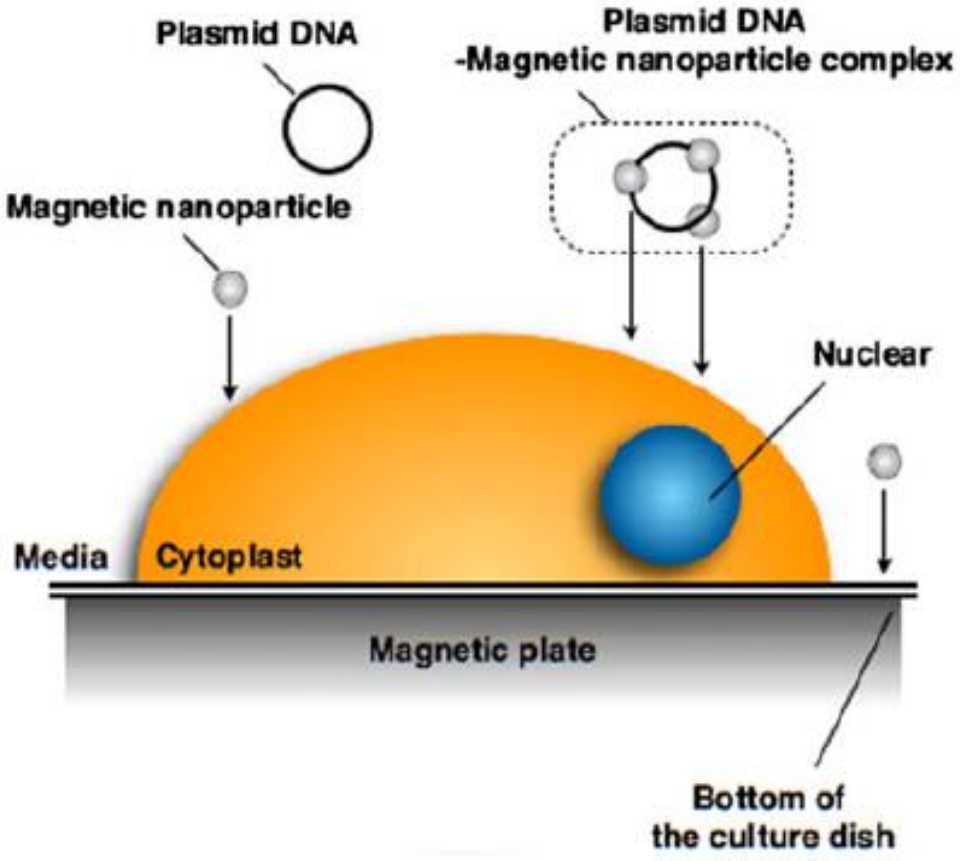

Figure 29. Schematic representation of magnetofection. Plasmid conjugated magnetic nanoparticles moved to the cell surface on the magnetic sheet upon application of magnetic force. Then, the magnetic force drove this complex toward and into the target cells. Journal of Artificial Organs, Efficient transfection method using deacylated polyethylenimine-coated magnetic nanoparticles, 14, 2011, 215, Daisuke Kami, With permission of Springer

Although numbers of surface modification strategies have been developed for magnetic nanoparticle based gene delivery vector, cationic polymer polyethylenimine (PEI) remains to be the most efficient modification reagent and is often used in combination with other

polymers.[167] However, its role in magnetofection still remains to be discovered. *Amal Rose* et al. showed that PEI played a critical role in controlling the sizes and surface charges of MNP vectors as well as DNA binding.[168] The coating with PEI resulted in smaller aggregates with narrower size distribution compared to uncoated ones probably because of the repulsions caused by the electrostatic charges and steric stabilization. Additional PEI might be required for a decent transfection although contrary result has also been reported with iron-oxide silica nanoparticles.[169]

Besides linear PEI modified magnetic nanoparticles, dendrimeric polymer has also been applied. Transfection efficiency depends heavily on the generation of dendrimer and the presence of magnetic field.[170] *Huang Shiwen* et al. prepared a six generation poly-amidoamine dendrimer modified superparamagnetic nanoparticle which can be used to improve the transfection efficiency of PEI.[171] High level gene expression was achieved even with a rather short incubation time and low DNA dose when magnetic field was applied. It is possible that magnetic field quickly gathered the magnetic gene complex to the surface of cell and enhanced the subsequent cellular uptake.

Gold nanoparticle has its own advantage in cellular uptake and biocompatibility. The decoration of gold nanoparticle with PEI has also been demonstrated. Gold nanoparticles provide high surface to volume ratio which could maximize the grafting density of PEI. *Alexander M. Klibanov* et al. conjugated 2 kD PEI to the surface of gold nanoparticle through thiol chemistry. These gold particles showed better transfection efficiency compared to that of 25 kD PEI.[172] Moreover, it was shown that gold nanoparticles conjugated with 2 kD PEI were safe for the cornea and thus can potentially be useful for corneal gene therapy *in vivo*.[173] *Zhuo Renxi* et al. reported that 800 D PEI decorated gold nanoparticles can transfect cells 3-4 folds more efficient than 800 D PEI alone.[174] TEM experiments revealed that gold nanoparticles with higher PEI grafting density on their surfaced led to more compact and smaller complexes with DNA. Notably, the transfection ability of gold/PEI vectors retained even in the presence of serum.

Interestingly, the combination of silica inorganic nanoparticle with PEI can reduce the toxicity of PEI while maintaining its transfection ability. *Huang Shiwen* et al. demonstrated that the cytotoxicity of PEI-silica nanoparticle prepared through one pot synthesis was

significant lower than conventional used PEI.[175] Meanwhile, the efficiency of these nanoparticles was also better than that of PEI in the presence of serum.

Inorganic nanoparticle – Lipid hybrids

Liposomes formed by the assembly of cationic lipids have been shown to be highly efficient in gene transfection, for example the widely used commercially available vector Lipofectamine. Thus, coating of inorganic nanoparticle with lipids has been developed to improve the cellular uptake and endosomal release ability of nanoparticle/gene complexes. Also, the unique physical and chemical properties of inorganic nanoparticles could be used to improve the transfection ability of cationic lipid.

Huang Leaf et al. prepared calcium phosphate nanoparticles coated with traditional cationic lipid 1, 2-dioleoyloxy-3-(trimethylammonio) propane chloride (DOTAP) and helper lipid cholesterol.[176] Calcium phosphate nanoparticle is expected to disassemble after entering the cell due to the low pH in the endosomes which results in endosome swelling and bursting to release the entrapped siRNA. The release ability of this system was confirmed by the increase of intracellular Ca^{2+} concentration through a calcium specific dye. As a result, the application of calcium phosphate improved the silencing effect 3–4 folds *in vitro* compared to previous formulation.

Interestingly, *Erkang Wang* et al. reported a new class of cationic lipid coated gold nanoparticles (DDAB-AuNPs).[177] Although these nanoparticles cannot transfect cells when applied alone, they could enhance the efficiency of other cationic liposomes mediated transfection. It was found that more DNA molecules were bound to cationic lipids upon the addition of DDAB-AuNPs. Flow cytometry results showed that the cellular uptake efficiency of DNA molecules was also increased which might explain the improved transfection.

Another merit of decoration of spherical inorganic nanoparticle with liposomes is to improve the capacity and stability of liposome. Also targeted delivery and controlled release properties could be realized. *C. Jeffery Brinker* et al. reported an elegant porous nanoparticle supported lipid bilayers that synergistically combined the properties of liposomes and nanoparticles as depicted in Figure 30.[178-180] In this system, cationic liposomes were fused to a spherical, high-surface-area, porous silica core to obtain supported lipid bilayer structures. The silica core could suppress large-scale bilayer fluctuations which result in a better stability

than unsupported liposomal bilayers. Additionally, other functional moieties such as targeting peptide, PEG and fusogenic peptide can be added to liposome coating. The combination of these molecules thus could improve the capacity, selectivity and stability of liposomes and also enable targeted delivery and controlled release of cargos. The most interesting property of this system is that it can be loaded simultaneously with combinations of therapeutic agents such as siRNA, toxins and diagnostic agents. They demonstrated that all these cargos were successfully transported into cells through endocytotic pathway. The release of cargo was proposed to depend on the destabilization of lipid bilayer triggered by endosome acidification. The gene transfection ability of this system was shown to be correlated with the sizes of nanoparticles. Transfection efficiency dramatically decreased when the sizes were increased.

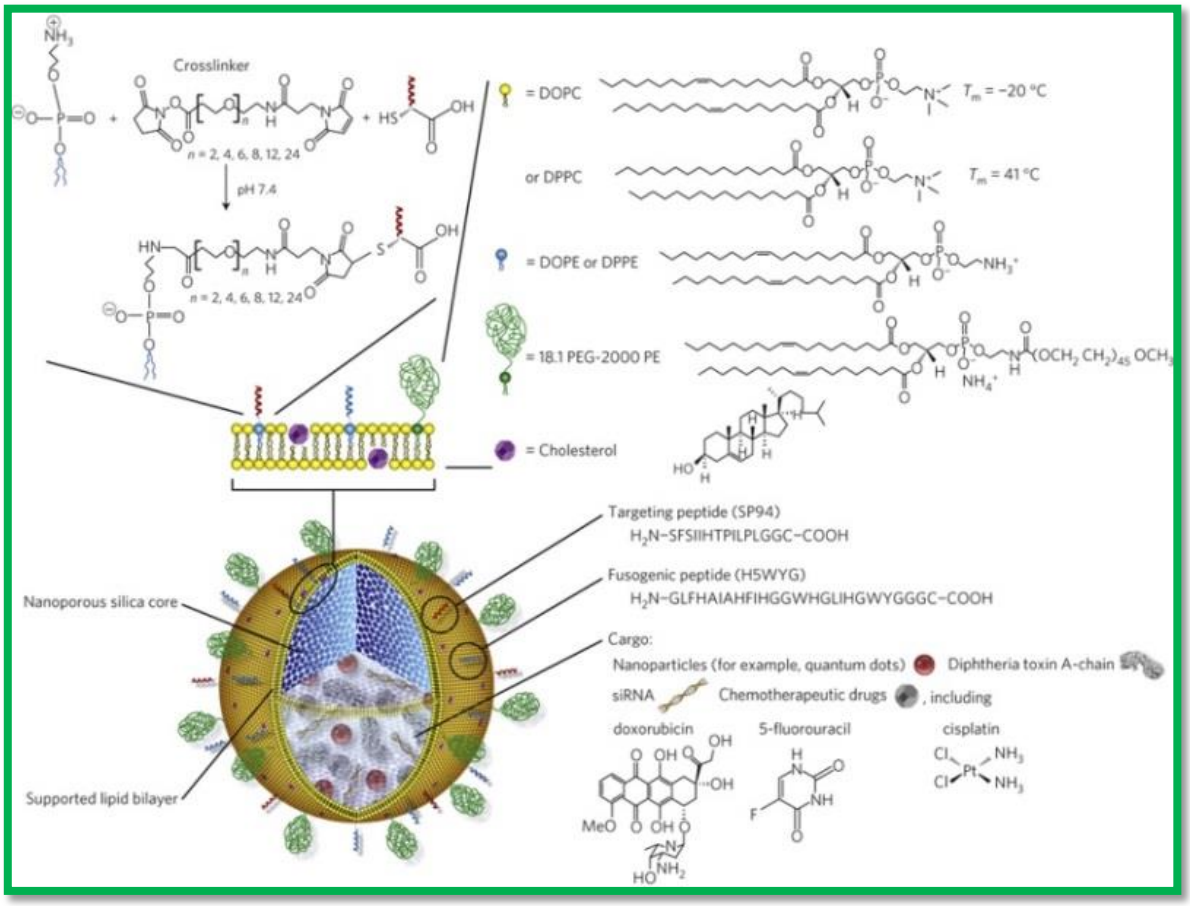

Figure 30. Schematic illustration of the nanoporous particle-supported lipid bilayer, depicting the disparate types of therapeutic and diagnostic agent that can be loaded within the nanoporous silica core, as well as the ligands that can be displayed on the surface. Reprinted by permission from Macmillan Publishers Ltd: [Nature materials] (reference 180), copyright (2011)

Inorganic nanoparticle – Cell penetrating peptide hybrids

The combination of inorganic nanoparticles and cell penetrating peptides to enhance cellular uptake has been extensively studied in the field of cellular labeling and molecular imaging during last decade.[181,182] The pioneering work of *Weissleder* et al. demonstrated that a 100-fold higher efficiency of intracellular magnetic labeling with dextran-coated superparamagnetic iron oxide nanoparticle could be achieved when it was conjugated with HIV-Tat peptide.[183,184] However, applications of such systems in gene delivery are less explored. One possible reason is that large amount of cell penetrating peptide is relatively more difficult to obtain for the decoration of inorganic nanoparticles. Nevertheless, the excellent biocompatibility of cell penetrating peptides makes it an interesting decoration strategy for inorganic nanoparticle based gene delivery vector.

Wang Shu et al. reported the hybridization of magnetic nanoparticles and cell penetrating HIV-Tat peptide can be used for gene transfection experiments (Figure 31).[185] The magnetic ion beads were first coated with PEI to condense plasmid DNA. A cysteine residue containing Tat peptide was added subsequently. The resulting complexes exhibited a 4-fold improvement in gene transfection compared to its counterpart without Tat peptide *in vitro*. The enhancement of transfection could still be observed *in vivo*. Additionally, the injected DNA complexes could respond to a moving magnetic field. Shifting away the magnetic field from the injection site resulted in transgene expression in a remote region.

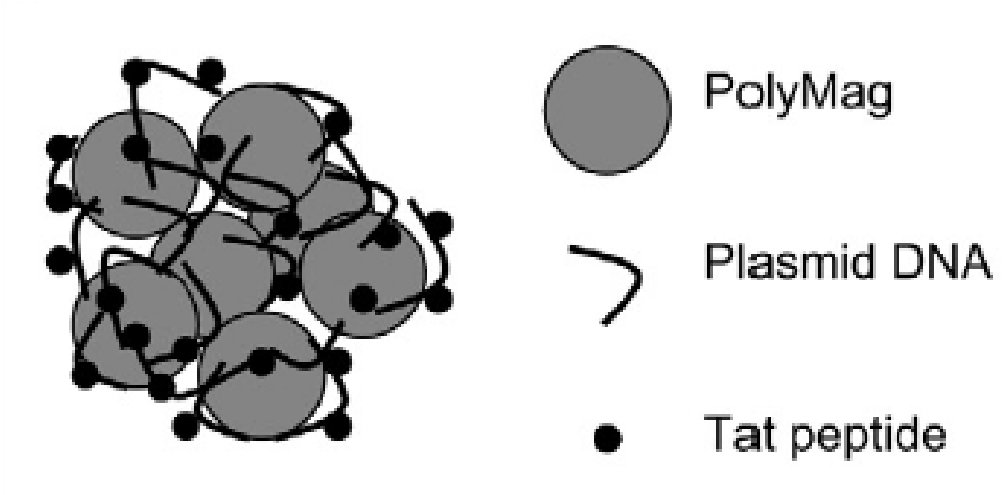

Figure 31. Schematic illustration of the structure of PolyMag/DNA/Tat complex. "Reprinted from reference 185, copyright (2016), with permission from Elsevier

The combination of calcium phosphate nanoparticle and arginine rich cell penetrating

peptide for gene delivery has also been reported by *Cory Berkland* et al.[186] Condensation of nascent CPP/DNA complex with $CaCl_2$ provided rather small and stable nanoparticles which led to a higher gene expression than PEI. It also showed negligible cytotoxicity *in vitro* and can still function in the presence of serum.

To summarize, gene therapy is now considered to be an extremely promising technique for the treatment of a variety of diseases. However, the lack of suitable gene delivery vectors for clinical trials limit its potentials. Despite the numerous non-viral vectors developed during the last 30 years, optimal vectors with efficient gene delivery ability comparable to viral vectors and excellent compatibility both *in vitro* and *in vivo* still remain to be realized. Development of such gene delivery vectors is in high demand.

2.3 Peptide assembly

Two approaches have been developed to fabricate nanomaterials: top-down and bottom-up approaches.[23,187] Top-down approach is essentially the breaking down of macro-materials to create nanoscale devices by techniques such as machining and etching. It is most useful in micro-patterning techniques such as photolithography and inkjet printing. For example, this approach is often applied in semiconductor industry to fabricate an integrated circuit on a silicon wafer.[188] Bottom-up approach, in contrast, relies on the chemical property of individual atoms or molecules to self-organize and self-assemble to construct macroscopic structures.[189] In particularly, materials generated from self-assembling strategy possess unique properties such as fast response towards external stimuli and structural unity in nanoscale. Self-assembled materials have been applied in the design of chemical sensors, regenerative medicines and tissue engineering etc.[20]

The building blocks for assembling process are rationally designed and allowed to interact with each other through non-covalent forces such as π-π stacking, hydrogen bonding and hydrophobic interactions. Supramolecular chemistry has developed several strategies to achieve efficient and controlled self-assembling.[190] Among them, peptide based materials are particular interesting due to their biocompatibility, easy preparation and versatility of functionalization. Several peptide self-assembling systems have been developed. Depending on the structure of basic building block, they can be classified as amphiphilic peptides, cyclic peptides, amyloid and collagen peptides etc.

2.3.1 Amphiphilic peptide assembly

Self-assembling of amphiphilic molecules is the one of the most widely used strategy in constructing supramolecular nanomaterials. Amphiphilic molecules usually contain a hydrophobic domain and a hydrophilic head group. They can self-assemble into a variety of nanostructures (Figure 32) depending on their chemical structures, solvents, concentration and temperature etc.[191-193] A well-established model theory has been developed by *Israelachvili* et al. to predict the aggregation morphology from the chemical structures of individual amphiphile. [194]

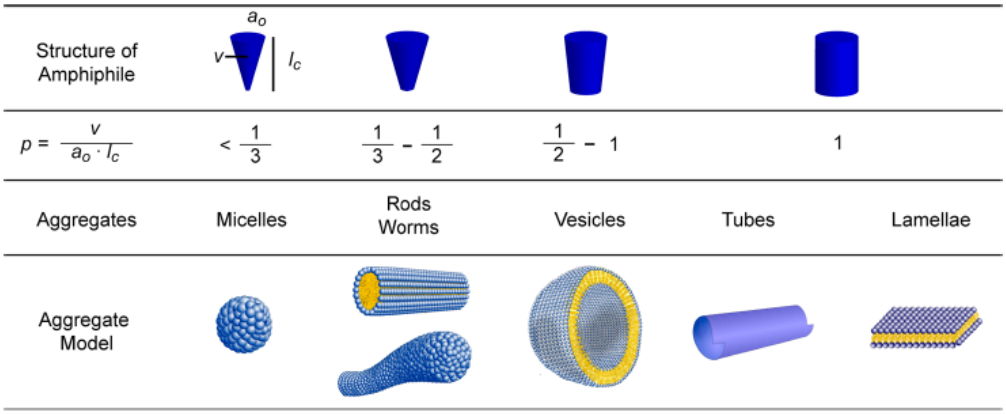

Figure 32. Schematic representation of amphiphilic molecules and assembly. Reprinted with permission from Reference 193. Copyright (2016) American Chemical Society."

In the assembly of amphiphilic peptides, the hydrophobic domain provides the main driving force through hydrophobic interactions. The head groups, built from short peptides, could interact with each other through hydrogen bonds. Three types of hydrophobic domains have been developed: aliphatic tails, aromatic rings and hydrophobic amino acid residues.

2.3.1.1 Aliphatic tails

The research on amphiphilic peptide assembly was pioneered by *Samuel Stupp* et al.[20] In 2001, they reported the self-assembly and mineralization of a peptide amphiphile nanofiber.[195] The research was inspired by the structure of bone tissue which essentially constructed through the organization of collagen fibers and hydroxyapatite (HA) crystals. Thus, an alkyl tail with 16 carbon atom was attached in the N-terminus of an ionic peptide (Figure 33A, 1). This peptide could assemble into cylindrical micelles in water due to the overall conical shape. The alkyl tail then packed in the center of micelle which consequently exposed the hydrophilic peptide segment on the surface.

In the peptide segment, four cysteine amino acid residues were incorporated to covalently link the assembled nanofibers through oxidation of thiol groups (Figure 33A, 2). Phosphorylate group, being highly efficient in the formation of calcium phosphate minerals, was introduced to nucleate the formation of HA in proper environment (Figure 33A, 4). Additional RGD peptide sequence was coupled to the N-terminus to facilitate the adhesion of cells (Figure 33A, 5). They found out that inorganic material was concentrated on the surface

of nanofibers 10 minutes after the treatment with $CaCl_2$. Shortly after, plate-shaped polycrystalline mineral was visible throughout the surface of the fibers. The *c* axes of the HA crystals were co-aligned with long axes of the fibers which may be of interest to the design of materials.

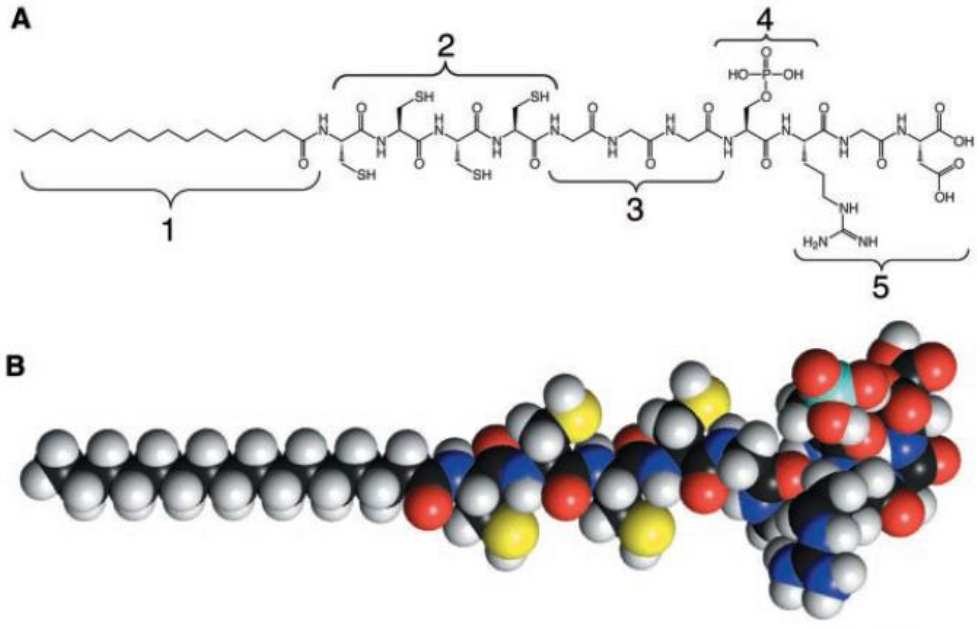

Figure 33. (A) Region 1 is a long alkyl tail, region 2 is composed of four consecutive cysteine residues for cross-linking, region 3 is a flexible linker region, region 4 is a single phosphorylated serine residue to interact with calcium ions, region 5 displays the cell adhesion ligand RGD. (B) Molecular model of the peptide amphiphile. From reference 195. Reprinted with permission from AAAS

In 2005, they applied the same strategy to realize the recognition between peptide fibers and avidin receptor protein.[196] Biotin molecules were introduced onto a branched peptide amphiphile which assembled into fibers in water. The binding of chromophore-conjugated avidin protein to biotinylated nanofibers was confirmed by measurement of fluorescence signals.

Later, *Stupp* et al. investigated the influences of amino acid sequences and the length of alkyl tails in the formation of nanofibers.[197] Twelve derivatives of peptide amphiphiles were studied. Nanofibers varying in morphology, surface chemistry, and potential bioactivity were thus obtained. Two methods of self-assembling, drying on surfaces and addition of divalent ions such as calcium, were established. However, the formation of these peptide fibers required a relatively low pH (~4). They then explored that efficient self-assembly could be

achieved at physiological pH when two oppositely charged peptide amphiphiles bearing different biological signals were mixed in aqueous solution.[198]

Jeffrey D. Hartgerink et al. studied the self-assembling process of peptide amphiphiles by systematic modification of the hydrogen bonding and amphiphilic packing ability.[199] A series of 26 PA derivatives, including 19 N-methylated variants and 7 alanine mutants were obtained by solid phase synthesis. A combination of the results obtained from circular dichroism spectroscopy, Fourier transform infrared spectroscopy, rheology and vitreous ice cryo-transmission electron microscopy provided a detailed insight in the mechanism of self-assembling of peptide amphiphiles. It was found that the four amino acids closest to the core of nanofiber were crucial in the formation of peptide fibers. These residues were hydrogen-bonded with each other which resulted in a β-sheet conformation oriented primarily down the *Z*-axis of the nanofiber in the hydrophilic peptide region. Disruption of these hydrogen bonds led the peptide amphiphiles to assemble into spherical micelles instead of elongated, cylindrical fibers. Amino acids further away from the core of the nanofiber played however a less important role in the stabilization of nanofiber, thus may accommodate a variety of functionalities.

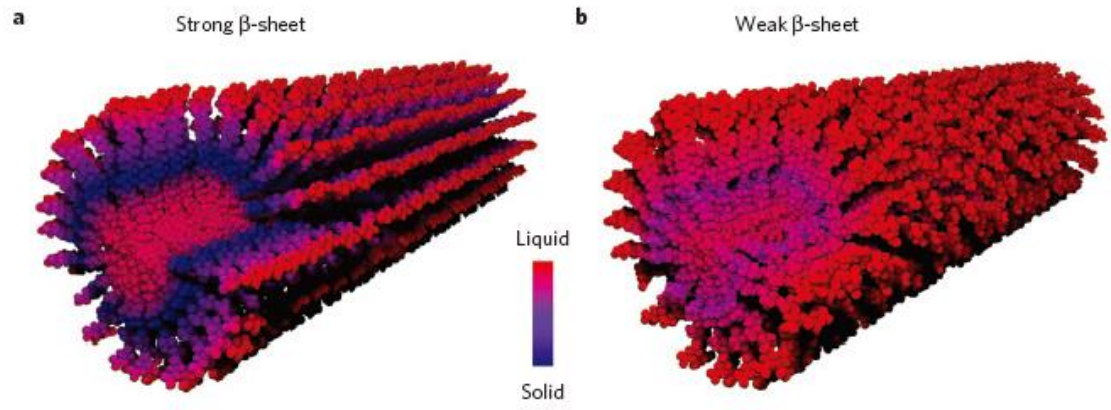

Figure 34. Schematic molecular-graphics representation of peptide amphiphile nanofibers. The vertical bar indicates the gradient of solid-like to liquid-like dynamics (blue and red, respectively) through the nanofibers' cross-sections. Reprinted by permission from Macmillan Publishers Ltd: [Nature materials] (reference 200), copyright (2014)

Moreover, using site-directed spin labelling and electron paramagnetic resonance spectroscopy, *Stupp* et al. examined the conformational dynamics of self-assembled nanofiber

in water through its 6.7 nm cross-section.[200] It was found that the innermost residues and adjacent sites of peptide amphiphile fiber had a rather low dynamic behavior which suggested a solid-like shell surrounding the viscous core (Figure 34). This result experimentally confirmed the simulations from molecular dynamics.

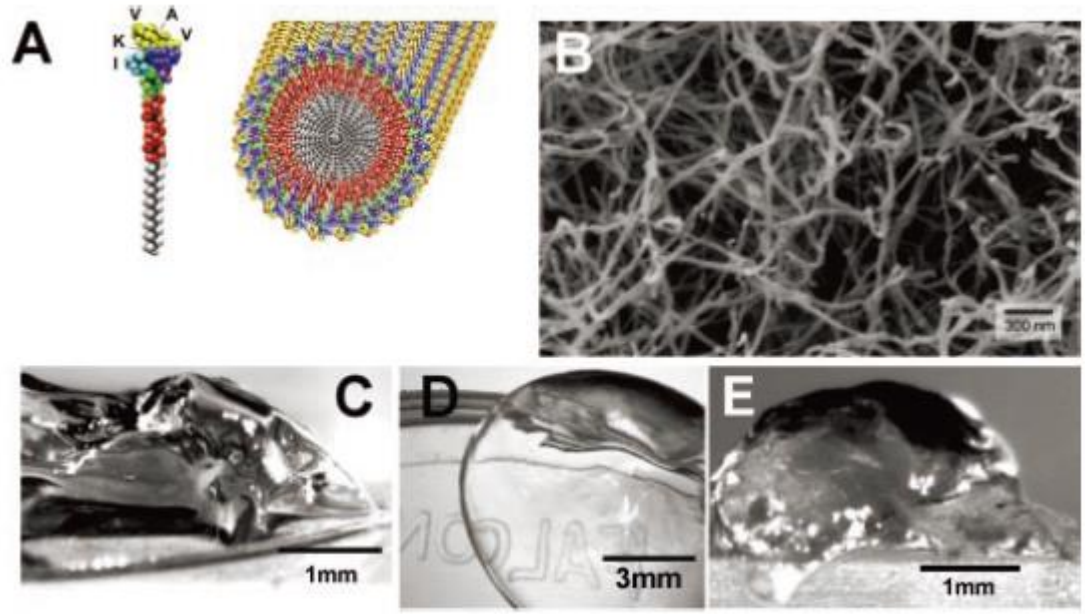

Figure 35. (A) Molecular graphics illustration of an IKVAV-containing peptide amphiphile. B) Scanning electron micrograph of an IKVAV nanofiber. (C and D) Micrographs of the gel formed by adding to IKVAV peptide amphiphile solutions (C) cell culture media and (D) cerebral spinal fluid. (E Micrograph of an IKVAV nanofiber gel surgically extracted from an enucleated rat eye. From reference 201. Reprinted with permission from AAAS

Stupp et al. then extended the application of peptide amphiphile to the selective differentiation of neural progenitor cells.[201] A pentapeptide epitope isolucinelysine-valine-alanine-valine (IKVAV), known to promote neurite sprouting and to direct neurite growth, was incorporated into the peptide amphiphile (Figure 35A). Another feature of this amphiphile was the utilization of glutamic acid residue to provide a net negative charge at pH 7.4 so that the cationic species in cell culture mediums can screen electrostatic interactions and trigger self-assembly when cell suspensions were added. These nanofibers were shown to form 3D networks and produced a gel-like solid with cell culture media (Figure 35C, D, E). Moreover, these artificial peptide based nanofiber scaffold induced very rapid differentiation of cells into neurons, while the development of astrocytes was suppressed. They also

demonstrated that replacement of IKVAV epitope with RGD peptide sequences in such peptide amphiphiles could successfully entrap osteoblast precursor cell lines.[202] In the presence of polyvalent metal ions, the assembling process was triggered by adding PA solutions to cell culture media or other physiological fluids. The cells entrapped in the nanofibrillar matrix could survive in culture for at least three weeks. Afterwards, the peptide fibers were internalized by the cells and possibly were utilized in the metabolic pathways.

In addition of bioactive peptide sequences, other types of functional moieties could be incorporated into peptide amphiphiles.[203-205] For example, pyrene moiety could be conjugated to the aliphatic tail. The self-assembly process thus can be studied with fluorescence measurement in solution owing to the excimer formation property of pyrene.[206] It was demonstrated that pyrene excimer can only be observed when the peptide amphiphile assembled into cylindrical fibers, not spherical aggregates. Covalently linking a derivative of 1,4,7,10-tetraazacyclododecane- 1,4,7,10 tetraacetic acid (DOTA) to peptide amphiphile resulted in magnetic resonance (MR) active molecules that could enhance relaxation time.[207]

Even large moieties such as inorganic nanoparticles and carbon nanotubes can be applied to decorate the fibers formed by these peptide amphiphiles. In 2005, *Stupp* et al. showed that one dimensional inorganic assembly could be templated with peptide fibers.[208] The peptide amphiphile used to form fibers was modified with thymine in the hydrophobic aliphatic tail. Gold nanoparticles were decorated with lipophilic diaminopyridine. Due to the high binding efficiency between thymine and diaminopyridine in aprotic environments, gold nanoparticles were linearly aligned on the surface of peptide fibers which could be observed with transmission electron microscope. The length of the array of gold nanoparticles extended for several microns.

The nanofibers formed by peptide amphiphiles also possess excellent ability to form hydrogel which could be applied for injectable therapies in regenerative medicine. A series of peptide amphiphiles with different peptide sequences were thus synthesized to study their gelation kinetics.[209] *Stupp* et al. found out that gelation time increases with the bulkiness and number of polar groups in the PA molecule. Circular dichroism (CD) spectroscopy measurements suggested the pre-existence of hydrogen-bonded aggregates in the solution state even before the trigging of self-assembly process. It was proposed that these aggregates

acted as nuclei to accelerate the gelation kinetics following typical nucleation-based mechanism for self-assembly. They further observed that large birefringent domains occurred in gels formed from heated solutions, whereas those formed from unheated solutions appeared completely isotropic with no birefringence.[210] The former solution could be dragged on a surface covered by a thin layer of this medium (Figure 36).

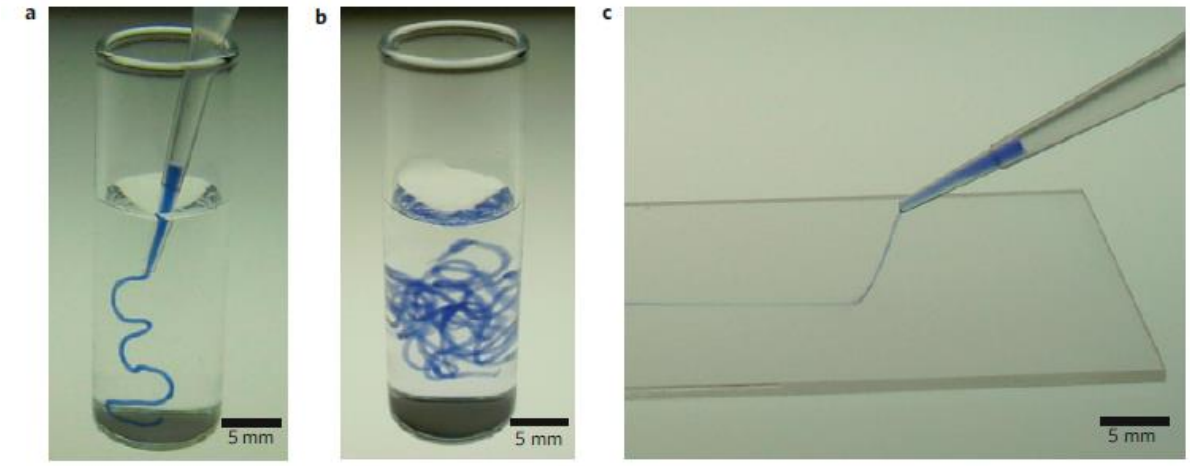

Figure 36. Schematic representation of amphiphilic peptide and nanofiber. (a, b) A peptide amphiphile solution coloured with trypan blue injected into phosphate-buffered saline after heat treatment. (c) The same solution dragged through a thin layer of aqueous $CaCl_2$ to form a noodle-like string. Reprinted by permission from Macmillan Publishers Ltd: [Nature materials] (reference 210), copyright (2010)

2.3.1.2 Aromatic peptide amphiphiles

The low cost for the preparation of dipeptide and amino acids relative to longer peptides and proteins makes them attractive in the design of self-assembling system. These low molecular weight molecules can function as hydrogelators which can fundamentally achieve all the hydrogel features associated with longer peptides as described above.[211]

One of the earliest amino acids based hydrogels was reported in 1921 (Figure 37).[212] However, it was not until 1995 that this hydrogel network had been examined with modern instrumental techniques.[213,214] It was then confirmed that the hydrogel consisted of fibrils around 50 nm in diameter that entangled in solution. X-ray crystal structure revealed that the gel fiber was held together by a favorable backbone orientation enhanced by hydrogen-bonding and π- π stacking interactions.

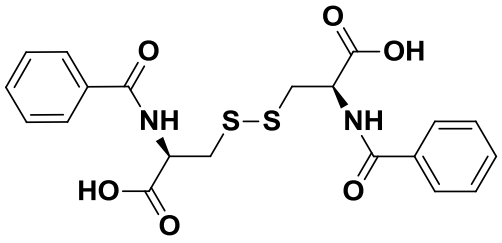

37

Figure 37. Chemical structure of aromatic peptide gelator **37**

In 2003, *Ehud Gazit* et al. reported that H-Phe-Phe-OH dipeptide, derived from Alzheimer's β-amyloid diphenylalanine structural motif, self-assembled into discrete and stiff nanotubes in water.[215] Reduction of ionic silver within the nanotubes, followed by enzymatic removal of the outer shell of peptide nanotubes, resulted in the production of discrete nanowires. This peptide is however unable to form a hydrogel. Fmoc-Phe-Phe-OH, the precursor of diphenylalanine peptide, was thus tested for its self-assembling property (Fmoc: 9-fluorenylmethoxycarbonyl).[216,217] Besides the expected hydrophobic interactions between Fmoc groups, the introduction of aromatic functionality in the N-terminus provided additional stacking interactions. Dissolving of this peptide at higher concentration thus resulted in the formation of a hydrogel which consisted of a fibrous network with fibril diameters ranging from 10 to 100 nm. Compared to the original tubular structure assembled from diphenylalanine peptide, the fibers formed with Fmoc protected diphenylalanine peptide were much more flexible with branching characteristics. Further experiments showed that the hydrogel can be used to encapsulate fluorescein, a small organic molecule. A slow release of fluorescein was observed when the gel containing the fluorescent molecule was covered with water.

Rein V. Ulijn et al. characterized the assembly behavior of Fmoc-FF peptide in detail.[218] Circular dichroism experiments showed a negative peak at 218 nm which was in consistent with β-sheet structure for molecular assembly. Fourier transform infrared spectroscopy (FT-IR) spectrum of Fmoc-FF gel had two peaks, at 1630 and 1685 cm^{-1}, which further confirmed the β-sheet structure and possibly implied an anti-parallel arrangement of the peptides. In addition, fluorescence spectroscopy revealed an excitation maximum absorption at 350 nm, significantly red shifted when compared to the absorption of Fmoc alone, clearly indicating a large degree of π- π stacking interactions between the fluorenyl groups.

Combining the information described above, if Fmoc-FF were stacked in an antiparallel β-sheet arrangement, the fluorenyl group would be too far from each other for π- π stacking interactions (Figure 38A). However, the fluorenyl groups could interlock with one another when the second stack of Fmoc-FF was placed alongside the first sheet but staggered by one peptide (Figure 38B).

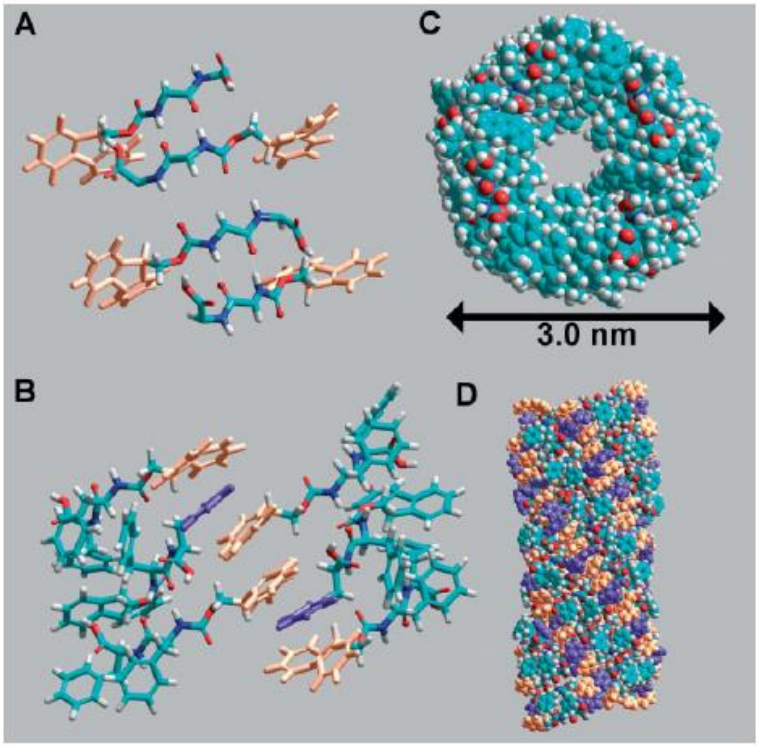

Figure 38. Model structure created for Fmoc-FF peptide. (A) Fmoc-FF peptides arranged in an anti-parallel β-sheet pattern. (B) Interlocking of Fmoc groups from alternate β-sheets to create π-stacked pairs with interleaved phenyl rings. Top view (C) and side view (D) of the structure created in (B). Reference 218, copyright (2016) Wiley. Used with permission from John Wiley and Sons.

Another important feature of Fmoc-FF peptide is that it can self-assemble at physiological pH. This feature is actually intriguing since the free carboxylic acid group in the C-terminus would be negatively charged under this condition (pKa of -COOH: 3.5). Charge repulsions should then prevent the fiber formation. However, it was found that the self-assembling process of Fmoc-FF resulted in two apparent pKa shifts of ~6.4 and ~2.2 pH units above the theoretical pKa (3.5).[219] Therefore, self-assembly of Fmoc-FF resulted in a suppressed ionization which led to dramatic pKa shifts related to significant structural transitions.

Introduction of phosphorylated amino acids in the design of Fmoc based short peptide

endowed a unique property to the self-assembling system.[220,221] In 2004, *Zhimou Yang* et al. reported a rather simple approach to develop assays based on the hydrogelation ability of short peptides for the detection of enzyme inhibitors.[222] In this system, the precursor which acted as the substrate of an enzyme could transform into a hydrogelator. When the inhibitor inhibited the function of an enzyme, such conversion were thus blocked which resulted in a macroscopic sol – gel transition (which can be observed visually).

They later demonstrated that following this strategy, even a hydrophobic molecule can unprecedentedly form supramolecular hydrogel (Figure 39).[223] A phosphatase was applied to convert hydrophilic precursor **38** to hydrophobic **39**. Interestingly, molecule **38** was not able to form hydrogel when it was tested alone due to its poor solubility. However, when **39** was conversed from **38**, an opaque hydrogels were formed. They suggested that the nanofibers were mainly formed by **39** and doped with hydrophilic **38** which provided the stability of nanofibers in aqueous solutions. *Rein V. Ulijn* et al. also observed similar transition from a micellar solution into a fibrous hydrogel upon enzymatic de-phosphorylation.[224]

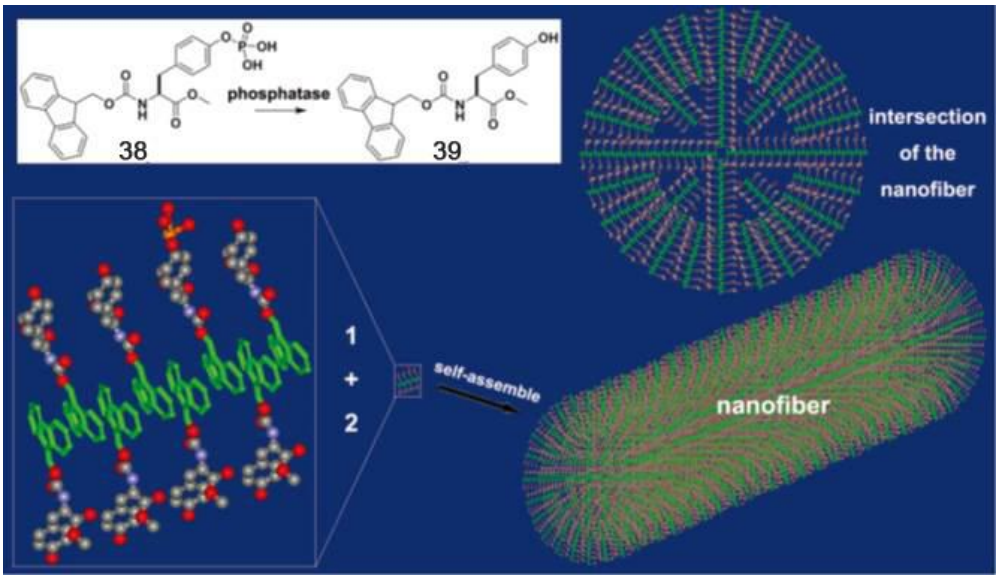

Figure 39. Schematic illustration of enzymatic conversion of **38** and **39** in nanofibers. Reprinted with permission from Reference 223. Copyright (2016) American Chemical Society.

Bing Xu et al. demonstrated that this process can be reversed.[225] A kinase/phosphatase switch was used to control the phosphorylation and de-phosphorylation process of the short aromatic peptide amphiphile containing tyrosine residue. The kinase and phosphatase can thus function as external regulations for the formation of hydrogel. In the presence of adenosine

triphosphates (ATP), adding kinase to the short peptide phosphorylated the tyrosine and thus altered the amphiphilic nature of peptide. This eventually resulted in the disruption of self-assembly and induced a gel-sol phase transition. On the other hand, treating the resulting solution with a phosphatase dephosphorylated the tyrosine residue, thus restored the self-assembly of short peptide to form the hydrogel.

Replacement of the Fmoc group with other aromatic molecules such as naphthalene in peptide amphiphile still preserved their self-assembly behavior. In 2007, *Bing Xu* et al. prepared a series of molecular hydrogelators based on the conjugates of dipeptide and (naphthalen-2-yloxy) acetic acid.[226] The chirality of the dipeptide dictated the handedness of resulting nanofiber: fibers formed with D-amino acid were left-handed and those obtained from L-amino acids were right-handed. They further demonstrated that introduction of D-glucosamine, a naturally occurring aminosaccharide, could allow these peptide based hydrogelator to be applied to wound healing.[227] The mice treated with these hydrogels exhibited a much faster wound healing process and smaller scars compared to those of control group.

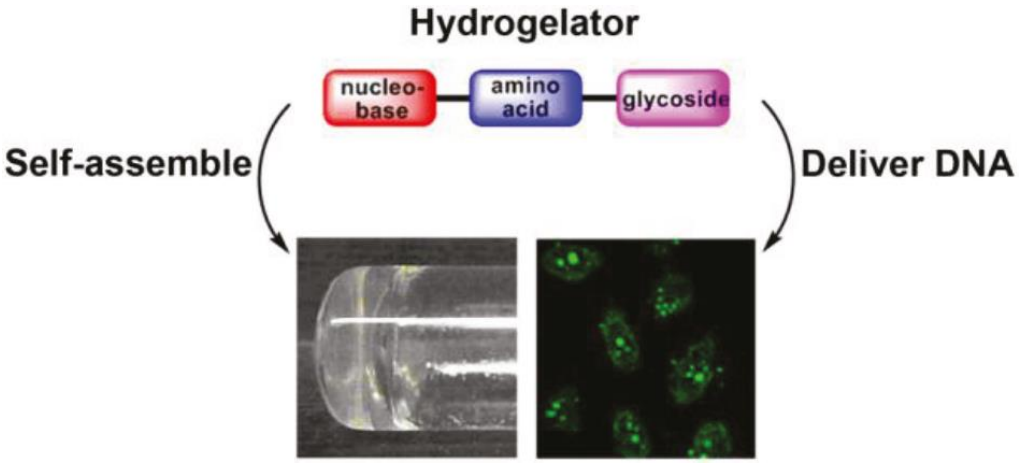

Figure 40. Multifunctional short peptide based hydrogelator. Reprinted with permission from Reference 228. Copyright (2016) American Chemical Society.

Later, *Bing Xu* et al. reported a novel class of multifunctional supramolecular hydrogelators based on a short peptide (Figure 40).[228] The hydrogelators consisting of nucleobase, amino acid, and glycoside not only exhibited excellent biocompatibility but also facilitated the transfer of nucleic acids into cytosol and nuclei of cells. This result highlighted the possibility of utilizing basic building blocks (i.e. nucleobase, amino acid, and glycoside) of the three

major bio-macromolecules (i.e. nucleic acid, proteins, and glycans) to build complex nanostructures. Compared to glycosyl-nucleoside-lipid based hydrogelators, the inclusion of a peptide imparts more diverse functions than a lipid does.

2.3.1.3 Hydrophobic amino acid residues

Peptide amphiphiles could also be constructed with hydrophobic amino acid residues instead of aliphatic tails and aromatic rings. In 2002, *Shuguang Zhang* et al. designed several surfactant-like short peptides that exhibited self-assembling properties as shown in Figure 41.[229] Each peptide contained seven to eight amino acids residues with a length around 2 nm. Charged residues such as aspartic acid and lysine were applied as hydrophilic head group. Non polar alanine, valine and leucine residues were incorporated as hydrophobic domain. Thus, these peptides were amphiphilic in nature when dissolved in water. These peptides were able to form nanotubes and vesicles with an average diameter of 30-50 nm with a helical twist. Dynamic laser scattering measurements revealed a rather narrow size distribution of these peptides which implied the good regularity of the assembled structures. Visualization of these structures with transmission electron microscopy from quick-freeze/deep-etch sample preparation showed a network of open-ended nanotubes and vesicles.

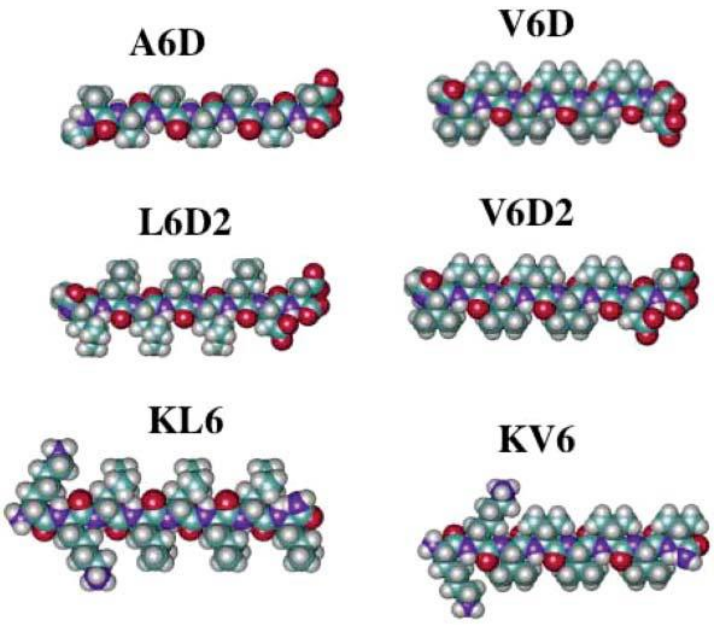

Figure 41. Chemical structure of surfactant-like short peptides. Reference 229, reproduced by permission of The Royal Society of Chemistry.

The authors then proposed a mechanism for the self-assembling process. First, two peptide

monomers pack in dimeric tail-to-tail fashion to form a bilayer creating a unilamellar shell. Owing to the intrinsically twisted nature of individual peptide monomer, these bilayer structures would have a curvature. As consequence, each peptide may interact with one another to form closed rings which in turn stack on top of one another to form tubular structure. Subsequently stacking of the tubular arrays through noncovalent interactions ultimately led to longer nanotubes.

Inspired by the shape of natural lipid, *Shuguang Zhang* et al. also designed a cone-shaped amphiphilic lipid-like peptide Ac-GAVILRRNH$_2$ with the larger part made of arginine and smaller part made of glycine (Figure 42, left).[230] Atomic force microscopy experiments found that this peptide assembled into donut-shape structures. It is plausible that at low concentration, peptide Ac-GAVILRRNH$_2$ was randomly oriented and distributed in solution (Figure 42A, right). When the concentration increased above critical micelle concentration, spherical micelles were formed similarly to common surfactants (Figure 42B, right). At even higher concentration, fusion or elongation of these spherical micelle occurred which led to the formation of short nano-pipes (Figure 42C, right). These short nano-pipes tended to bend gradually to form donut like structures to reduce the surface free energy as a result of the geometry restriction of cone-shaped peptide monomer (Figure 42D, right).

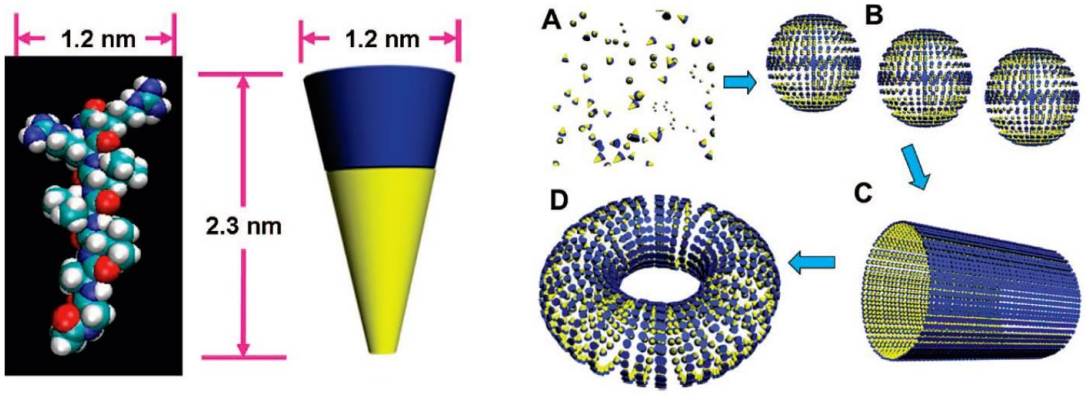

Figure 42. Modelled structure of peptide Ac-GAVILRRNH2 and its assembling mechanism. Reprinted with permission from Reference 230. Copyright (2016) American Chemical Society.

These short amphiphilic peptides are excellent candidates to model bilayer membrane structures. It is known that membrane proteins are crucial in almost every aspect of cellular activities. However, their structures and functions are poorly studied due to the lack of suitable surfactants. In 2006, *Shuguang Zhang* et al. demonstrated that peptide surfactants

were capable of stabilizing a well characterized membrane protein bovine rhodopsin.[231] In the presence of lipids and common surfactants, these short peptides not only enhanced the stability of bovine rhodopsin, but also significantly stabilized rhodopsin even under thermal denaturation conditions. In 2011, they further showed that these short peptides can be used to address another critical issue related to membrane proteins.[232] Using peptide surfactants in commercial *Escherichia coli* cell-free systems, milligram quantities of G protein coupled receptors (GPCRs) could be obtained. These receptors were nicely soluble and had α-helical secondary structures, suggesting that they were properly folded.

2.3.2 Cyclic peptide assembly

Nanotubes (NTs) structures are particular interesting in the development of nanomedicines, sensors and nanotechnology engineering etc. Since the first synthesis of carbon nanotube in the early 1990's, interests in fabrications of other types of nanotubes have grown rapidly.[233] For example, a variety of inorganic nanotubes such as tungsten (IV) sulfide and titanium dioxide have been prepared and exhibited unique mechanical, optical and electrical properties.[234-237] However, the drawbacks of these materials including poor solubility, toxicity and lack of uniformity limited their applications. Therefore, supramolecular organic nanotube constructed with the assembly of cyclic peptides emerges as alternative and promising nanomaterials with tubular structures. Additionally, the well-established peptide chemistry provides excellent toolbox for the preparation and versatile functionalization of such materials.

2.3.2.1 Design of cyclic peptide nanotube

The utilization of cyclic peptides to prepare nanotubes was first realized by *M. Reza Ghadiri* et al. in 1993.[238] In their pioneering paper entitled "Self-assembling Organic Nanotube Based on Cyclic Peptide Architecture", a cyclic peptide constructed from eight amino acid residues (Figure 43) was rationally designed. An even number of alternating D and L amino acids were used in order to adopt a low energy ring shaped flat conformation in which all the amide functionalities were positioned approximately perpendicular to the plane of the ring. Of the eight amide groups, four carbonyl groups were placed above the ring whereas the adjacent –NH groups pointed downwards. The main driving force for the

self-assembling process was thus the hydrogen-bonding interactions between each cyclic peptide backbone to produce a continuous β-sheet structure. Moreover, because of the alternating D and L amino acids composition, the side chains of peptides must lie on the outside of entire assembly which resulted in the tubular structure.

As expected, they observed in TEM that this cyclic peptide assembled into bundle-like structures when a suitable pH was applied. Cryo-TEM revealed that each bundle consisted of hundreds of tightly packed nanotubes with a spacing of 14.9 Å as expected for the center to center distance of the peptide rings. Electron diffraction patterns of this cyclic peptide sample showed a 4.73 Å axial periodicity. This distance was ideal for an antiparallel β-sheet structure which suggested that each nanotube was made up of several stacked rings. Modelling results confirmed the assembling mechanism since the only way to pack two peptides to within 4.7 Å was to let the peptide backbones hydrogen bonding with each other.

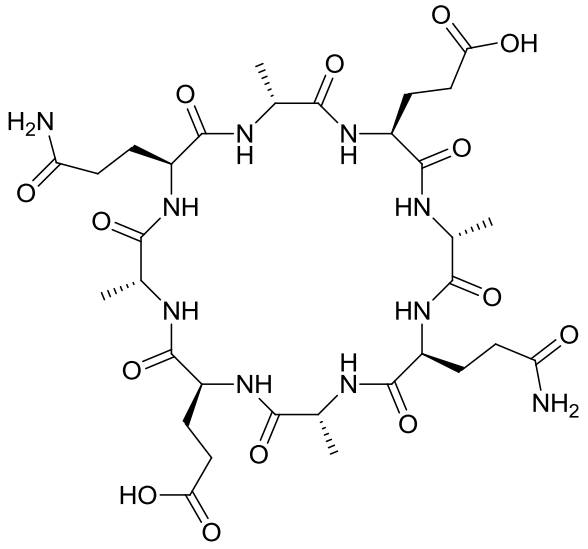

Figure 43. Chemical structure of a cyclic peptide

The length of this type of nanotube assembled from cyclic peptides is however very difficult to control owing to their inherent assembling mechanism which was determined through the study of assembling thermodynamics with N-alkylated cyclic peptide analogues.[239-242] Alkylation resulted in the hydrogen bonding interactions occurred only at one face of the ring, which leads to dimer formation instead of nanotubes. The equilibrium constant for the dimer was determined to be in the vicinity of 3000 M^{-1}, far lower than would be expected for supramolecular nanotubes.[243-245] Considering the remarkable stability of non-alkylated cyclic peptide nanotubes, this suggested a cooperative growing mode for their

formation. Additionally, *Jeffrey D. Hartgerink* et al. reported that the stability of peptide nanotubes can be attributed to the highly cooperative nature of the noncovalent interactions.[246] Enthalpically driven hydrogen bonding interactions between each stacked rings were reinforced with entropically driven hydrophobic interactions in aqueous solutions.

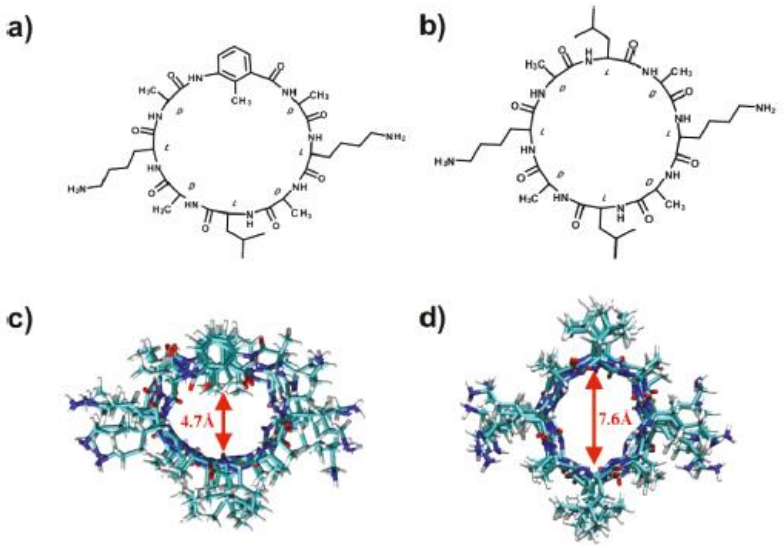

Figure 44. Chemical structures of (a) Mba-8CP and (b) its conventional analogue 8CP. Snapshots of equilibrium structures calculated from molecular dynamics simulations, showing cross-sectional (c,d) views of Mba-8CP and 8CP nanotubes respectively. Reprinted with permission from Reference 251. Copyright (2016) American Chemical Society.

The internal diameter of cyclic peptide nanotubes is relatively easy to optimize. Simple adjustment of the number of amino acid residues in the ring would effectively change the diameter of final assembled nanotubes. For example, *Ghadiri* et al. reported the internal diameter of cyclic peptide nanotubes constructed with eight residues was around 7-8 Å.[238] Since then, a number of nanotubes varying in their diameters assembled from different cyclic peptides have been realized. Cyclic peptides with four, six and ten amino acid residues are all capable of forming nanotubes with diameters ranging from 2 Å to 13 Å.[247-250] Interestingly, *Rami Hourani* et al. recently reported a different route to generate cyclic peptide nanotubes with tunable interiors.[251] An unnatural amino acid 3-amino-2-methylbenzoic acid (Mba) was incorporated into the D, L-alternating primary sequence of a cyclic peptide (Figure 44a). Molecular dynamic (MD) simulations suggested that the methyl group pointed into the interior of the pore as designed. This placement of the hydrophobic methyl group significantly reduced the internal diameter to an estimated 4.7 Å. As comparison, the pore size of the

original cyclic peptide was around 7.6 Å. The incorporation of non-natural amino acid Mba did not altered the self-assembling ability of cyclic peptide as tubular structures were readily observed in acetonitrile. The hydrogen bonding interaction between each stacked ring was confirmed with FT-IR measurements. Moreover, 2D NOESY spectra of Mba-8CP dissolved in d^6-DMSO revealed the through space correlation between the methyl group's proton with the protons in amide. This result further confirmed the structure obtained with MD simulations as shown in Figure 44c.

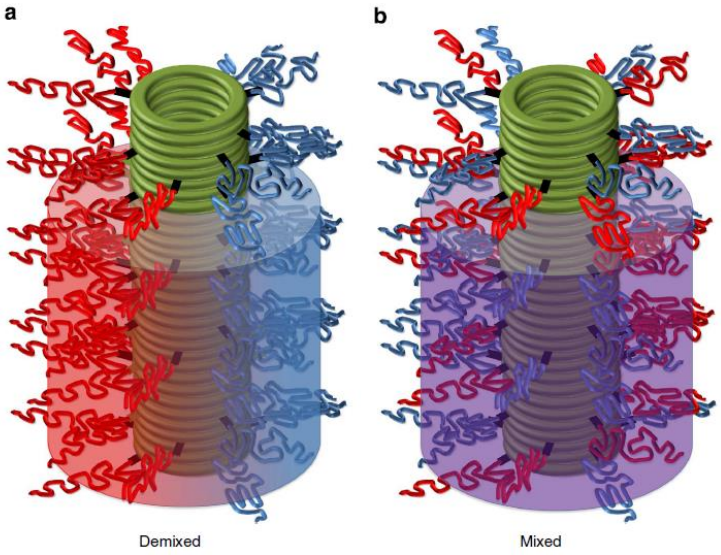

Figure 45. Cyclic peptide–polymer nanotubes with two corona configurations. (a) Janus assembly with 'demixed' corona. (b) Hybrid assembly with 'mixed' corona. Reprinted by permission from Macmillan Publishers Ltd: [Nature materials] (reference 252), copyright (2013)

A major advantage to construct nanotubes with cyclic peptides is that it allows facile functionalization of the exterior of nanotube. The side chains of amino acids residues such as lysine and glutamic acid provide ideal active sites for a variety of modifications. *Maarten Danial* et al. reported a self-assembling cyclic peptide–polymer nanotube with dual functionality in the form of either a Janus or mixed polymeric corona (Figure 45).[252] The polymers used in this study were terminated with either thiol or alkyne functionalities. Well-known click chemistry of thiol-ene reaction and copper catalyzed azide-alkyne cycloaddition (CuAAC) were used to conjugate different polymers to cyclic peptide. The self-assembling ability of cyclic peptide was not affected by the conjugation of polymers as determined by FT-IR and dynamic light scattering studies. Small-angle neutron scattering (SANS) experiments confirmed the formation of nanotubes in deuterated chloroform. More

importantly, the Janus character of this type of polymer decorated nanotube may create a new way to access synthetic transmembrane protein channel mimics.

Robert Chapman et al. described the assembly of polymer–cyclic peptide conjugates into nanotubes in solution through *in situ* measurements.[253] A series of polymers with degrees of polymerization (DPs) ranging from 16 to 195 were conjugated to a cyclic peptide. The assembled nanotubes have a remarkable stability. Even in neat TFA, a highly competitive solvent, it still took several hours to completely break up the nanotubes. They further demonstrated that the length of nanotubes can be controlled by varying the degree of polymerization of outer polymers due to steric bulkiness. Also by selectively deuterating one block of the polymer shell, the internal structures of nanotubes were altered.

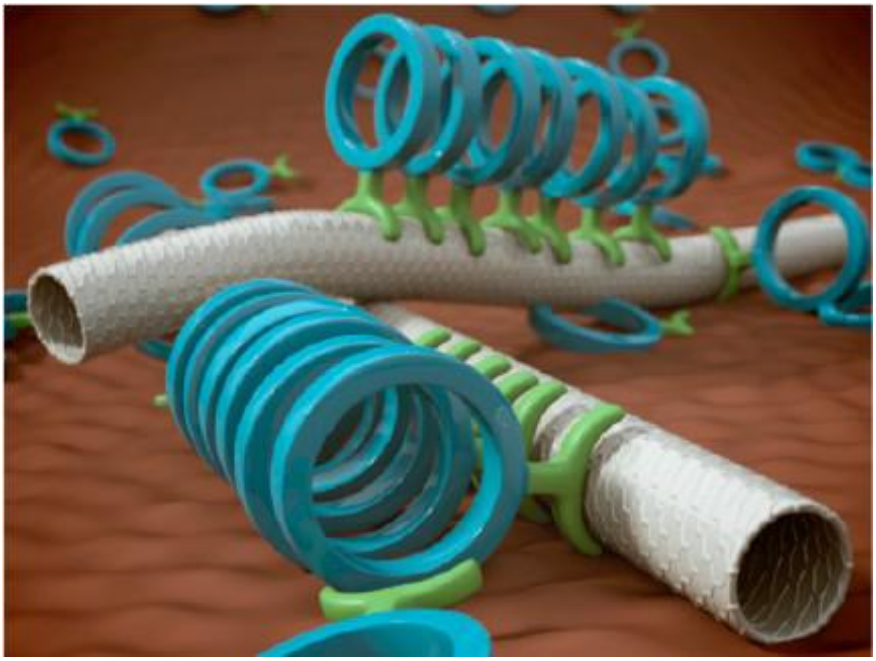

Figure 46.Coupled cyclic peptide nanotubes (blue) and carbon nanotubes (white). Reprinted with permission from Reference 256. Copyright (2016) American Chemical Society.

Besides polymers, other molecules such as fullerene and naphthalene tetracarboxylic diimide (NDI) could also be used to decorate the surface of cyclic peptide nanotubes.[254,255] Recently, *Javier Montenegro* et al. successfully coupled two main types of nanotubes, carbon nanotubes and cyclic peptide nanotubes together (Figure 46).[256] To achieve such design, one of the lysine residues in cyclic peptides was modified with a pyrene “paddle”. This pyrene paddle can establish efficient π-π stacking interactions with carbon nanotubes in water. They found out that carbon nanotubes functioned as template to assist the formation of cyclic

peptide nanotubes. The hybrid nanotubes exhibited semiconducting properties in aqueous dispersions rather than metallic carbon nanotubes.

2.3.2.1 Application of cyclic peptide nanotubes

The main applications of cyclic peptide nanotubes are in the field of biochemical science such as ion channels and antibacterial agents.[257] Other applications including gene delivery inhibitor, responsive materials and electronic devices have also been reported but less explored.[258-260]

In 1994, *M. Reza Ghadiri* et al. demonstrated that cyclic peptide nanotube could be used as artificial transmembrane ion channels.[261] A planar lipid bilayer was selected to model cell membranes. The cyclic peptide was constructed with alternating L-tryptophan and D-leucine residues. Two forces can contribute to the self-assembling process when the peptide monomer was mixed with lipids. The main driving force remained to be the hydrogen bonding interaction between each stacked peptide subunit. Another contribution came from the increase of entropy for the lipid chains when they were interacted with the side chains of tryptophan and leucine. FT-IR experiments supported the formation of transmembrane channels resulted from the assembly of cyclic peptide nanotubes. This system displayed ion-transport activity with rates around 10^7 per second for both sodium and potassium cations which was comparable to naturally occurring transmembrane channels such as gramicidin A. Shortly after, they demonstrated that glucose, a small organic hydrophilic molecule, can also across through bilayer membrane with assistance from cyclic peptide nanotubes.[248] For the passage of glucose through the cylindrical cavity of the tubular structure, a pore size >9 Å was required. Therefore, a ten residue cyclic peptide was designed and synthesized. The assembled peptide nanotubes displayed uniform 10 Å internal diameter and efficiently allowed glucose to across model membrane.

Owing to its pore formation ability in bilayer membrane, cyclic peptides were also tested as potential antibacterial agents. The nanotubes can easily form within bacterial membrane without involving proteins and specific receptors which makes them attractive over traditional antibiotics. The princinples of cyclic peptide nanotubes as antibacterial agens were first demonstrated by *M. Reza Ghadiri* et al. in 2001 (Figure 47).[262]

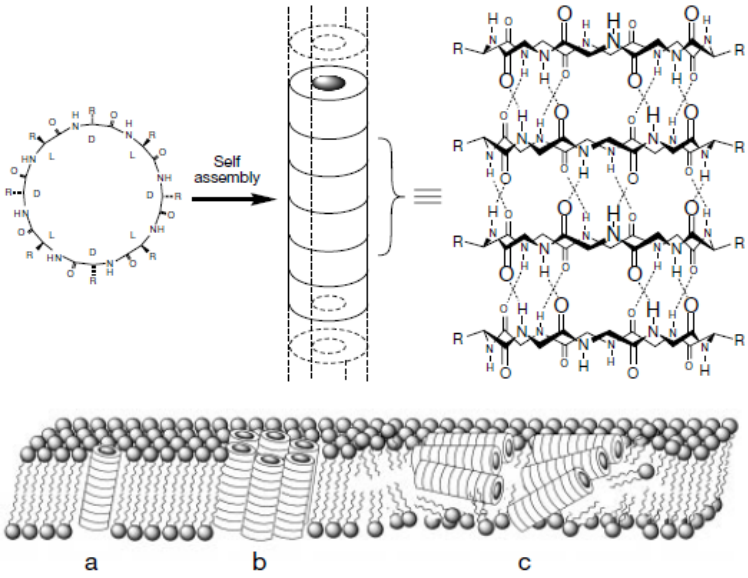

Figure 47. Tubular architecture of the assembled cyclic peptide and modes of membrane permeation. a, intramolecular pore; b, barrel stave; and c, carpet-like (cyclic peptides are depicted as ring structures). Reprinted by permission from Macmillan Publishers Ltd: [Nature] (reference 262), copyright (2010)

It was previously observed that amphiphilic cyclic peptides composed of three consecutive hydrophilic residues and five L-tryptophan and D-leucine residues self-assembled into nanotubes in synthetic membranes. Thus, a series of six- and eight-residue amphiphilic cyclic peptides were synthesized to examine their antibacterial activity. *Escherichia coli* and methicillin-resistant *S. aureus* (MRSA) were selected as target bacteria. It was found that glutamic acid residue had a deleterious effect on the antibacterial activity whereas basic amino acid residues were preferred. This is most likely due to the unfavorable electrostatic interactions of the carboxylate side chain with negatively charged cell membrane. Moreover, linear control peptides with identical amino acids sequences displayed little activity against MRSA. This highlighted the role of cyclic D, L-peptide structure in the formation of functional tubular assembly in bacteria membrane. In overall, the effectiveness of this class of cyclic peptides provides a promising new type of candidate in the developments of antibiotics.

James T. Fletcher et al. developed a combinatorial approach that could rapidly identify hexamer cyclic peptide sequences for the application of antibacterial agents.[263] Gram-positive MRSA and gram-negative *E. coli* and two eukaryotic marine algae, *Ulva linza* and *Navicula perminuta* were screened. A reliable, high-throughput assay was established to facilitate the

examination by correlating toxicity to the fluorescence intensity of chlorophyll. Previous results showed that the selectivity of cyclic peptide against bacteria was highly sensitive to minor changes in amino acid composition. This finding was then extended to the scope of eukaryotic species as well.

Leila Motiei et al. prepared a series of cationic cyclic peptides bearing D-glucosamine, D-galactose, or D-mannose glycosyl side chains.[264] This design was inspired by the discovery and structure elucidation of a new class antibiotic named mannopeptimycin in 2002.[265] Mannopeptimycin is in striking structural similarity to the previous described self-assembling cyclic peptide. The major difference in mannopeptimycin is the glycosylation in the side chain of tyrosine (Figure 48). Thus, the authors envisioned the introduction of glycosyl chains could improve the performance of cyclic peptide based antibacterial agents. Indeed, they found out that specific glycosylation not only preserved their activities against drug-resistant gram-positive bacteria but also significantly reduced their toxicity.

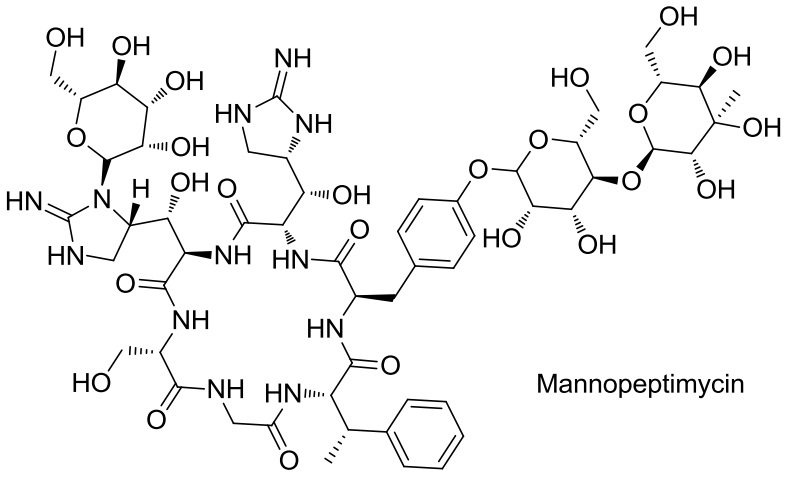

Figure 48. Chemical structure of mannopeptimycin

2.3.3 Other peptides assembly

Peptide assembly can be achieved with a variety of structurally different peptide based building blocks. Besides amphiphilic peptides and cyclic peptides, there are several other rather efficient peptide based assembling systems.[22] For example, coiled-coil peptides, in which several helices are coiled together, have been shown to be able to assemble into cages.[266] β-hairpin peptides can fold with itself and induce gelation process.[267,268] Peptides with strong tendency to form β-sheet can assemble into tape-like aggregates.[269,270]

2.3.3.1 Metal-peptide assembly

Peptide self-assembling trigger by metal ions is emerging as a quite active field of research nowadays.[271] Supramolecular structures assembled with the combination of peptides and metal ions are extremely interesting in the application of biomaterials and biomedicines due to the fact that natural proteins often require metal ions as cofactor to fulfill their functions. Additionally, the coordination with metal ion can change the conformation of peptides which could in turn alter and regulate their physiological properties.

To achieve peptide assembly with metal ions, appropriate ligands are in most cases incorporated into the amino acids sequences. In 2005, *Mary Elizabeth Williams* et al. synthesized two peptides with pyridine or bipyridine ligands.[272] Titrations with Cu^{2+} and Fe^{2+} showed that both peptides bound stoichiometric quantities of transition metals. Interestingly, the peptides bearing bipyridine ligands cross-linked with each other through metal ion centers to form duplex structures. Modelling results suggested that the backbones of this peptide served as a scaffold for the directed assembly of copper cations.

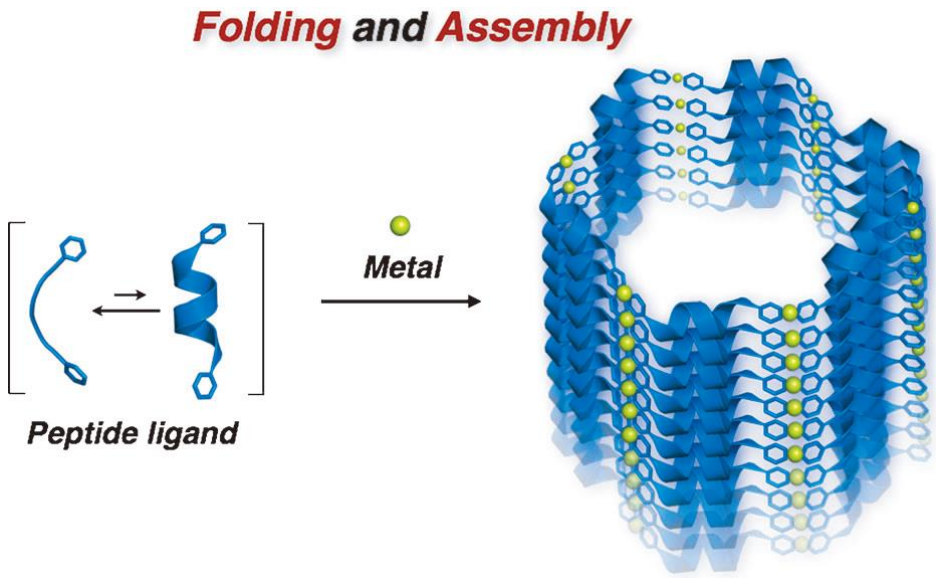

Figure 49. Concept of peptide Gly-Pro-Pro assembly with metal ions. Reference 273, copyright (2016) Wiley. Used with permission from John Wiley and Sons.

Similarly, *Tomohisa Sawada* and *Makoto Fujita* et al. constructed a short proline containing peptide with two pyridine ligands on both terminals (Figure 49).[273] The rather simple peptide Gly-Pro-Pro was able to assemble into polyproline-II helices through the coordination of silver ion with pyridine ligand in aqueous alcohol. Crystallographic studies revealed two

unique helical channel structures in this material. The larger one was approximately 2 nm in diameter and able to encapsulate guests such as BF_4^- anion, chiral organic molecules and linear penta-saccharides.

Futoshi Fujimura et al. designed a cyclic tri-β-peptide having a terpyridine ligand.[274] The peptide itself was not able to form nanotubes due to the introduction of bulky terpyridine groups that prevented the intermolecular hydrogen bonding interactions. However, the rod-shaped crystals obtained from the cyclic tripeptide can efficiently bind to copper cations and exhibited weak fluorescence. *Masatoshi Ikemi* et al. reported a *ca*. 9 nm $M_{12}L_{24}$ coordination sphere coated with 24 hexa-peptide aptamers.[275] The sphere was assembled from 12 Pd (II) ions and 24 terpyridine containing peptide (Arg–Lys–Leu–Pro–Asp–Ala) ligands at their convex. The formation of nano-sphere was confirmed by diffusion-ordered NMR spectroscopy (DOSY).

Nitrilotriacetic acid (NTA) is a strong chelating agent for metal ions such as Ca^{2+}, Cu^{2+} and Fe^{3+}. Variant of NTA is widely used for protein isolation and purification in the His-tag method. *Jean Chmielewski* et al. then designed a triple helical peptide modified with a His moiety on its C-terminus and a NTA unit on its N-terminus in order to create collagen-based supramolecular assemblies.[276] Upon addition of metal ions, the self-assembling process is triggered and higher ordered aggregates such as sheet-like structures and nanoparticles can be observed in solution. This process was fully reversible when EDTA, a competing metal cHeLating agent, was added to the assemblies. They further demonstrated that the final morphologies of assemblies were controllable by defining the number of Pro-Hyp-Gly repeating units in collagen peptide.

2.3.3.2 Amyloid peptide assembly

The aggregation of amyloid β-peptide (Aβ) into oligomers or fibrils is now considered as a key cause of Alzheimer's disease (AD).[277,278] Amyloid β-peptides, normally containing 36-43 amino acids, are the main component of the amyloid plaques found in the brains of Alzheimer patients. The assembling property of Aβ peptide has thus inspired numbers of researches.[279-281]

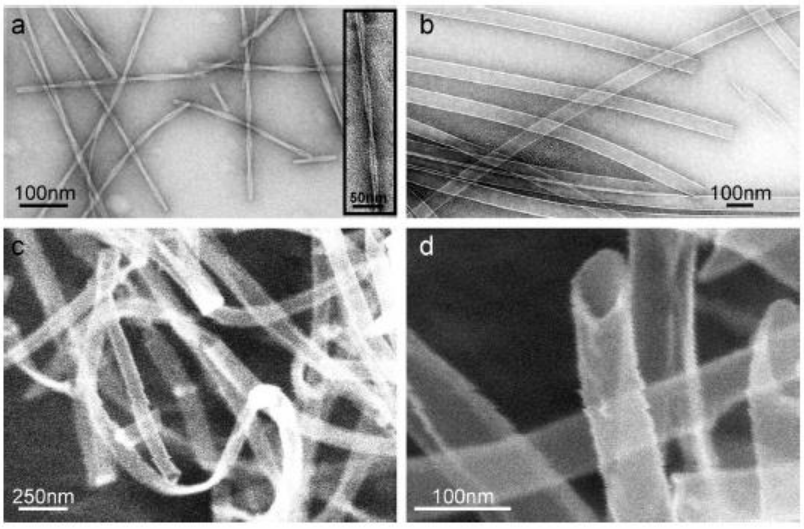

Figure 50. Assembly of Aβ (16-22) peptide fibers and nanotubes a) pH 6 (b, c, d) pH 2. Reprinted with permission from Reference 282. Copyright (2016) American Chemical Society.

Anil K. Mehta et al. found out that the short Aβ (16-22) peptide, a segment from Aβ peptide, assembled into amyloid fiber which was morphologically identical from the full-length peptide fiber.[282] However, this peptide was also capable of forming different structures under distinct conditions. At slight acidic solutions, long and unbranched amyloid fibrils were observed with TEM. Decreasing the pH to 2 resulted in the formation of nanotubes as shown in Figure 50. Molecular dynamic simulations showed that these fibers were featured with both a polar and a nonpolar face, while the same side chains displayed on each face of tubes.

Aβ peptide is thought to contain a set of structures when dissolved in solution. As consequences, it cannot be crystallized and most structural knowledge on this peptide comes from NMR and molecular dynamics. *James S. Nowick* et al. then incorporated a key region of Aβ into a macrocyclic peptide that could stabilize oligomers.[283] This strategy facilitated the structural elucidation by X-ray crystallography. Crystallographic structures were thus obtained from the macrocycle containing Aβ (15−23) peptide. Later, they showed that macrocycle containing both Aβ (15−23) peptide and Aβ (15−23) hybrid strand could also be crystallized.[284] An extended β sheet comprised of two dimers interacting through hydrophobic interactions was observed in solid state. This eventually led to fibril-like assembly formation that ran the length of the crystal lattice.

Interestingly, *David G. Lynn* et al. demonstrated the switching ability of amyloid formation with metal ions.[285] By examining the structures of fibrils formed by Aβ (10-35) peptides, they

noticed that the side chains of the histidine residues at positions 13 and 14 were directed to opposite surfaces of the β sheet which provided an ideal site for Zn^{2+} chelating. The results showed that in the absence of Zn^{2+}, a nucleation phase lasting several hours was observed which was followed by a longer growth phase. Addition of Zn^{2+} to Aβ (10-35) peptide solution, however, diminished the nucleation phase. They further demonstrated that varying the concentrations of Zn^{2+} dramatically altered both self-assembly kinetics and fibril morphology. With higher Zn^{2+} concentration, the nucleation time was significantly eliminated (Figure 51b). In the rapid assembly process, formation of helical thick ribbons could be observed in both AFM and TEM.

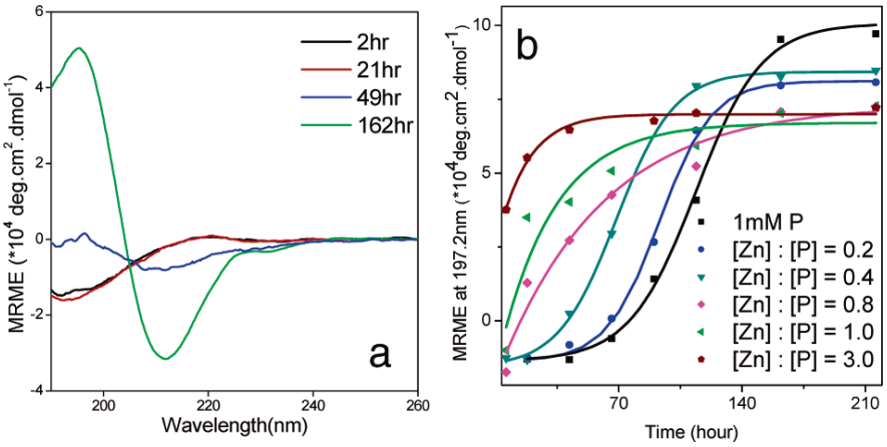

Figure 51. (a) CD spectra over time of Aβ peptide at pH 5.6. (b) Mean residue molar ellipticity as a function of time for Aβpeptide in the presence of different Zn^{2+}concentrations. Reprinted with permission from Reference 2854. Copyright (2016) American Chemical Society.

2.3.3.3 Collagen peptide assembly

Collagen is the most abundant protein in mammals and the main component of connective tissues. However, collagen isolated from natural sources is difficult to modify and can induce immunological side effects. Synthetic peptides which could assemble into collagen-like structures thus attract many interests. In 2008, *Ronald T. Raines* et al. reported that short collagen fragments prepared through conventional solid phase peptide synthesis could also self-assemble into triple helices, characteristic structure of collagen.[286] Cysteine residues were incorporated to hold together the three strands by disulfide bonds. The self-assembling of this peptide is comprised of two processes. Firstly, individual peptide fragments formed a triple-helix through intramolecular hydrogen bonding interactions. Afterwards, intermolecular

hydrogen bonding interactions allowed elongated fibril formation. CD and TEM measurements revealed that these fibrils resembled the triple helix structure of natural collagen and were longer (400 nm) than any known collagens.

Jeffrey D. Hartgerink et al. designed a peptide that replicated each steps of the self-assembling of typical collagens (Figure 52: peptide chains to triple helices to nanofibers and finally to hydrogel).[287] This peptide utilized the proline–hydroxyproline–glycine repeating units of collagen with additional salt-bridged hydrogen bonds between lysine and aspartate residues to stabilize the triple helix. The hydrogel formed with collagen mimetic peptides can be degraded by collagenase and it is also temperature sensitive due to the unfolding property of triple helix at 40℃.

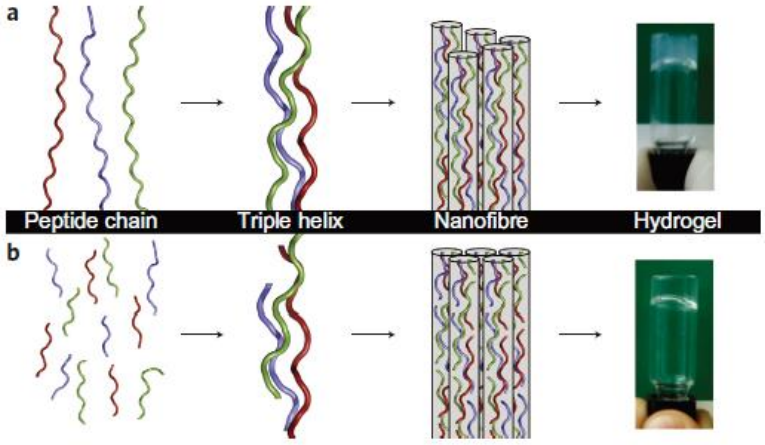

Figure 52.Self-assembly of collagen (a) compared to that of collagen mimetic peptide (b). Reprinted by permission from Macmillan Publishers Ltd: [Nature chemistry] (reference 287), copyright (2011)

The assembling property of collagen peptides can be used to construct other types of supramolecular structures.[288-291] For example, *Tushar Gore* et al. demonstrated that adding lipophilic tails can control the assembly morphology of model collagen peptides.[292] Short tails such as C12 and C14 resulted in the formation of spherical micelles. Increasing the length of tails led to the formation of disk-like micelles. Double tails with lengths of C18 and C20 gave rise to crystalline structures. *Armando E. Reimer* et al. reported that when aromatic FITC moiety was attached to a non-helical collagen peptide, tubular structures were well observed.[293]

3. PROJECT AND OBJECTIVES

Peptide based materials have gained much interests in recent years due to its functional versatility and biocompatibility. Applications such as gene delivery vector and self-assembled nanomaterials have been widely explored. On the other hand, the excellent anion recognition ability of GCP moiety provides another useful tool for applications regarding anions such as DNA and peptides. Therefore, we hypothesized that the combination of GCP and peptide scaffold could largely improve the performance of peptide based materials in the above applications. This hypothesis is thus demonstrated in the following projects.

3.1 Development of novel cell penetrating peptide

Among the various strategies which have been applied in drug delivery so far, cell penetrating peptides are considered highly promising owing to their biocompatibility and functional versatility. These peptides are mostly featured in the use of cationic amino acid residues especially arginine due to the anionic nature of cell membrane. Although the exact mechanism of cellular entry of arginine rich cell penetrating peptides have not been fully understood, it is clearly shown that cell surface proteoglycan played an important role in this process.

Based on these findings, we hypothesized that enhancing the hydrogen bonding ability of arginine rich cell penetrating peptides could improve their interactions with glycosaminoglycan on cell surface (Figure 53). GCP moiety has previously been demonstrated high binding affinity toward oxoanions. Therefore, we envisioned that introduction of GCP groups into the side chains of peptides could provide a more effective peptide in cellular uptake.

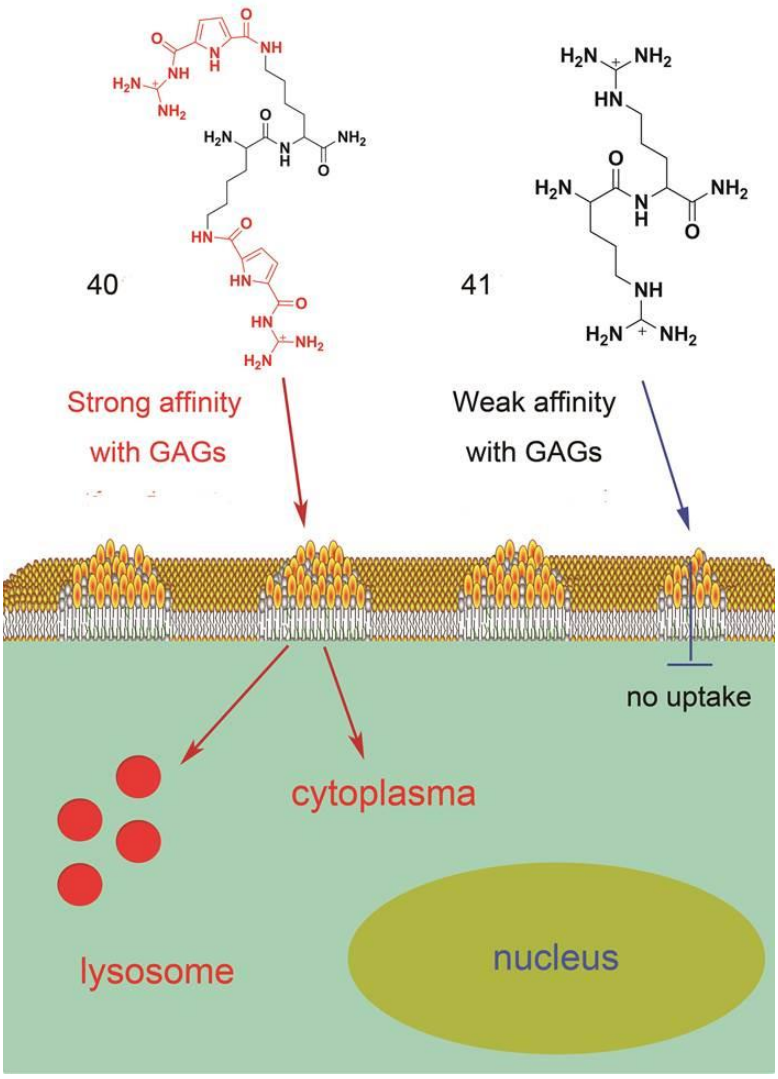

Figure 53. Schematic representation of the designing principles

3.2 Development of cell penetrating peptide based gene transfection vector

Peptide based gene transfection vectors have attracted increasing interests in recent years due to their ease of synthesis, lower toxicity at least compared to polymeric transfection vectors and versatility of functionalization. Of the most often used peptidic vector, arginine rich cell penetrating peptides have been identified as being highly efficient in cellular uptake and thus are widely tested as gene delivery vectors. However, at least 8 to 9 arginines were still necessary for decent gene transfection even with these amphiphilic arginine oligomers. The transfection efficacy as well cytotoxicity of these peptides requires further improvement,

with regard to future applications.

Although other cationic peptides such as lysine oligomers have been used for gene transfection, their efficacies are usually even worse than arginine rich peptides. Owing to the superior anion binding ability of GCP moiety, we hypothesized that the replacement of guanidine with GCP in arginine-rich cell penetrating peptides (CPPs) should further improve the binding ability between CPPs and both DNA and the cell membrane which might result in a better performing vector (Figure 54).

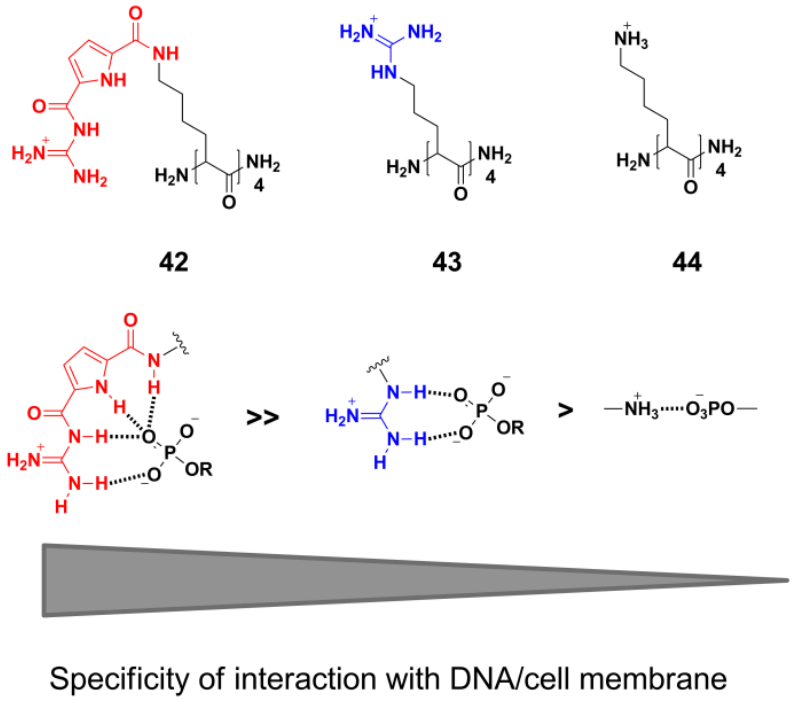

Figure 54. Schematic representation of the designing principles

3.3 Development of cyclic peptide nanotube based gene transfection vector

Besides individual peptides, self-assembled peptide aggregates have also been tested as gene transfection vectors. For example, *M. Yolamanova* et al. recently reported that an amphiphilic 12-amino acid peptide derived from the HIV-1 glycoprotein gp120 forms cationic nanofibers which boost virus mediated gene transfection.[294] Only the nanofibers, not individual peptides, enhanced gene transfection probably by functioning as an "electrostatic nanobridge" between virus and cell membrane. It has also been reported that nanotubes formed from cationic dipeptides bind single strand DNA.[295] Upon dilution these nanotubes

rearrange into vesicles which are taken up by cells.

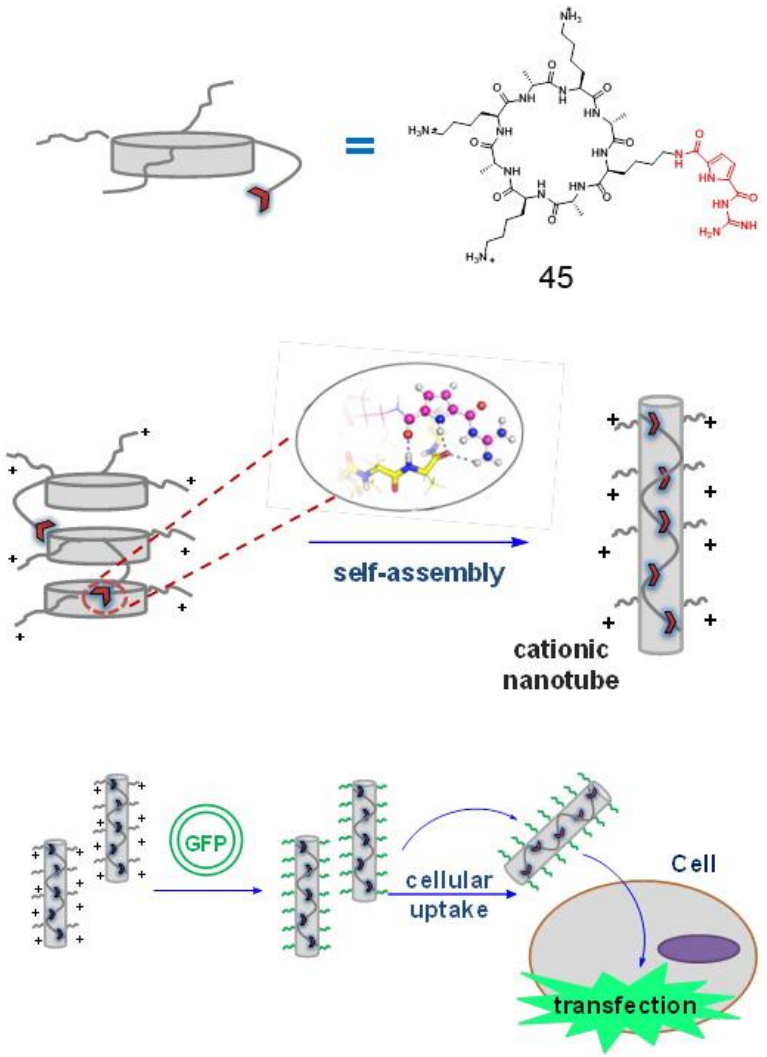

Figure 55. Schematic representation of the designing principles

Cyclic peptide nanotubes have become a highly interesting scaffold for a variety of applications since their first discovery in the 90's. However, cyclic peptide nanotubes normally cannot be positively charged under physiological conditions since charge repulsion then prevents tube formation. Unfortunately, positive charges are usually critical for DNA binding and also gene transfection due to the anionic nature of DNA. Hence, cyclic peptide nanotubes were not used for DNA binding or even gene transfection so far. Therefore, we hypothesized that functionalization of a cationic cyclic peptide with our GCP group could significantly alter its self-assembly and DNA binding features (Figure 55).

3.4 Development of supramolecular β-helix mimetic peptide

One current goal of supramolecular chemistry is to design artificial self-assembling systems that could mimic biological important helix structures under biomimetic conditions. A variety of assembly strategies based on peptide building blocks have been thus developed. However, while peptide assembly aiming to resemble α-helix structure has been demonstrated by several studies, reports on β-helix mimics are rare. Mainly because α-helix is one of the most common secondary structures of proteins and therefore examples on such structures are abundant. On the other hand, there are only very few peptides which exhibit β-helix properties and thus are poorly studied due to insufficient data.

Gramicidins are fascinating examples of such structures designed by nature. It is generally believed that this peptide can only form a unique head-to-head associated dimer of two single stranded β-helices (the channel form) in the presence of membrane mimics, such as vesicles. In organic solvents it exists in totally different structures, such as a double strand inter-twined helix (the non-channel form). Although there have been reports that demonstrated that similar structural properties as of gramicidin A can be realized with artificial non peptidic systems such as aromatic hydrazide oligomer and synthetic triazole compounds, they normally require carefully designs and adjustments. A strategy for a self-assembling peptide forming a β-helix structure has not yet been developed.

The interaction of a GCP moiety with carboxylates in water is sufficiently strong as described above. Therefore, we hypothesized that this supramolecular recognition pair (GCP—COO^-) can be applied to stabilize a β-helix structure and might also provide additional self-assembling property when it is approximately positioned (Figure 56).

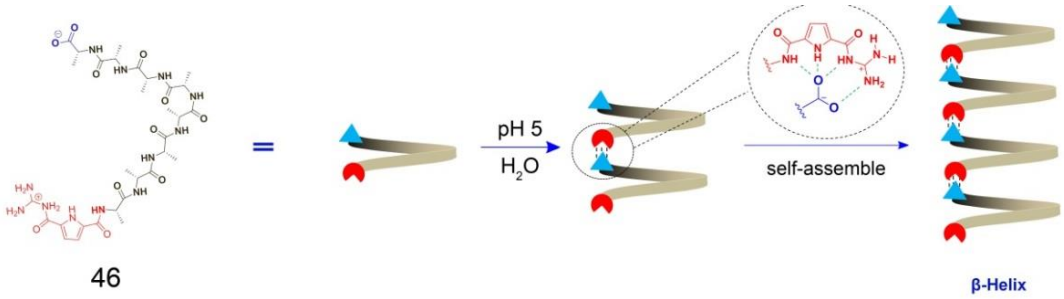

Figure 56. Schematic representation of the designing principles

3.5 Development of functionalized amphiphilic peptide assembly

Self-assembling Fmoc-based dipeptides are highly interesting in the development of supramolecular materials. Their assembling properties are rather robust and can be realized in aqueous conditions. However, the variety of Fmoc-based dipeptides is limited. Hydrophobic amino acid residues are in most cases required to achieve efficient peptide assembly. Post-assembly modification of this system is thus difficult to achieve compared to that of amphiphilic peptides with aliphatic chains.

Therefore, we hypothesized that the introduction of a GCP moiety in the side chains of Fmoc-based dipeptides could provide further manipulation of the assembled peptide fibers (Figure 57). The GCP moiety is most likely not protonated under neutral conditions due to its low pKa value (~7). This property renders a hydrophobic domain in the side chains of peptide **47** which is structurally similar to the Fmoc-FF peptide but with additional anion binding ability. Post-assembly modification is thus plausible through the anion recognition ability of GCP moiety arrayed on the surface of fibers. This property allows us to further manipulate the assembled peptide fibers with other components such as monomers which can be covalently polymerized, small organic molecules which could chelate metal ions etc. Thus, this peptide could serve as a platform or a template for a variety of applications including DNA binding and hybrid material fabrication.

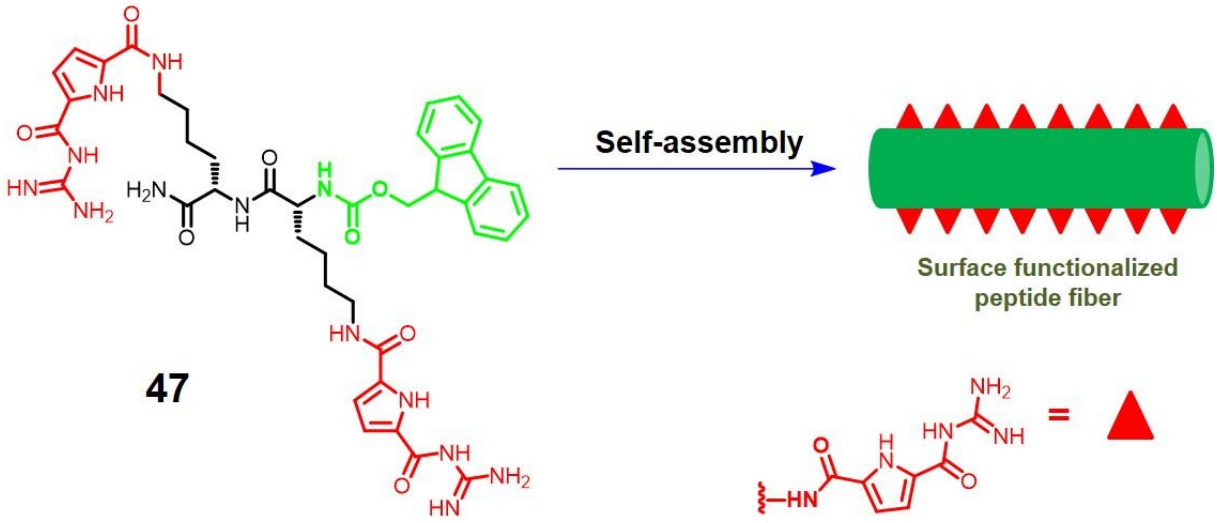

Figure 57. Schematic representation of the design principle

4. RESULTS AND DISCUSSION

In this chapter, we describe that through the utilization of the excellent anion binding ability of GCP moiety, a variety of artificial peptides could be obtained which showed interesting properties in cellular uptake (section 4.1), gene delivery (section 4.2 and 4.3), and supramolecular assembly (section 4.4 and 4.5).

4.1 Development of novel cell penetrating peptide

4.1.1 Synthesis of GCP moiety

In order to introduce the extremely strong anion binding motif GCP into the designed systems, it must be synthesized before peptide preparation. The route of synthesis for GCP is well established in the *Schmuck* laboratory as shown in Figure 58.

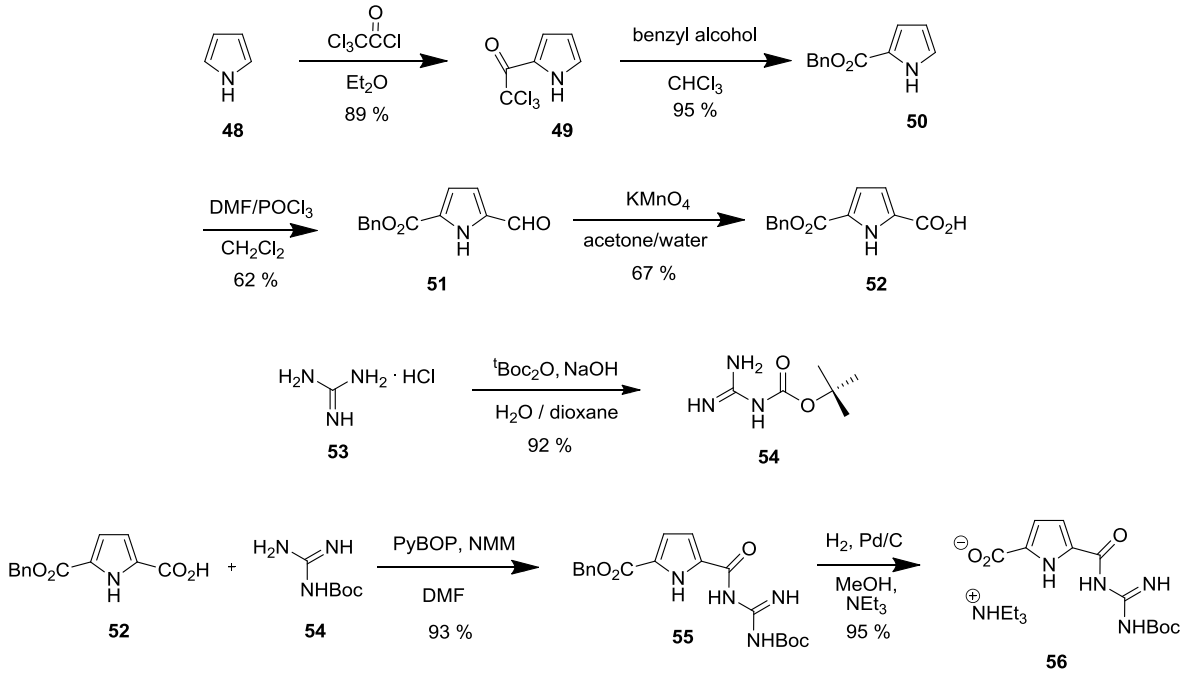

Figure 58. Synthetic route of GCP moiety (**56**)

The synthesis of GCP started form commercial available pyrrole. Pyrrole (**48**) was first acylated with trichloroacetyl chloride in diethyl ether to give the trichloroacetyl-pyrrole (**49**). Trichloroacetyl-pyrrole **49** was then subjected to attack with benzylate and liberation of the trichloromethane anion directly yielded the benzyl ester **50**. *Vilsmeier–Haack* formylation was then conducted on **50** to introduce an aldehyde functional group in the 5 position of pyrrole.

The *Vilsmeier* reagent, preformed from phosphoryl chloride and dimethylformamide, was added slowly under cooling to **50** and the reaction gave rise to 2’5-substituted pyrrole **51**. Subsequently oxidation with potassium permanganate resulted in **52**. Afterwards, molecule **52** was allowed to couple with a tert-butyloxycarbonyl (Boc)-protected guanidino moiety using PyBop as coupling reagent. The activation is necessary due to the low reactivity of the carboxyl group in **52**. The guanidinocarbonylpyrrole benzyl ester **55** directly precipitated when water was added to the reaction mixture. Finally, the benzyl ester group was cleaved off by hydrogenation with a catalytic amount of palladium to yield **56** as a while solid. GCP building block **56** possesses a carboxylate group which can facilitate the following modifications in peptides. The whole procedure can be operated on gram scale with an overall yield of 50%.

4.1.2 Synthesis of dipeptide analogue

4.1.2.1 Synthesis of dipeptide analogue 40

To examine the effect of GCP modification on the cellular uptake ability of cell penetrating peptides, a dipeptide analogue **40** was first designed. GCP units were introduced into the side chains of lysine through conventional coupling reactions. The preparation of **40** was performed on solid phase using Fmoc strategy (Figure 59). Rink amide MBHA resin was selected because it provide an amide functionality at the C-terminus after final cleavage. Commercially available amino acid Fmoc-Lys(Alloc)-OH was used to build the peptide scaffold (step 2). De-protection of the Alloc group with $Pd(PPh_3)_4$ resulted in free amine groups on the side chains of lysine (step 3). Subsequently coupling with GCP moiety (step 4), Fmoc de-protection (step 5) and cleavage from the resin (step 6) yielded the crude product. Purification with MPLC resulted in peptide **40** in 25 % yield with 96 % purity.

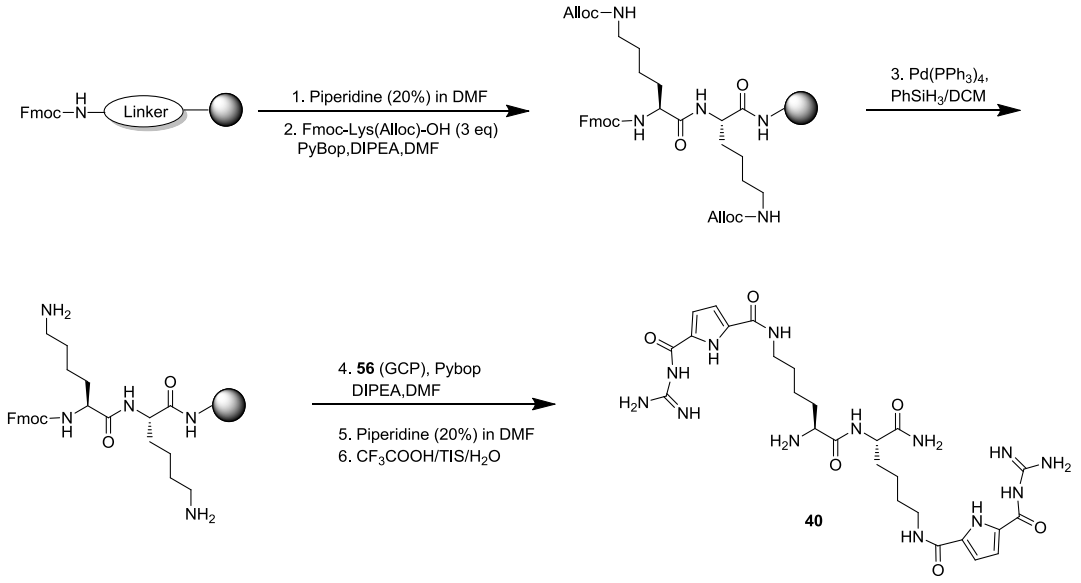

Figure 59. Synthetic route of dipeptide analogue (**40**)

4.1.2.2 Synthesis of dipeptide 41

For comparison of binding affinities with glycosaminoglycan, we also synthesized peptide **41**, comprised of two arginine residues, as control peptide. The preparation of **41** was performed on solid phase using Fmoc strategy (Figure 60). Rink amide MBHA resin was selected. Commercial available amino acid Fmoc-Arg(Pbf)-OH was used to construct the peptide scaffold (step 2). Subsequently deprotection (step 3) and cleavage from the resin (step 4) and purification with MPLC yielded peptide **41** as a white solid in 25 % yield.

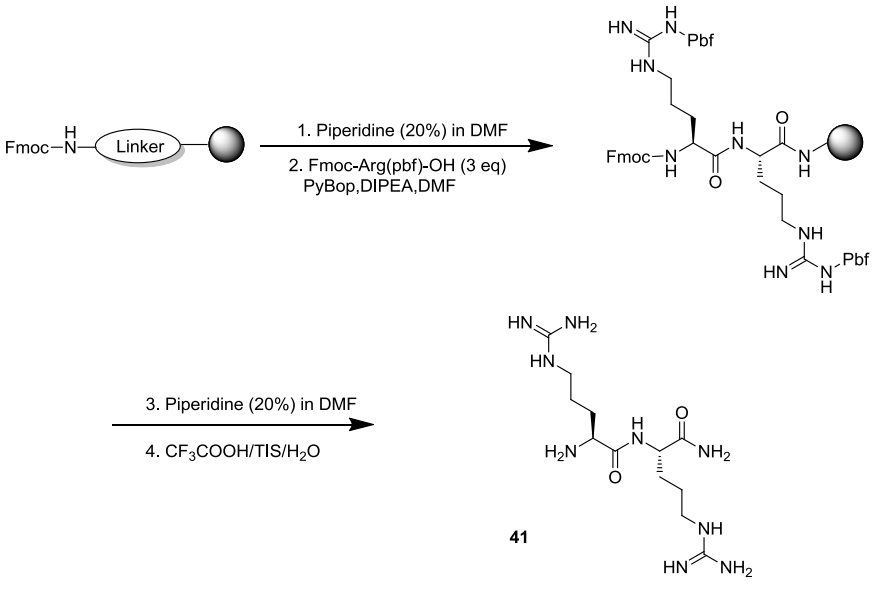

Figure 60. Synthetic route of dipeptide (**41**)

4.1.2.3 Synthesis of labeled dipeptide analogue 58

The cellular uptake ability of peptides can be examined in several ways. For example, the hydrophobicity of a molecule can be defined with partition experiment in which a two phase system (typically octanol and water) is constructed to measure the layer permeation ability of target molecule. The most often used and indeed most reliable method is to label the studied peptide with a fluorescent group and examine its cellular uptake directly. For this purpose, we labeled peptide analogue **40** with rhodamine B through conventional coupling reaction protected from light (Figure 61). Purification with flash chromatography resulted in a red solid **58** (38 % yield).

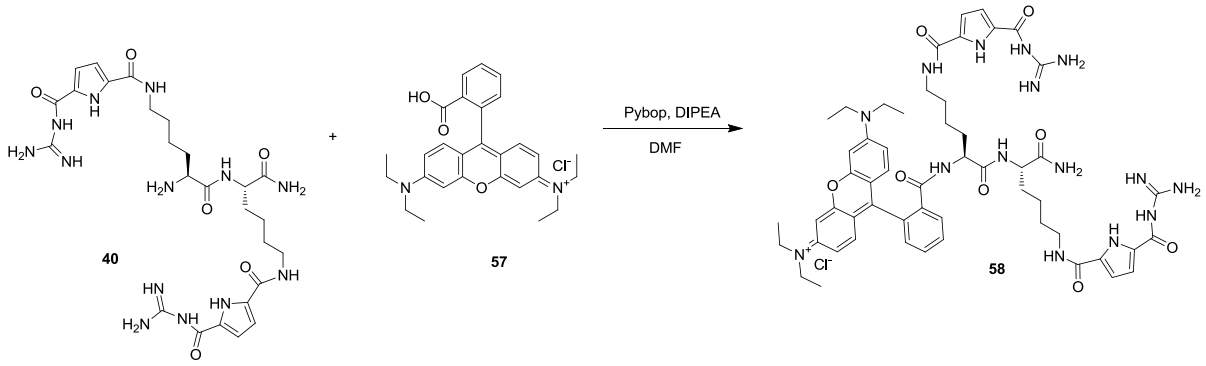

Figure 61. Synthetic route of labeled dipeptide analogue (**58**)

4.1.2.4 Synthesis of labeled dipeptide analogue 60

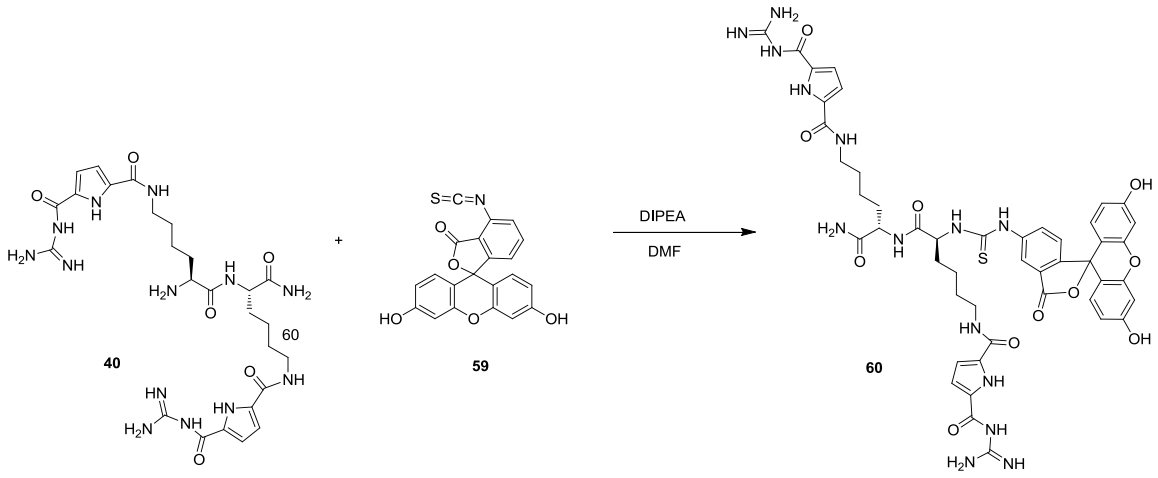

Figure 62. Synthetic route of labeled dipeptide analogue (**60**)

We also labeled peptide analogue **40** with fluorescein to confirm the results and also exclude

any artifacts caused by the property of the fluorophores. Fluorescein isothiocyanate was used to modify the N-terminus of peptide **40** through conventional conjugate addition reaction protected from light (Figure 62). Purification with flash chromatography resulted in a yellow solid **60** (90 % yield).

4.1.3 Binding study with glycosaminoglycan

Although the exact mechanism of cellular entry of arginine rich CPPs has not been fully understood yet, it has been clearly demonstrated that cell surface proteoglycans played an important role in this process. The binding affinity of both peptides with glycosaminoglycan was therefore tested by isothermal titration calorimetry (ITC). ITC is at present the most effective tool to characterize the thermodynamic profile of interactions of small molecules with macromolecules such as DNA and proteins, providing valuable information about the enthalpic and entropic contributions to the Gibbs energy. Commercially available heparin sodium, a sulfated glycosaminoglycan (GAG), was selected as model due to its close structural similarity with respect to cell surface proteoglycans (Figure 63).

The binding between control peptide **41** and heparin was negligible. Only the dilution effect of heparin can be observed when it was titrated into a solution of peptide **41** (Figure 64). However, in sharp contrast to this, the binding between dipeptide analogue **40** and heparin was extremely strong (10^7) as shown in Table 1. Considering the structural similarity between the two peptides, clearly the favorable interactions between the GCP moiety in **40** and the oxoanions in heparin are mainly responsible for this enhancement. Moreover, the thermodynamic signature for the binding process between heparin and **40** were rather unusual. The enthalpy contribution in the binding process of peptide **40** with heparin reached to -60.5 kJ/mol. This was however compensated with an unfavorable entropy change. Such classical enthalpy-entropy compensation indicated that the binding between peptide **40** and heparin was very specific.

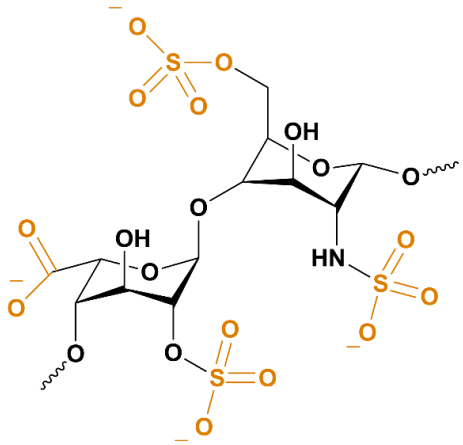

Figure 63. Chemical structure of heparin disaccharide

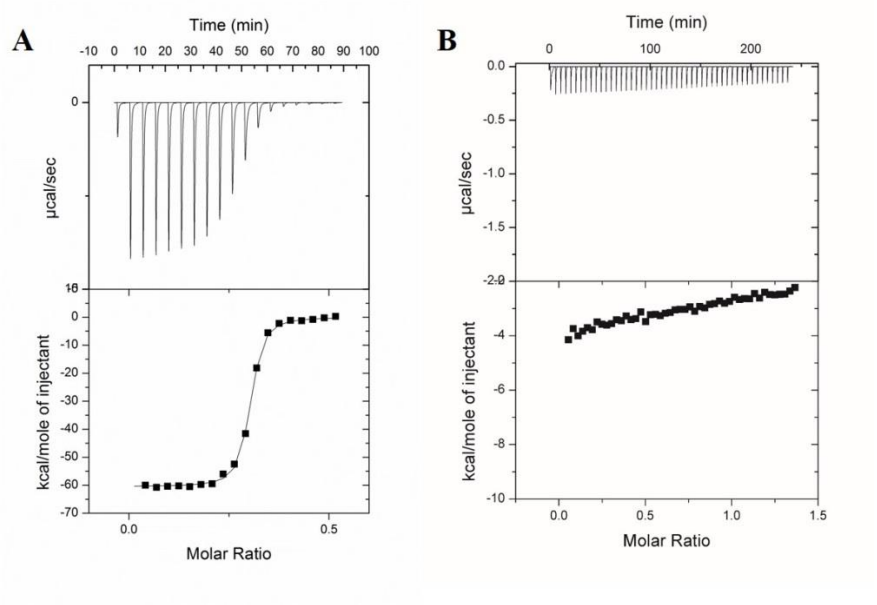

Figure 64. ITC titration curves of peptides **40** (A) and **41** (B) with heparin. Note that the heat exchange for the titration to **41** (-0.25) is 64 fold smaller compared to **40** (-16). Heparin (1 mM) was titrated into peptides **40** and **41** (50 µM) pH 7.4 cacodylate buffer solution, respectively.

Table 1. Thermodynamic binding profiles of peptides **40** and **41** with heparin

	K_d (M^{-1})	**N**	**ΔH (kJ/mol)**	**TΔS (kJ/mol)**
40	2.31×10^7	0.29	-60.5 ± 0.3	-50.4 ± 5.0
41	no binding detected	-	-	-

4.1.4 Cellular uptake study

As described above, peptide **40** obviously exhibited rather high binding affinity with model glycosaminoglycan, we thus determined to test its cellular uptake ability in HeLa cell lines. Rhodamine labeled peptide **58** and fluorescein labeled peptide **60** was added to cell culture medium respectively and incubated for one hour at 37 ℃. After washing the cells with buffered water three times, they were directly examined with confocal fluorescence microscopy to determine cellular uptake ability. The cell experiment was conducted with the cooperation from prof. Shirley Knauer in biology department with Stefanie Schlesiger.

The results clearly showed that peptide **58** entered into the cells after the incubation (Figure 65). It is also can be seen that the cellular distribution of peptide **58** is concentration dependent. At lower concentration, the internalized peptides seemed to be entrapped in cell compartments. However, when the concentration increased to 20 μM, peptide **58** was well distributed in both cytosol and nucleus. These results were further confirmed with peptide **60** bearing a green fluorophore (Figure 66).

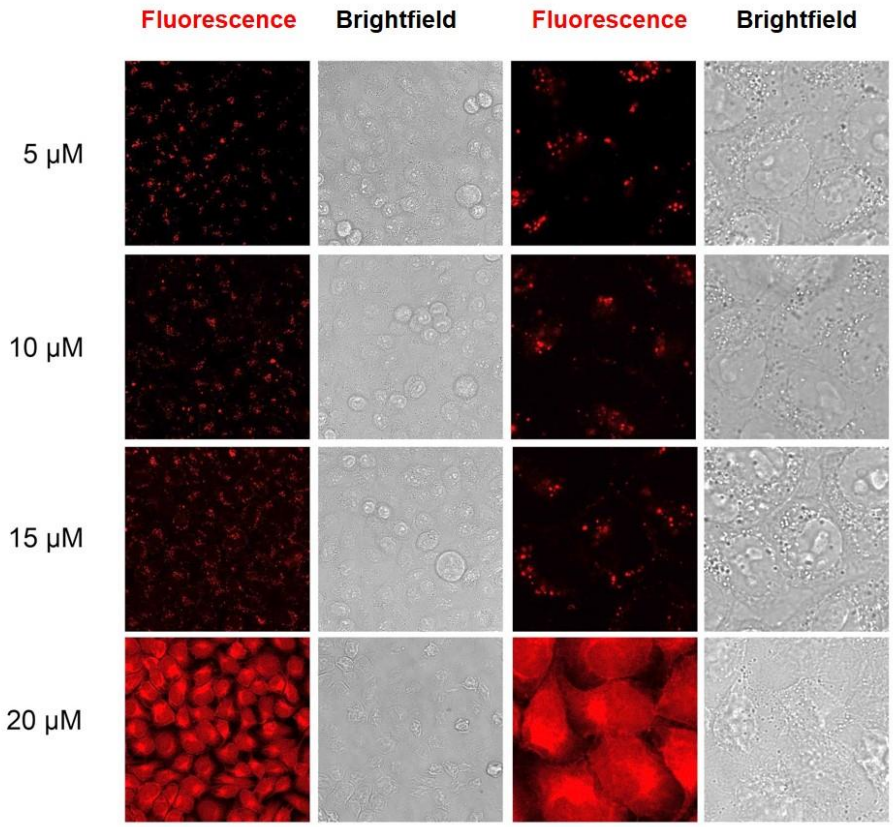

Figure 65. Confocal microscopy images of HeLa cells with peptide **58**

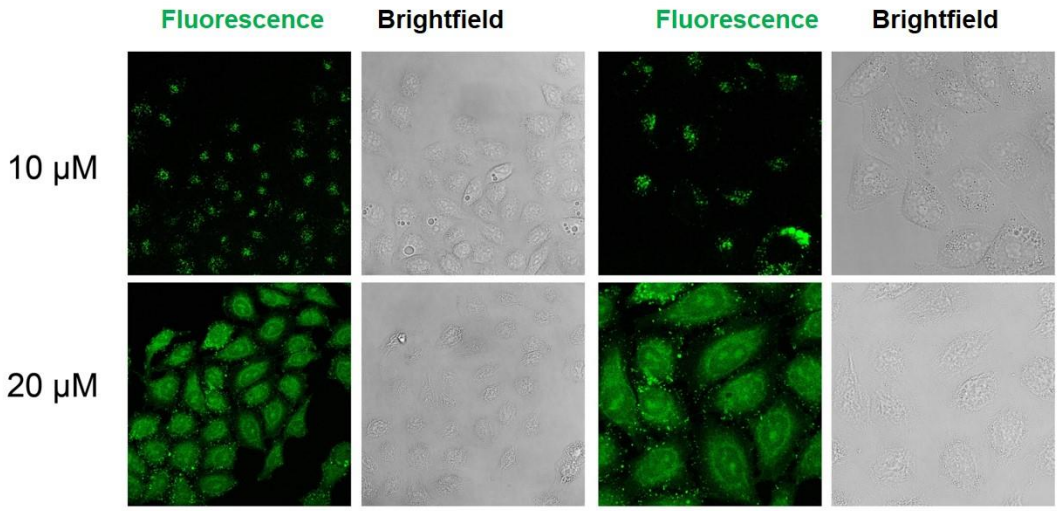

Figure 66. Confocal microscopy images of HeLa cells with peptide **60**

Therefore, we tested the cellular distribution property of peptide **58** in co-localization experiments. Cell co-localization was conducted with 10 μM peptide **58** due to the fact that **58** obviously entered into cytosol at higher concentration. Three cell organelles, Golgi apparatus, endosome and lysosome were stained with green fluorophore respectively. DAPI, a nucleic acid specific dye exhibiting blue fluorescence, was used to stain cell nucleus in each case.

As shown in Figure 67, peptide **58** did not co-localize with the Golgi apparatus in HeLa cell lines. We then labeled endosomes with a green fluorophore. Endosomes are in most cases the necessary pathway for endocytosis mediated cellular uptake. However, the internalized peptide **58** did not co-localize with endosomes neither which might suggest that endocytosis pathway was not mainly responsible for the cellular uptake process of peptide **58** (Figure 68).

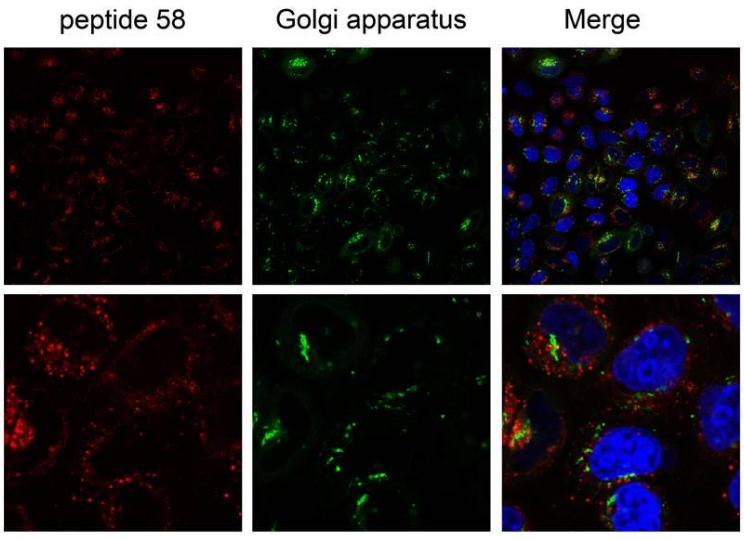

Figure 67. Co-localization images of Golgi apparatus with 10 μM peptide **58**

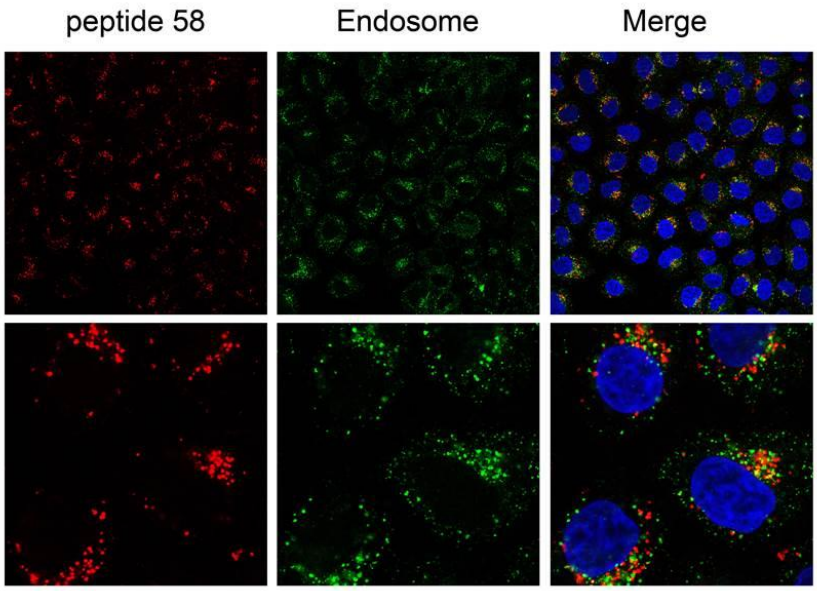

Figure 68. Co-localization images of endosome with 10 μM peptide **58**

We next labeled lysosomes, another cell organelle containing the materials taken up by the cells, with green fluorophore. The results shown in Figure 69 clearly demonstrated that most peptide **58** internalized by cells ended up in lysosomes under this concentration. Thus, the results implied that peptide **58** with its two GCP group modifications, ultimately ended up in lysosomes after 1 h incubation time with cells. However, this might be due to the incubation time for peptide **58** is too long that it already passes through other endocytosis related organelles such as endosome.

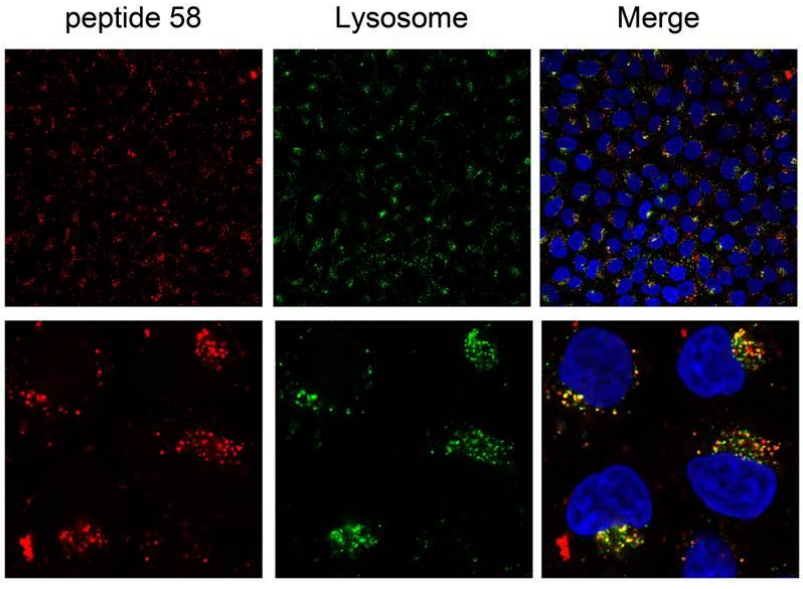

Figure 69. Co-localization images of lysosome with 10 μM peptide **58**

Importance for any future applications of cell penetrating peptides is their toxicity. Therefore, the cytotoxicity of the novel cell penetrating dipeptide analogue **40** was examined with alamar blue assay by means of metabolic activity. Different concentrations of peptide **40** were tested in HeLa cell lines. The results showed that peptide **40** is essentially not toxic at least *in vitro* (Figure 70). Even treatment with 100 μM of peptide **40**, a concentration well above the concentration tested in cellular uptake studies, exhibited negligible cytotoxicity.

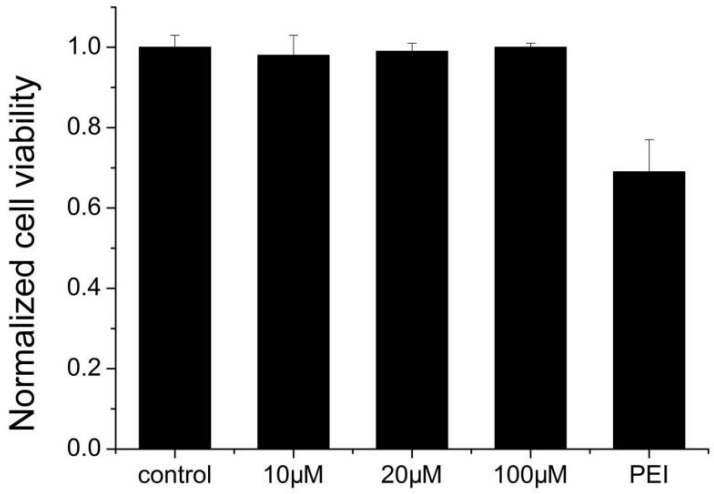

Figure 70. Normalized cell viability of different concentrations of peptide **40** in HeLa cell lines

In summary, the introduction of the GCP moiety into short peptides exhibited astonishing ability in the enhancement of cell penetration. In contrast to the common strategy of adding lipophilic tail, the combination of weak non-covalent forces, i.e. hydrogen bonds and ion pairs, provided the smallest cell penetrating peptide analogue known so far to be best of our knowledge. With its small size and negligible cytotoxicity, we envisioned peptide **40** would largely benefit the development of drug carriers.

4.2 Development of cell penetrating peptide based gene delivery vector

The first project successfully demonstrated that modification of short peptides with GCP moieties can enhance their cell penetrating ability. Therefore, we determined to utilize the same strategy to develop novel cell penetrating peptides based gene delivery vectors.

4.2.1 Synthesis of tetra peptide analogues

We thus designed and synthesized a series of tetra peptide analogues with different numbers of GCP modifications on the side chains to evaluate their transfection efficiency (Figure 71).

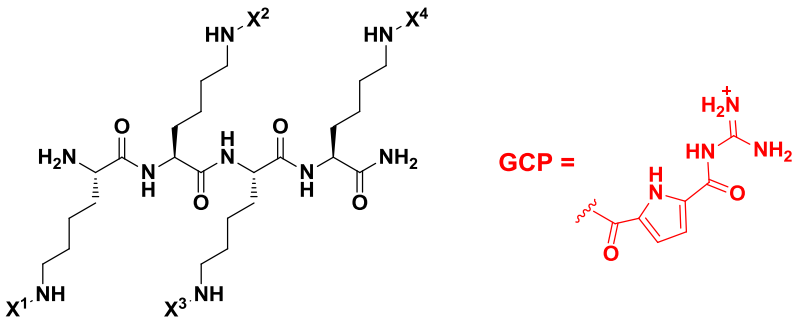

42 (G'G'G'G') : $X^1 = X^2 = X^3 = X^4$ = GCP
61 (G'G'G'K) : $X^1 = X^2 = X^3$ = GCP, X^4 = H
62 (KG'G'G') : X^1 = H, $X^2 = X^3 = X^4$ = GCP
63 (G'KKG') : $X^1 = X^4$= GCP, $X^2 = X^3$= H
64 (G'KKK) : X^1= GCP, $X^2 = X^3 = X^4$= H,
43 (RRRR) : Arginine tetramer
44 (KKKK) : Lysine tetramer

Figure 71. Chemical structures of designed tetra peptide analogues

4.2.1.1 Synthesis of GCP modified tetra-peptide analogues

The strategy of synthesis for the tetra-peptide series was very similar. Alloc protected lysine was applied in each case for the coupling of GCP moiety into the side chain. An example of synthesis route for peptide **42** is shown in Figure 72. Synthesis for other GCP modified peptides can be found in experimental section 6.4.2. The preparation of **42** was performed on solid phase using Fmoc strategy. Rink amide MBHA resin was selected to provide an amide

group at the C-terminus after cleavage. Commercial available amino acid Fmoc-Lys(Alloc)-OH was used to build the tetra peptide scaffold (step 2). De-protection of the four Alloc groups in the side chains with $Pd(PPh_3)_4$ resulted in free amine groups on the side chains (step 3). The amine groups are in close proximity with each other which may suppress their reactivity. Therefore, a prolonged reaction time (8 h) and large excess of GCP were used to ensure the full coupling of amines (step 4). Subsequently de-protection (step 5) and cleavage from the resin (step 6) yielded the crude product. The resulting solid was purified by MPLC to obtain **42** as white solid (5 % yield) with 93 % purity by analytical RP-HPLC.

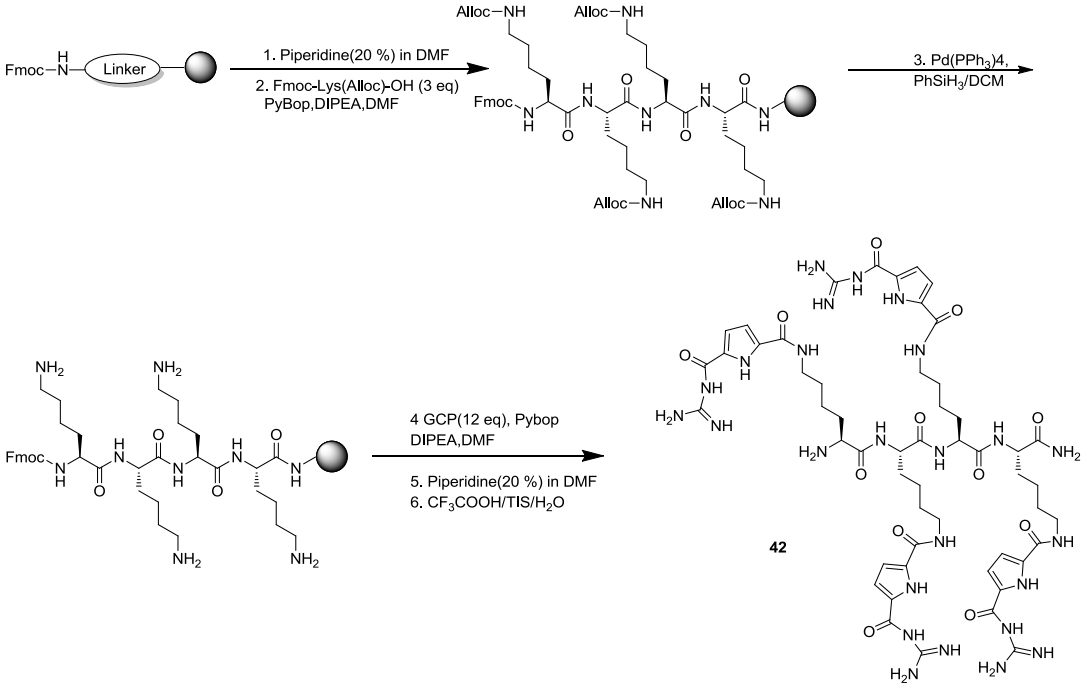

Figure 72. Synthetic route of tetra peptide **42**

4.2.1.2 Synthesis of control tetra peptide 43 and 44

Two control peptides arginine tetramer **43** and lysine tetramer **44** were synthesized for comparisons in DNA binding and gene transfection experiments. Commercially available amino acid Fmoc-Arg(Pbf)-OH was used to synthesize peptide **43** (Figure 73) After de-protection (step 3) and cleavage from the resin (step 4), the resulting solid was purified by MPLC to obtain **43** as white solid (19% yield) with 90 % purity by analytical RP-HPLC.

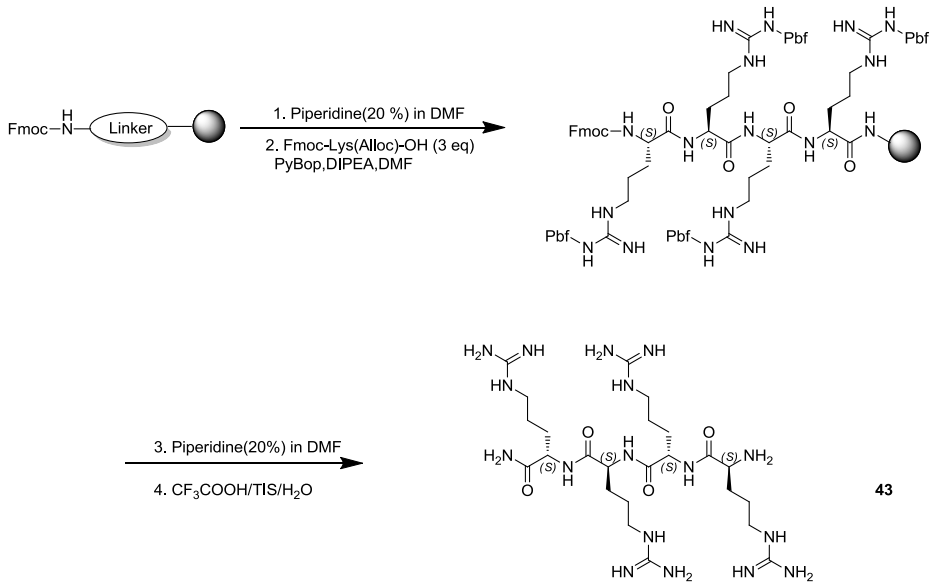

Figure 73. Synthetic route of tetra peptide **43**

Lysine tetramer **44** was prepared with commercially available amino acid Fmoc-Lys(Boc)-OH (Figure 74). After de-protection (step 3) and cleavage from the resin (step 4), the resulting solid was purified by MPLC to obtain **44** as white solid (10 % yield) with 90 % purity by analytical RP-HPLC. .

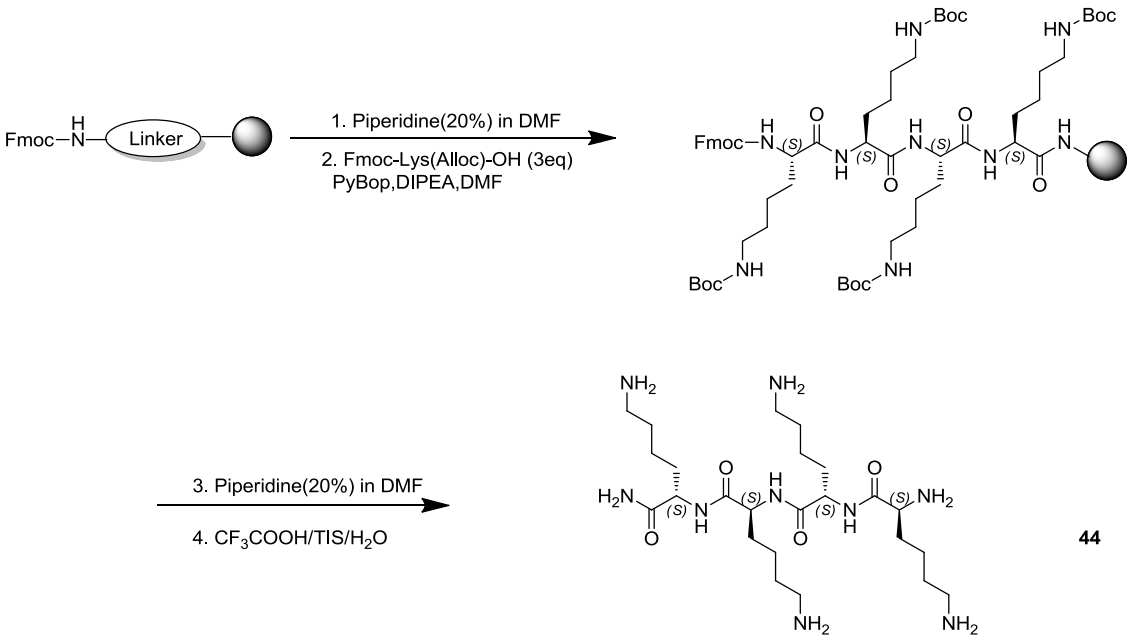

Figure 74. Synthetic route of tetra peptide **44**

4.2.2 DNA binding study

The binding affinity of these GCP modified tetra peptide analogues with DNA was first

studied with isothermal titration calorimetry (ITC) and ethidium bromide (EB) displacement assay. Both techniques serve as reliable means to examine the binding affinity of designed DNA binding molecules. Additional thermodynamic binding profiles can be obtained with ITC experiments. Commercially available fragmented calf thymus DNA (ctDNA) was selected as model DNA.

Ethidium bromide is a red phenanthridine dye which can intercalate into nucleic acids. Its fluorescence emission at 600 nm increases by a factor of 50-100 upon binding to DNA. Ethidium bromide ́s binding constant with DNA was determined around 10^6 M^{-1} in buffered water at pH 7.5. Addition of DNA-binding molecules such as the tetra peptide analogues could displace ethidium bromide from its EB/DNA complex which consequently results in a reduction of the EB emission band around 600 nm. The amount of ligand necessary to displace EB (EC_{50}) is the most important information obtained from EB displacement assay to evaluate the binding affinity. However, it should be noted that only differences of ca. one order of magnitude or greater can be considered as significant due to the approximative character of EC_{50} value. Furthermore, EC_{50} values are only comparable for the same type of DNA due to different binding modes of ligands to nucleic acid sequences.

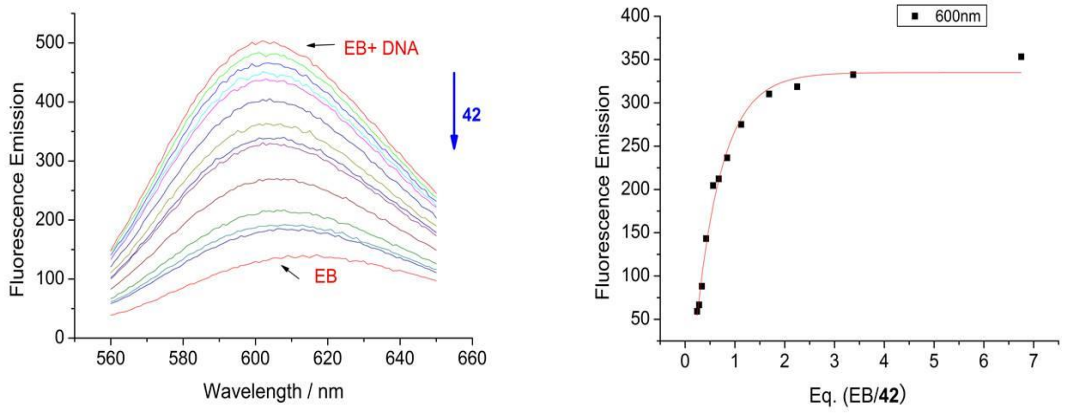

Figure 75. EB displacement titration assay. **42** was added in aliquots (left); Excerpt at 600 nm corrected for EB ́s own emission, fitted with exponential decay first order function (right).

Ethidium bromide (0.75 µM) was pre-incubated with ctDNA (3.0 µM) for 15 minutes. Afterwards, peptide **42** was added to the solution EB/DNA. The aliquot addition of **42** resulted in decrease of the fluorescence emission intensity at 600 nm indicating that peptide **42** displaced EB molecules through its binding with DNA (Figure 75). Other peptides

displayed similar behavior when they were added to EB/DNA solution (see experimental section). The EC_{50} values for each peptide were thus obtained as shown in Table 2.

Table 2. EC_{50} values of different peptides obtained in EB displacement assay. 0.01M sodium cacodylate buffer at pH 7: [ctDNA] = 3.00 μM, [EB] = 0.75 μM.

peptide	**42**	**62**	**63**	**64**	**43**	**44**
EC_{50} (μM)	0.85	1.51	1.50	1.31	0.89	0.85

As can be seen above, the concentrations of peptide analogues necessary to displace half of the EB molecules from its DNA complex were very similar to each other. Although tetra GCP modified peptide **42** and control peptides arginine tetramer **43** and lysine tetramer **44** required less amounts, such difference is negligible in EB displacement assay. This result indicated that all these tetra peptide analogues bind to DNA with similar affinity.

ITC experiments were thus conducted to study the thermodynamic signature of these tetra peptide analogues with DNA. The binding constants of each peptide with DNA were directly obtained as well the contributions from enthalpic and entropic forces (Table 3). The results suggested that functionalization with GCP groups significantly enhanced the binding affinities of these peptides (10^6) about one magnitude compared to original tetra lysine peptide (10^5). However, these peptide analogues did not exhibited stronger binding with DNA compared to tetra arginine peptide. Moreover, the differences in the binding constants between these peptide were not significant taking into account the experimental and calculation errors in ITC.

Table 3. ITC binding data of peptide analogues (50 μM) with DNA (0.7 mM to 1.4 mM) in 0.01M pH 7.4 cacodylate buffer.

Peptide	**Sequence**	**K_d** M^{-1}	**ΔH** kcal/mol	**TΔS** kcal/mol
42	NH_2-G'G'G'G'-$CONH_2$	$2.19 \cdot 10^6$	-25.6	-16.9
62	NH_2-KG'G'G'-$CONH_2$	$9.05 \cdot 10^6$	-23.3	-13.8
63	NH_2-G'KKG'-$CONH_2$	$1.35 \cdot 10^6$	-2.86	5.55
64	NH_2-KKKG'-$CONH_2$	$1.24 \cdot 10^6$	-1.63	6.71
43	NH_2-RRRR-$CONH_2$	$9.23 \cdot 10^6$	-12.3	-2.84
44	NH_2-KKKK-$CONH_2$	$2.52 \cdot 10^5$	-2.87	4.64

Despite the overall similar binding affinities of these peptide analogues, their thermodynamic profiles of the binding process with DNA were quite different. Table 3 clearly showed that the binding between DNA and control peptide **44**, lysine tetramer, was mainly driven by entropy. However, modification of tetra lysine with GCP groups demonstrated amazing ability of shifting the thermodynamic signature to an enthalpically derived binding as GCP moiety has a much stronger hydrogen bonding ability. In sharp contrast to **44**, the binding profiles of peptide **42** and **62** with DNA shifted strongly towards enthalpy. Enthalpy contribution for peptide **62** increased to - 23.3 kcal/mol which was almost 10 fold stronger as that of **63** (-2.86 kcal/mol). The enhancement in enthalpy contribution was even more significant in the case of peptide **42**. Most likely, this enhancement in enthalpy is due to the fact that both peptides possess more GCP groups than positively charged ammoniums. Thus the binding contributions from the recognitions between GCPs and DNA phosphates overwhelmed the contributions from simple charge interactions. The binding processes of peptides **63** and **64** with DNA were still mainly driven by entropy with minor contributions from enthalpy. This is not surprising since there are less GCP groups than positively charged

ammoniums in both peptides. As consequence, their bindings with DNA is mostly driven by the release of counter cations from DNA backbone.

Taken together, the results suggested that with more GCP group modifications, the binding between peptide and DNA became more enthalpy favored. However, entropic contribution to the binding process became significantly negative along with more GCP modifications. Plotting of entropy with enthalpy contributions of the binding data resulted in a fine linear relationship which is a typical sign of entropy-enthalpy compensation (Figure 76). Such entropy-enthalpy compensation is characteristic of specific complex formation.[296]

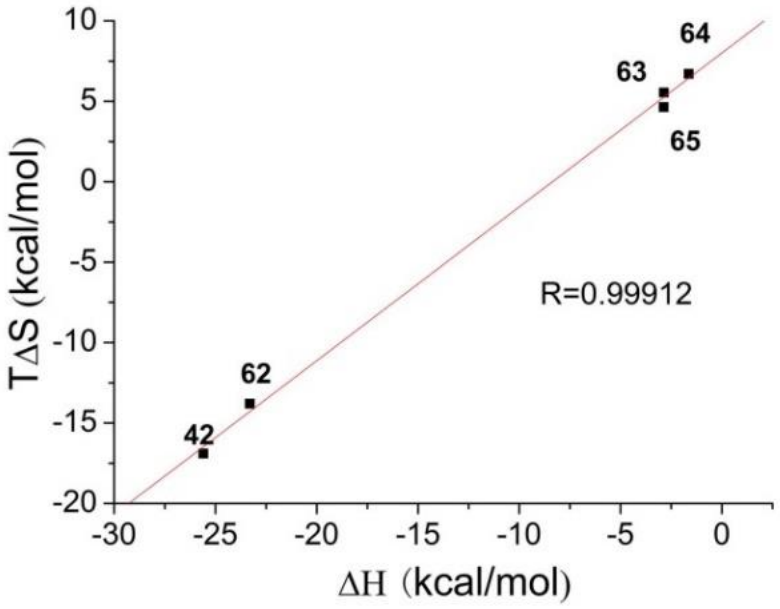

Figure 76. Plot of entropy with enthalpy contributions of binding data

Notably, similar compensation effect has been reported earlier with totally different peptide sequences containing GCP group modifications.[297] Thus, the ability of GCP moiety of shifting the binding thermodynamics towards enthalpy is independent on the sequence of the peptides. It is also worth pointing out that GCP group not only enhanced the hydrogen bonding abilities of these peptide analogues, they also became more hydrophobic compared to unmodified peptide **44** as determined by their elution profiles of HPLC.

The condensation ability of these tetra peptide analogues with DNA was tested by dynamic laser scattering (DLS) and atomic force microscopy (AFM). DLS measurements can provide information on the size and charge state of the formed DNA/peptide complexes. AFM results

are valuable in the determination of the morphology of those complexes or aggregates.

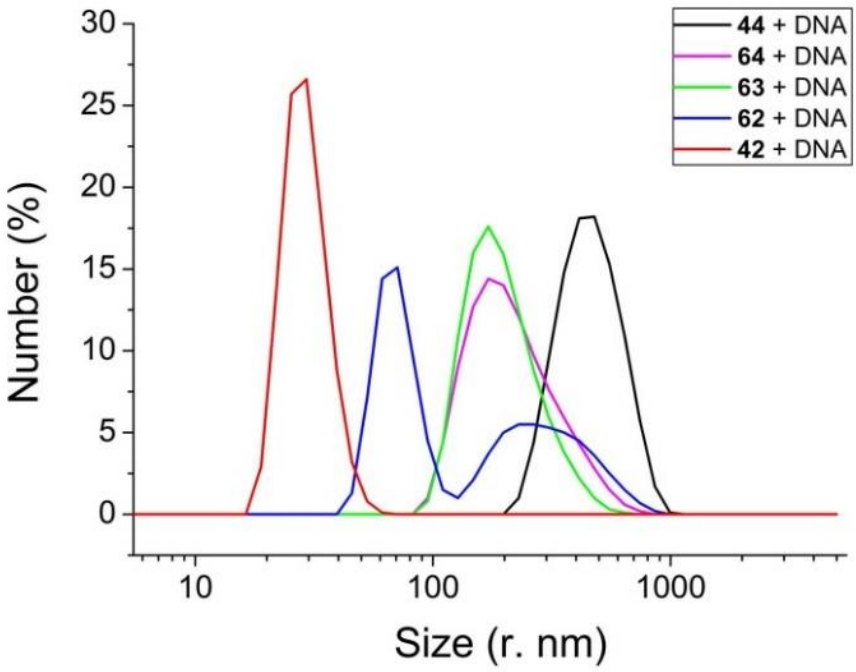

Figure 77. Number distribution of the size of aggregates formed by 3 eq. peptide analogues (150 μM) and DNA (50 μM) in pH 7.4 cacodylate buffer

DLS results demonstrated that all peptides exhibited excellent DNA condensation ability. For each measurement, three equivalence of peptide analogues (relative to DNA phosphate concentration) were used to complex DNA. Aggregates with sizes ranging from 20 nm to 500 nm were well observed in cacodylate buffer solution for the studied peptide analogues (Figure 77). However, the DNA condensation abilities of these peptides were quite different. Control peptide lysine tetramer **44** was only able to condense DNA into complexes or aggregates around 500 nm. Two GCP groups modified peptide **63** and mono-GCP peptide **64** exhibited better condensation ability as the size of both aggregates formed were around 200 nm. In contrast to this, tetra-GCP peptide **42** and tri-GCP peptide **62**, which were characterized by their enthalpic binding mode with DNA, exhibited significantly enhanced DNA condensation ability. The aggregates formed by peptide **42** and **62** with DNA (20 nm and 60 nm, respectively) were much smaller than that of **63** and **64**. Clearly, with more GCP group modifications, the binding between peptide analogues and DNA became more enthalpy favorable which eventually resulted in the formation of more compacted aggregates.

This result was also confirmed with AFM studies. Figure 78 showed that those peptide

analogues formed particle–like aggregates with DNA under this ratio. The particles formed from tetra-GCP modified peptide **42** with DNA were significantly smaller compared to that of lysine tetramer **44**.

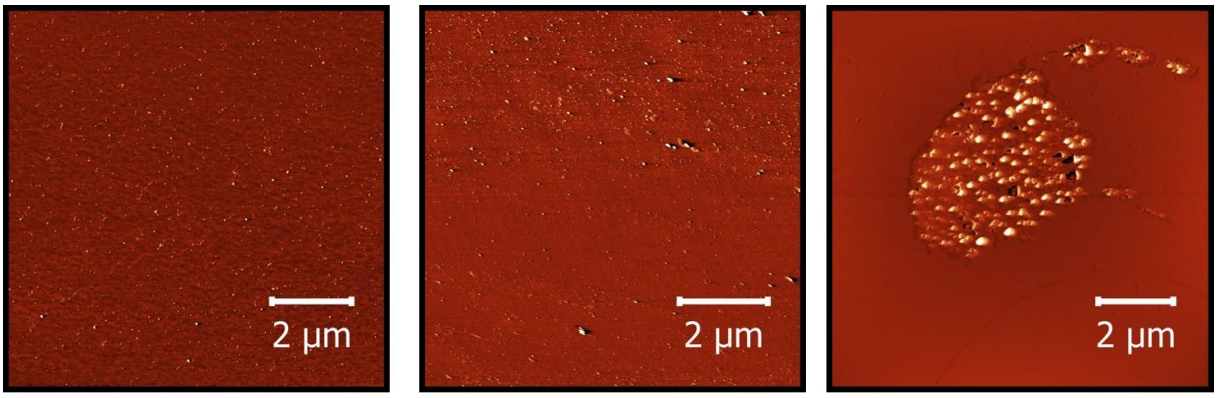

Figure 78. AFM phase images of aggregates formed by 3eq. peptide analogues and DNA

Another important feature of DNA aggregates for potential gene transfection experiments is their charge state. Cell membrane is highly negatively charged. Therefore, aggregates with negative charges are generally considered not favorable in the cellular uptake process for gene delivery. Charge state can be examined with DLS. As shown in Figure 79, DNA molecules were highly negatively charged (-30 mV) before the addition of peptide analogues. Upon addition of positively charged peptides, DNA was condensed stepwise to neutralize the negative charges. Tetra lysine peptide **44** exhibited rather weak neutralization ability. Six equivalences of **44** were required to achieve full neutralization. Tetra arginine **43** displayed better condensation ability as the negative charges of DNA were neutralized with three equivalences of **43**. Modification with GCP moiety significantly improved the neutralization ability of tetra lysine **44**. For example, addition of three equivalences of peptide **61** and **62**, both with three GCP groups functionalization, were sufficient to fully neutralize DNA molecules. Moreover, the complexes formed with peptide **61** and **62** under this ratio possessed more positively charges (+20 mV). This phenomenon is even more significant in the case of tetra-GCP peptide **42**.

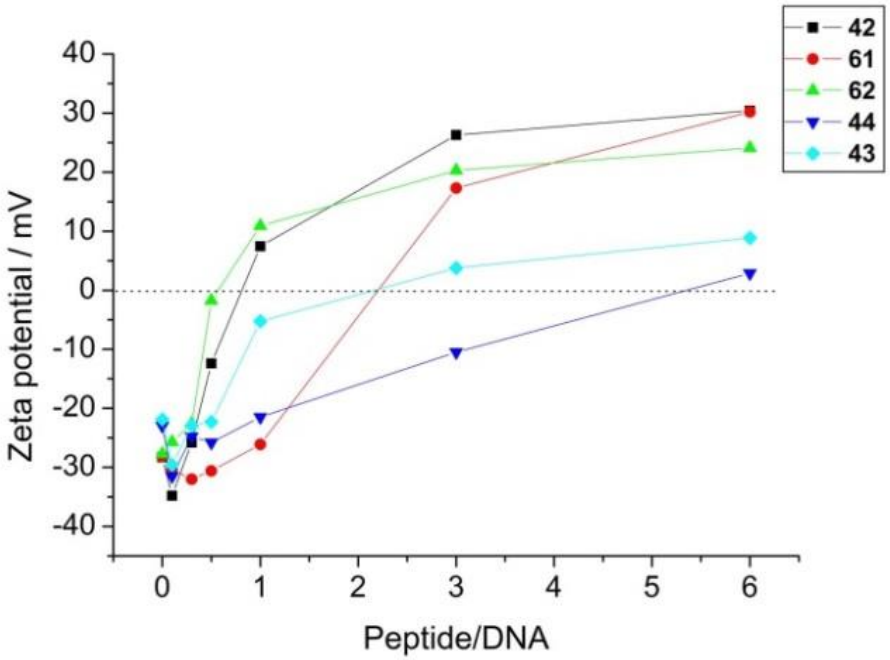

Figure 79. Zeta potential measurements of different ratio of peptide analogues and DNA

4.2.3 Gene delivery study

Since these peptide analogues are capable of condensing DNA into particle-like positively charged aggregates, we next tested their gene transfection ability in HeLa cell lines. Different concentrations of peptides were used to study their gene delivery ability. Commercial available PEI was applied as positive control. These peptides were directly mixed with green fluorescence protein (GFP) plasmid DNA, a typical reporter gene used in gene delivery study. No other reagents were required such as helper lipid which is normally necessary for other transfection systems. The mixture was allowed to incubate for 5 minutes at room temperature to ensure completely DNA condensation. Afterwards, the mixtures was added to cell culture medium and the transfection results were examined 24 and 48 hours after incubation. The expression of GFP gene in cell nucleus results in the production of green fluorescence protein which can be observed with fluorescence microscopy. The cell experiment was conducted with the cooperation from prof. Shirley Knauer in biology department with the help of Stefanie Schlesiger.

4.2.3.1 Gene transfection ability

Transfection with peptides with less than four GCP modifications, however, did not

succeed (Figure 80). Only very few cells displayed fluorescence signals after 24h and 48h incubations in the case of tri-GCP modified peptides **61** and **62**. Such weak signals indicated that the plasmid DNA complexes formed with these peptide analogues either did not enter into cells or failed to escape from endosomes. Also, it can be concluded that peptide sequences have no influences on the gene transfection ability of these peptides.

Transfection with tetra-GCP modified peptide **42** resulted in significantly different results. As can be seen in Figure 93, **42** successfully transported plasmid DNA into cells. Most of the cells transfected with **42** exhibited green fluorescence similar to that of positive control PEI. The transfection efficiency of **42**, defined as the percentages of transfected cells, was even better than the current golden standard PEI. Considering the low molecular weight and the number of charges of peptide analogue **42** relative to PEI, the transfection ability of **42** was even more remarkable. In comparison, tetra lysine peptide **43** and arginine tetramer **44** did not showed any transfection which in consistent with previous reports that cationic peptides require at least eight positive charges to achieve decent transfection. Moreover, the difference in the transfection results of peptide **42** with respect to **61** and **62** was very surprising. Both **61** and **62** possessed three GCP group modifications, one less than that of **42**. However, such a small structural difference resulted in a totally different transfection outcome.

We also tested the transfection ability of peptide **42** under different concentrations. The results showed that peptide **42** delivered plasmid DNA into cells in a concentration-dependent manner. A minimum amount (0.05 mM) of peptide **42** was required as can be seen in Figure 81. When the concentration increased to 0.25 mM per well, the efficiency of transfection with **42** decreased possibly due to its toxicity at this concentration.

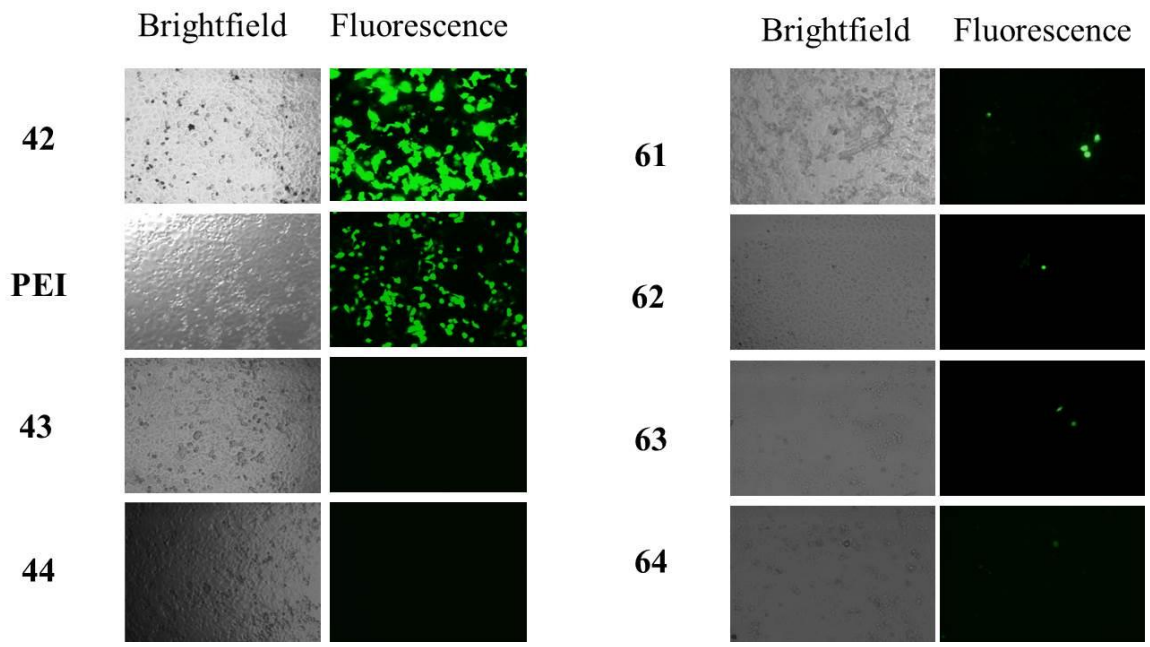

Figure 80. Transfection results of 0.15 mM peptide and 2 μg GFP plasmid in each well

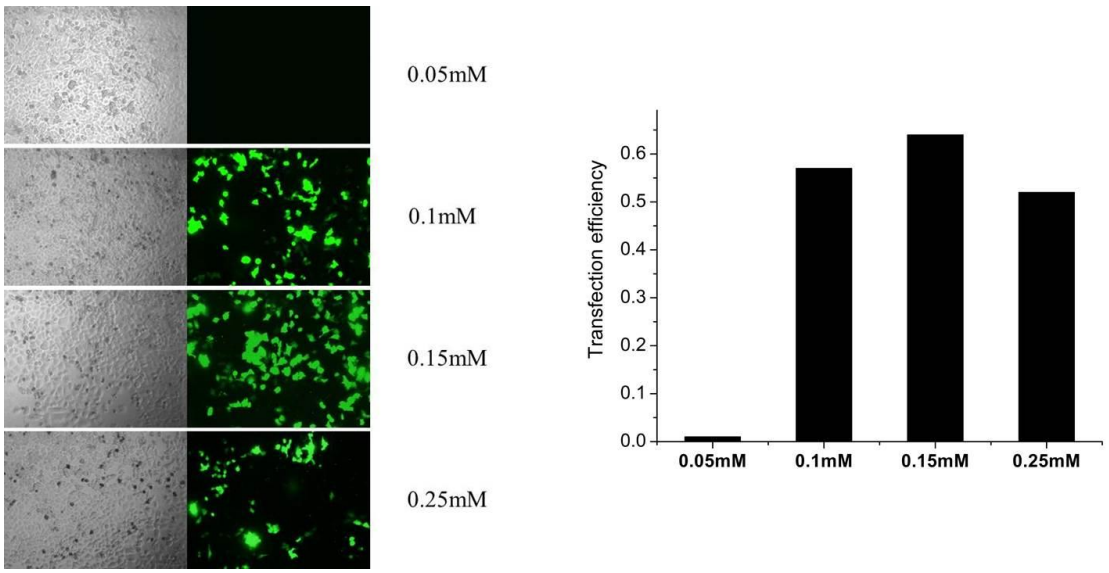

Figure 81. Transfection results with different concentrations of peptide **42**

To further confirm the transfection results obtained above, these tetra peptides were also tested in human embryonic kidney cell line HEK-293 and in murine embryonic fibroblast cell line NIH/3T3. As shown in Figure 82, only tetra-GCP modified peptide **42** enabled successful transfection of the cells with a plasmid encoding GFP. Other peptide analogues did not show any detectable transfection. This result implicated that peptide **42** can be applied as a general gene transfection vectors irrespective of the type of cells.

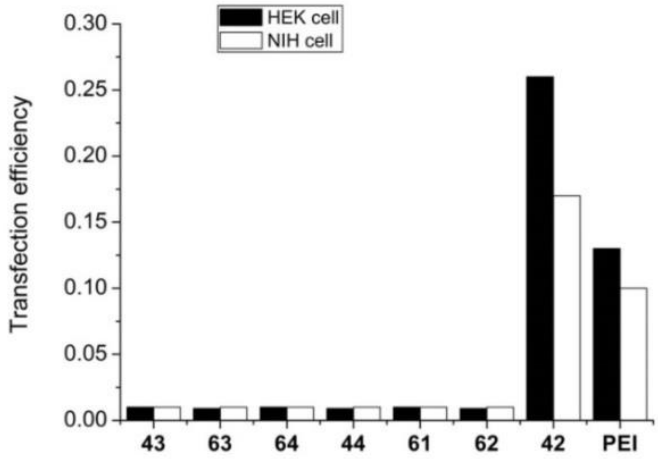

Figure 82. Transfection efficiency of peptide analogues in HEK and NIH cell lines. 0.15 mM peptide and 2 μg GFP plasmid were incubated with HEK and NIH cells for 24 hours and examined with fluorescence microscopy.

4.2.3.2 Gene transfection mechanism

To elucidate the origin of the dramatically improved transfection efficiency of tetra-GCP peptide analogue **42** compared to the other tetra peptides, transfection experiments with the addition of chloroquine or bafilomycin were conducted.

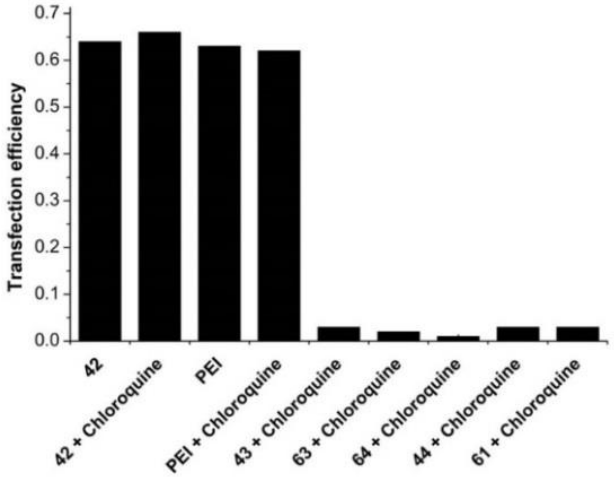

Figure 83. Transfection efficiency of peptide analogues with the addition of chloroquine

The release of the transported DNA from the endosome into the cytosol is often a critical step in gene transfection. The addition of chloroquine, a weak organic base, increases the

buffer capacity within the endosome and facilitates cargo release. However, chloroquine had no effect on the cells transfected by other tetra peptides including arginine tetramer **43** and lysine tetramer **44** (Figure 83). This suggested that hardly any cellular uptake occurred in the case of **43** and **44**. Thus, the main reason for the increased transfection efficiency of peptide analogue **42** relative to other peptide analogues is its enhanced cellular uptake, which most likely originates from a more specific binding interaction between the GCP group in **42** and negatively charged groups on the cell membrane. Moreover, chloroquine did not increased the transfection efficiency of peptide **42** which indicated that the DNA molecules transfected into cells by **42** were not entrapped in endosomes.

Besides the better uptake of **42**, the low pKa value of the GCP group also results in an increased buffering capacity within the endosomes, which facilitates endosomal escape by the proton-sponge effect. Accordingly, DNA transfection by **42** was completely inhibited by bafilomycin, which blocks the endosomal acidification process (Figure 84). In consequence, the DNA stayed trapped within the endosome and was degraded there before transfection occurs. This effect can also be observed with PEI mediated gene transfection process. PEI vector is known to utilize proton sponge effect to release the condensed DNA from endosome. The replacement of arginine by an artificial GCP-containing amino acid thus not only enormously enhances the endosomal uptake of peptide/DNA complexes by cells, but also facilitates the necessary release of the DNA from the endosomes to ultimately enable gene transfection.

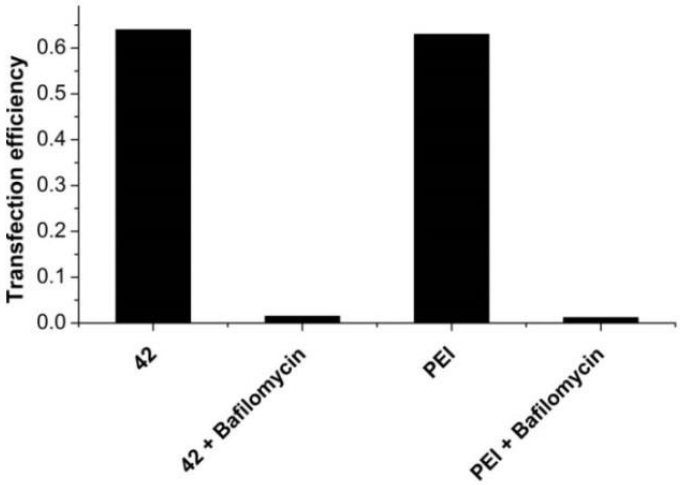

Figure 84. Transfection efficiency of peptide analogues with the addition of bafilomycin

4.2.3.3 Cell cytotoxicity

Important for the applications of a new artificial transfection vector is its cytotoxicity, which for these tetra peptide analogues was examined in HeLa cells by measuring metabolic activity as an indicator of cell viability. Toxicity was negligible at 0.15 mm, the concentration at which **42** mediated DNA transfection experiments, while in the case of PEI, cell viability was reduced by nearly 70% (Figure 85).

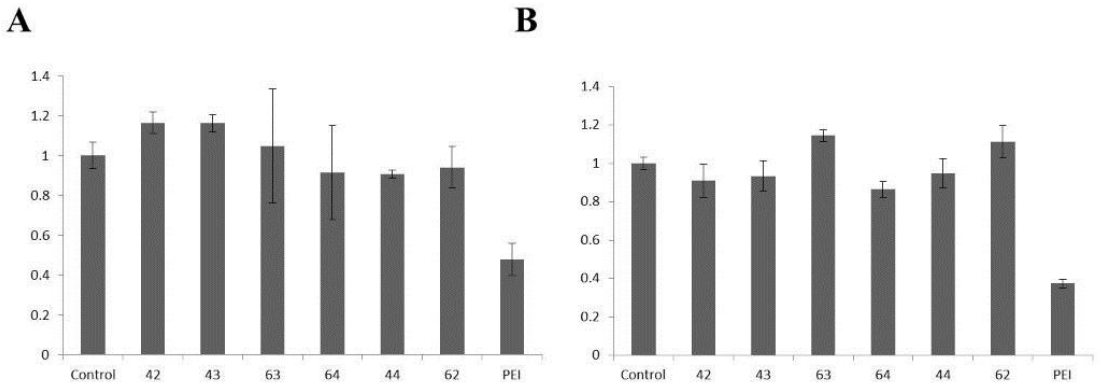

Figure 85. Alamar blue assay of 0.15 mM each peptide in gene transfection experiment A) 24 hours B) 48 hours after transfection. Cytotoxicity was normalized for control group without any treatment.

In conclusion, the introduction of the GCP moiety in the side chain of tetra lysine resulted in a novel strategy to shift the thermodynamic signature of peptide DNA binding. Enthalpy contribution to binding process was significantly enhanced when the interaction between GCP and DNA were dominant. The exclusively enthalpically driven binding mode of peptide **42** with DNA eventually led to higher compacted peptide-DNA complexes. This enormously enhances the cellular uptake of corresponding peptide/DNA polyplexes relative to peptides with only natural amino acids. Tetra-peptide **42** with only four of these artificial GCP groups is a highly efficient transfection vector, even better than the commercial reagent PEI but at the same time with significant lower cytotoxicity.

4.3 Development of a cyclic peptide nanotube based gene delivery vector

The enhancement of cellular uptake and gene transfection ability of GCP moiety on short peptides was successfully demonstrated by the last two projects. We therefore determined to introduce GCP group into a cationic cyclic peptide. Cyclic peptides constructed with alternative D and L amino acids possess unique properties of assembling into nanotubes. However, this type of nanotubes normally cannot be positively charged under physiological conditions since charge repulsion then prevents tube formation. Unfortunately, positive charges are usually critical for DNA binding and also gene transfection due to the anionic nature of DNA. We thus designed a cyclic octamer peptide **45** and control peptide **65** to study their aggregation behavior and gene transfection ability (Figure 86).

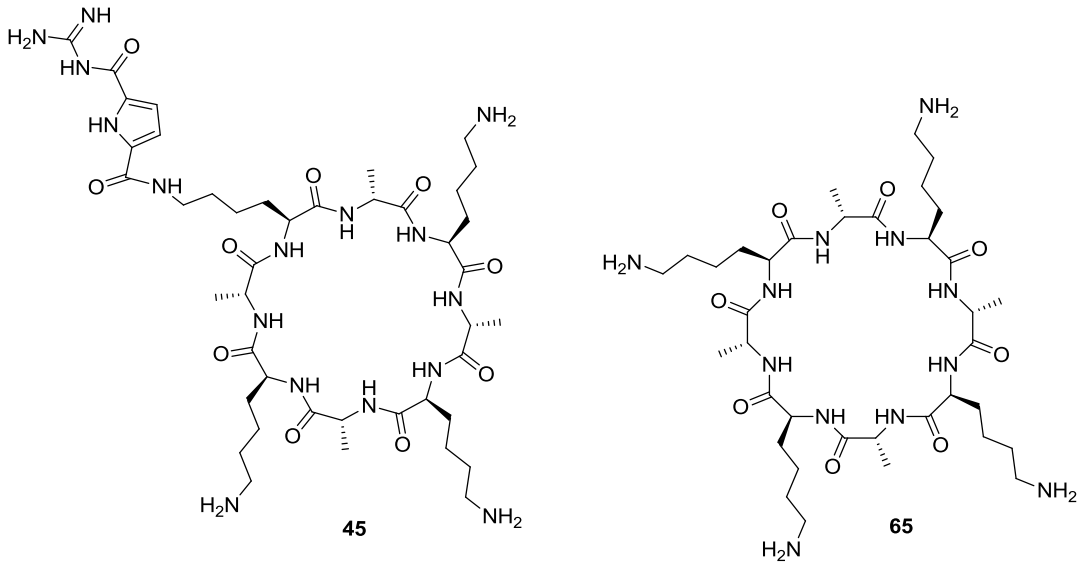

Figure 86. Chemical structures of cyclic peptide **45** and **65**.

4.3.1 Synthesis of cyclic peptides

Cyclic peptides are more difficult to synthesize. The cyclization process is always accompanied by unwanted polymerization reaction. Two strategies of cyclization have thus been developed for the preparation of cyclic peptides: on-resin cyclization and in solution cyclization. On-resin strategy utilizes the *pseudo* dilution effect of solid phase which suppresses the formation of oligomers. On the other hand, in solution cyclization requires highly diluted conditions and careful adjustments of reaction parameters such as temperature,

stirring speed etc. Nevertheless, the advantage of this strategy is that it allows the preparation of large quantity of cyclic peptide. Therefore, we decided to use the in solution method to synthesize the target cyclic peptides.

4.3.1.1 Synthesis of cyclic peptide 45

The linear precursor of **45** was first synthesized on solid phase using Fmoc strategy. 2-chlorotrityl chloride resin was selected. This resin is featured with a 2-chlorotrityl chloride functional group. The first amino acid can thus be attached to this resin through esterification under argon protection. Cleavage with acids results in a free carboxyl group in the C-terminus (Figure 87).

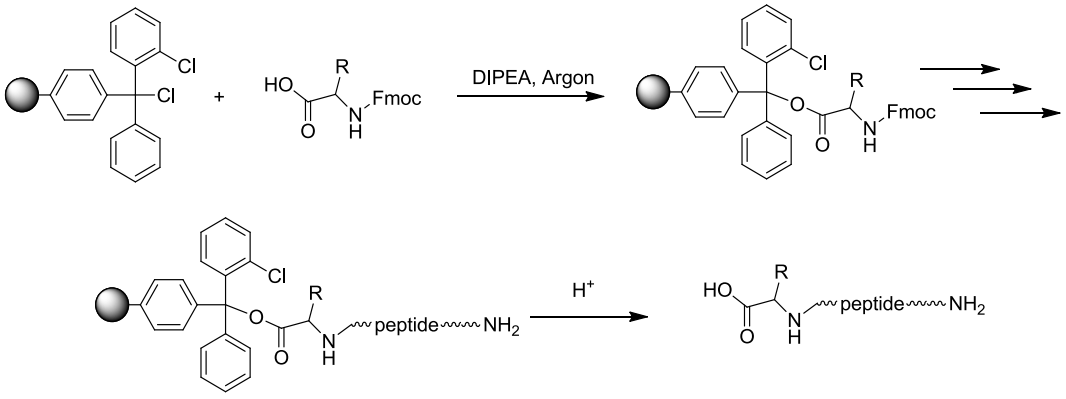

Figure 87. Attachment on 2-chlorotrityl chloride resin and the final cleavage

Commercially available amino acids Fmoc-*d*-Ala-OH, Fmoc-*l*-Lys(Boc)-OH and Fmoc-*l*-Lys(Alloc)-OH were used to build the peptide scaffold (Figure 88). De-protection of the Alloc groups in the side chain with $Pd(PPh_3)_4$ resulted in free amine group on the side chain (step 3). Subsequently GCP coupling (step 4) and Fmoc de-protection (step 5) yielded the linear precursor on the solid phase. Special cares must be taken in the next step of cleavage from resin. The cleavage of peptide segment from 2-chlorotrityl chloride resin requires acidic condition. However, the reaction condition cannot be too acidic avoiding de-protection of the Boc groups on the side chains of lysine. Therefore, a very mild condition with 1% TFA was used to yield the linear precursor **70**.

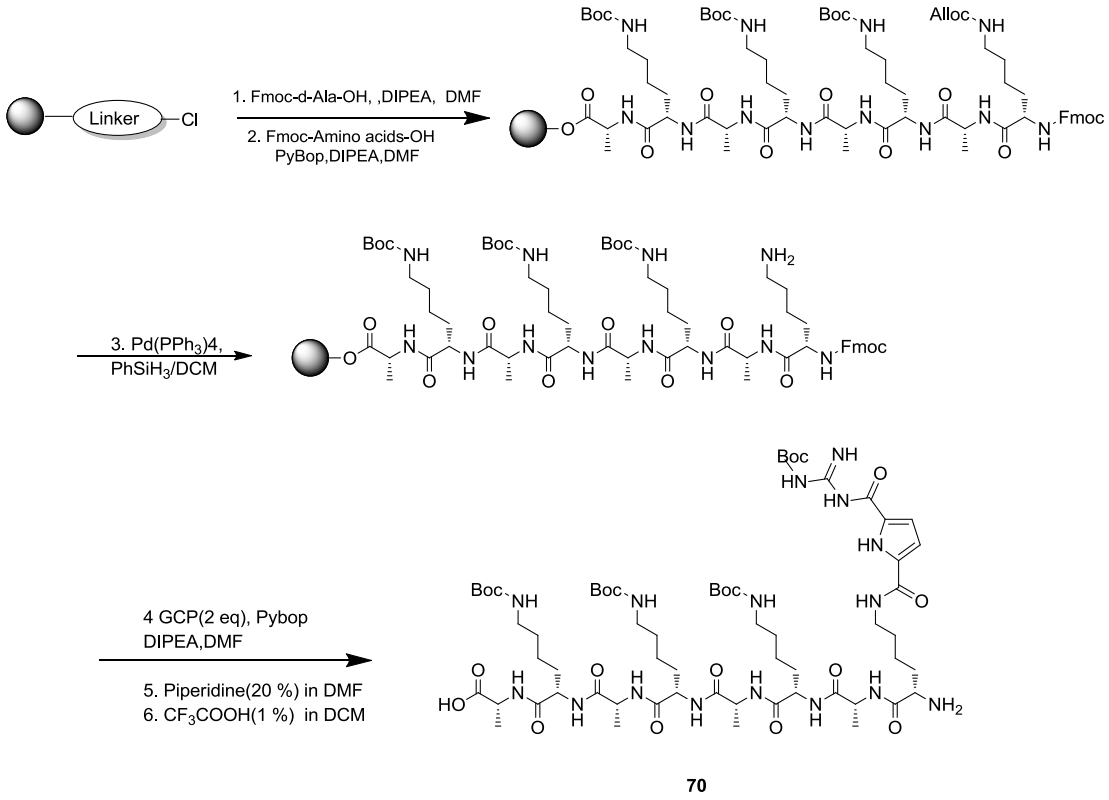

Figure 88. Synthetic route of linear precursor **70**

The linear precursor **70** was directly used for cyclization reaction without purification. Due to the presented carboxyl group and amine group on both terminals, **70** is easily subjected to polymerization or oligomerization through intermolecular coupling reaction. Thus, a highly diluted condition (~0.2 mM) was used for the cyclization process. Moreover, the solution of **70** needs to be cooled down to 0 ℃ before the addition of coupling reagent. Afterwards, DIPEA was added as catalyst slowly under cooling conditions. This procedure is to prevent intermolecular reactions before the fully mixing of the starting material. The cyclization of **70** yielded protected cyclic peptide **71**. Final deprotection and purification gave rise to crude product of **45** as a white solid (Figure 89). The crude product was purified by MPLC on C18 reversed-phase silica gel to obtain **45** as white solid (5 % yield) with 91 % purity determined by analytical RP-HPLC.

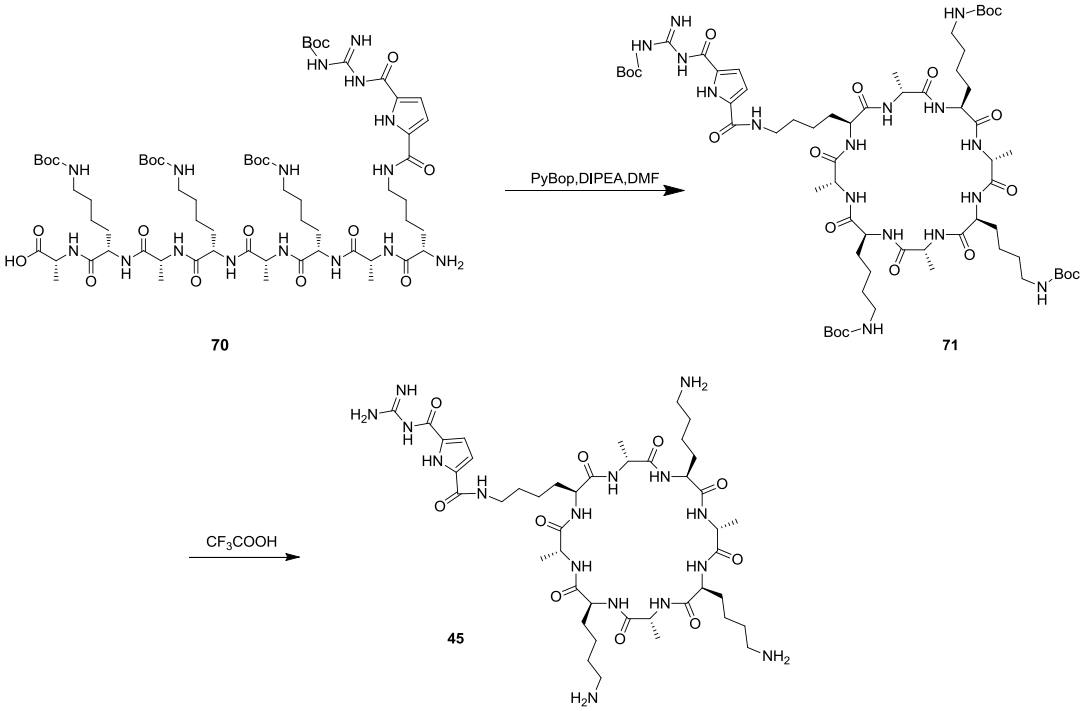

Figure 89. Synthetic route of cyclic peptide **45**

4.3.1.2 Synthesis of cyclic peptide 65

The synthesis strategy for peptide **65** is similar to that of **45**. The linear precursor of **65** was first synthesized on solid phase using Fmoc strategy with 2-chlorotrityl chloride resin. Commercially available amino acid residues Fmoc-*d*-Ala-OH and Fmoc-*l*-Lys(Boc)-OH were used to build the peptide scaffold (Figure 90). Subsequently Fmoc de-protection (step 3) and cleavage yielded the linear precursor **72** as a white solid.

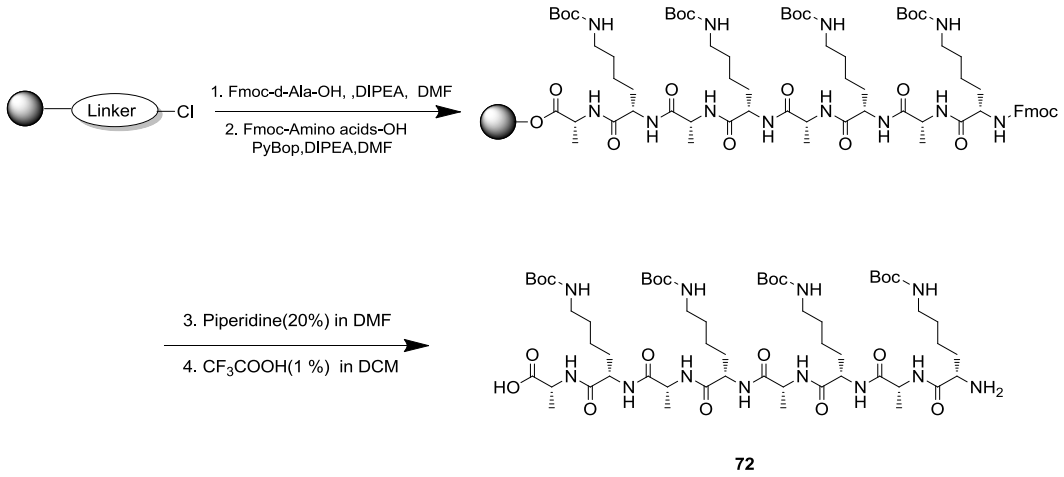

Figure 90. Synthetic route of linear precursor **72**

The linear precursor **72** was directly used for cyclization without further purification. A highly diluted condition (~0.2 mM) was used for the cyclization process under cooling condition as described above. The cyclization of **72** yielded protected cyclic peptide **73**. Final de-protection and purification gave rise to crude product of **65** as a white solid (Figure 91). The crude product was purified by MPLC on C18 reversed-phase silica gel to obtain **65** as white solid (6.5 % yield) with 90 % purity by analytical RP-HPLC.

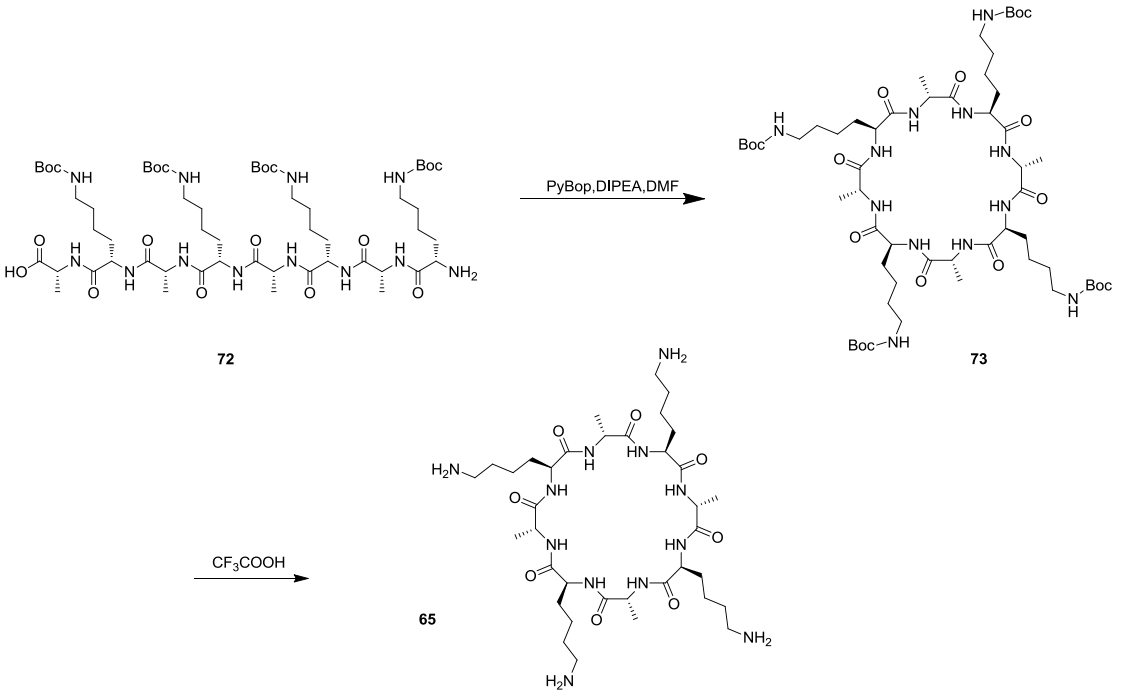

Figure 91. Synthetic route of cyclic peptide **65**

4.3.2 Assembling property of cyclic peptides

The self-assembling abilities of both peptides were first tested by AFM and TEM. As expected, cyclic peptide **65** did not form any ordered nanostructure at pH 7.4 in water (Figure 92). Most likely charge repulsion between the positively charged ammonium groups in the lysine side chains hindered the hydrogen bond induced aggregation of the cyclic peptides. This result was also confirmed with dynamic light scattering (DLS) in solution as no aggregates could be detected.

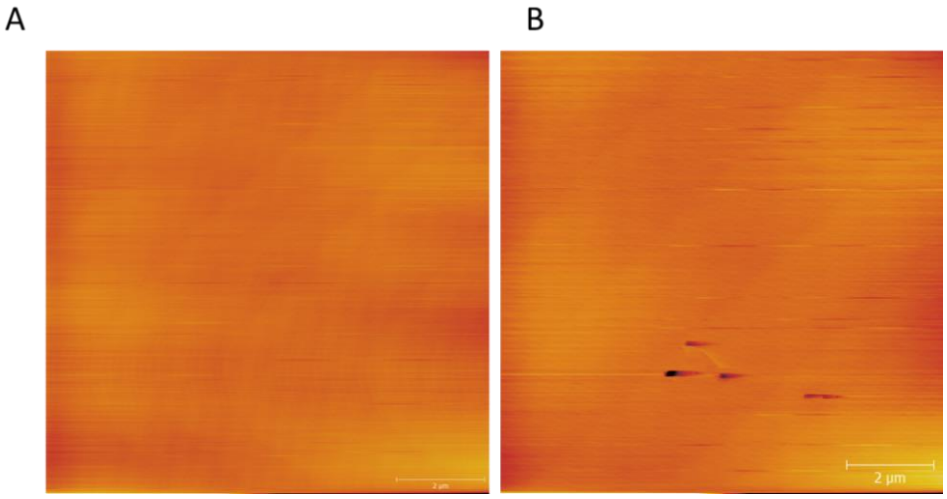

Figure 92. AFM images of 0.1 mM (A) and 0.5 mM (B) of peptide **65** in pH 7.4 H2O.

However, to our surprise, modification of peptide **65** with only a single GCP moiety completely changed the self-assembly behavior. DLS clearly showed that peptide **45** formed large aggregates in buffered water at pH 7.4 (Figure 93); a pH value at which the weakly basic GCP might not yet be fully protonated but the remaining three lysine residues are (amine: pKa~10, GCP: pKa~7). Therefore, as expected at this pH the aggregates are overall positively charged as determined by Zeta potential measurements (+4.08 mV). The size of the aggregates assembled from cyclic peptide **45** was around 1 µm with a rather narrow size distribution.

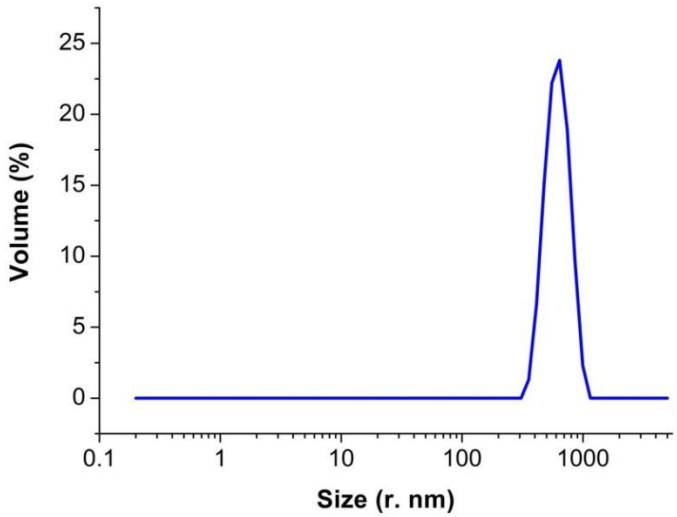

Figure 93. Volume distribution of peptide **45** (0.4 mM) in pH 7.4 cacodylate buffer

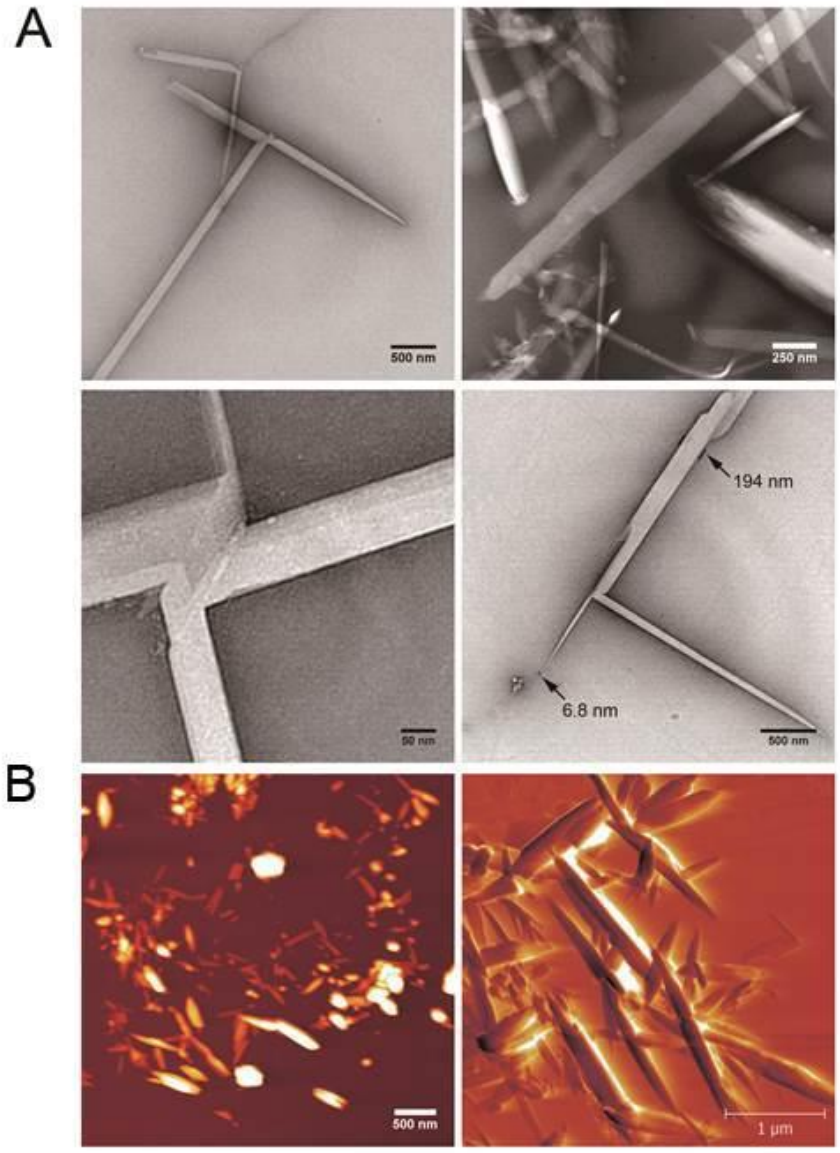

Figure 94. A) TEM and B) AFM images of peptide **45** (0.4 mM, pH 7.4) in water

Moreover, we studied the morphology of the aggregates formed by **45** with transmission electron microscopy (TEM). Due to the organic nature of these peptide assemblies, it must be stained with uranyl formate solution for the visualization of the nanostructures. Tubular structures as typically seen for other self-aggregated cyclic peptides were observed in TEM images (Figure 94A). The lengths of these nanorods-like structures were in the range of micrometers. The majority of assemblies was around 200 nm in width. The smallest ones we could find in the images had a width of ca. 7 nm. Therefore, it can be deduced that the observed the larger assemblies should possess at least 20 smaller units. As consequence, the

wall thickness cannot be obtained convincingly from those images. In AFM images rods or particles with lengths less than 100 nm were also found (Figure 94B). This might due to the different sample preparation protocols for AFM and TEM which could influence the observed nanostructures in microscopy. Nevertheless, the results from AFM and TEM clearly showed that peptide **45** can form nanorod or nanofiber structures at neutral pH. However, the exact internal structure of these aggregates remains so far, unclear.

To elucidate the assembling mechanism of peptide **45**, molecular modelling experiment was conducted by Martin Ehlers. The results suggested that the GCP group in **45** could stabilize the nanotubes by binding to the backbone of an adjacent cyclic peptide (Figure 95). Hence, the GCP groups could function as "extra-clamps" between the stacked cyclic peptides. This binding interaction could provide enough extra stabilization to overcome the charge repulsion of the remaining lysine allowing nanotube formation even for a positively charged cyclic peptide.

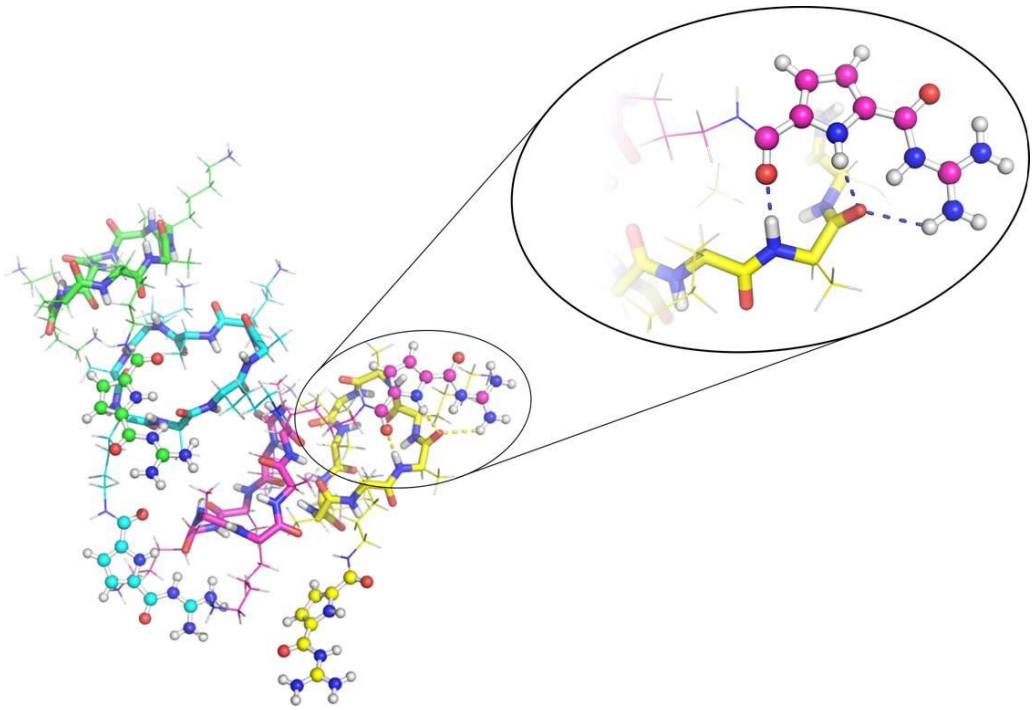

Figure 95. Molecular modelling of peptide **45**

There might be other aspects for the explanation of the assembly behavior of peptide **45**. One further point worth mentioning for example is that peptide **45** is significantly more hydrophobic than peptide **65** as e.g. determined by the retention time of HPLC elution profile (10 % to 40 % methanol/water, 0.1 % TFA: peptide **45** in 17.6 minute, peptide **65** in 6.6

minute). This property may also favor the aggregation of peptide **45** in water relative to **65**. Nevertheless, it is without doubt that a positively charged cyclic peptide nanofiber or nanotube was formed through the assembling of **45**.

4.3.3 Transfection study of cyclic peptides

4.3.3.1 DNA binding ability

We next tested the DNA binding ability of these cationic nanotubes, the premise for any gene transfection vector. Addition of ctDNA solution to the aggregates form by peptide **45** did not significantly change their overall size (Figure 96). The size of peptide **45**/DNA complexes was around 900 nm which correlated well with the size of the assembly formed by peptide **45** (1 μm). This indicated that DNA molecules did not disrupt the assembled tubular structures of peptide **45**.

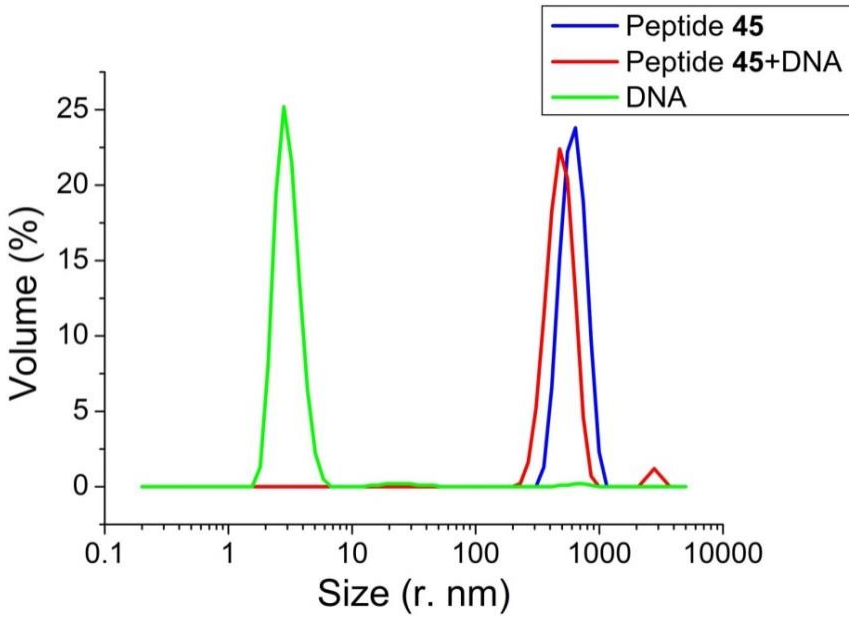

Figure 96. Volume distribution of peptide **45** (0.4mM) and its mixture with ctDNA in pH 7.4 cacodylate buffer

The morphology of the assembly formed with **45** was also retained as shown in Figure 97. Tubular structures were well observed in TEM images after the addition of ctDNA. Moreover, it can be seen that DNA molecules were attached on the surface of nanotubes. This is most likely due to the cationic nature of peptide **45** which provides attractive electrostatic

interactions with negatively charged DNA backbones.

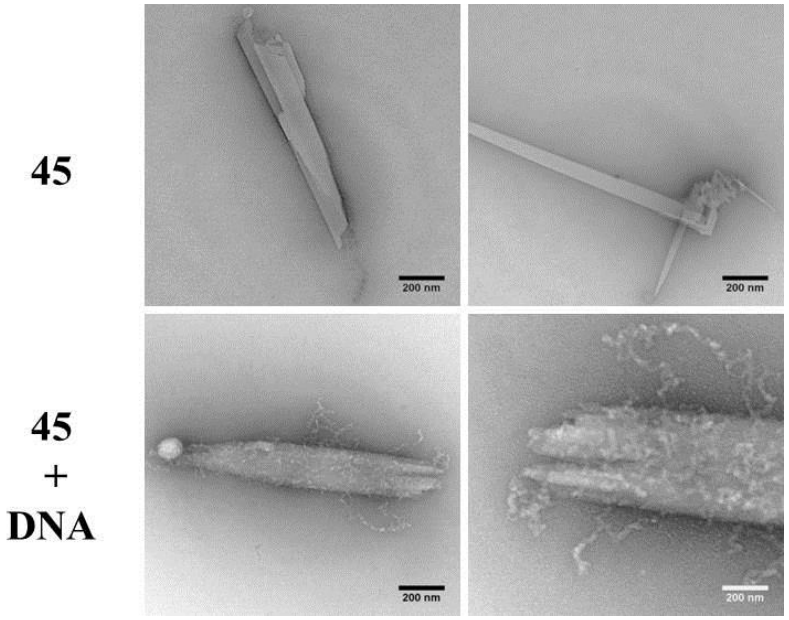

Figure 97. TEM images of peptide **45** and its mixture with ctDNA in pH 7.4 H_2O

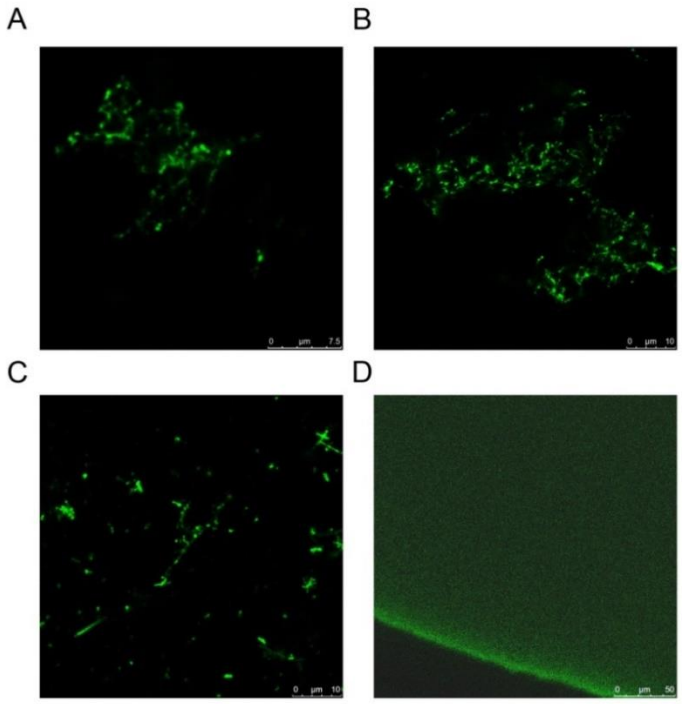

Figure 98. Fluorescence images: (A, B, C) mixture of peptide **45** and labeled DNA; (D) droplet of labeled DNA

To further confirm the results, we labeled plasmid DNA with green fluorophore with the PromoFluor-500 Nick Translation Labeling Kit (PromoKine) according to the manufacturer's

instructions and mixed it with peptide **45**. The resulting mixture was directly examined with confocal fluorescence microscopy. Figure 98 clearly showed that labeled DNA was successfully attached onto the peptide nanotubes which must be formed from the assembling of peptide **45**. As comparison, only diffusive fluorescence signals can be observed in a single droplet of the labeled DNA without the addition of peptide **45** nanotube.

4.3.3.2 Gene transfection ability

As DNA obviously attaches to the nanotubes, we determined whether the peptide nanotubes could be applied as vectors in gene delivery. Therefore, green fluorescent protein (GFP) plasmid, a typical used reporter DNA in gene transfection, was mixed with the peptide nanotubes. The resulting mixture was directly subjected to HeLa cells. No other helper molecules such as lipids were added which are often required for other artificial transfection vectors to enable gene transfection. The widely used, commercial available polycationic polymer polyethyleneimine (PEI) was used as a positive control. The cell experiment was conducted with the cooperation from prof. Shirley Knauer in biology department with the help of Stefanie Schlesiger.

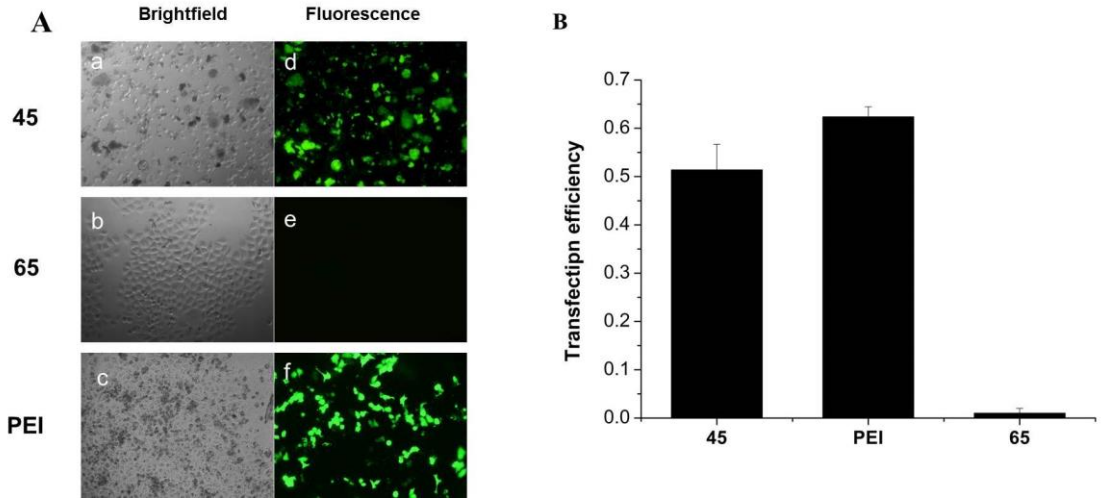

Figure 99. A) Transfection results with 2 µg pF143-GFP plasmid using **45**, **65**, or PEI (all 0.4 mM). Brightfield (a–c) and fluorescence images (d–f) of HeLa cells 24 h after transfection with **45** (a, d), **65** (b, e), or PEI (c, f) B) Transfection efficiency of peptide **45**, **65**, or PEI (all 0.4 mM)

Transfection results were imaged 24h after incubation with HeLa cells. As shown in Figure

99A, peptide **65**, being even more positively charged than **45** but not forming any nanotubes, was not able to transfer plasmid into cells. In striking contrast to this, the nanotubes formed by peptide **45** successfully transported the GFP plasmid into cells as seen by the expression of the green fluorescent protein. Moreover, the transfection efficacy of peptide **45** was even comparable to PEI (Figure 99B) which highlighted the utilization of supramolecular nanotubes in gene transfection experiments.

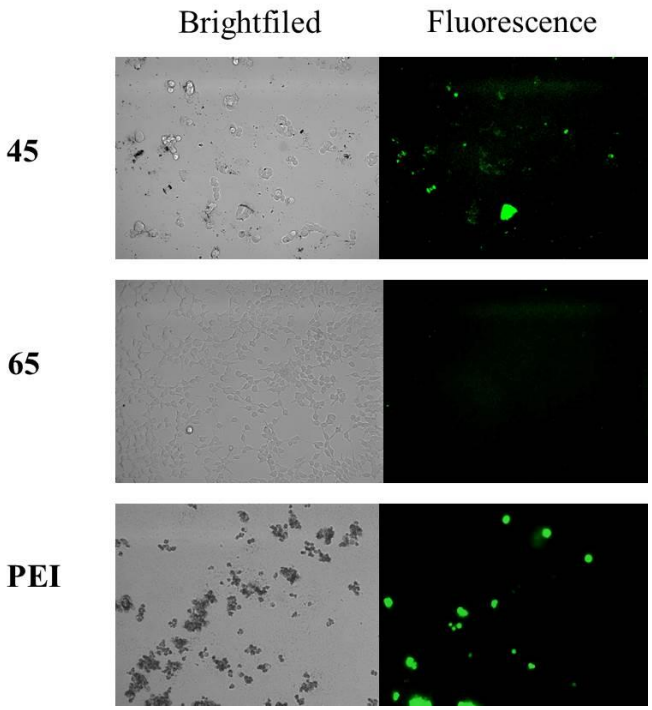

Figure 100. Transfection results with 2 μg pF143-GFP plasmid using **45**, **65**, or PEI (all 0.4 mm) in HEK cell lines 24h after incubation

The transfection ability of cyclic peptide analogue **45** was also confirmed in human embryonic kidney HEK-293 cell lines. As shown in Figure 100, control peptide **65**, unable to form any nanotubes, did not show any detectable transfection. In contrast, peptide **45** still enabled the transfection of plasmid DNA into HEK cells although with a lower transfection efficiency than in HeLa cells. The reason for the decreased efficiency is however unclear. Anyway, cyclic peptide nanotubes formed from the assembling of **45** has the potential to serve as an universal gene delivery vector in future study.

4.3.3.3 Gene transfection mechanism

To further elucidate the mechanism of gene transfection result by peptide **45**, transfection experiments with the addition of either chloroquine or bafilomycin were conducted. Chloroquine can enhance endosomal release of cargo molecules trapped within endosomes after cell uptake while bafilomycin can block this process by inhibiting the acidification of the endosomes. The addition of chloroquine prior to transfection did not improve the transfection efficiency of peptide **45** (Figure 101A). This suggested that either the plasmid DNA entered into cells already successfully escaped from endosome or, the internalization of plasmid DNA was endocytosis independent.

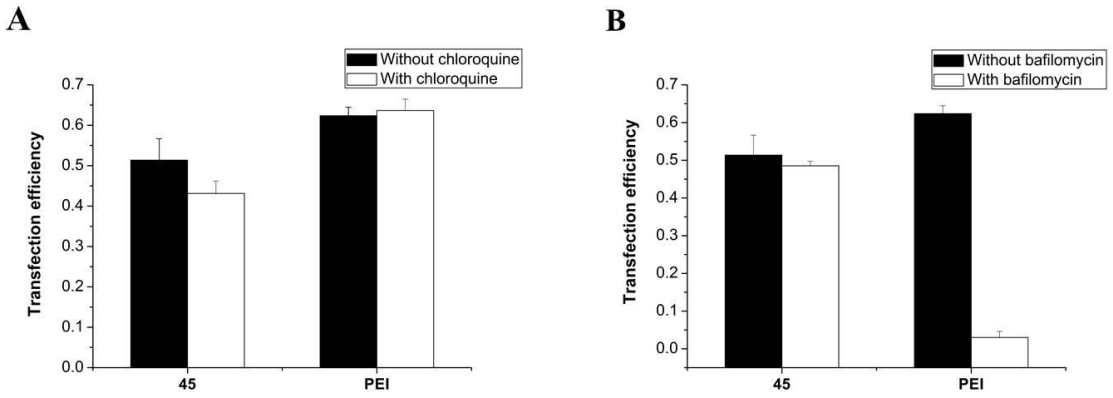

Figure 101 Transfection efficiency of **45** and PEI (all 0.4 mm) with the addition of chloroquine or bafilomycin prior to incubation in HeLa cells

It has been demonstrated that endocytosis is the major uptake pathway for PEI mediated gene transfection. Thus, when the cells were treated with bafilomycin prior to transfection, the endocytosis pathway was blocked and accordingly transfection with PEI was completely inhibited (Figure 101B). However, bafilomycin did not have any effect on the gene transfection by our peptide **45** which again underlined an alternate cellular uptake mechanism other than endocytosis. One possible mechanism could be direct membrane translocation through the interactions between the positively charged peptide nanotube **45** and negatively charged cell membrane.

Taken together, the above results indicated that an endocytic pathway was unlikely responsible for the cellular uptake process in **45** mediated gene transfection. Thus, a more

reasonable explanation is that nanotubes formed by cyclic peptide **45** function as an electronic-bridge between DNA and cell membrane so that DNA molecules could enter into cells without the involvement of endocytosis.

4.3.3.4 Cytotoxicity of cyclic peptide

To apply any newly developed gene transfection vector in future appications, its toxicity in cells must be examined. We therefore conducted alamar blue cytotoxicity assay to determine the influence of transfection with peptide **45** in the metabolic activity of cells. The results showed that this novel type gene transfection vector was less toxic than the common used gene transfection standard PEI (Figure 102).

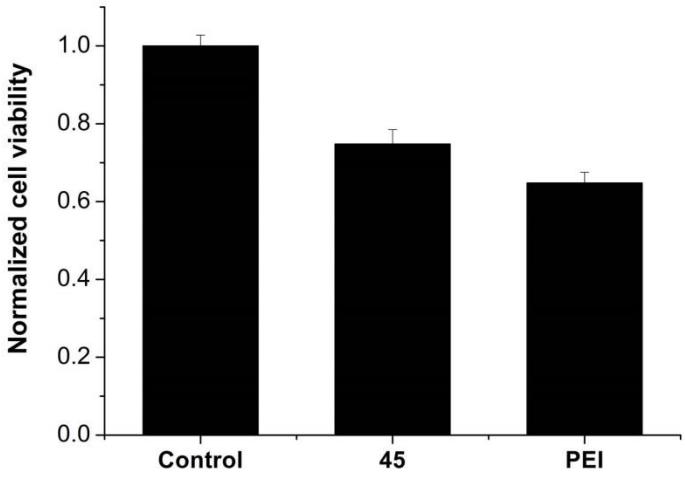

Figure 102. Alamar blue cell viability assay. The graph illustrates the fluorescence level of the redox indicator 24 h after transfection with **45** and PEI.

In summary, the functionalization of a cyclic peptide with a GCP group resulted in a novel peptide nanotube. The interactions between GCP group and cyclic peptide backbone possibly stabilized the tubular structure by offsetting charge repulsions. Hence, a positively charged cyclic peptide nanotube was obtained under physiological conditions. The resulting nanotube could bind with negatively charged DNA and showed an astonishing ability in gene transfection.

4.4 Development of a supramolecular β-helix mimetic peptide

Peptide assembly aiming to resemble α-helix structure has been demonstrated by several studies.[298-300] However, self-assembling systems mimicking a β-helix are rarely reported. One of the reasons might be that α-helix is among the most commonly observed secondary structures in protein and enzymes. Examples on such structures are thus abundant. We then determined to apply the superior anion recognition ability of GCP moiety to design self-assembling system that could mimic β-helices.

4.4.1 β-helix structure

The structural feature of α-helix is well studied. An α-helix is a right-handed coil of amino acid residues on a polypeptide chain, typically ranging between 4 and 40 residues. It normally adopts a spiral conformation (helix) in which every backbone amide NH group donates a hydrogen bond to the backbone carbonyl group of another amino acid residue. Such a hydrogen bond is formed exactly every 4 amino acid residues (O_i to N_{i+4}), and every complete turn of the helix requires 3.6 amino acid residues. The structure repeats itself every 5.4 Å along the helix axis, i.e. the α-helix has a pitch of 5.4 Å. In proteins, individual α-helices are connected by loops to form more complex structures.

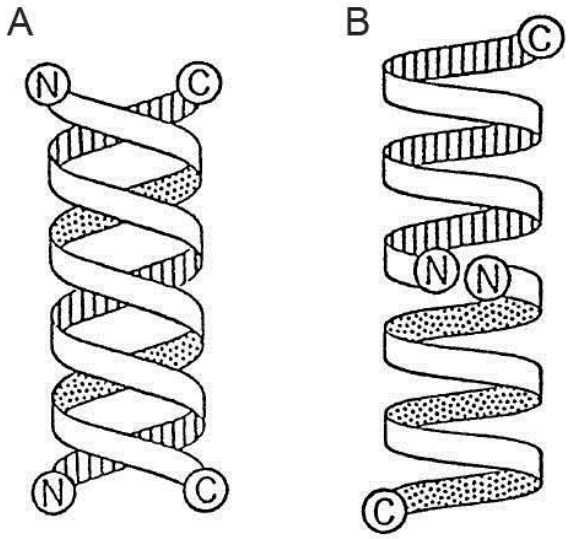

Figure 103. The non-channel form (A) and channel form (B) of gramicidin A. Reprinted from reference 302, copyright (2016), with permission from Elsevier

On the other hand, the structure of β-helix is significantly different. The term ‘‘β-helix’’

was first used to describe the structure of gramicidin in 1980's.[301] Gramicidin can form transmembrane ion channels which are selective for cations. Natural mixture of gramicidin consisted mostly of gramicidin A, a linear pentadecapeptide constructed by alternative D and L amino acids. It can easily incorporate into cell membrane since the amino acid composition of gramicidin A is highly hydrophobic with no charged or hydrophilic side chains present. In addition, both the N- and C-terminus are blocked, the former with a formyl group and the latter with an ethanolamine group.[302] As consequence, it is generally believed that gramicidin A can only form a unique head-to-head associated dimer of two single stranded β-helices (the channel form) in the presence of membrane mimics, such as vesicles (Figure 103B). In organic solvent it exists in totally different structures such as double strand intertwined helix (Figure 103A, the non-channel form).[303,304] Both forms are composed of β-sheet-like secondary structures with their side chains protruding on one surface due to the alternating L- and D-amino acids. The β-helix is then produced by rolling up of these β-sheets.

Another β-helix related structure is a parallel β-helix. It refers to the structure which uses β-sheet alone to form complex structures connected by repeating individual coils. A typical parallel β-helix is a three-stranded parallel β-helices. [305,306] These structures are constructed by a single polypeptide chain in which three parallel β-sheets are separated by three turns forming a single rung of a larger helical structure. The top view of this structure reveals a pore inside the parallel β-helix. The whole helix is mostly stabilized by hydrogen bonds.

4.4.2 Synthesis of β-helix mimetic peptide

Peptide **46** was designed to mimic gramicidin A by using alanine as basic building block. Alanine has a strong preference to form helix structure and it is also a weak former of β-sheet structure.[307] It has a moderate hydrophobicity which makes it suitable to be applied in aqueous conditions. GCP moiety was coupled to the N-terminus of an alanine octamer to establish multiple H-bond interactions with carboxylate group in the C-terminus.

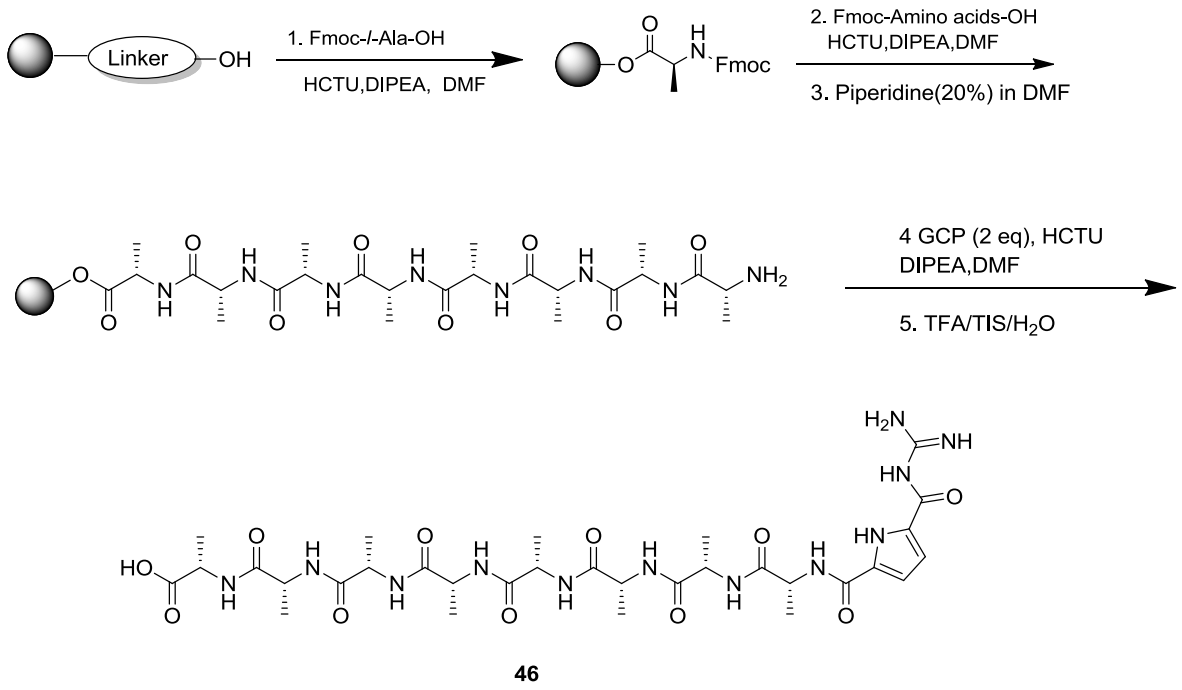

46

Figure 104. Synthetic route of peptide **46**

The synthesis was achieved with Fmoc solid phase peptide synthesis. Wang resin was selected to leave a free carboxylate group at the C-terminus. Commercially available Fmoc-*d*-Ala-OH and Fmoc-*l*-Ala-OH were used to build the peptide scaffold (Figure 104). The first attachment of amino acid residue with Wang resin was done under argon atmosphere with HCTU and DIPEA (step 1). Subsequent coupling and de-protection gave rise to a free amino group at the N-terminus of peptide (step 2 and 3). GCP moiety was then coupled and cleavage with TFA yielded the crude product. Purification with MPLC resulted in peptide **46** as a white solid in 10 % yield with 97 % purity.

A control peptide **66** without GCP group modification was also synthesized as shown in Figure 105. Commercially available Fmoc-*d*-Ala-OH and Fmoc-*l*-Ala-OH were used to build the peptide scaffold. The target peptide **66** was obtained as a white solid in 20 % yield with 93 % purity.

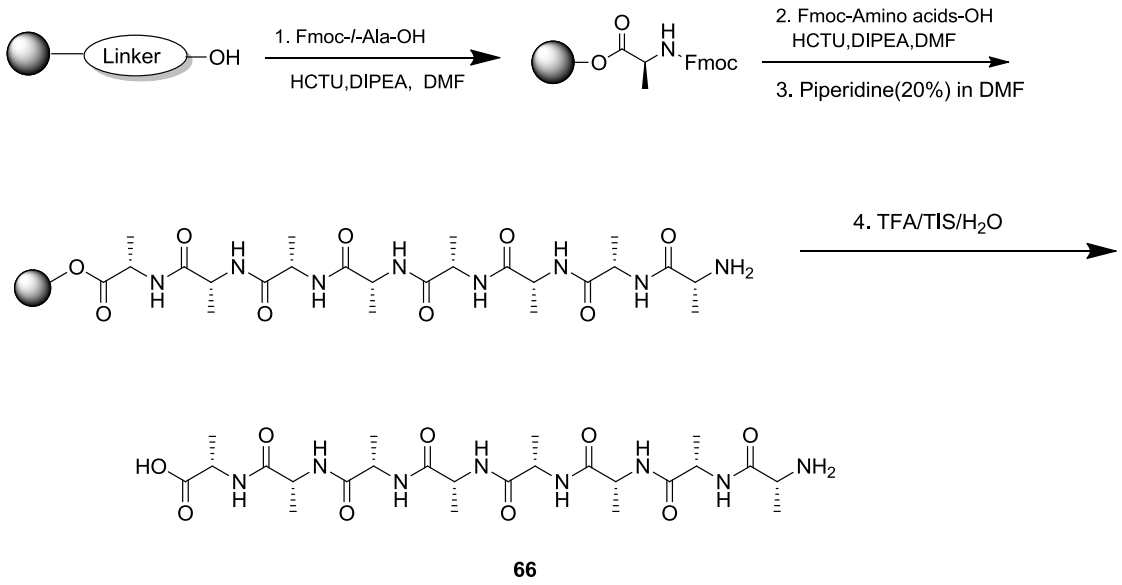

66

Figure 105. Synthetic route of peptide **66**

4.4.3 Structure determination for β-helix mimetic peptide

Circular dichroism (CD) experiment was measured with the cooperation from prof. Ivo Piantanida by Dr. Marijana Radić Stojković. CD was first applied to study the structures of both peptides in pH 5.0 water. At this pH, GCP moiety (pKa~7) on the N terminus is positively charged while carboxylate group (pKa~3-4) on the C terminus is negatively charged. Thus both peptides existed as zwitterion in water which is ideally for self-assembling. The results showed that the CD spectrum of peptide **46** was concentration dependent. At lower concentration, only very weak CD signal of β-helix (positive band at 220 nm and negative band at 230 nm) was observed (Figure 106A). It is possibly that the assembling of peptide **46** did not occur when it was dissolved in a diluted condition. However, when the concentration increased to 0.1 mM, the CD spectrum showed characteristic signals for β-helix structures which were in excellent agreement with the signals of gramicidin A in distearoylphosphatidylcholine (DSPC) vesicles (Figure 106B).[308]

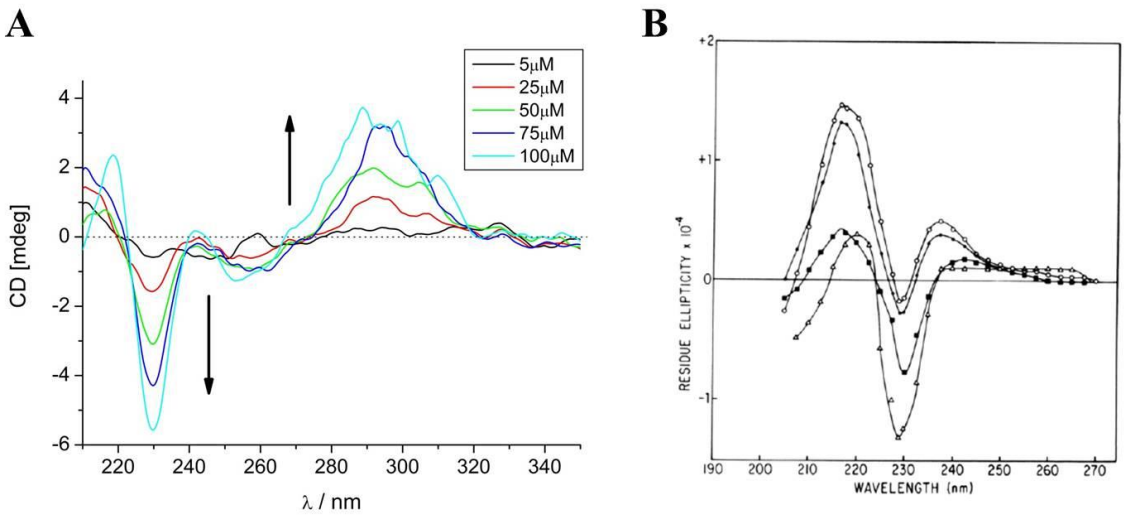

Figure 106. A) CD spectra of different concentrations of peptide **46** in pH 5.0 water B) CD spectrum of gramicidin A in (○) DLPC, (●) DMPC (■) DPPC, and (△) DSPC at 20℃ (lipid/peptide=30:1). Reprinted with permission. Copyright (2015) American Chemical Society

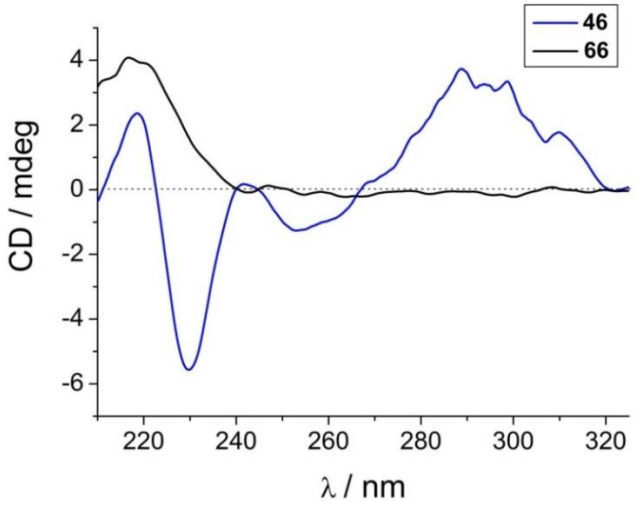

Figure 107. CD spectra of peptide **46** and **66** in pH 5.0 water

As shown in Figure 107, a strong positive peak at 220 nm and even stronger negative peak at 230 nm were well observed. A weaker positive peak around 242 nm was also found. It is known that the long lipid chains in vesicle components could help the stabilization of β-helix conformation of gramicidin A since such signals cannot be observed in organic solvent. However, in sharp contrast to this, peptide **46** was able to adopt same structure even without the presence of vesicles. Compared to peptide **66** which did not demonstrate any characteristics of β-helices, most likely the favorable interactions between GCP moiety and

carboxylate stabilized the β-helix conformation of peptide **46** which eventually allowed hydrogen bonding interactions between each adjacent peptide backbones to occur.

The strong and broad positive peak at around 300 nm, which corresponds to the adsorption of pyrrole, indicated that the GCP groups were aligned in a helical fashion in the assembly of peptide **46**. Indeed, molecular modelling study (done by Martin Ehlers) suggested that the GCP groups incorporated only in peptide **46** interacted with adjacent carboxylate groups (Figure 108A).

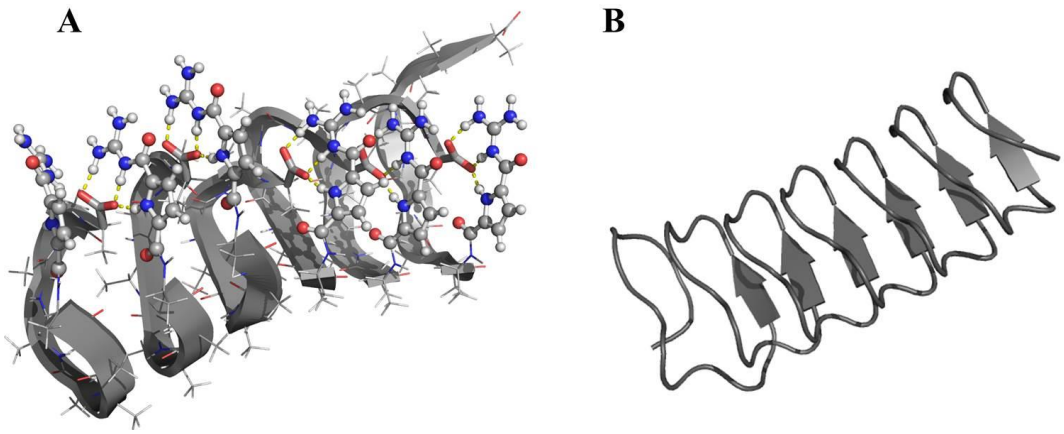

Figure 108. Molecular modelling of peptide **46** (A) and its comparison with (B) insect antifreeze protein (PDB code: 1EZG)

The modelled structure of peptide **46** was compared with the known crystal structure of β-helix insect antifreeze protein (Figure 108B).[309] The structure of insect antifreeze protein demonstrated that the individual β-sheets in its β-helix were connected with loops comprised of peptide chains. In comparison, the modelled structure of peptide **46** showed that the individual β-sheets, constructed with alanine residues, were linked by the recognition between N-terminal GCP and C-terminal carboxylate. This result indicated that supramolecular recognition motif (GCP^{+}-COO^{-}) can be applied to simulate bio-conjunction to construct secondary structures.

Furthermore, we determined the solvent accessible surface area for the modelled structure of peptide **46**. A top view of the solvent accessible surface area model of peptide **46** clearly demonstrated the existence of a pore which is characteristic of β-helix structure (Figure 109). It can also be seen that the side chains of alanine residues were pointed out of the modelled structure. This is in consistent with the feature of β-helix structure of gramicidin due to the

alternative D and L amino acid composition.

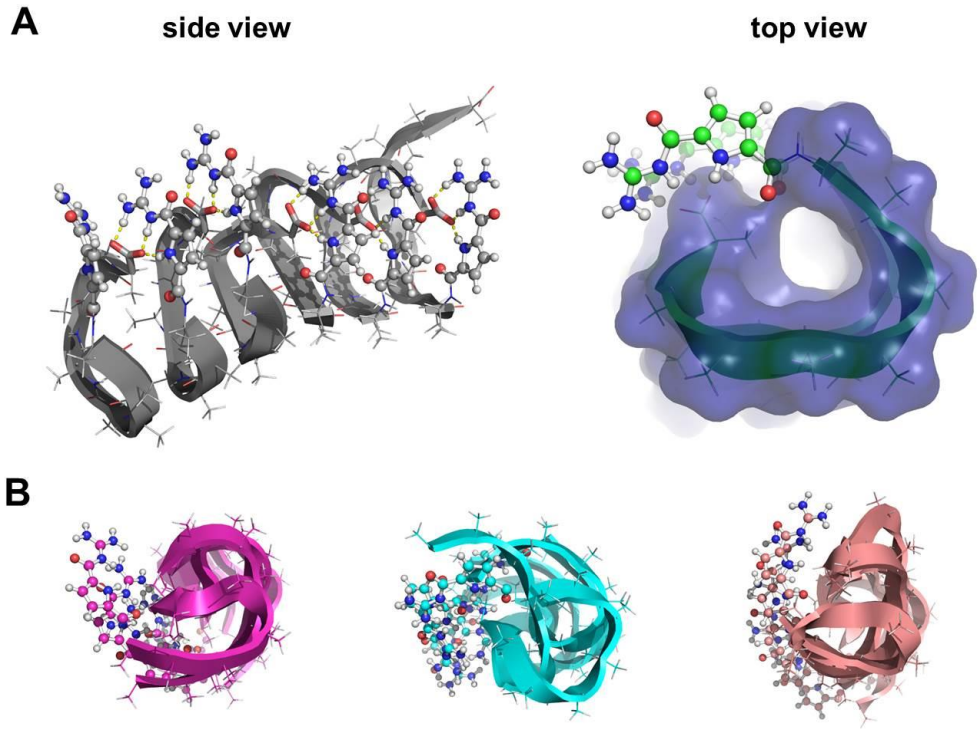

Figure 109. A) Side view of the modelled structure of **46** and top view of the solvent accessible surface area [1.4 Å radius for water] B) Additional images of the modelled structure of **46**

4.4.4 Growth process of β-helix mimetic peptide

4.4.4.1 Assembly of β-helix mimetic peptide

We further studied the structure of peptide **46** and **66** by atomic force microscopy (AFM) and transmission electron microscopy (TEM). As expected, peptide **66** did not form any ordered structures in water (Figure 110). Also DLS experiments did not detect any aggregates of **66** in water solution. This suggested that the modification with GCP moiety is required to trigger the self-assembly process.

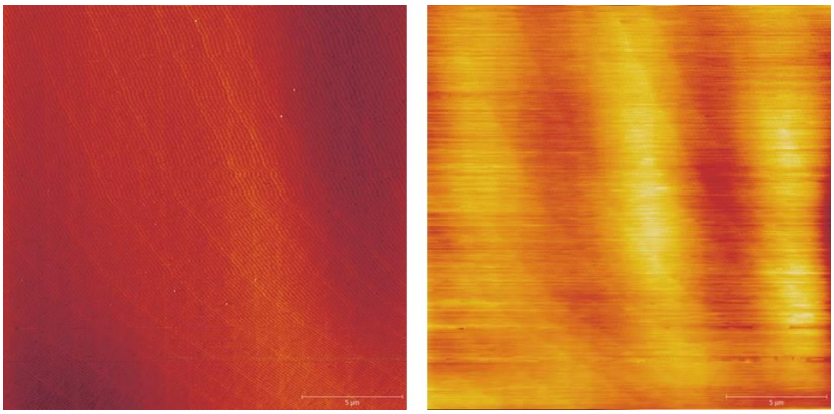

Figure 110. AFM images of 0.1 mM peptide **66** in pH 5 water.

Left: Amplitude image; Right: Height image.

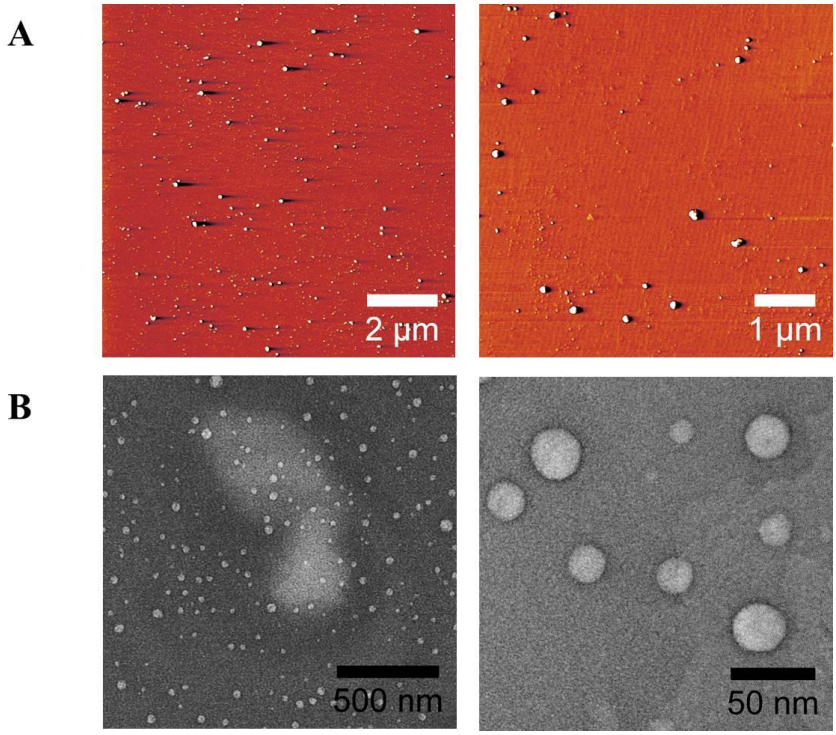

Figure 111. AFM (A) and TEM (B) images of a fresh prepared 0.1 mM peptide **46** in pH 5 water

Surprisingly, we observed that peptide **46** exhibited aging effect in water. For freshly prepared sample of peptide **46**, only small particles can be found in both AFM and TEM (Figure 111). The sizes of those particles were ranging from 20 nm to 35 nm. They exhibited a spherical shape which possibly was formed through the aggregation of individual helices. However, the morphology of these particles significantly changed when the sample solution was aged at room temperature. We found in AFM images that after 5 days incubation, the particles observed in the beginning transformed into short rod-like structures. As can be seen in Figure 112, these rods, varying in their lengths, were composed of smaller nanoparticles

which suggested that peptide **46** continued the self-assembling process even after the particles were formed. Therefore, the morphology of the assembly formed by peptide **46** was time dependent.

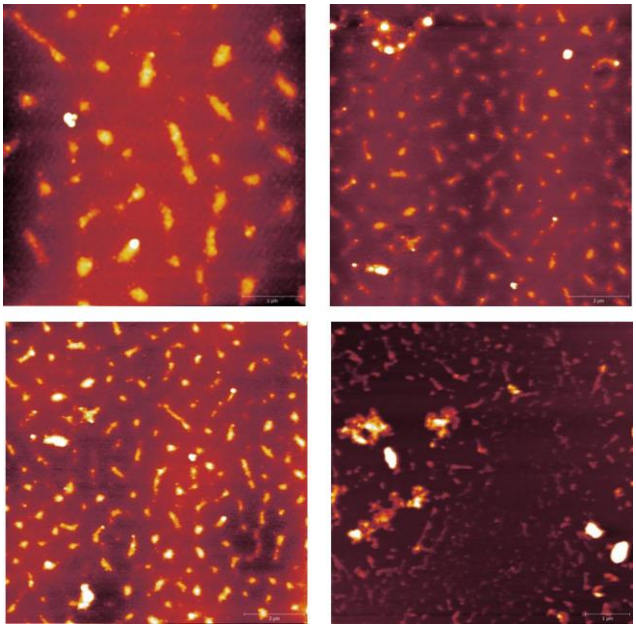

Figure 112. AFM height images of 5 days old sample of 0.1 mM peptide **46** in pH 5 water

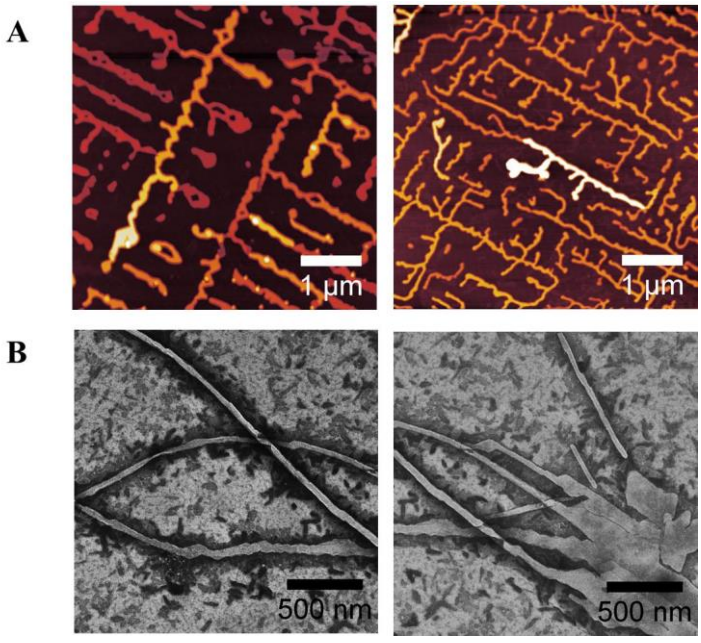

Figure 113. AFM (A) and TEM (B) images of 8 days old sample of 0.1 mM peptide **46** in pH 5 water

After 8 days incubation of the same sample solution at room temperature, the morphology of the aggregates formed by peptide **46** was completely different from the structures observed before. Fibrous structures with length of several micrometers were well distributed in solution as shown in both TEM and AFM images (Figure 113). Curiously, these fibers seemed to be

intertwined with each other in a helical fashion as can be seen in AFM images (Figure 113A). Regular wounded fibers were observed throughout the sample plate. Small rod-like structures can also be found in TEM images (Figure 113B). This might indicate a growth process for the long fibers assembled from **46**.

Therefore, the morphology of the assemblies formed by peptide **46** significantly changed through the aging process. It first formed small particles around 20 nm in diameter. Afterwards those particles transformed into short rod-like structures which eventually evolved into long fibers.

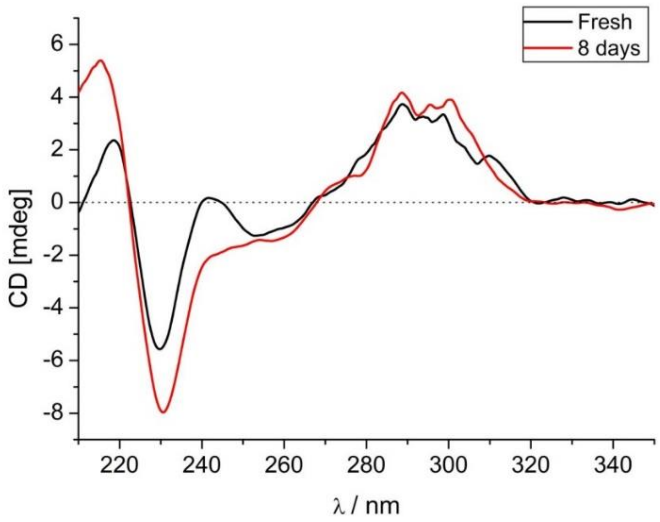

Figure 114. CD spectra of fresh prepared (black), 8 days (red) and 10 days (green) old sample of 0.1 mM peptide **46** in pH 5 water

Correlated to the different morphology of the assembly of peptide **46**, the CD signals also changed accordingly. Figure 114 clearly showed that after 8 days incubation at room temperature, the intensity of both peaks at 220 nm and 230 nm was significantly enhanced. Meanwhile, the positive peak at 280 nm - 320 nm, corresponding to the absorbance of pyrrole, was unaffected, indicating that the conformation of GCP moiety in peptide **46** remained unchanged during the aging process. The shape of CD curve for the aged sample was identical to freshly prepared samples which suggested that the overall β-helix structure of peptide **46** was retained. The enhancement of the intensity of CD signals should then only reflect more β-helix conformation contents of peptide **46** in its water solution. Therefore, it is reasonable to assume that in the freshly prepared sample solution of peptide **46**, individual monomer

co-existed with oligomers in equilibrium. During the aging process, these monomers could further assemble into higher ordered structures such as fibers which could stabilize the β-helices. It is indeed observed in AFM and TEM images that the small particles formed by peptide **46** transferred into fibers after several days' incubation at room temperature.

4.4.4.2 Growth mode of β-helix mimetic peptide

For the growth process of supramolecular polymerization, two aggregation modes have been proposed: isodesmic and cooperative modes. Isodesmic mode is featured with a single equilibrium constant in the elongation process of the assembly. As shown in Figure 115A, the addition of each monomeric unit to previous aggregates is governed by the same thermodynamics. In the cooperative mode, however, nuclei are firstly formed to activate the following growth process (Figure 115B). This step is thus named "nucleation" which is featured with a larger nucleation equilibrium constant than the elongation equilibrium constant ($K_2 > K_e$). Afterwards, a rapid growth of self-assembly is occurred which eventually leads to the formation of final aggregates.

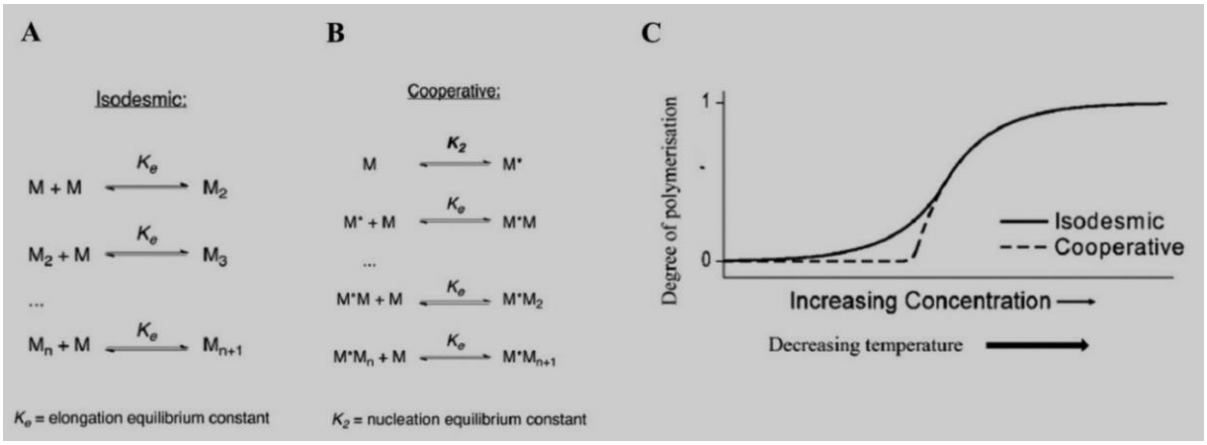

Figure 115. A) the isodesmic and B) the cooperative self-assembly mechanism for monomers M. C) Schematic representation of the degree of aggregation, α, versus concentration and temperature

We then studied the growth process of peptide **46** with dynamic laser scattering experiment in solution. It was found that the hydrodynamic size of the aggregates formed by peptide **46** correlated well with the results from AFM and TEM. For freshly prepared samples of **46**, only very small aggregates with sizes around 20 nm can be found. This size was in agreement with the size of the particles found in AFM and TEM. After 8 days, very large aggregates were

observed in water solution with sizes around 1 μm. Following the hydrodynamic diameter of aggregates during the aging process revealed a cooperative-like growth mode. As can be seen in Figure 116, the size of aggregates remained unchanged until 137h. Afterwards a fast growth of the sizes of aggregates formed by peptide **46** was observed which corresponded well with the nucleation-elongation mechanism in supramolecular systems. Thus, the particles formed in the fresh prepared sample of peptide **46** may rearrange itself during the aging process to form the nuclei. The fibers which were observed after 8 days then represented the final thermodynamically stable assembly.

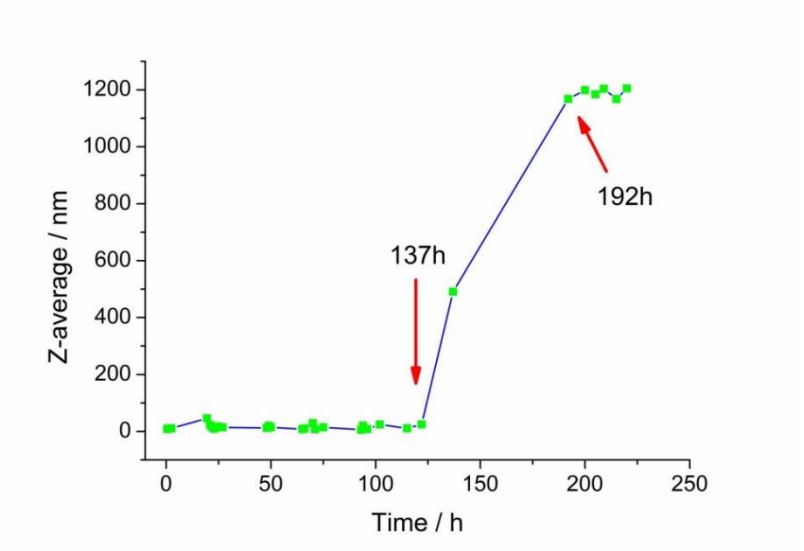

Figure 116. Hydrodynamic diameters of peptide **46** in pH 5.0 water during the aging process obtained with DLS.

To confirm the nucleation-elongation mechanism for the assembling of peptide **46**, we monitored the UV-vis adsorptions of an aged sample at different temperatures. The adsorption of pyrrole in GCP units (295 nm) and peptide backbone (241 nm) were both followed along with the increases of temperature. It was shown in Figure 117 that the disassembling process of those fibers formed by peptide **46** followed the typical nucleation-elongation mechanism. Both adsorptions from 295 nm and 241 nm decreased dramatically when the temperature increased to 305 K which implied the sudden break-up of the whole assembly. The degree of aggregation was calculated based on the assumption that at 290 K, the aggregation of peptide **46** was fully completed thus representing degree of aggregation of 1.When the temperature increased to 335 K, the assembly formed by **46** was disassembled which means the degree of

aggregation is 0. The adsorption data thus can be transferred to the degree of aggregation as shown in Figure 117B. This result then further demonstrated the cooperative growth mode of peptide **46**

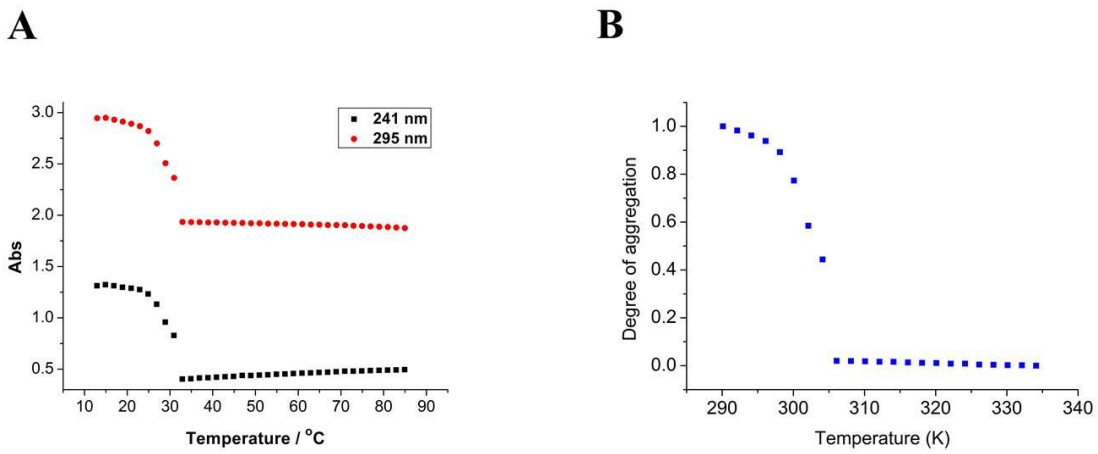

Figure 117. A) Temperature-dependent UV-vis adsorption of peptide **46** in pH 5.0 water. B) Degree of aggregation calculated from the adsorption on 295 nm.

4.4.5 pH response of β-helix mimetic peptide

Additionally, the helical fibers formed by peptide **46** were responsive towards pH stimuli. When sodium hydroxide solution was added to an old sample of peptide **46** to adjust the pH to 10, the helical fibers were immediately transformed into vesicles (Figure 118A). This is not surprising because the pKa of GCP moiety is around 7. At pH 10, the GCP groups are not protonated anymore therefore the recognition between the GCP and carboxylate are not strong enough to induce fiber formation. Peptide **46** at basic pH is just a simple amphiphile which accordingly formed vesicles (Figure 118A). The sizes of the vesicles were around 25 nm. Similarly, DLS results showed that the sizes of the aggregates formed by peptide **46** in water changed from ca. 1000 nm at pH 5 to 25 nm at pH 10 (Figure 118B).

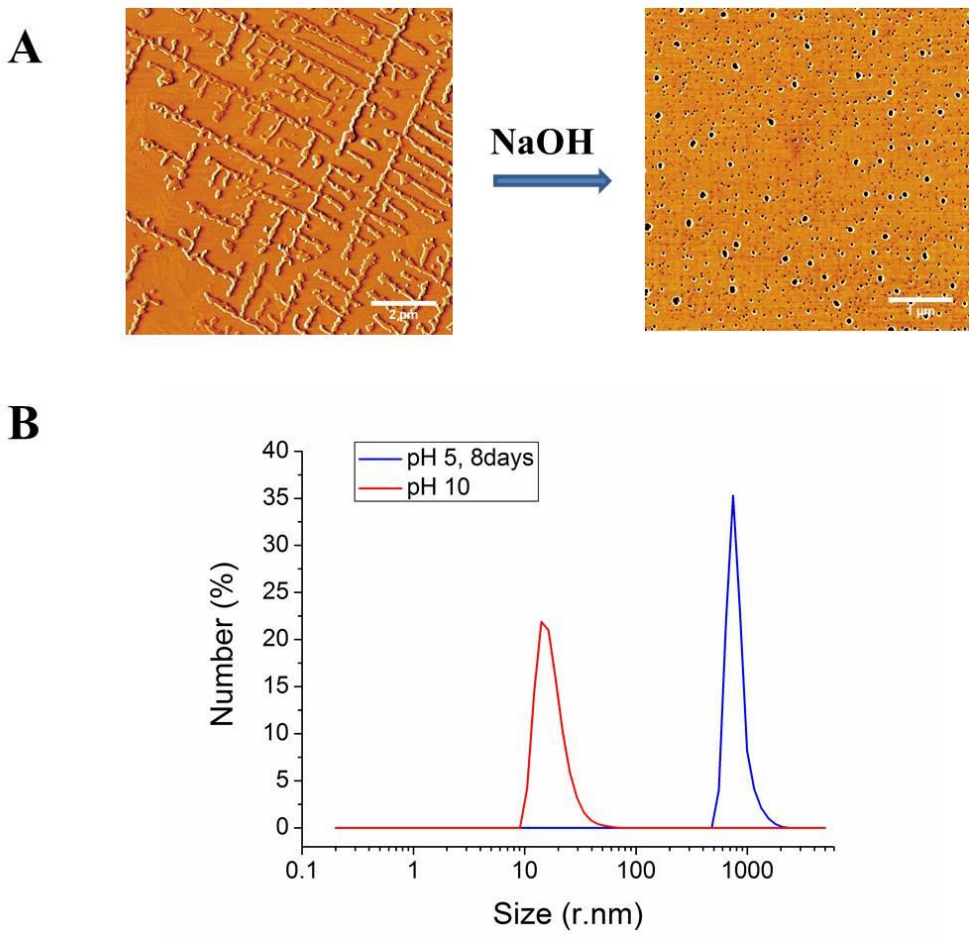

Figure 118. AFM phase images (A) and DLS number distribution (B) of 0.1 mM peptide **46** at pH 5 and pH 10 water

Also no aging effect was observed when peptide **46** was dissolved in pH 10 water solutions. As shown in Figure 121, the differences in the CD spectrum of peptide **46** were negligible after incubation for 8 days. Yet at this basic pH, the CD signals of peptide **46** within 200-240 nm range still resembled the signals of gramicidin A and CD signals of **46** at pH 5 (Figure 119), but the intensity of GCP-attributed CD band at 295 nm was much weaker (Figure 114; only 20% intensity of the signals at 220 and 230 nm at pH 5). Such almost negligible CD band suggested that GCP moiety was not uniformly oriented within the peptide chiral helix, which again pointed to the importance of protonation of GCP-guanidine at pH 5. Most likely, the binding between neutral-GCP and carboxylate is not strong enough to maintain fiber configurations but still provides sufficient stabilization for β-helix conformation to an extent.

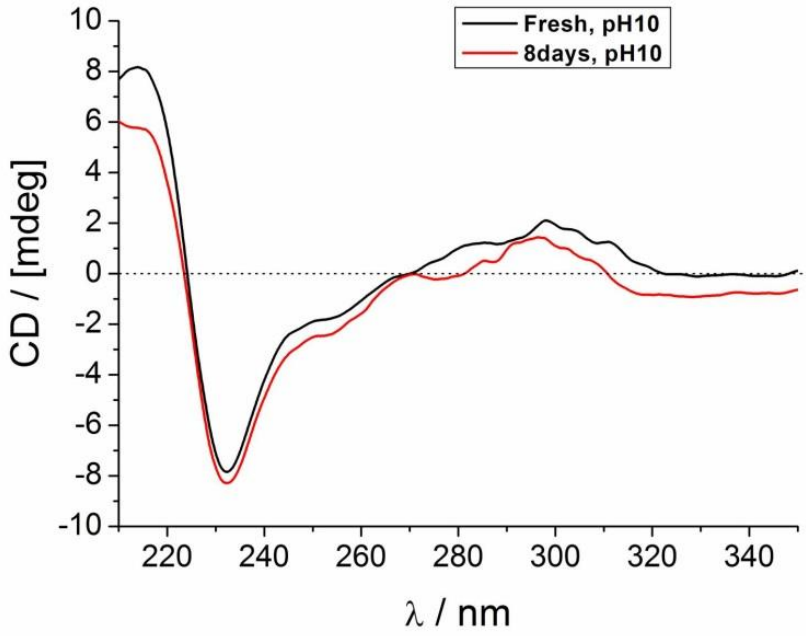

Figure 119. CD spectrum of freshly prepared (black) and 8 days old sample (red) of 0.1 mM peptide **46** at pH 10

In conclusion, peptide **46** is not only the first example for a self-assembled supramolecular β-helix in pure water but it also highlights the application of supramolecular recognition motifs for obtaining such secondary structures. Without the tailor made GCP binding motif no β-helix is formed in this case. The pH dependent switch of peptide **46** between fibers and vesicles also showed interesting potentials in constructing responsive materials.

4.5 Development of functionalized amphiphilic peptide assembly

Fmoc-based dipeptide assembling systems are highly interesting in the development of supramolecular materials. However, due to the use of hydrophobic amino acid residues, the exterior surface of the resulting assembly (fiber, sheet etc.) usually cannot be modified. Therefore, we hypothesized that introduction of GCP moiety in the side chains of Fmoc containing dipeptide could allow further manipulation of the assembled peptide nanostructures. Two dipeptides with GCP group modification were thus designed.

4.5.1 Synthesis of Fmoc-dipeptide analogues

Dipeptide analogue **47** was first designed and synthesized. GCP units were introduced into the side chains of lysine through conventional coupling reactions. The preparation of **40** was performed on solid phase using Fmoc peptide synthesis strategy (Figure 120). Rink amide MBHA resin was again selected because it could leave amide functionality at the C-terminus after final cleavage. Commercial available amino acid Fmoc-*l*-Lys(Alloc)-OH was used to build the peptide scaffold (step 2). De-protection of Alloc group with $Pd(PPh_3)_4$ resulted in free amino groups on the side chains of lysine (step 3). Subsequently coupling with GCP moiety (step 4) and cleavage from the resin (step 5) yielded the crude product of peptide **47**. The crude product was purified by MPLC on C18 reversed-phase silica gel to obtain **47** as white solid (38 % yield) with 93 % purity determined by analytical RP-HPLC.

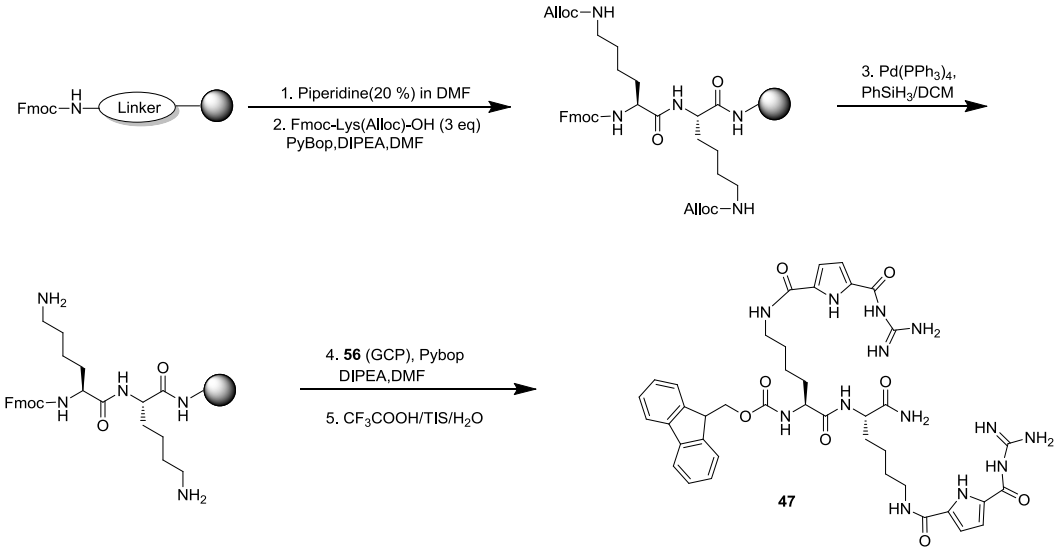

Figure 120. Synthetic route of Fmoc-dipeptide analogue (**47**)

Dipeptide analogue **67** was also designed and synthesized similar to that of **47**. However, peptide **67** was constructed with D amino acid residues instead of L amino acid (Figure 121). Thus, commercially available Fmoc-*d*-Lys(Alloc)-OH was selected to build the peptide scaffold (step 2). The crude product was purified by MPLC on C18 reversed-phase silica gel to obtain **67** as white solid (19 % yield) with 94 % purity.

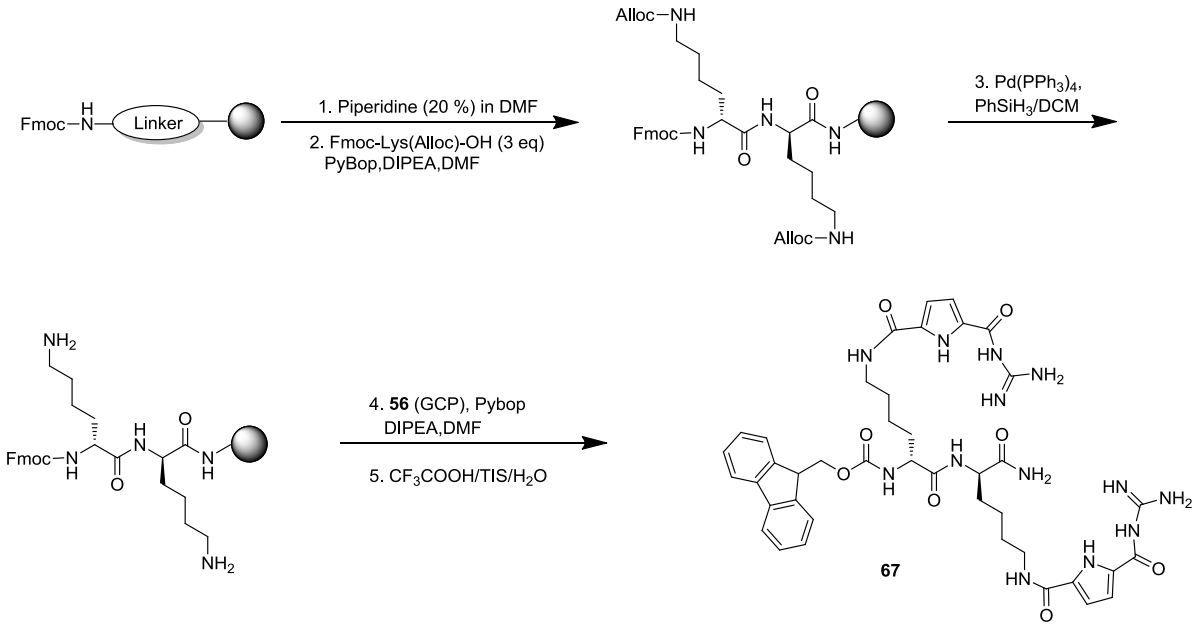

Figure 121. Synthetic route of Fmoc-dipeptide analogue (**67**)

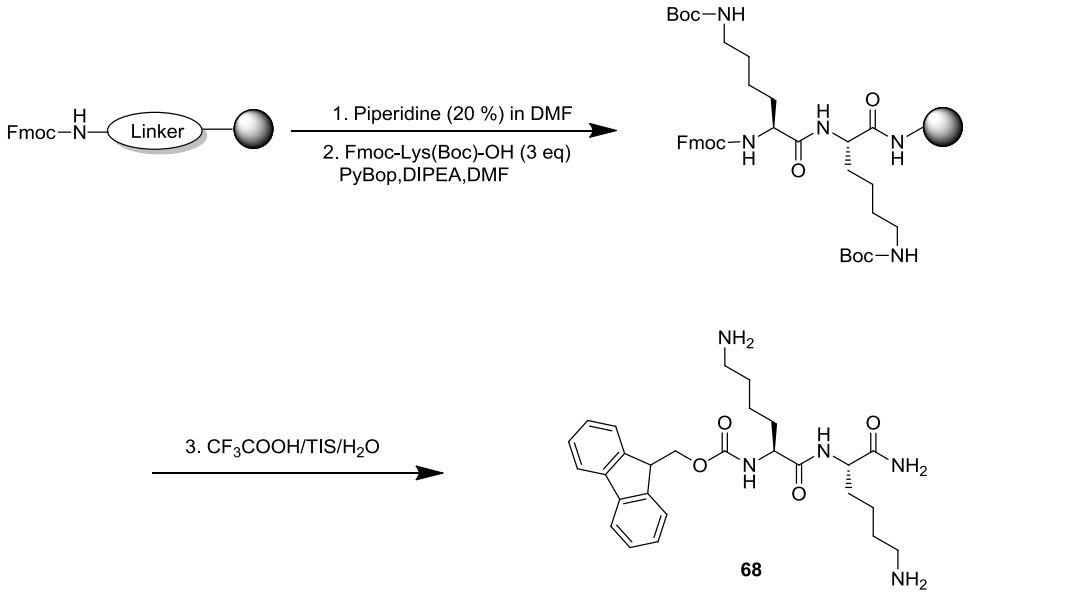

Figure 122. Synthetic route of Fmoc-dipeptide (**68**)

For the comparison of assembling property, we also synthesized peptide **68**, composed of

two lysine residues, as control group. The preparation of **68** was performed on solid phase using Fmoc peptide synthesis strategy (Figure 122). Rink amide MBHA resin was selected. Commercially available amino acid Fmoc-*l*-Lys(Boc)-OH was used to construct the peptide scaffold (step 2). The crude product was purified by MPLC on C18 reversed-phase silica gel to obtain **68** as yellow solid (19 % yield) with 94 % purity determined by analytical RP-HPLC.

4.5.2 Assembling of Fmoc-dipeptide analogues

The assembling properties of these Fmoc based peptide analogues were studied with circular dichroism (CD) in solution and also with atomic force microscopy (AFM), transmission electron microscopy (TEM).

4.5.2.1 AFM and TEM study

The assembling behavior of peptide **47** was firstly studied with AFM. Fmoc-containing short peptide is known to assemble in water. Therefore, peptide **47** was first dissolved in pure water to form a white suspension. Heating at 70 ℃ for 3 minutes resulted in a transparent solution which was cooled down to room temperature gradually. The pH of the solution of peptide **47** was adjusted to 7 and directly examined with high resolution AFM.

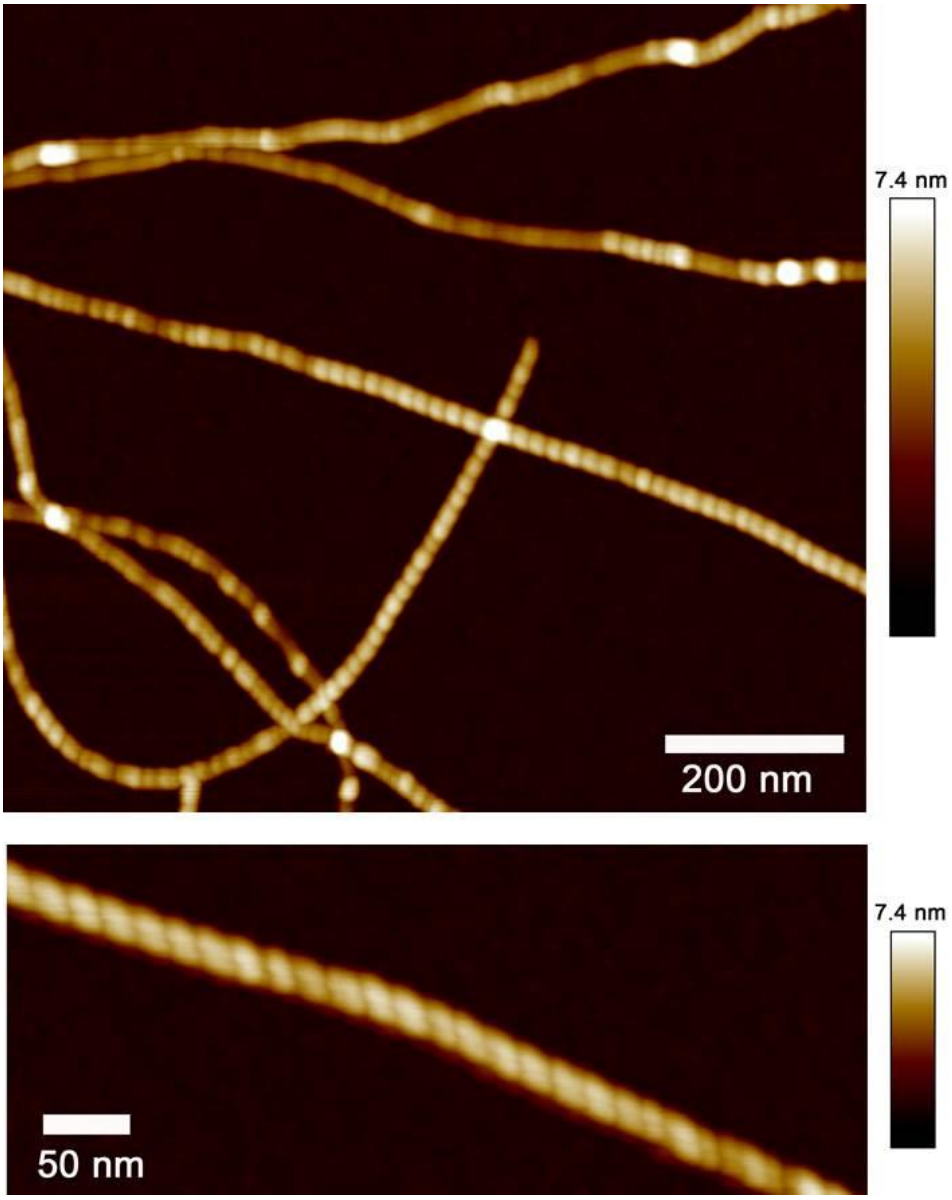

Figure 123. AFM height images of 0.1 mM **47** in water

As shown in Figure 123, peptide **47** readily assembled into fibers in water. The length of these fibers exceeded several micrometers with diameters around 20 nm. It can also be clearly seen in the AFM images that these fibers were helical in nature. Most likely, the chirality of lysine residues endowed the right handedness of the assembled fibers.

The fibers formed with **47** were also examined with TEM. Due to the organic nature of **47**, the sample was stained with uranyl formate prior to the examination. We found in TEM images that these fibers were well distributed throughout the sample plate around several micrometers in length (Figure 124). Similarly, the fibers formed by **67** were also exceeded several micrometers in length and well distributed throughout sample plate (Figure 125). The

average diameter of fibers found in TEM was around 7.5 nm, corresponded well with the height of the fibers found in AFM (7.4 nm).

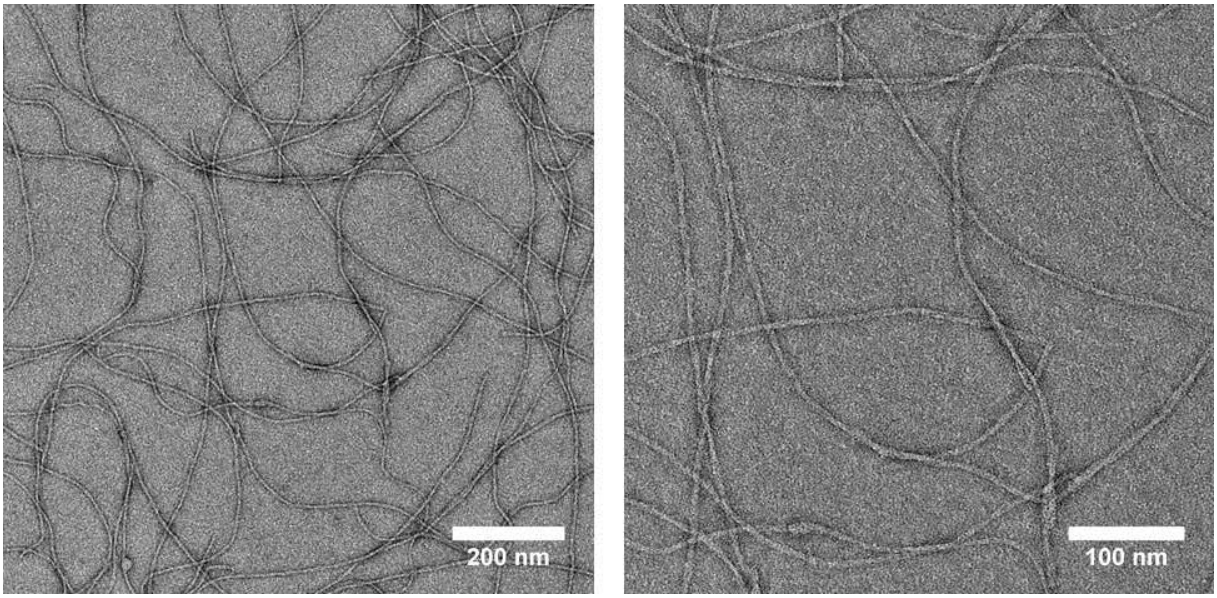

Figure 124. TEM images (negative stain) of 0.1 mM **47** in water

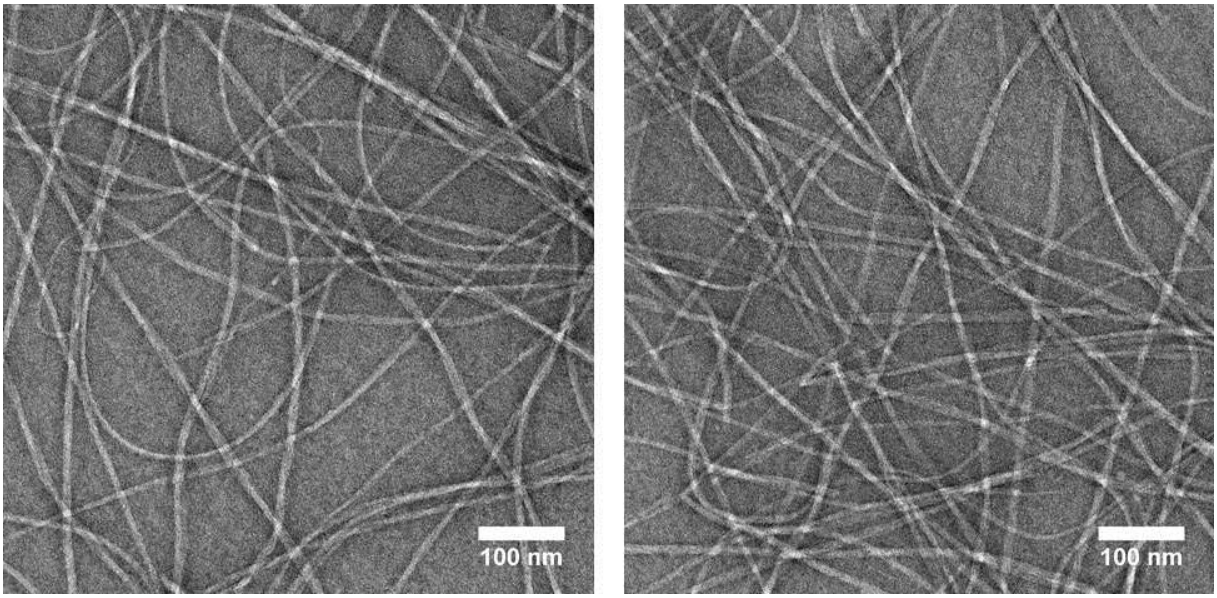

Figure 125. TEM images (negative stain) of 0.1 mM **67** in water

In comparison to peptide **47** and **67**, control peptide **68** without GCP group modifications did not show any detectable self-assembling when it was dissolved in water at the same conditions. Moreover, only very few particle-like structures were observed even when a rather high concentration of **68** (1.0 mM, ten folds as **47**) was used as shown in Figure 126. This is most likely because of the pKa value of the amine group on the side chain of lysine (~ 9). As

consequence, the side chains in **68** were both positively charged at pH 7. The charge repulsions then prevented the formation of any higher ordered supramolecular structures.

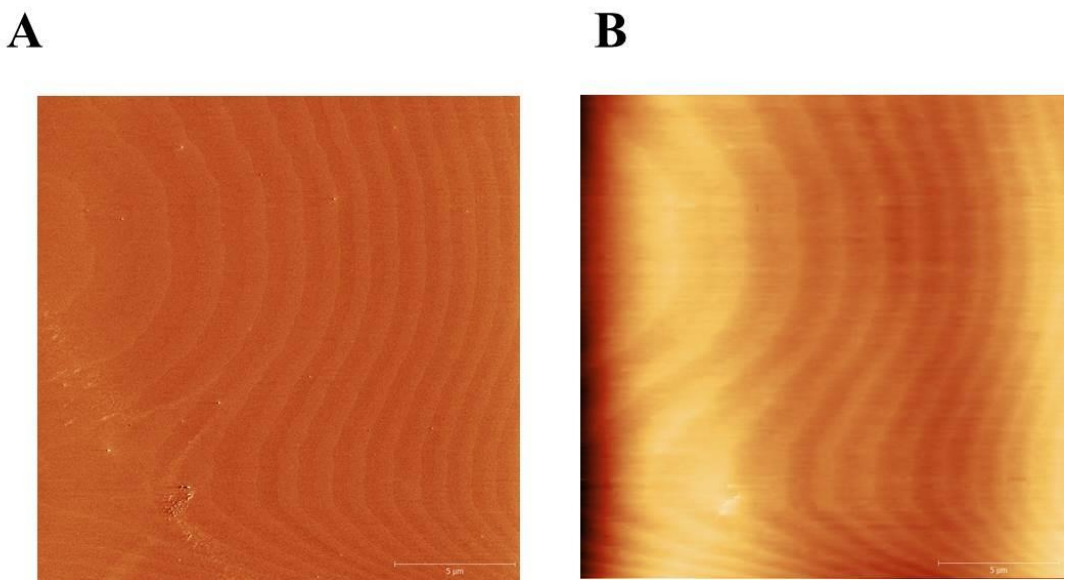

Figure 126. AFM phase (A) and height images (B) of 1.0 mM **68** in water

4.5.2.2 CD spectroscopy study in solution

The aggregation property of these GCP modified peptides was also studied with CD spectroscopy in solution. Different concentrations of peptide **47** were first tested. The CD experiment was measured with the cooperation from prof. Ivo Piantanida by Dr. Marijana Radić Stojković.

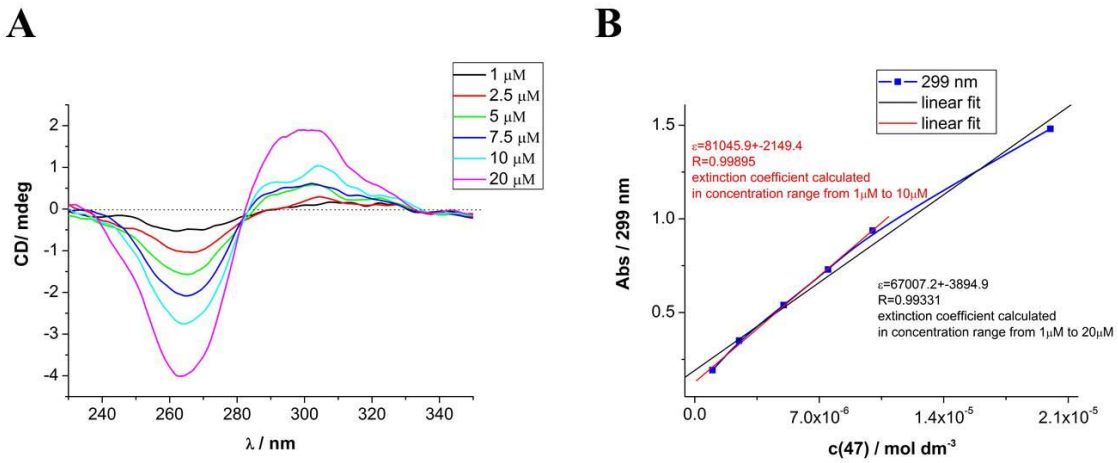

Figure 127. CD spectra (A) and absorption at 299 nm (B) of different concentrations of peptide **47** in water

As shown in Figure 127A, peptide **47** displayed two peaks in its CD spectrum. A strong

negative peak at 262 nm and a positive peak at 299 nm were observed. The peak at 262 nm was assigned to the absorption of the Fmoc fluorenyl group while the positive peak at 299 nm was from the combination of Fmoc and GCP. The intensity of both peaks was significantly enhanced when the concentration of peptide **47** increased from 1 μM to 20 μM. The biggest enhancement was achieved when the last aliquot of the stock solution of **47** was added. Accordingly, the last aliquot caused a slight deviation from *Lambert-Beer* law (Figure 127B). The extinction coefficient deviated from 81045 to 67007 when the last addition was included in the calculation. This deviation hinted that the aggregation of peptide **47** might be triggered within the concentration range from 10 μM to 20 μM.

Owing to its D amino acid compositions, peptide **67** exhibited opposite CD curves when it was dissolved at the same concentration (Figure 128A). A strong positive peak at 262 nm and a negative peak at 299 nm were observed. The intensity of both peaks was also concentration dependent. Similar deviation of extinction coefficient from 81471 to 63839 occurred when the concentration of **67** reached to 20 μM (Figure 128B).

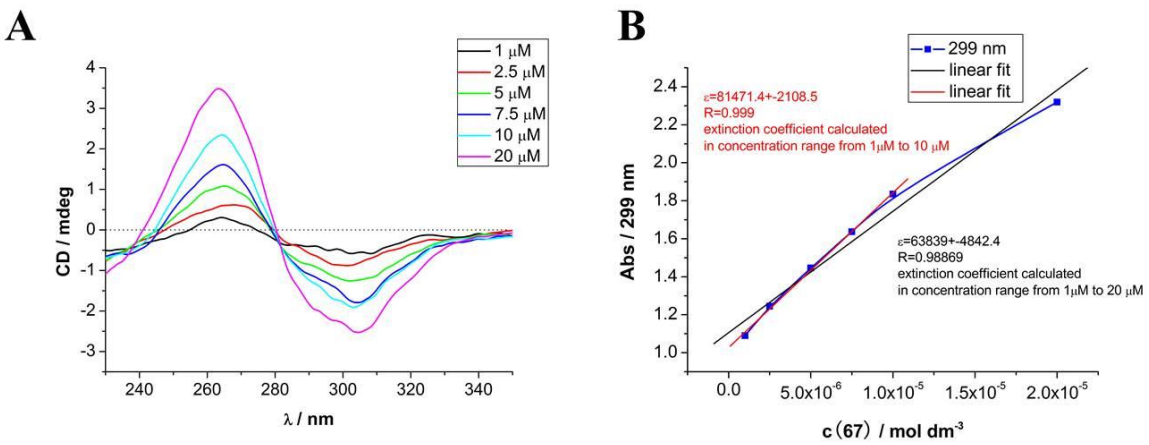

Figure 128. CD spectra (A) and absorption at 299 nm (B) of different concentrations of peptide **67** in water

In comparison, peptide **68** displayed very weak signals in CD spectroscopy as shown in Figure 129. The absorption at 260 nm was negligible which indicated that the Fmoc group in peptide **68** was not aligned helically. This further highlighted that GCP groups indeed boosted the assembling of Fmoc based peptide system in water.

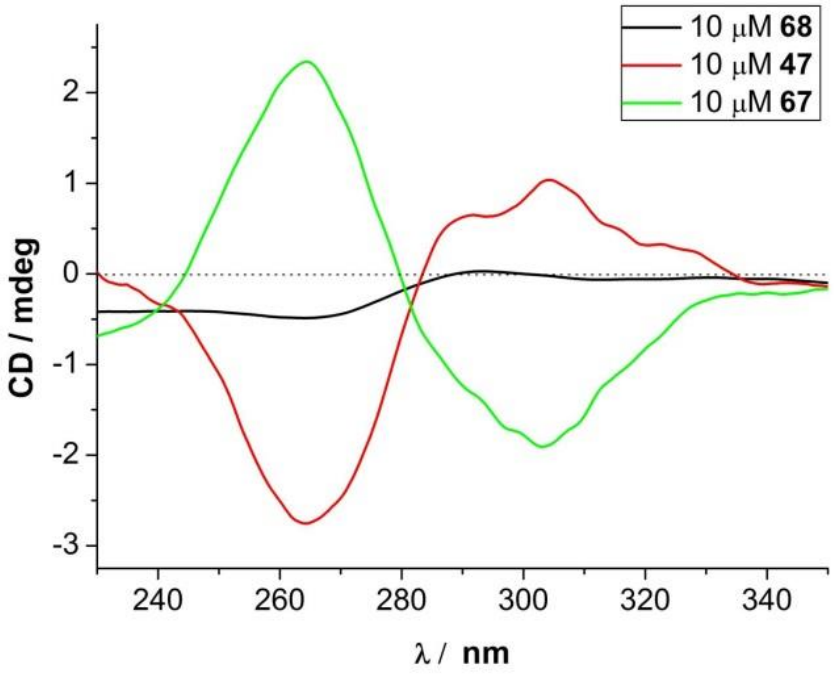

Figure 129. CD spectra of 10 μM peptide **47**, **67** and **68** in water

4.5.2 Application of Fmoc-dipeptide analogues

The results from AFM and CD demonstrated that peptide **47** and **67** with GCP group modification indeed assembled into fibers when they were dissolved in water. The GCP groups on the surface should be able to recognize anionic species which might provide unique property to these fibers. Therefore, we studied the application of these fibers with two anionic moieties respectively: bio-macromolecule DNA and small organic molecule terpyridine.

4.5.2.1 Interaction with DNA

We first studied the interaction of these GCP functionalized fibers with DNA using AFM. Calf thymus DNA was selected as model DNA. Peptide **47** and **67** were dissolved in water and the pH was adjusted to 7, respectively. Afterwards, an equivalence of DNA was added and the mixture was incubated for 5 minutes. The resulting mixture was then examined with AFM. As can be seen in Figure 130A, the fibers formed by peptide **47** were transformed into particles when the DNA was added. It might due to the interactions between Fmoc group and the base pairs in DNA that disrupted the assembly of peptide. Similar transition was also observed with peptide **67** which demonstrated that the interaction of these fibers with DNA is

independent of the chirality of amino acid composition (Figure 130B).

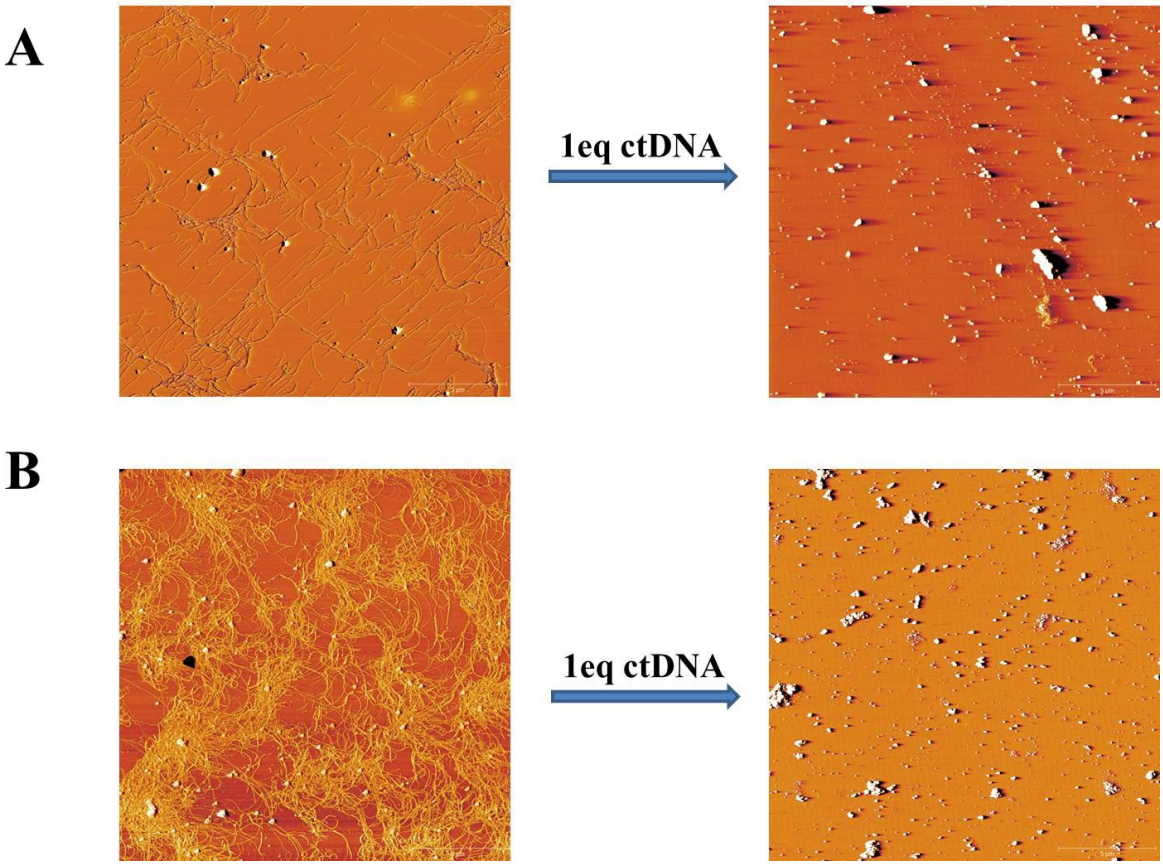

Figure 130. AFM images of peptide **47** (A) and **67 (B)** before and after the addition of DNA

4.5.2.2 Gene transfection of 47

We hypothesized that the transition of peptide **47** from fibers to nanoparticles might also provide gene transfection ability. Therefore, peptide **47** was mixed with GFP plasmid in buffered water and incubated for 5 minutes. The resulting mixture was directly applied to transfect HeLa cells. Transfection result was imaged 24 hours after the incubation.

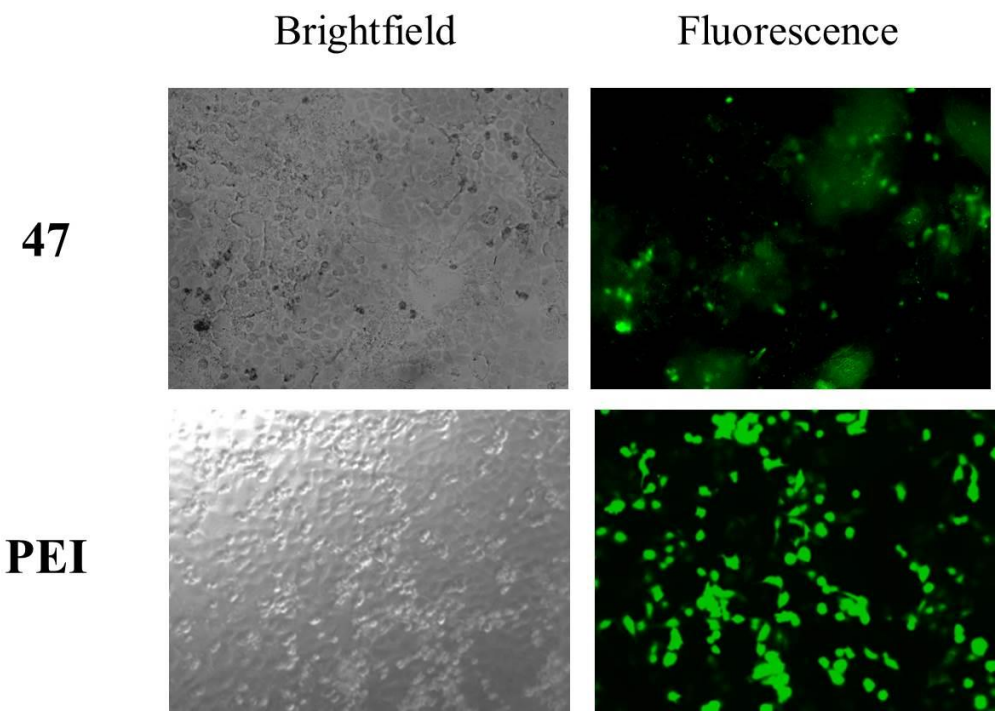

Figure 131. Transfection results of 0.4 mM peptide **47** and **PEI** with 2 μg GFP plasmid in HeLa cells

As shown in Figure 131, peptide **47** successfully transported the GFP plasmid into cells. The transfection efficiency was however, lower than that of PEI. Notably, some fibrous structures can also be observed in the brightfield image of the cells treated with **47**. This might indicate that the fibers formed by peptide **47** did not fully transformed into particles when plasmid DNA was added.

4.5.2.3 Interaction with terpyridine

We next tested a post-assembly modification with a small organic molecule. A carboxyl group functionalized terpyridine **69** was added to the fibers formed by peptide **47**. Due to the favorable ion-pair assisted hydrogen bonding interaction between GCP and carboxylate (Figure 132A), terpyridine molecule **69** was thus attached on the surface of the fibers formed by peptide **47**. After incubation at room temperature for 5 minutes, iron (II) chloride was added. It is well known that the nitrogen atoms in terpyridine can coordinate with metal ions to form rather stable complex (Figure 132B). Therefore, the iron (II) atoms acted as “glue” to strengthen the terpyridine decorated surfaces. A metal-organic nanowire was thus obtained with peptide fibers as template.

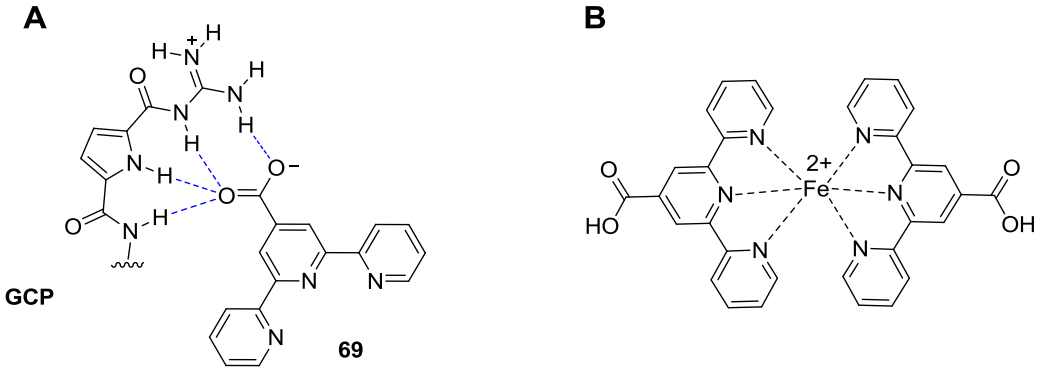

Figure 132. Anion recognition of GCP and carboxylate (A) and terpyridine-Fe(II) coordination (B)

We therefore examined the resulting metal-organic nanowire with AFM and TEM. AFM images showed that the addition of terpyridine and metal ions did not change the morphology of the assembly of peptide **47**. Long fibers or wires were again observed in the AFM sample plate (Figure 133A). However, the helical property of **47** was clearly altered as shown in Figure 133B. The helicity found in the fibers formed by **47** alone was around 19 nm. Addition of terpyridine and iron (II) thus completely altered the helicity in **47** to around 53 nm. This is the first hint that terpyridine molecules were aligned on the surface of peptide **47** and the addition of Iron (II) significantly resulted in different nanowires.

The presence of metal ions on the surface of those nanowires was confirmed with TEM. Organic molecules such as peptide **47** are not visible in TEM experiment. A staining solution for example, uranyl formate is required to increase the electron density of the nanostructures formed with organic materials. In contrast, the fibers observed in Figure 125A should be visible in TEM without staining step owing to the presence of iron (II) atoms. Indeed, we found in TEM images that nanowires with length around several micrometers were well distributed in the sample (Figure 134). Notably, the diameter of these nanowires (12 nm) was slightly bigger than the fibers formed by peptide **47** alone (7.4 nm). This further supported the presence of terpyridine molecules and metal ions on the surface of nanowires.

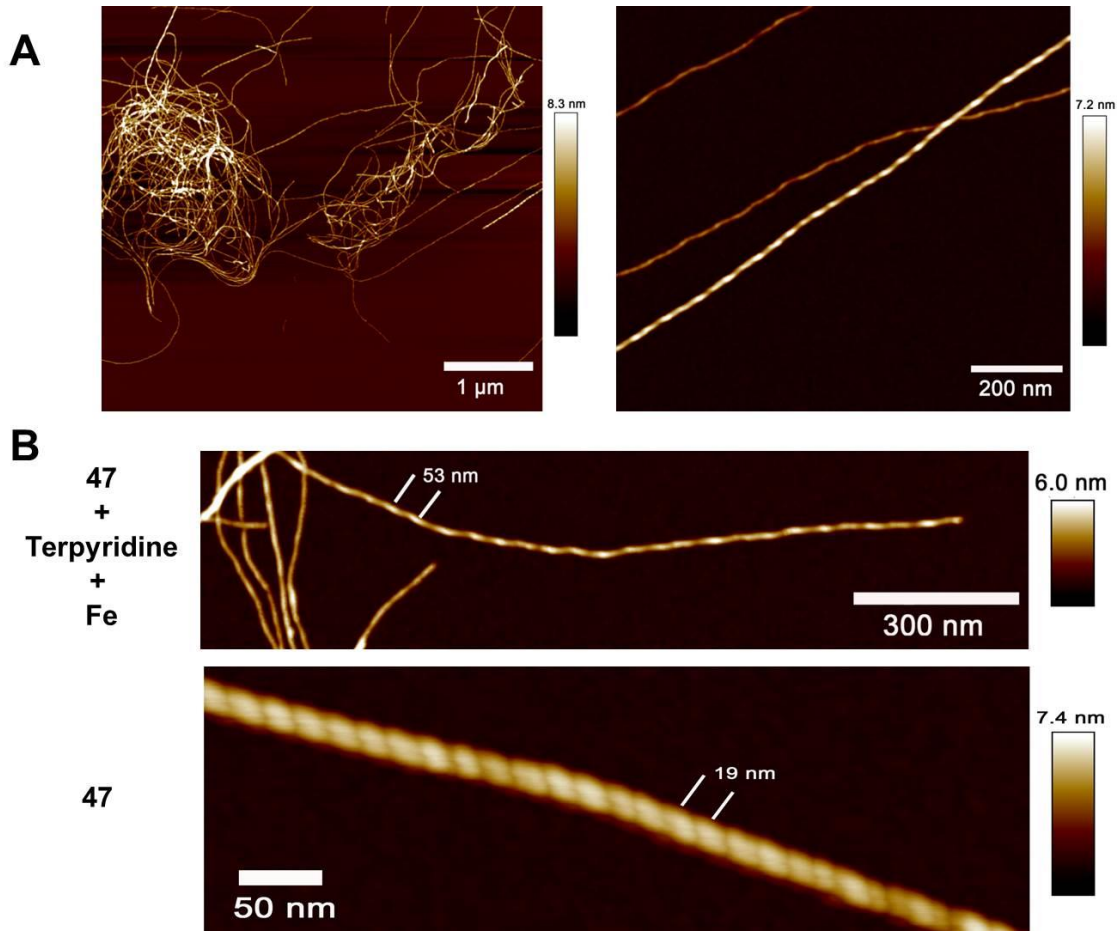

Figure 133. (A) AFM images of the mixture of 0.5 mM peptide **47** + 1 eq. terpyridine + 1 eq. $FeCl_2$ and (B) Comparison of the helicity of **47**+ terpyridine + Fe (upper channel) with **47** (lower channel)

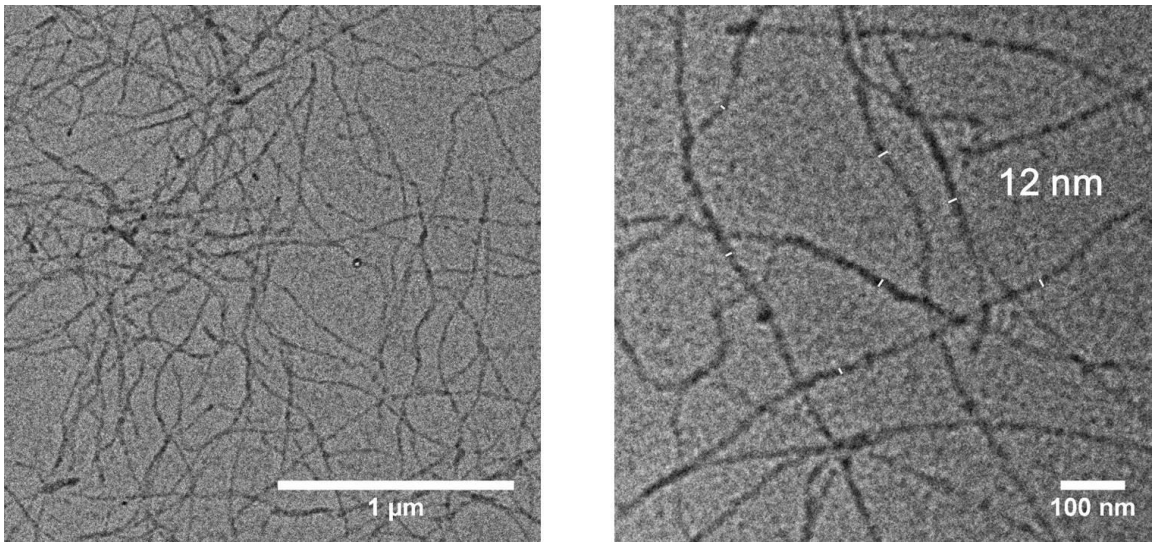

Figure 134. TEM images (**no stain**) of the mixture of 0.5 mM peptide **47** + 1 eq. terpyridine + 1 eq. $FeCl_2$

In conclusion, we demonstrated in this project that through the introduction of an anion recognition moiety GCP into the side chains of a Fmoc containing short peptide, a novel class of peptide fibers was obtained through its assembly process. Owing to the GCP presented on the surface of the nanofibers assembled from **47**, the fibers could interact with anionic macromolecules such as DNA and shuttle DNA into cells. More interestingly, we showed that metal ions such as iron (II) could be adsorbed on the surface of the peptide fibers using a carboxylate functionalized terpyridine ligand. Metal-organic hybrid nanofibers were thus obtained which could benefit the future preparation of supramolecular nanomaterials.

5. SUMMARY AND OUTLOOKS

5.1 Development of novel cell penetrating peptide

Functionalization of a short peptide with GCP moiety resulted in a novel peptide analogue **40** (Figure135). Owing to the superior anion binding ability of the GCP groups on the side chains of **40**, its binding affinity with model glycosaminoglycan, heparin, reached to the magnitude of 10^7.

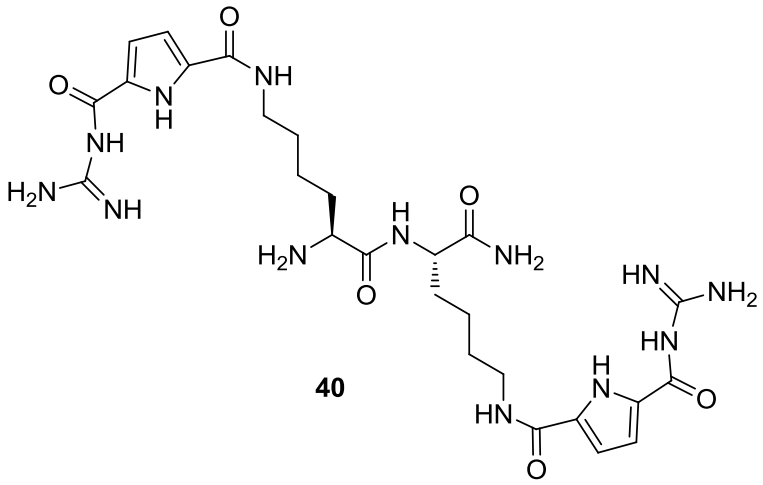

40

Figure 135. Chemical structure of peptide **40.**

The enhanced affinity with glycosaminoglycan eventually led to a significantly improved cellular uptake behavior. Peptide **40**, with only two amino acid residues, is the smallest cell penetrating peptide which has been reported. Moreover, the cellular distribution of this short peptide was concentration dependent. At lower concentration, the internalized peptides were mostly entrapped in lysosomes. When the concentration reached to 20 μM, peptide **40** was well distributed in cytosol.

In summary, the designed peptide **40** demonstrated amazing ability of cell penetration. We envisioned that the small size of **40** would make it an ideal carrier for the transport of a variety of drug molecules into cells. However, the exact cell penetration mechanism is still not clear. The role of glycosaminoglycan on cell membrane in the cellular uptake process of **40** should be further explored.

5.2 Development of a novel cell penetrating peptide based gene delivery vector

In this project, seven tetra peptide analogues with different number of GCP modifications were prepared (Figure 136). Their binding properties with DNA were thoroughly studied with ITC, EB displacement assay. The DNA condensation ability was also examined with DLS and AFM. We demonstrated that with more GCP modification, the binding process with DNA became more enthalpy favored. This might provide a unique strategy to shift the thermodynamic profiles of peptide/DNA binding.

The transfection with these tetra peptide analogues gave rise to a surprising result. Peptide **42** successfully transfect GFP plasmid into cells while peptide **61** and **62**, with only one less GCP modification than **42**, did not show any transfection. The reason for that is not clear at present. One possible reason might be that **42** condensed DNA into smaller particles which were suitable for cellular uptake.

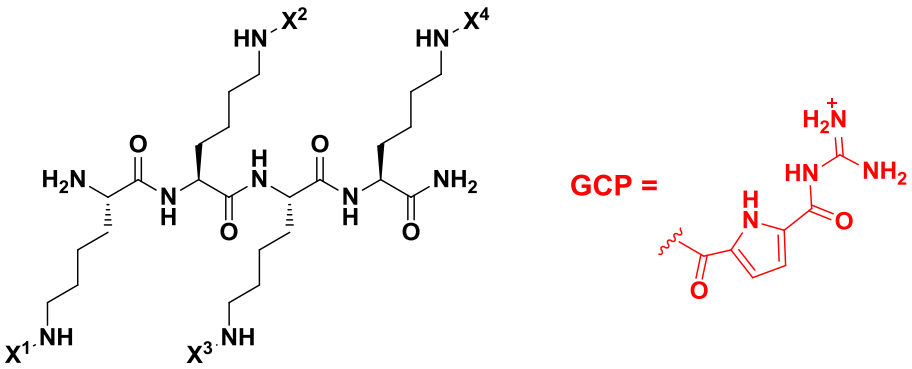

42 (G'G'G'G') : $X^1 = X^2 = X^3 = X^4$ = GCP
61 (G'G'G'K) : $X^1 = X^2 = X^3$ = GCP, X^4 = H
62 (KG'G'G') : X^1 = H, $X^2 = X^3 = X^4$ = GCP
63 (G'KKG') : $X^1 = X^4$= GCP, $X^2 = X^3$= H
64 (G'KKK) : X^1= GCP, $X^2 = X^3 = X^4$= H,
43 (RRRR) : Arginine tetramer
44 (KKKK) : Lysine tetramer

Figure 136. Chemical structures of designed tetra peptide analogues

In summary, this research highlights the potential of specific tailor-made anion binding sites, such as our GCP group, to improve CPP mediated gene delivery. Such supramolecular

binding motifs not only allow for more specific interactions with the DNA but also with the cell membrane. This enormously enhances the cellular uptake of corresponding peptide/DNA polyplexes relative to peptides with only natural amino acids. Tetra peptide **42** with only four of these artificial GCP groups is a highly efficient transfection vector, even better than the commercial reagent PEI but at the same time with significant lower cytotoxicity.

5.3 Development of a cyclic peptide nanotube based gene delivery vector

The synthesis of a cyclic peptide **45** with a GCP group modification on the side chain of lysine was achieved (Figure 137). This strategy resulted in a novel cationic peptide nanotube. As far as we know, peptide **45** is the first example that a positively charged cyclic peptide forms nanotubes under physiological conditions. Modelling results suggested that the interactions between GCP group and cyclic peptide backbone stabilized the tubular structure by offsetting charge repulsions.

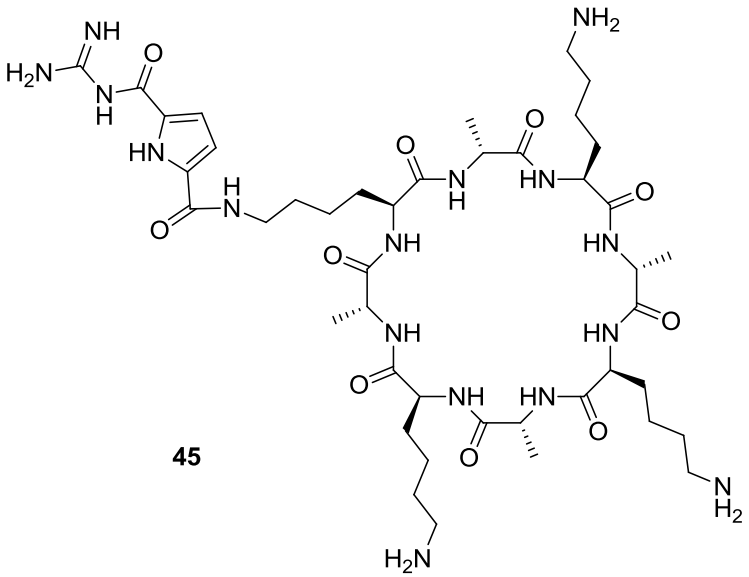

45

Figure 137. Chemical structure of peptide **45.**

Moreover, we demonstrated that peptide **45** can be applied as gene delivery vector. DNA was successfully attached on the surface of nanotubes. The resulted nanotube showed an astonishing ability in gene transfection through non-endocytic cellular uptake pathway. Nanotubes formed by cyclic peptide **45** functioned as a bridge between DNA and cell membrane so that DNA molecules could enter into cells without the involvement of

endocytosis. To the best of our knowledge, this is the first report that a cyclic peptide nanotube can be applied as gene transfection vector.

However, it should be noted that the exact internal structure of the nanotube formed by peptide **45** is not clear due to the detection limit of the method used. Further studies of the role of GCP modifications are in process.

5.4 Development of supramolecular β-helix mimetic peptide

The first example of artificial peptide forming β-helix structure was described in this project. The alternative D and L alanine construction designed to mimic the structure of gramicidin A endowed the helical property of peptide **46** (Figure 138). However, in sharp contrast to typical β-helix structures which have been reported so far, the β-helix formation of peptide **46** required no involvement of membrane mimics. Characteristic CD signals for β-helix of peptide **46** were observed in pure water. It is known that the overall hydrophobic nature of gramicidin A played an important role for its conformation in membranes. Therefore, endeavors to mimic its structure have focused on hydrophobic residues to construct peptides. As consequence, these peptides can only be applied to organic solvents which limited their further application. We now firstly demonstrated that peptide constructed from only alanine, a moderate hydrophobic residue, can successfully mimic β-helix structures in water without the addition of vesicles. Molecular modelling results suggested that the binding between N-terminal GCPs and C-terminal carboxylates were the key force to form energetically stable β-helix structures. Similar structural property can be found in native insect antifreeze proteins (AFP) in which the individual β-sheets were connected with loops to stabilize the β-helix conformation. While in the case of peptide **46**, the individual β-sheets were connected by supramolecular recognition motif (GCP^{+}-COO^{-}). Thus, the ability of peptide **46** to adopt β-helix conformation in water represented a rather simple and promising strategy to construct secondary structures in biological system.

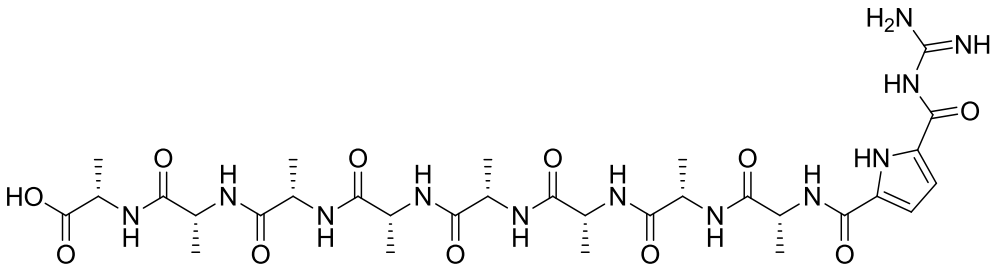

46

Figure 138. Chemical structure of peptide **46**

The aging effect of peptide **46** in water is really intriguing. Based on the results of CD spectroscopy, the overall curve shape which corresponded to β-helix conformation is retained during the aging process. The intensity enhancements of CD signals should then only reflect more β-helix conformation contents of peptide **46** water solution. Therefore, it is reasonable to assume that in the freshly prepared sample solution of peptide **46**, individual monomer co-existed with oligomers in equilibrium. During the aging process, these monomers could further assemble into higher ordered structures such as fibers which would stabilize the β-helix conformation. It is indeed observed in AFM and TEM that the small particles formed by peptide **46** transferred into fibers after several days' incubation at room temperature. However, the curious aspect for the fibers formed by peptide **46** is that these fibers seemed to be intertwined with each other regularly which can be better observed in AFM. One possible reason which cannot be ruled out is that the drying process for the sample preparation of AFM may influence the resulting morphology of the fibers formed by peptide **46**. Nevertheless, the growth process of peptide **46** fiber followed the classical nucleation-elongation mechanism in supramolecular self-assembly as determined by variable temperature experiment.

In overall, the self-assembly of peptide **46** not only demonstrated the first supramolecular β-helix mimic in water but also highlighted the application of supramolecular recognition motif in constructing secondary structures. The switch of peptide **46** between fibers and vesicles also showed interesting potentials in constructing responsive materials.

5.5 Development of functionalized amphiphilic peptide assembly

In this project, GCP group was introduced into Fmoc-containing dipeptide. Due to its low pKa value, GCP groups facilitated the assembly of peptide **47** and **67** (Figure 139). These two

peptides formed helical fibers in water as demonstrated by AFM and CD studies. In comparison, peptide **68** without GCP modifications did not show any assembling property. Thus, peptide **47** and **67** represented a novel class of peptide assembly. The surface of the fibers formed by **47** and **67** were modified with GCP moiety which provided the possibility of post-assembly modification.

We then demonstrated that the fibers formed by **47** were bifunctional. It can interact with DNA and transform into nanoparticles upon DNA binding. This property led to a successful gene transfection which made **47** a new type of gene delivery vector.

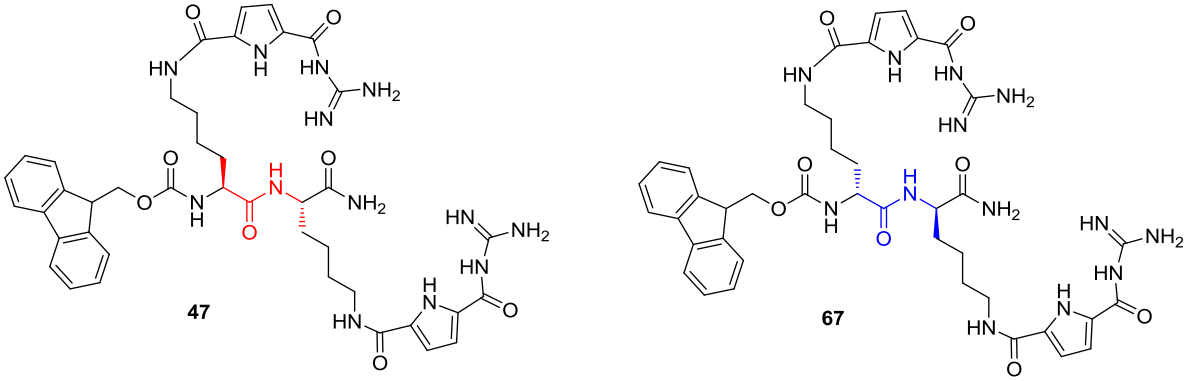

Figure 139. Chemical structure of peptide **47** and **67**

On the other hand, it can also act as a template for the fabrication of other materials. We showed that simple addition of an organic ligand terpyridine and metal ions led to the preparation of metal-organic nanowires. This could benefit the future development of supramolecular nanomaterials.

6. EXPERIMENTAL SECTION

6.1 General remarks and analytical methods

Solvents and Chemicals

All solvents were dried before use. DCM was distilled from calcium hydride. Methanol was distilled. THF and diethyl ether were distilled from sodium with benzophenon as indicator. DMF was distilled from calcium hydride under reduced pressure (the first 100 mL were discarded). Water used in all measurements was purified with *TKA* MicroPure ultrapure water system. All other solvents and reagents were utilized as supplied from the manufacturer.

Cell lines and DNA

The human embryonic kidney cell line HEK293T (ATCC-No. CRL-1573), the Human cervix carcinoma cell lines HeLa (ATCC-No.CCL-2), and the murine fibroblast cell line NIH/3T3 (ATCC-No. CRL-1658) were obtained from the *American Type Culture Collection* and maintained as recommended in complete Dulbecco`s Modified Eagle Medium (DMEM) supplemented with 10 % fetal bovine serum, 1 % Glutamine and 1 % Antibiotic-Antimycotic (*Invitrogen)* at 37 ° C in a humidified atmosphere of 5 % CO_2. Calf thymus DNA (ctDNA) was obtained from *Aldrich*, dissolved in sodium cacodylate buffer (0.05 M, pH 7), cooled to 4 ° C for 20 h, sonicated (8 × 4 sec) and filtered through a 0.45 μm PTFE filter.

Magnetic Stirrer

Reactions were stirred and heated with the help of magnetic stirring bars and a MR 3001 K magnetic stirrer from *Heidolph*.

Inert Gas

Reactions under inert gas were carried out with Argon (99.998 %) from *Air Liquide* dried with Silica Gel Orange.

Thin layer Chromatography (TLC)

Analytical TLC was carried out on aluminium foils ALUGRAM-SIL-G/UV254 from *Macherey-Nagel*. The spots were visualized upon irradiation with UV light of 254 nm.

Column Chromatography

Flash chromatography was done on columns packed with Silica gel 60M with a spherical size of 40-63 μm from *Macherey-Nagel*.

Vacuum Pumps

Vacuum was generated with a *Vacuubrand* CVC3000 pump. High vacuum was achieved with a RC6 chemistry hybrid pump.

Rotary Evaporator

Removal of solvent from the reaction mixture and eluents from chromatography were performed under reduced pressure with a *Heidolph* Hei-VAP Advantage rotary evaporator at 40 °C.

Orbital Shaker for Peptide Synthesis

Room temperature solid phase peptide synthesis was carried out on a *Yellowline* OS 5 basic orbital shaker from *Heidolph*.

Microwave used in Peptide Synthesis

Mircowave-assisted solid phase peptide synthesis was carried out with a *CEM* Discover single mode microwave.

Analytical HPLC

The analysis of peptides was carried out with an HPLC apparatus from *Dionex* containing the following components: P680 HPLC-pump, ASI-100 Automated Sample Injector, UVD 340U detector. The YMC ODS-A RP18 column with a spherical size of 5 μm and a pore size of 12 nm was utilized. Commercial available ultrapure water and HPLC-grade solvents were used for elution.

Preparative HPLC

Separation of milligram scales of peptides were performed on a *Merck* SepTech preparative HPLC apparatus equipped with a Knauer Dynamic Mixing Chamber and a Shimadzu SPD-10A UV detector. The YMC ODS-A RP18 column (15 cm × 3.0 cm, 5 μm) was utilized and the conditions were optimized via analytical HPLC on the corresponding YMC column.

Preparative MPLC

Purification of peptides was conducted with reversed phase preparative MPLC on a Liquid Chromatography Flash apparatus from *Armen Instrument*. Glass columns were packed with YMC Gel ODS-A RP18 silica of 12 nm pore size and 5 μm diameter. Distilled solvents and ultrapure water were used as eluents. UV detector was applied for the detection of the products.

Centrifuge

Precipitates in water solution were centrifuged with a Rotofix 32 from *Hettich*.

Lyophilization

Lyophilization of aqueous solutions of peptides was carried out with an Alpha 1-4 LD plus drying apparatus obtained from *Christ.*

Mass Spectrometry

MALDI-TOF and ESI MS spectra were received by using a *Bruker* BioTOF III.

pH Measurement

The pH of sample solution was adjusted with pH-Meter 766 Calimatic from *Knick*.

Nuclear Magnetic Resonance (NMR)

500 and 300 MHz NMR spectra in $CDCl_3$ and d^6-DMSO were recorded with DRX 500 and DMX300 from *Bruker* at 298K. The spectra were calibrated with residual peaks of the deuterated solvents as internal standard: DMSO-d6 (δ [1H] = 2.50 ppm), $CDCl_3$ (δ [1H] = 7.26 ppm). The chemical shifts are reported as δ values in ppm. Coupling constants are reported in Hz. The following abbreviations are utilized for the signal multiplicity: s = singlet, d = doublet, t = triplet, q = quartet, m = multiplet, br. = broad.

UV/Vis Spectroscopy

UV spectrum was recorded with *JASCO* V-660 spectrometer in 10 mm quartz cuvette with following parameters: range = 295 nm, sensitivity = standard, scanning speed = 200nm/min, data pitch = 0.1 nm, bandwidth = 1 nm, response = 1 sec. All spectra are corrected for the background (buffer solution).

Fluorescence Spectroscopy

Fluorescence spectra were recorded with a *Varian* Carey Eclipse spectrometer in standard quartz fluorescence micro-cuvettes of 1 cm width.

CD Spectroscopy

Experiments were carried out in 10mm quartz cuvette (total volume of cuvette=2000 µl) with *JASCO* J-815 CD Spectrometer. Instrument parameters: range=500-230 nm, sensitivity=standard (100mdeg), scanning speed=200nm/min, data pitch=0.2 nm, bandwindth=2nm, response=1 sec, accumulation=3.

Isothermal Titration Calorimetry

ITC measurements were performed with a VP-ITC Microcalorimeter purchased from *MicroCal*. Ultrapure, degassed water was used to fill the reference cell. All samples were dissolved in degassed, ultrapure buffered water and filtered before measurement. The data were analyzed with Origin 7 from *Origin Lab* including an ITC plugin from *MicroCal*.

Dynamic Light Scattering

All measurements were carried out at 25 °C in UV-transparent microcuvettes (1 cm) equipped with a stopper. Peptide solution in water was prepared and filtered prior to measuring. The pH was adjusted with sodium hydroxide solution accordingly. The autocorrelation functions of the backscattered light fluctuations were analyzed with the DTS 6.20 software from *Malvern* providing the hydrodynamic diameter (Z-average), polydispersity, size distribution (NNLS analysis).

Atomic Force Microscopy

The according samples were prepared and adjusted the pH with sodium hydroxide solution. AFM samples were prepared by spin-coating (66rps) the solutions onto a freshly cleaved mica surface (Plano GmbH) for 2 minutes. AFM images were obtained in tapping mode using a NanoDrive Controller with an Innova Scanning Probe Microscope (*Veeco Germany*, Mannheim) and N-type silicon cantilever (AC 160TS OLYMPUS). The scan rate was about 5 µm/s. The AFM data were analyzed using Gwiddion-2.20 software.

Transmission Electron Microscope

The according samples were prepared and adjusted the pH with sodium hydroxide solution. A drop of a freshly prepared and 8 days old sample solution was placed on 400-mesh formvar copper grid coated with carbon, respectively. About 2 min after the deposition the grid was tapped with filter paper to remove remaining solvent from the surface. Negative staining was performed by addition of a drop of an ethanol solution of uranyl acetate (0.5 %) onto the copper grid. After 1 min, the liquid on the surface of the grid was removed by tapping it with a filter paper. TEM images were obtained using a CM 200 FEG (*Phillips Company*).

6.2 General procedure for solid phase peptide synthesis

Solid phase peptide synthesis was performed in Schlenck glass vessels equipped with frit and stopper under argon atmosphere while shaking. The solvent was removed through vacuum filtration after the reaction is finished.

Kaiser test

To examine the free amino groups on the resin, ninhydrin (1.00 g) and phenol (40 g) were dissolved in 10 mL ethanol, respectively. A small amount of resins were then suspended in a mixture of 0.5 mL of each of the two solutions and heated for 1-2 min at 110 ℃. Consequently, resins with free amines showed deeply blue color while resin without free amino functions remained white.

Fmoc Deprotection

The resin was shaken with 20 % piperidine in DMF two times for 20 min in order to remove Fmoc protecting groups. Afterwards, it was thoroughly washed six times with DMF. The reaction is monitored with *Kaiser* test.

Alloc Deprotection

The removal of Alloc group was achieved by treatment with $Pd(PPh_3)_4$ (0.1 eq) in the presence of $PhSiH_3$ (24 eq) in DCM. This procedure was repeated two times for 20 min. Then the resin was washed three times with DCM and DMF for 5 min. The reaction is monitored with *Kaiser* test.

Coupling Procedure

The amino acid (3 eq) was attached to the resin using PyBop (3eq) as the coupling reagent and DIPEA (6 eq) as base in distilled DMF under argon atmosphere at room temperature by shaking the reaction mixture for 8h. Then the resin was washed with DMF for three times each for 5 min. For the attachment of each amino acid, the coupling and washing steps were repeated twice. The reaction is monitored with *Kaiser* test.

6.3 General Procedures for Microwave-Assisted SPPS

Microwave-assisted solid phase peptide synthesis was performed in a microwave-transparent polyethylene tubes using *CEM* Discover microwave apparatus equipped with a frit. The reaction mixtures were bubbling with argon.

Fmoc Deprotection

Fmoc protecting group was removed with 20% piperidine in DMF. For each deprotection, the reaction was carried out under irradiation condition (20W, T_{max}= 60 °C, ΔT = ±5 °C) two times for 1.5 min and 5 min, respectively. Then the resin was thoroughly washed six times with DMF each for 2min with argon bubbling. The reaction is monitored with *Kaiser* test.

Alloc Deprotection

The removal of Alloc protecting group was performed by treatment with $Pd(PPh_3)_4$(0.1 eq) in the presence of PhSiH3 (24 eq) in DCM for 10 min under irradiation condition (20W, T_{max}= 30 ℃). Then the resin was washed three times with DCM and DMF each for 2 min with the help of argon bubbling. The reaction is monitored with *Kaiser* test.

Coupling Procedure

The amino acid was attached to the resin using PyBop as the coupling reagent and DIPEA as base in distilled DMF. The reaction was facilitated by irradiation condition (20W, Tmax= 60 °C, ΔT = ±5 °C) and repeated two times each for 20 min with the help of argon bubbling. Then the resin was washed with DMF for three times each for 5 min. The reaction is monitored with *Kaiser* test.

6.4 Synthesis of peptide analogues

6.4.1 Synthesis of dipeptide analogues

Microwave Assisted Solid-Phase Peptide Synthesis of (40):

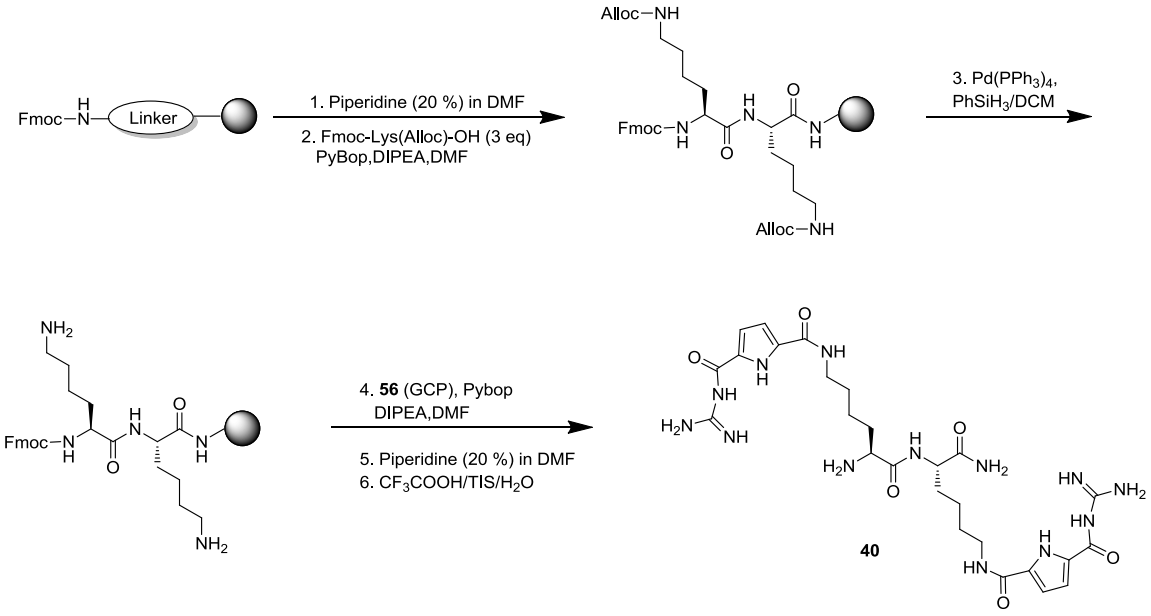

The reaction was carried out in a microwave-transparent 25 ml polyethylene column with a CEM Discover microwave apparatus. Rink-Amide MBHA resin (200 mg, 0.62mmol/g) was swollen in DCM (5 ml) for 2 h. Fmoc removal was achieved by irradiating the resin in 20 % piperidine/DMF (5 ml) for 1 min and 5 min at 20 W and a maximum temperature of 60 °C followed by washing with DMF (6 × 5 ml). The first residue Fmoc-Alloc-Lys-OH (169 mg, 0.37 mmol, 3 eq) was attached to the resin by microwave irradiation for 20 min at 20 W and a maximum temperature of 60 °C under argon atmosphere with PyBOP (194 mg, 0.37 mmol, 3 eq), DIPEA (130 µl, 0.74 mmol, 6 eq) in DMF (5 ml) and consequent washing with DMF (3 × 5 ml). Coupling and washing steps were repeated. After Fmoc deprotection the second residue Fmoc-Alloc-Lys-OH was attached to the resin as described above, also repeating coupling and washing steps. Alloc removal was achieved by $Pd(PPh_3)_4$ (28 mg, 0.02 mmol, 0.2 eq), $PhSiH_3$ (183 µl, 1.50 mmol, 24 eq) in 7 ml DCM for 30 min at room temperature under argon bubbling and consequent washing with DMF (3 × 5 ml). The deprotection and washing process was repeated. The GCP groups (197 mg, 0.99 mmol, 4 eq) were attached to the resin by microwave irradiation for 20 min at 20 W and a maximum temperature of 60 °C under

argon atmosphere with PyBOP (258 mg, 0.55 mmol, 4 eq), DIPEA (168 µl, 0.99 mmol, 8 eq) in DMF (5 ml) and consequent washing with DMF (3 × 5 ml). The coupling process was repeated until *Kaiser Test* showed negative result. After Fmoc deprotection the resin was washed with DCM (3 × 5 ml), methanol (3 × 5 ml), and DCM (3 × 5 ml) and dried under reduced pressure for one hour. To cleave the product, the resin was transferred to a flask equipped with a frit onto a Heidolph Rotamax 120 shaker. There it was shaken under argon atmosphere in a mixture containing 95 % TFA, 2.5 % water, and 2.5 % TIS for three hours and washed twice with the cleavage mixture. The filtrates were combined and concentrated in high vacuum at room temperature. Diethyl ether (40 ml) was added and the resulting suspension was centrifuged. The supernatant solvent was decanted and the solid was washed with diethyl ether and centrifuged again. After decanting, the raw product was dissolved in little methanol, water (30 ml) was added, and the mixture was freeze-dried in vacuum. The resulting solid was purified by MPLC on C18 reversed-phase silica gel (10 % to 50 % methanol/water in 45 min, 0.1 % TFA) to obtain **40** as white solid (20 mg, 25 %) with 96 % purity determined by analytical RP-HPLC.

^{1}H-NMR (500 MHz, d^{6}-DMSO): δ [ppm] = 1.36-1.38 (m, 4H, Lys-CH_2), 1.48-1.50 (m, 4H, Lys-CH_2), 1.71-1.73 (m, 4H, Lys-CH_2), 3.21-3.23 (t, 4H, J = 5 Hz, Lys-CH_2), 3.80-3.81 (m, 1H, Lys-CH), 4.22-4.25 (m, 1H, Lys-CH), 6.85 (s, 2H, pyrrole-CH), 7.05 (s, 1H, pyrrole -NH), 7.37 (s, 2H, pyrrole-CH), 7.50 (s, 1H, pyrrole -NH), 8.12-8.13 (m, 3H, amide-NH), 8.46-8.52 (m, 10H, guanidine-NH), 11.70 (s, 2H, amine-NH_2), 12.31 (s, 2H, amide-NH_2).

^{13}C-NMR (125 MHz, d^{6}-DMSO): δ [ppm] = 21.7 (Lys-CH_2), 22.9 (Lys-CH_2), 28.6 (Lys-CH_2), 28.8 (Lys-CH_2), 31.0 (Lys-CH_2), 31.9 (Lys-CH_2), 38.6 (Lys-CH_2), 38.7 (Lys-CH_2), 52.1 (Lys-CH), 52.7 (Lys-CH), 112.4 (pyrrole-CH), 115.9 (pyrrole-CH), 125.4 (Cq), 132.9 (Cq), 155.4 (Cq), 159.1 (Cq), 159.2 (Cq), 159.7 (Cq), 158.5 (Cq), 173.2 (Cq).

MALDI-TOF-MS (pos.) m/z calculated for $C_{26}H_{39}N_{13}O_6$ $[M + H]^+$ 630.31, found 630.33

Microwave Assisted Solid-Phase Peptide Synthesis of (41):

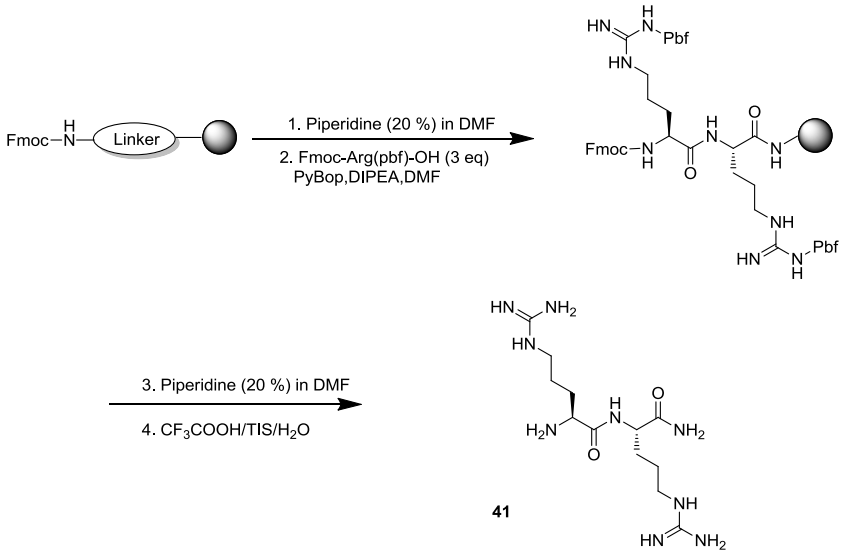

Rink-Amide MBHA resin (200 mg, 0.62mmol/g) was swollen in DCM (5 ml) for 2 h. Fmoc removal was achieved by irradiating the resin in 20 % piperidine/DMF (5 ml) for 1 min and 5 min at 20 W and a maximum temperature of 60 °C followed by washing with DMF (6 × 5 ml). The first residue Fmoc-Arg(Pbf)-OH (242 mg, 0.37 mmol, 3 eq) was attached to the resin by microwave irradiation for 20 min at 20 W and a maximum temperature of 60 °C under argon atmosphere with PyBOP (193 mg, 0.37 mmol, 3 eq), DIPEA (127 µl, 0.74 mmol, 6 eq) in DMF (5 ml) and consequent washing with DMF (3 × 5 ml). Coupling and washing steps were repeated. After Fmoc deprotection the second residue Fmoc-Arg(Pbf)-OH was attached to the resin as described above, also repeating coupling and washing steps. After Fmoc deprotection the resin was washed with DCM (3 × 5 ml), methanol (3 × 5 ml), and DCM (3 × 5 ml) and dried under reduced pressure for one hour. To cleave the product, the resin was shaken under argon atmosphere in a mixture containing 95 % TFA, 2.5 % water, and 2.5 % TIS for three hours and washed twice with the cleavage mixture. The filtrates were combined and concentrated in high vacuum at room temperature. Diethyl ether (40 ml) was added and the resulting suspension was centrifuged. The supernatant solvent was decanted and the solid was washed with diethyl ether and centrifuged again. After decanting, the raw product was dissolved in little methanol, water (30 ml) was added, and the mixture was freeze-dried in vacuum. The resulting solid was purified by MPLC on C18 reversed-phase silica gel (5 % to 50 % methanol/water in 45 min, 0.1 % TFA) to obtain **41** as white solid (10

mg, 25 %).

^{1}H-NMR (500 MHz, D_2O): δ [ppm] = 1.67-1.72 (m, 4H, Arg-CH_2), 1.84-1.85 (m, 2H, Arg-CH_2), 1.97-1.98 (m, 2H, Arg-CH_2), 3.22-3.25 (m, 4H, Arg-CH_2), 4.13 (s, 1H, Arg-CH), 4.32-4.35 (m, 1H, Arg-CH).

^{13}C-NMR (125 MHz, D_2O): δ [ppm] = 23.4 (Arg-CH_2), 24.4 (Arg-CH_2), 28.0 (Arg-CH_2), 28.1 (Arg-CH_2), 40.4 (Arg-CH_2), 40.6 (Arg-CH_2), 52.6 (Arg-CH), 53.6 (Arg-CH), 156.8 (guanidine-C), 169.8(Cq), 175.9 (Cq).

ESI-MS (pos.) m/z calculated for $C_{12}H_{28}N_9O_2$ $[M + H]^+$ 330.2, found 330.2

Synthesis of Rhodamine labeled peptide (58):

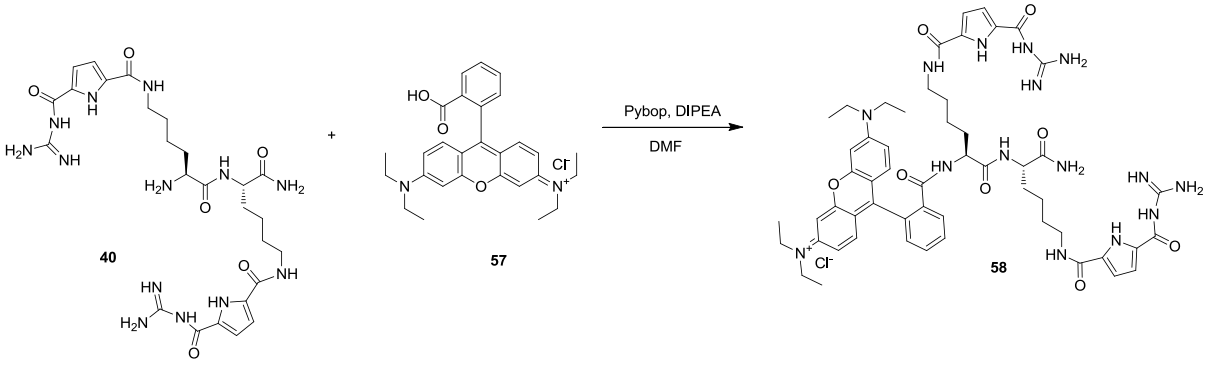

To a reaction mixture of **57** (9.6mg, 0.02 mmol) in 10 mL DMF, PyBop (12mg, 0.024mmol) and DIPEA (4.1µl, 0.024mmol) were added under argon atmosphere at room temperature avoid of light. The solution was stirred for 30 minutes and peptide **40** (12mg, 0.02mmol) was added subsequently. The reaction solution was stirred for overnight at room temperature. Afterwards, DMF was removed under reduced pressure. 20 mL water was then added to the residue oil and lyophilized. The crude product was purified with MPLC on C18 reversed-phase silica gel (10 % to 100 % methanol/water in 45 min, 0.1 % TFA) to obtain **58** as red solid (8 mg, 38%).

^{1}H-NMR (500 MHz, d^{6}-DMSO): δ [ppm] = 1.20-1.23 (m, 8H, Lys-CH_2), 1.42-1.44 (m, 12H, Lys-CH_2, Rhodamine-CH_3), 1.45-1.49 (m, 4H, Lys-CH_2), 2.83 (m, 2H, Lys-CH_2), 3.14-3.28 (m, 10H, Lys-CH_2, Rhodamine-CH_2), 3.92-4.08 (m, 1H, Lys-CH), 4.09-4.10 (m, 1H, Lys-CH), 6.32 (s, 2H, pyrrole-CH), 6.83 (s, 2H, pyrrole-CH), 6.90-7.10 (m, 7H, amide-NH, pyrrole-NH), 7.43-7.53 (m, 4H, amide-NH), 7.75-7.80 (m, 3H, amide-NH), 8.35-8.40 (m,

10H, guanidine-NH), 11.14 (s, 2H, amide-NH), 12.29-12.33 (m, 2H, amide-NH_2).

^{13}C-NMR (125 MHz, d^6-DMSO): δ [ppm] = 12.3 (Rhodamine-CH_3), 12.4 (Rhodamine-CH_3), 13.9 (Rhodamine-CH_3), 22.1 (Lys-CH_2), 28.1 (Lys-CH_2), 28.4 (Lys-CH_2), 28.7 (Lys-CH_2), 29.0 (Lys-CH_2), 31.2 (Lys-CH_2), 32.3 (Lys-CH_2), 38.6 (Lys-CH_2), 43.7 (Rhodamine-CH_2), 45.2 (Rhodamine-CH_2), 46.2 (Rhodamine-CH_2), 52.1 (Lys-CH), 52.7 (Lys-CH), 112.3 (pyrrole-CH), 114.4 (pyrrole-CH), 115.4 (pyrrole-CH), 125.3 (Rhodamine-CH), 132.8 (Rhodamine-CH), 152.6 (Rhodamine-CH), 155.0 (Rhodamine-CH), 158.0 (Cq), 158.7 (Cq), 158.9 (Cq), 159.5 (Cq), 167.3 (Cq),172.9 (Cq).

MALDI-TOF-MS (pos.) m/z calculated for $C_{54}H_{69}N_{15}O_8$ $[M + H]^+$ 1055.54, found 1056.47

Synthesis of FITC labeled peptide (60):

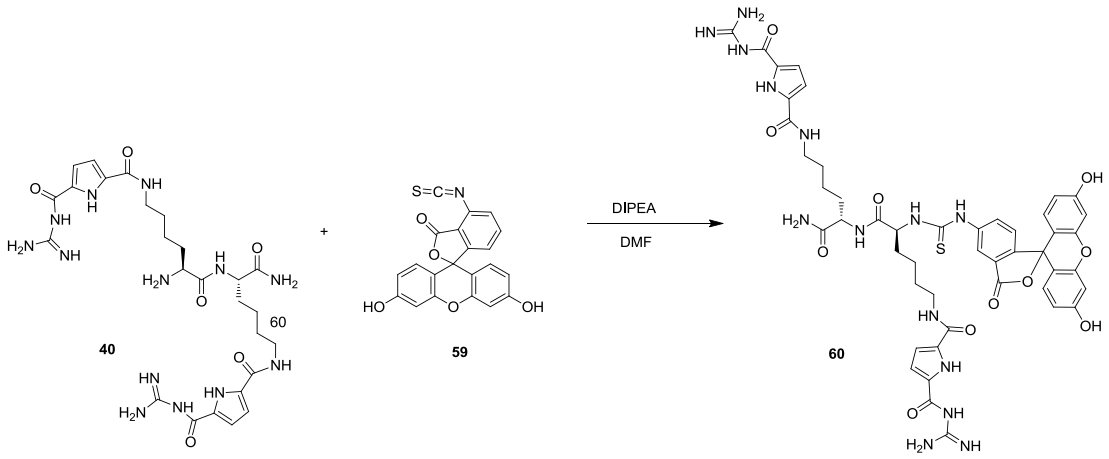

To a reaction mixture of **59** (7.8 mg, 0.02 mmol) in 10 mL DMF, DIPEA (4.1 µl, 0.024 mmol) was added under argon atmosphere at room temperature avoid of light. The solution was stirred for 30 minutes and peptide **40** (12mg, 0.02 mmol) was added subsequently. The reaction solution was stirred for 2 hours at room temperature. Afterwards, DMF was removed under reduced pressure. 20 mL water was then added to the residue oil and lyophilized. The crude product was purified with MPLC on C18 reversed-phase silica gel (10 % to 100 % methanol/water in 45 min, 0.1 % TFA) to obtain **60** as yellow solid (18 mg, 90%).

^{1}H-NMR (500 MHz, d^{6}-DMSO): δ [ppm] = 1.53-1.54 (m, 8H, Lys-CH_2), 1.55-1.59 (m, 4H, Lys-CH), 1.70-1.83 (m, 2H, isothiocyanate-NH), 3.23-3.24 (m, 4H, Lys-CH_2), 3.75 (m, 1H, Lys-CH), 4.23 (m, 1H, Lys-CH), 4.91 (s, 1H, FITC-OH), 6.54-6.56 (m, 3H, FITC-CH), 6.58-6.60 (m, 2H, FITC-CH), 6.67-7.32 (m, 7H, amide-NH, pyrrole-NH, pyrrole-CH), 7.75 (s, 1H, amide-NH), 8.20-8.23 (m, 8H, guanidine-NH), 8.42-8.43 (m, 2H, guanidine-NH), 10.12-10.19 (m, 2H, amine-NH), 11.05 (s, 2H, amine-NH), 12.34 (m, 2H, amide-NH_2).

^{13}C-NMR (125 MHz, d^{6}-DMSO): δ [ppm] = 13.9 (Lys-CH_2), 22.0 (Lys-CH_2), 22.4 (Lys-CH_2), 23.0 (Lys-CH_2), 24.4 (Lys-CH_2), 28.7 (Lys-CH_2), 28.8 (Lys-CH_2), 29.0 (Lys-CH_2), 31.2 (Lys-CH_2), 31.6 (Lys-CH_2), 32.1 (Lys-CH_2), 52.5 (Lys-CH), 56.7 (Lys-CH), 82.9 (FITC-CH), 102.2 (FITC-CH), 109.6 (FITC-CH), 112.2 (pyrrole-CH), 112.5 (pyrrole-CH), 115.4 (pyrrole-CH), 125.2 (FITC-CH), 129.0 (FITC-CH), 132.9 (FITC-CH), 151.8 (Cq), 154.8 (Cq), 157.8 (Cq), 158.0 (Cq), 158.9 (Cq), 159.4 (Cq), 173.4 (Cq),179.9 (Cq).

ESI-MS (pos.) m/z calculated for $C_{47}H_{52}N_{14}O_{11}S$ $[M + H]^{2+}$ 510.2, found 510.7

6.4.2 Synthesis of tetra-peptide analogues

Microwave Assisted Solid-Phase Peptide Synthesis of (42):

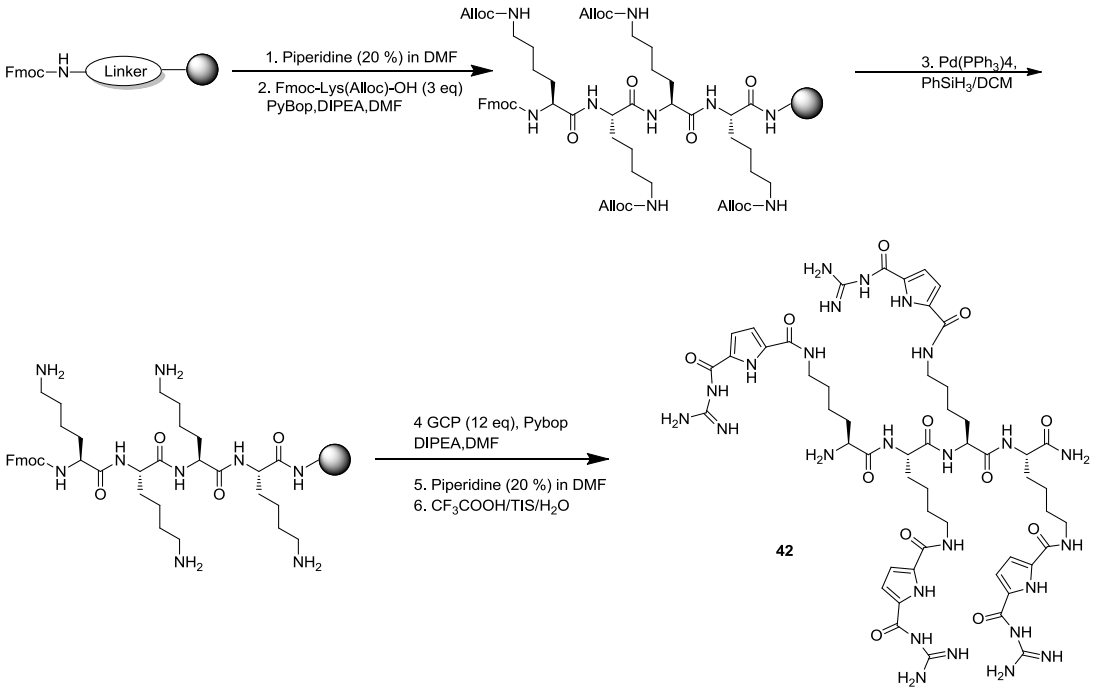

The reaction was carried out in a fritted, microwave-transparent 25 ml polyethylene column with a CEM Discover microwave apparatus. Rink-Amide MBHA resin (200 mg, 0.62mmol/g) was swollen in DCM (5 ml) for 2 h. Fmoc removal was achieved by irradiating the resin in 20 % piperidine/DMF (5 ml) for 1 min and 5 min at 20 W and a maximum temperature of 60 °C followed by washing with DMF (6 × 5 ml). The first residue Fmoc-Alloc-Lys-OH (169 mg, 0.37 mmol, 3 eq) was attached to the resin by microwave irradiation for 20 min at 20 W and a maximum temperature of 60 °C under argon atmosphere with PyBOP (194 mg, 0.37 mmol, 3 eq), DIPEA (130 µl, 0.74 mmol, 6 eq) in DMF (5 ml) and consequent washing with DMF (3 × 5 ml). Coupling and washing steps were repeated. After Fmoc deprotection the second to the fourth residues Fmoc-Alloc-Lys-OH was attached to the resin as described above, also repeating coupling and washing steps. Alloc removal was achieved by $Pd(PPh_3)_4$ (57 mg, 0.05 mmol, 0.4 eq), $PhSiH_3$ (366 µl, 2.98 mmol, 24 eq) in 7 ml DCM for 30 min at room temperature under argon bubbling and consequent washing with DMF (3 × 5 ml). The deprotection and washing process was repeated. The GCP groups (591 mg, 1.48 mmol, 12 eq) were attached to the resin by microwave irradiation for 20 min at 20 W and a maximum

temperature of 60 ° C under argon atmosphere with PyBOP (774mg, 1.48 mmol, 12 eq), DIPEA (505 µl, 2.97 mmol, 24 eq) in DMF (5 ml) and consequent washing with DMF (3 × 5 ml). The coupling process was repeated until *Kaiser Test* showed negative result. After Fmoc deprotection the resin was washed with DCM (3 × 5 ml), methanol (3 × 5 ml), and DCM (3 × 5 ml) and dried under reduced pressure for one hour. To cleave the product, the resin was transferred to a flask equipped with a frit onto a Heidolph Rotamax 120 shaker. There it was shaken under argon atmosphere in a mixture containing 95 % TFA, 2.5 % water, and 2.5 % TIS for three hours and washed twice with the cleavage mixture. The filtrates were combined and concentrated in high vacuum at room temperature. Diethyl ether (40 ml) was added and the resulting suspension was centrifuged. The supernatant solvent was decanted and the solid was washed with diethyl ether and centrifuged again. After decanting, the raw product was dissolved in little methanol, water (30 ml) was added, and the mixture was freeze-dried in vacuum. The resulting solid was purified by MPLC on C18 reversed-phase silica gel (5 % to 45 % methanol/water in 45 min, 0.1 % TFA) to obtain **42** as white solid (8 mg, 5%) with 93% purity by analytical RP-HPLC.

^{1}H-NMR (500 MHz, d^{6}-DMSO): δ [ppm] = 1.29-1.40 (m, 8H, Lys-CH_2), 1.48-1.70 (m, 16H, Lys-CH_2), 3.20 (s, 8H, Lys-CH_2), 3.69-3.79 (m, 1H, Lys-CH), 4.16-4.22 (m, 2H, Lys-CH), 4.46 (s, 1H, Lys-CH), 5.32-5.52 (m, 1H, amino-NH), 6.83 (s, 4H, pyrrole-CH), 7.02-7.17 (m, 2H, amide-NH), 7.26-7.31 (m, 2H, amide-NH_2), 7.42(s, 4H, pyrrole-CH), 7.78(s, 1H, guanidine-NH), 7.93(br. s, 1H, guanidine-NH), 8.18-8.68 (m, 19H, amide-NH, guanidine-NH), 11.88 (br.s, 3H, guanidine-NH), 12.26 (br.s, 3H, guanidine-NH).

^{13}C-NMR (125 MHz, d^{6}-DMSO): δ [ppm] = 22.7 (Lys-CH_2), 22.9 (Lys-CH_2), 23.1 (Lys-CH_2), 28.9 (Lys-CH_2), 31.4 (Lys-CH_2), 31.7 (Lys-CH_2), 38.7 (Lys-CH_2), 52.2 (Lys-CH), 52.6 (Lys-CH), 52.9 (Lys-CH), 112.3 (pyrrole-CH), 113.4 (pyrrole-CH), 115.8 (pyrrole-CH), 125.4 (pyrrole-CH), 155.5 (Cq), 158.9 (Cq), 159.7 (Cq), 171.2 (Cq), 171.6 (Cq), 171.8 (Cq), 173.4 (Cq).

MALDI-TOF-MS (pos.) m/z calculated for $C_{52}H_{76}N_{25}O_{12}$ $[M + H]^+$ 1242.61, found 1242.01

Microwave Assisted Solid-Phase Peptide Synthesis of (62):

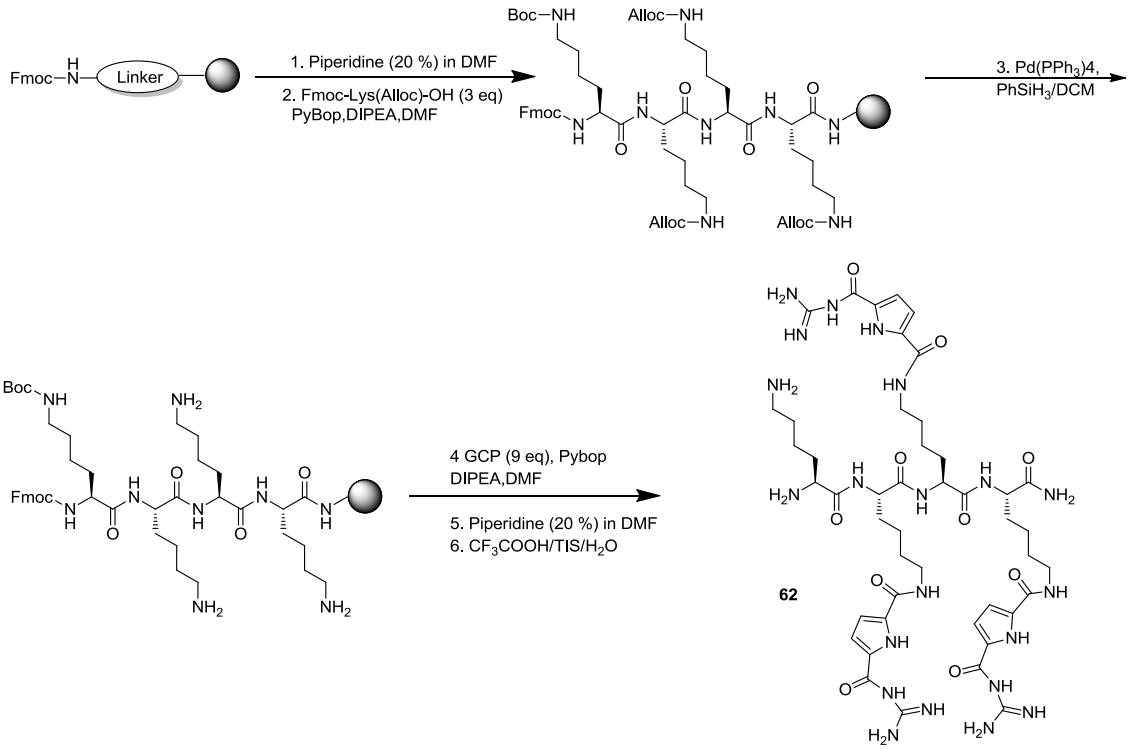

The reaction was carried out in a fritted, microwave-transparent 25 ml polyethylene column with a CEM Discover microwave apparatus. Rink-Amide MBHA resin (200 mg, 0.62mmol/g) was swollen in DCM (5 ml) for 2 h. Fmoc removal was achieved by irradiating the resin in 20 % piperidine/DMF (5 ml) for 1 min and 5 min at 20 W and a maximum temperature of 60 °C followed by washing with DMF (6 × 5 ml). The first residue Fmoc-Alloc-Lys-OH (169 mg, 0.37 mmol, 3 eq) was attached to the resin by microwave irradiation for 20 min at 20 W and a maximum temperature of 60 °C under argon atmosphere with PyBOP (194 mg, 0.37 mmol, 3 eq), DIPEA (130 µl, 0.74 mmol, 6 eq) in DMF (5 ml) and consequent washing with DMF (3 × 5 ml). Coupling and washing steps were repeated. After Fmoc deprotection the second to the third residues Fmoc-Alloc-Lys-OH was attached to the resin as described above, also repeating coupling and washing steps. Afterwards, the fourth residue Fmoc-Boc-Lys-OH (173mg, 0.37 mmol, 3 eq) was attached to the resin. Alloc removal was achieved by $Pd(PPh_3)_4$ (42 mg, 0.04 mmol, 0.3 eq), $PhSiH_3$ (366 µl, 2.98 mmol, 24 eq) in 7 ml DCM for 30 min at room temperature under argon bubbling and consequent washing with DMF (3 × 5 ml). The deprotection and washing process was repeated. The GCP groups (443 mg, 1.11 mmol, 9 eq) were attached to the resin by microwave irradiation for 20 min at 20 W and a

maximum temperature of 60 °C under argon atmosphere with PyBOP (580 mg, 1.11 mmol, 9 eq), DIPEA (379 µl, 2.22 mmol, 18 eq) in DMF (5 ml) and consequent washing with DMF (3 × 5 ml). The coupling process was repeated until *Kaiser Test* showed negative result. After Fmoc deprotection the resin was washed with DCM (3 × 5 ml), methanol (3 × 5 ml), and DCM (3 × 5 ml) and dried under reduced pressure for one hour. To cleave the product, the resin was transferred to a flask equipped with a frit onto a Heidolph Rotamax 120 shaker. There it was shaken under argon atmosphere in a mixture containing 95 % TFA, 2.5 % water, and 2.5 % TIS for three hours and washed twice with the cleavage mixture. The filtrates were combined and concentrated in high vacuum at room temperature. Diethyl ether (40 ml) was added and the resulting suspension was centrifuged. The supernatant solvent was decanted and the solid was washed with diethyl ether and centrifuged again. After decanting, the raw product was dissolved in little methanol, water (30 ml) was added, and the mixture was freeze-dried in vacuum. The resulting solid was purified by MPLC on C18 reversed-phase silica gel (5 % to 45 % methanol/water in 45 min, 0.1 % TFA) to obtain **62** as white solid (6 mg, 4%) with 95% purity by analytical RP-HPLC.

^{1}H-NMR (500 MHz, d^{6}-DMSO): δ [ppm] = 1.37-1.39 (m, 8H, Lys-CH_2), 1.51-1.72 (m, 16H, Lys-CH_2), 2.61-2.74 (s, 2H, Lys-CH_2), 3.20 (s, 6H, Lys-CH_2), 3.83 (s, 1H, Lys-CH), 4.16-4.22 (m, 2H, Lys-CH), 4.32 (s, 1H, Lys-CH), 6.85-6.87 (m, 2H, pyrrole-CH), 7.04-7.50 (m, 5H, amide-NH), 7.85(s, 4H, pyrrole-CH), 8.17-8.63 (m, 18H, amide-NH, guanidine-NH), 12.0 (s, 2H, amine-NH_2), 12.29(s, 2H, amide-NH_2).

^{13}C-NMR (125 MHz, d^{6}-DMSO): δ [ppm] = 21.6 (Lys-CH_2), 22.8 (Lys-CH_2), 22.9 (Lys-CH_2), 26.5 (Lys-CH_2), 28.4 (Lys-CH_2), 28.7 (Lys-CH_2), 30.8 (Lys-CH_2), 31.4 (Lys-CH_2), 31.5 (Lys-CH_2), 38.5 (Lys-CH_2), 51.9 (Lys-CH), 52.7 (Lys-CH), 112.3 (pyrrole-CH), 112.4 (pyrrole-CH), 115.8 (pyrrole-CH), 155.4 (Cq), 159.0 (Cq), 159.6 (Cq), 168.5 (Cq), 171.2 (Cq), 173.3 (Cq).

MALDI-TOF-MS (pos.) m/z calculated for $C_{45}H_{70}N_{21}O_{10}$ $[M + H]^+$ 1064.55, found 1065.36

Microwave Assisted Solid-Phase Peptide Synthesis of (63):

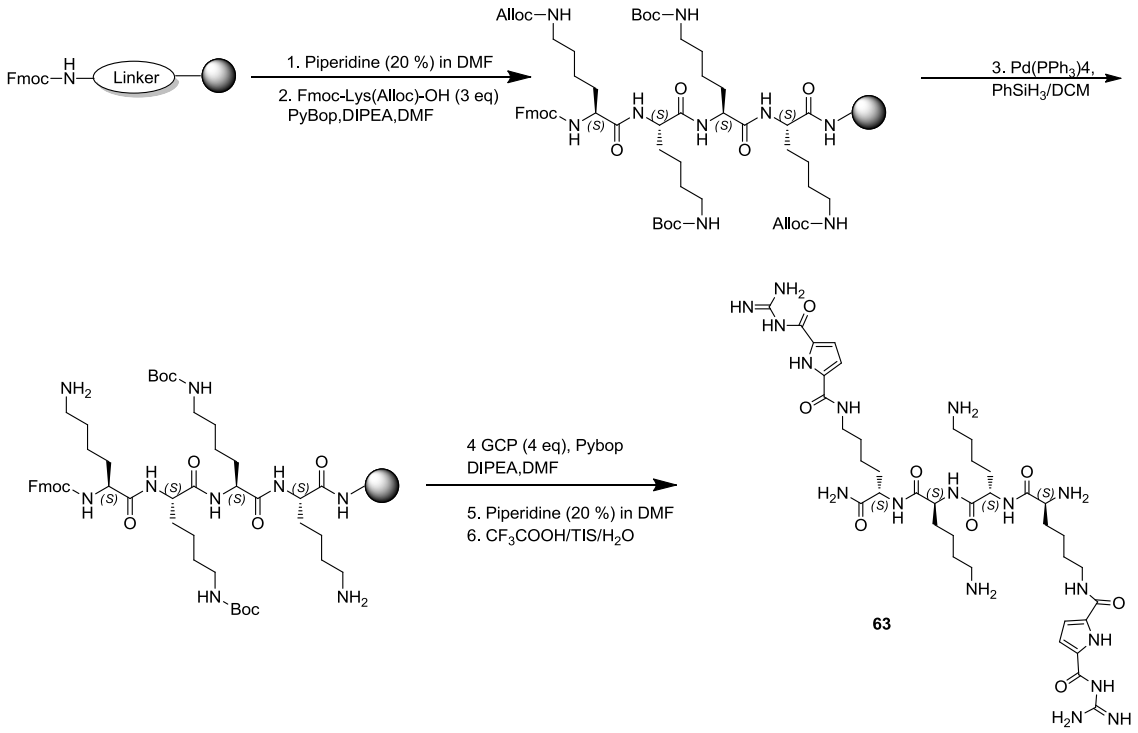

The reaction was carried out in a fritted, microwave-transparent 25 ml polyethylene column with a CEM Discover microwave apparatus. Rink-Amide MBHA resin (200 mg, 0.62mmol/g) was swollen in DCM (5 ml) for 2 h. Fmoc removal was achieved by irradiating the resin in 20 % piperidine/DMF (5 ml) for 1 min and 5 min at 20 W and a maximum temperature of 60 °C followed by washing with DMF (6 × 5 ml). The first residue Fmoc-Alloc-Lys-OH (169 mg, 0.37 mmol, 3 eq) was attached to the resin by microwave irradiation for 20 min at 20 W and a maximum temperature of 60 °C under argon atmosphere with PyBOP (194 mg, 0.37 mmol, 3 eq), DIPEA (130 µl, 0.74 mmol, 6 eq) in DMF (5 ml) and consequent washing with DMF (3 × 5 ml). Coupling and washing steps were repeated. After Fmoc deprotection the second to the third residues Fmoc-Boc-Lys-OH was attached to the resin as described above, also repeating coupling and washing steps. Afterwards, the fourth residue Fmoc-Alloc-Lys-OH (169mg, 0.37 mmol, 3 eq) was attached to the resin. Alloc removal was achieved by $Pd(PPh_3)_4$ (28 mg, 0.02 mmol, 0.2 eq), $PhSiH_3$ (366 µl, 2.98 mmol, 24 eq) in 7 ml DCM for 30 min at room temperature under argon bubbling and consequent washing with DMF (3 × 5 ml). The deprotection and washing process was repeated. The GCP groups (211 mg, 0.49 mmol, 4 eq) were attached to the resin by microwave irradiation for 20 min at 20 W and a maximum

temperature of 60 ° C under argon atmosphere with PyBOP (210 mg, 0.49 mmol, 4 eq), DIPEA (168 µl, 0.98 mmol, 8 eq) in DMF (5 ml) and consequent washing with DMF (3 × 5 ml). The coupling process was repeated until *Kaiser Test* showed negative result. After Fmoc deprotection the resin was washed with DCM (3 × 5 ml), methanol (3 × 5 ml), and DCM (3 × 5 ml) and dried under reduced pressure for one hour. To cleave the product, the resin was transferred to a flask equipped with a frit onto a Heidolph Rotamax 120 shaker. There it was shaken under argon atmosphere in a mixture containing 95 % TFA, 2.5 % water, and 2.5 % TIS for three hours and washed twice with the cleavage mixture. The filtrates were combined and concentrated in high vacuum at room temperature. Diethyl ether (40 ml) was added and the resulting suspension was centrifuged. The supernatant solvent was decanted and the solid was washed with diethyl ether and centrifuged again. After decanting, the raw product was dissolved in little methanol, water (30 ml) was added, and the mixture was freeze-dried in vacuum. The resulting solid was purified by MPLC on C18 reversed-phase silica gel (5 % to 45 % methanol/water in 45 min, 0.1 % TFA) to obtain **63** as white solid (8 mg, 7%) with 88% purity by analytical RP-HPLC.

^{1}H-NMR (500 MHz, d^{6}-DMSO): δ [ppm] = 1.33-1.35 (m, 8H, Lys-CH_2), 1.51-1.72 (m, 16H, Lys-CH_2), 2.75 (s, 4H, Lys-CH_2), 3.22 (s, 4H, Lys-CH_2), 3.72-3.83 (s, 1H, Lys-CH), 4.16-4.45 (m, 3H, Lys-CH), 6.87-6.89 (m, 1H, amide-NH), 7.03-7.12 (m, 2H, pyrrole-CH), 7.20-7.47 (m, 2H, pyrrole-CH), 7.82-7.88 (m, 8H, amide-NH, amine-NH_2, pyrrole-NH), 8.22-8.58 (m, 12H, amide-NH, guanidine-NH), 12.0 (s, 1H, amine-NH), 12.3 (s, 1H, amide-NH).

MALDI-TOF-MS (pos.) m/z calculated for $C_{38}H_{64}N_{17}O_8$ $[M + H]^+$ 886.50, found 886.84

Microwave Assisted Solid-Phase Peptide Synthesis of (64):

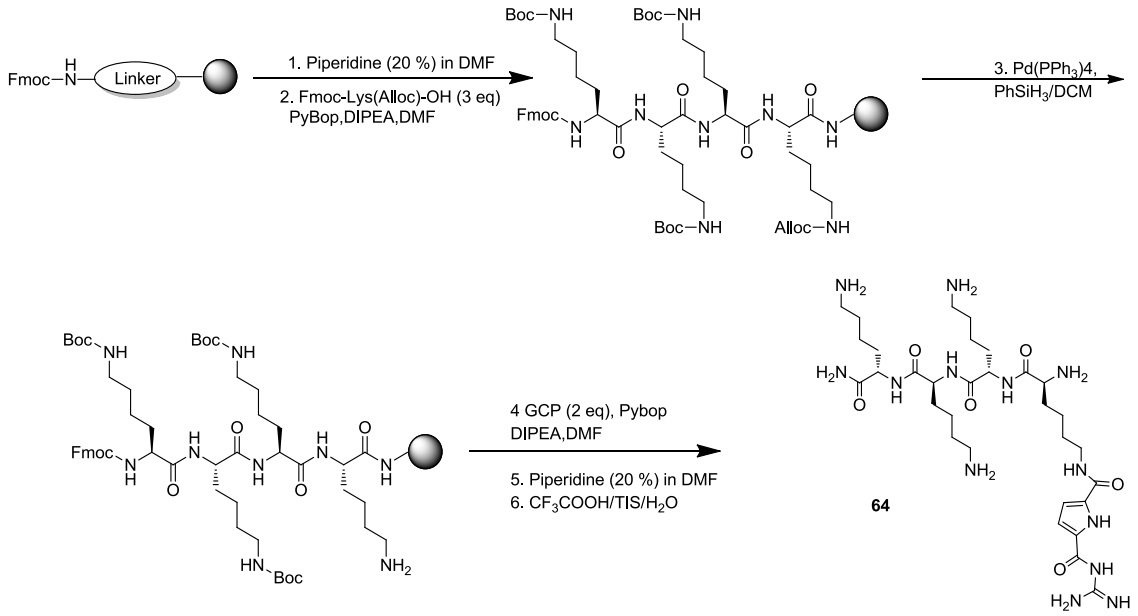

The reaction was carried out in a fritted, microwave-transparent 25 ml polyethylene column with a CEM Discover microwave apparatus. Rink-Amide MBHA resin (200 mg, 0.62mmol/g) was swollen in DCM (5 ml) for 2 h. Fmoc removal was achieved by irradiating the resin in 20 % piperidine/DMF (5 ml) for 1 min and 5 min at 20 W and a maximum temperature of 60 °C followed by washing with DMF (6 × 5 ml). The first residue Fmoc-Alloc-Lys-OH (169 mg, 0.37 mmol, 3 eq) was attached to the resin by microwave irradiation for 20 min at 20 W and a maximum temperature of 60 °C under argon atmosphere with PyBOP (194 mg, 0.37 mmol, 3 eq), DIPEA (130 µl, 0.74 mmol, 6 eq) in DMF (5 ml) and consequent washing with DMF (3 × 5 ml). Coupling and washing steps were repeated. After Fmoc deprotection the second to the fourth residues Fmoc-Boc-Lys-OH was attached to the resin as described above, also repeating coupling and washing steps. Alloc removal was achieved by $Pd(PPh_3)_4$ (28 mg, 0.02 mmol, 0.2 eq), $PhSiH_3$ (366 µl, 2.98 mmol, 24 eq) in 7 ml DCM for 30 min at room temperature under argon bubbling and consequent washing with DMF (3 × 5 ml). The deprotection and washing process was repeated. The GCP groups (106 mg, 0.25 mmol, 2 eq) were attached to the resin by microwave irradiation for 20 min at 20 W and a maximum temperature of 60 °C under argon atmosphere with PyBOP (105 mg, 0.25 mmol, 2 eq), DIPEA (84 µl, 0.49 mmol, 4 eq) in DMF (5 ml) and consequent washing with DMF (3 × 5 ml). The coupling process was repeated until *Kaiser Test* showed negative result. After Fmoc

deprotection the resin was washed with DCM (3 × 5 ml), methanol (3 × 5 ml), and DCM (3 × 5 ml) and dried under reduced pressure for one hour. To cleave the product, the resin was transferred to a flask equipped with a frit onto a Heidolph Rotamax 120 shaker. There it was shaken under argon atmosphere in a mixture containing 95 % TFA, 2.5 % water, and 2.5 % TIS for three hours and washed twice with the cleavage mixture. The filtrates were combined and concentrated in high vacuum at room temperature. Diethyl ether (40 ml) was added and the resulting suspension was centrifuged. The supernatant solvent was decanted and the solid was washed with diethyl ether and centrifuged again. After decanting, the raw product was dissolved in little methanol, water (30 ml) was added, and the mixture was freeze-dried in vacuum. The resulting solid was purified by MPLC on C18 reversed-phase silica gel (5 % to 45 % methanol/water in 45 min, 0.1 % TFA) to obtain **64** as white solid (6 mg, 7%) with 90% purity by analytical RP-HPLC.

^{1}H-NMR (500 MHz, d^{6}-DMSO): δ [ppm] = 1.51-1.58 (m, 8H, Lys-CH_2), 1.66-1.76 (m, 16H, Lys-CH_2), 2.74 (s, 6H, Lys-CH_2), 3.21 (s, 2H, Lys-CH_2), 3.86-3.90 (m, 1H, Lys-CH), 4.16-4.33 (m, 3H, Lys-CH), 6.91 (s, 1H, pyrrole-CH), 7.43(s, 1H, pyrrole-CH), 7.93-8.39 (m, 10H, amide-NH, guanidine-NH), 8.61 (s, 4H, amine-NH_2), 8.73-8.79 (m, 3H, amide-NH), 12.2 (s, 1H, amide-NH), 12.3 (s, 1H, amide-NH).

^{13}C-NMR (125 MHz, d^{6}-DMSO): δ [ppm] = 22.0 (Lys-CH_2), 22.1(Lys-CH_2), 22.2 (Lys-CH_2), 26.3 (Lys-CH_2), 26.4 (Lys-CH_2), 28.4 (Lys-CH_2), 30.7 (Lys-CH_2), 31.1 (Lys-CH_2), 31.3 (Lys-CH_2), 38.5 (Lys-CH_2), 51.9 (Lys-CH), 52.5 (Lys-CH), 112.5 (pyrrole-CH), 116.0 (pyrrole-CH), 125.2 (Cq), 132.9 (Cq), 155.6 (Cq), 159.0 (Cq),159.6 (Cq), 168.5 (Cq), 171.2 (Cq), 173.4 (Cq).

MALDI-TOF-MS (pos.) m/z calculated for $C_{31}H_{58}N_{13}O_6$ $[M + H]^+$ 708.46, found 708.59

Microwave Assisted Solid-Phase Peptide Synthesis of (43):

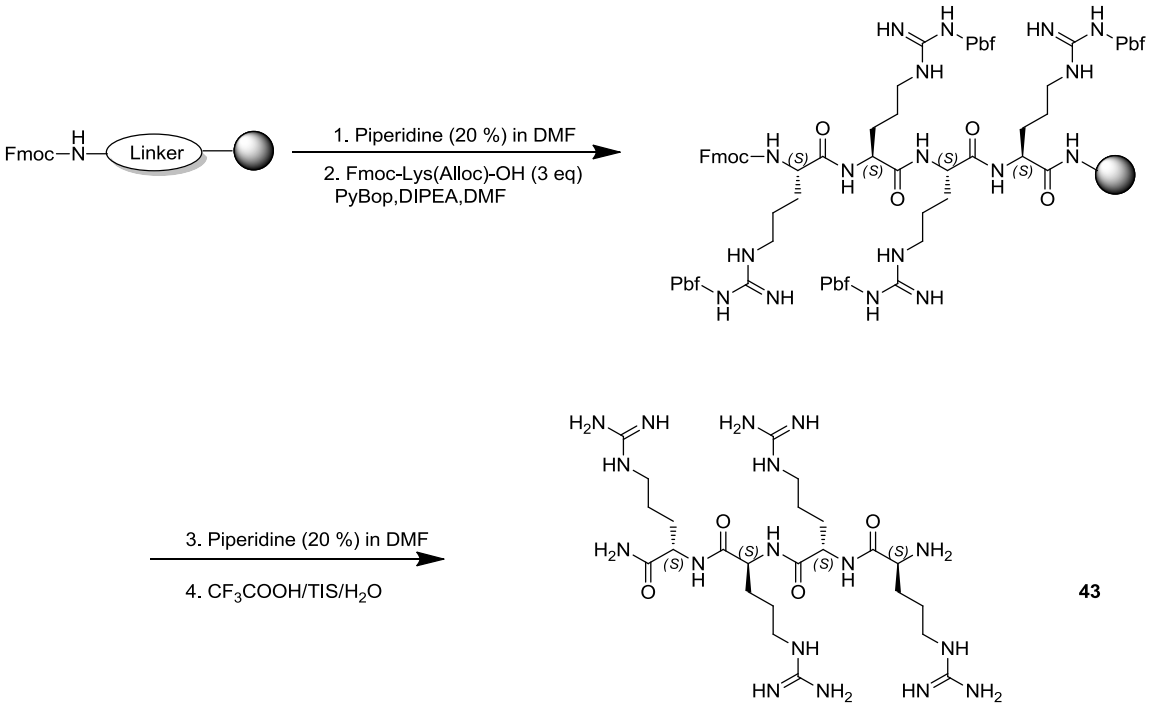

The reaction was carried out in a fritted, microwave-transparent 25 ml polyethylene column with a CEM Discover microwave apparatus. Rink-Amide MBHA resin (200 mg, 0.62mmol/g) was swollen in DCM (5 ml) for 2 h. Fmoc removal was achieved by irradiating the resin in 20 % piperidine/DMF (5 ml) for 1 min and 5 min at 20 W and a maximum temperature of 60 °C followed by washing with DMF (6 × 5 ml). The first residue Fmoc-Arg(Pbf)-OH (242 mg, 0.37 mmol, 3 eq) was attached to the resin by microwave irradiation for 20 min at 20 W and a maximum temperature of 60 °C under argon atmosphere with PyBOP (193 mg, 0.37 mmol, 3 eq), DIPEA (127 µl, 0.74 mmol, 6 eq) in DMF (5 ml) and consequent washing with DMF (3 × 5 ml). Coupling and washing steps were repeated. After Fmoc deprotection the second to the fourth residues Fmoc-Arg(Pbf)-OH was attached to the resin as described above, also repeating coupling and washing steps. After Fmoc deprotection the resin was washed with DCM (3 × 5 ml), methanol (3 × 5 ml), and DCM (3 × 5 ml) and dried under reduced pressure for one hour. To cleave the product, the resin was transferred to a flask equipped with a frit onto a Heidolph Rotamax 120 shaker. There it was shaken under argon atmosphere in a mixture containing 95 % TFA, 2.5 % water, and 2.5 % TIS for three hours and washed twice with the cleavage mixture. The filtrates were combined and concentrated in high vacuum at

room temperature. Diethyl ether (40 ml) was added and the resulting suspension was centrifuged. The supernatant solvent was decanted and the solid was washed with diethyl ether and centrifuged again. After decanting, the raw product was dissolved in little methanol, water (30 ml) was added, and the mixture was freeze-dried in vacuum. The resulting solid was purified by MPLC on C18 reversed-phase silica gel (5 % to 50 % methanol/water in 45 min, 0.1 % TFA) to obtain **43** as white solid (15 mg, 19%) with >90% purity by analytical RP-HPLC.

^{1}H-NMR (500 MHz, d^{6}-DMSO): δ [ppm] = 1.53-1.75 (m, 16H, Arg-CH_2), 3.10-3.12 (t, 8H, J = 5Hz, Arg-CH_2), 3.85-3.86 (m, 1H, Arg-CH), 4.11-4.17 (m, 1H, Arg-CH), 4.19-4.26 (m, 1H, Arg-CH), 4.29-4.33 (m, 1H, Arg-CH), 6.85 (br. s, 4H, guanidine-NH), 7.02 (s, 2H, amino-NH_2), 7.10 (s, 2H, guanidine-NH), 7.18 (s, 2H, guanidine-NH), 7.29 (br. s, 4H, guanidine-NH), 7.51-7.52 (m, 4H, amide-NH), 8.10-8.19 (m, 4H, guanidine-NH), 8.52-8.55 (m, 1H, amide-NH).

^{13}C-NMR (125 MHz, d^{6}-DMSO): δ [ppm] = 23.9 (Arg-CH_2), 24.9 (Arg-CH_2), 25.0 (Arg-CH_2), 25.1 (Arg-CH_2), 27.9 (Arg-CH_2), 28.3 (Arg-CH_2), 28.8 (Arg-CH_2), 28.9 (Arg-CH_2), 29.0 (Arg-CH_2), 29.1 (Arg-CH_2), 40.0 (Arg-CH_2), 40.1 (Arg-CH_2), 40.3 (Arg-CH_2), 40.4 (Arg-CH_2), 45.6 (Arg-CH_2), 51.7 (Arg-CH), 52.1 (Arg-CH), 52.4 (Arg-CH), 52.5 (Arg-CH), 156.6 (guanidine-C), 168.4(Cq), 158.9 (Cq), 170.9 (Cq), 171.0 (Cq), 171.2 (Cq), 173.2 (Cq), 173.4 (Cq).

MALDI-TOF-MS (pos.) m/z calculated for $C_{24}H_{52}N_{17}O_4$ $[M + H]^+$ 642.43, found 643.05

Microwave Assisted Solid-Phase Peptide Synthesis of (44):

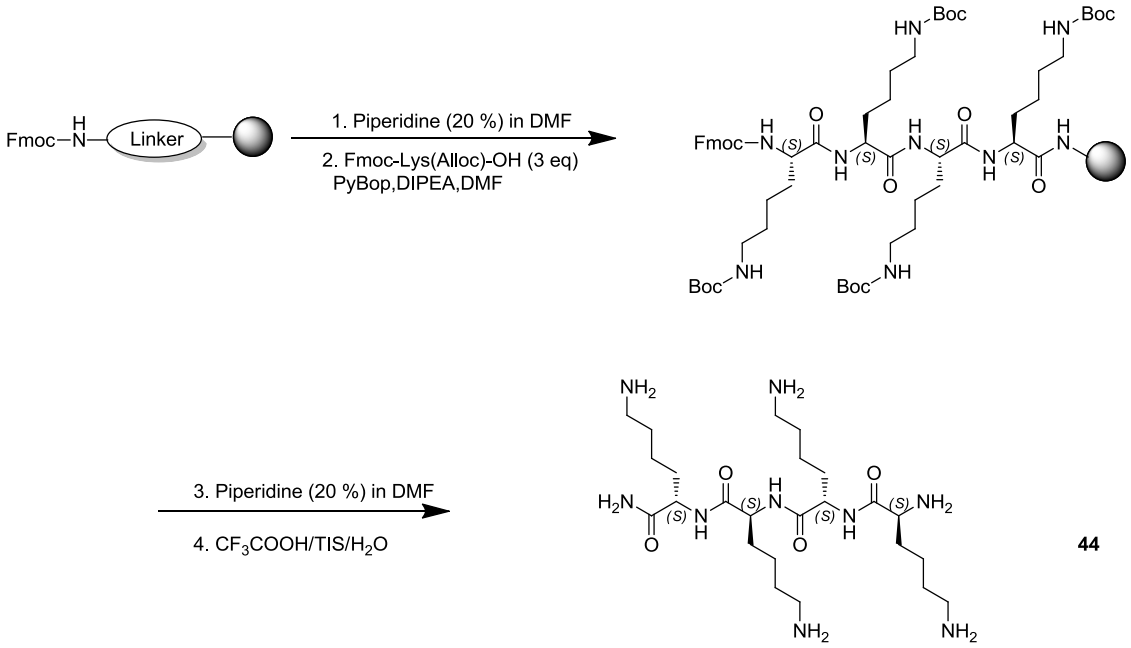

The reaction was carried out in a fritted, microwave-transparent 25 ml polyethylene column with a CEM Discover microwave apparatus. Rink-Amide MBHA resin (200 mg, 0.62mmol/g) was swollen in DCM (5 ml) for 2 h. Fmoc removal was achieved by irradiating the resin in 20 % piperidine/DMF (5 ml) for 1 min and 5 min at 20 W and a maximum temperature of 60 °C followed by washing with DMF (6 × 5 ml). The first residue Fmoc-Lys(Boc)-OH (175 mg, 0.37 mmol, 3 eq) was attached to the resin by microwave irradiation for 20 min at 20 W and a maximum temperature of 60 °C under argon atmosphere with PyBOP (194 mg, 0.37 mmol, 3 eq), DIPEA (127 µl, 0.74 mmol, 6 eq) in DMF (5 ml) and consequent washing with DMF (3 × 5 ml). Coupling and washing steps were repeated. After Fmoc deprotection the second to the fourth residues Fmoc-Lys(Boc)-OH were attached to the resin as described above, also repeating coupling and washing steps. After Fmoc deprotection the resin was washed with DCM (3 × 5 ml), methanol (3 × 5 ml), and DCM (3 × 5 ml) and dried under reduced pressure for one hour. To cleave the product, the resin was transferred to a flask equipped with a frit onto a Heidolph Rotamax 120 shaker. There it was shaken under argon atmosphere in a mixture containing 95 % TFA, 2.5 % water, and 2.5 % TIS for three hours and washed twice with the cleavage mixture. The filtrates were combined and concentrated in high vacuum at room temperature. Diethyl ether (40 ml) was added and the resulting suspension was centrifuged. The supernatant solvent was decanted and the solid was washed with diethyl

ether and centrifuged again. After decanting, the raw product was dissolved in little methanol, water (30 ml) was added, and the mixture was freeze-dried in vacuum. The resulting solid was purified by MPLC on C18 reversed-phase silica gel (0 % to 50 % methanol/water in 50 min, 0.1 % TFA) to obtain **44** as white solid (6.6 mg, 10%) with >90% purity by analytical RP-HPLC.

^{1}H-NMR (500 MHz, d^{6}-DMSO):δ [ppm] = 1.29-1.44 (m, 8H, Lys-CH_2), 1.57-1.73 (m, 16H, Lys-CH_2), 2.75 (s, 8H, Lys-CH_2), 3.87 (s, 1H, Lys-CH), 4.16-4.32 (m, 3H, Lys-CH), 7.12-7.48 (m, 2H, amino-NH_2), 7.97-8.04 (m, 10H, amino-NH_2, amide-NH), 8.26-8.27 (m, 2H, amino-NH_2), 8.85 (s, 1H, amide-NH).

^{13}C-NMR (125 MHz, d^{6}-DMSO): δ [ppm] = 20.9 (Lys-CH_2), 22.1 (Lys-CH_2), 26.3 (Lys-CH_2), 30.3 (Lys-CH_2), 30.9 (Lys-CH_2), 31.3 (Lys-CH_2), 38.3 (Lys-CH_2), 51.6 (Lys-CH), 52.1 (Lys-CH), 52.5 (Lys-CH), 52.6 (Lys-CH), 168.4 (Cq), 171.1 (Cq), 173.4 (Cq).

MALDI-TOF-MS (pos.) m/z calculated for $C_{24}H_{52}N_9O_4$ $[M + H]^+$ 530.41, found 530.21

6.4.3 Synthesis of cyclic peptide analogues

Synthesis of linear precursor (70):

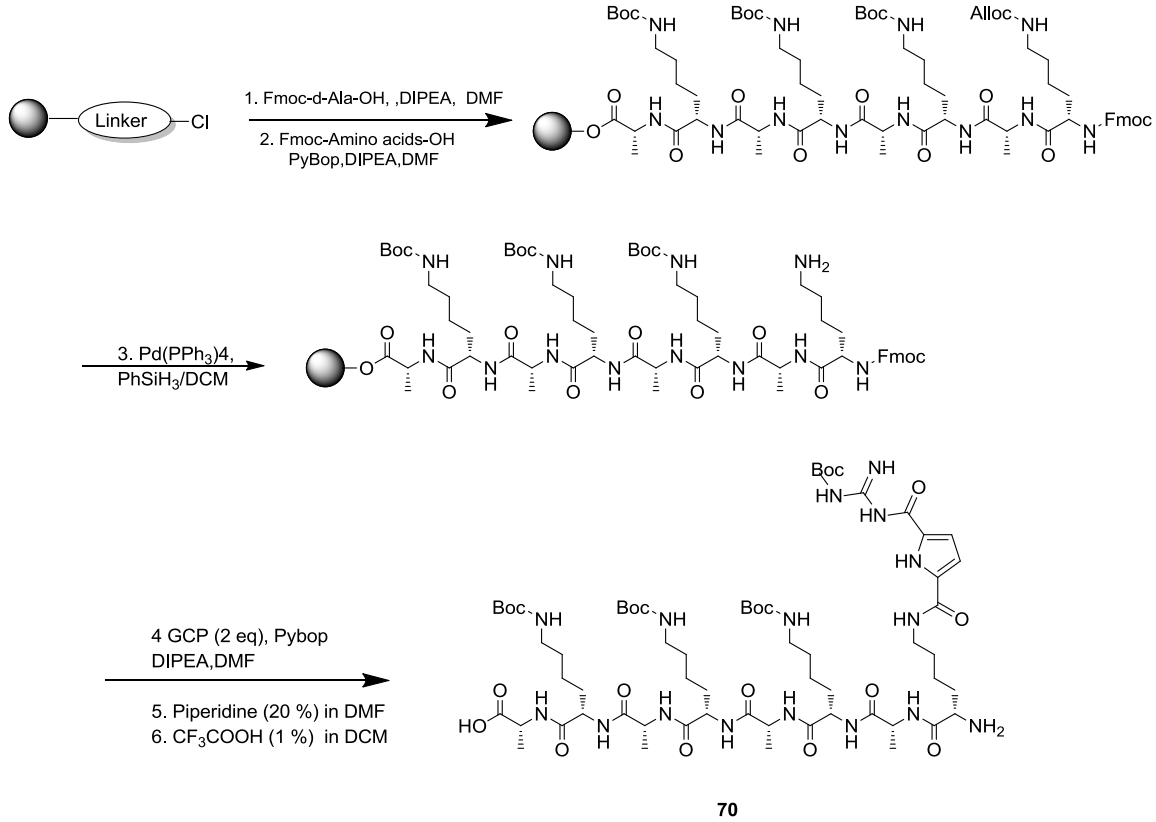

70

2-Chlorotrityl chloride resin (200 mg) was swollen in DMF (5 ml) for 2 h. The first residue Fmoc-D-Ala-OH (3 eq.) was attached to the resin at room temperature under argon atmosphere with DIPEA (6 eq.) in DMF (5 ml) for 2 h and consequent washing with DMF (3 × 5 ml). Coupling and washing steps were repeated. Methanol was then added to block remaining chloride residues. The resin was filtered and washed with DMF, DCM and methanol, and left to dry under vacuum. The Fmoc protecting group was then removed by stirring the resin in 20% piperidine in DMF solution for 20 mins. After Fmoc deprotection the remaining solid was washed intensively with DMF. A solution of PyBop (3eq.) and Fmoc-L-Lys-(Boc)-OH (3eq.) in DMF was added to the loaded resin, followed by the addition of DIPEA (6eq.). The mixture was left to stir in 2h and consequent washed with DMF. The reaction was repeated with fresh reagents. The resin was filtered and washed with DMF, DCM and methanol, and left to dry under vacuum. The Fmoc protecting group was then removed as described above, and the same procedure was done for the next five amino acids. After Fmoc removal, Fmoc-L-Lys-(Alloc)-OH (3eq.) was attached to the resin as described above, also

repeating coupling and washing steps. Alloc removal was achieved by $Pd(PPh_3)_4$ (0.1 eq.), $PhSiH_3$ (6 eq.) in 7 ml DCM for 30 min at room temperature under argon bubbling and consequent washing with DMF (3 × 5 ml). The deprotection and washing process was repeated. The GCP groupS (3 eq.) were attached to the resin under argon atmosphere with PyBop (6 eq.), DIPEA (337 µl, 1.98 mmol, 6 eq) in DMF (5 ml) and consequent washing with DMF (3 × 5 ml). The coupling process was repeated until Kaiser Test showed negative result. After Fmoc deprotection the resin was washed with DCM (3 × 5 ml), methanol (3 × 5 ml), and DCM (3 × 5 ml) and dried under reduced pressure for one hour.

To cleave the linear precursor, the resin was shaken under argon atmosphere in a mixture containing 1% TFA, 2.5 % water, and 2.5 % TIS in DCM for 20 minutes and washed twice with DCM. The filtrates were combined and concentrated in high vacuum at room temperature. Diethyl ether (20 ml) was added and the resulting suspension was centrifuged. The supernatant solvent was decanted and the solid was washed with diethyl ether and centrifuged again. After decanting, the raw product was dissolved in methanol, water (30 ml) was added, and the mixture was freeze-dried in vacuum. The resulting white solid (200 mg, 60%) was used to next step without further purification.

Synthesis of cyclic peptide (45):

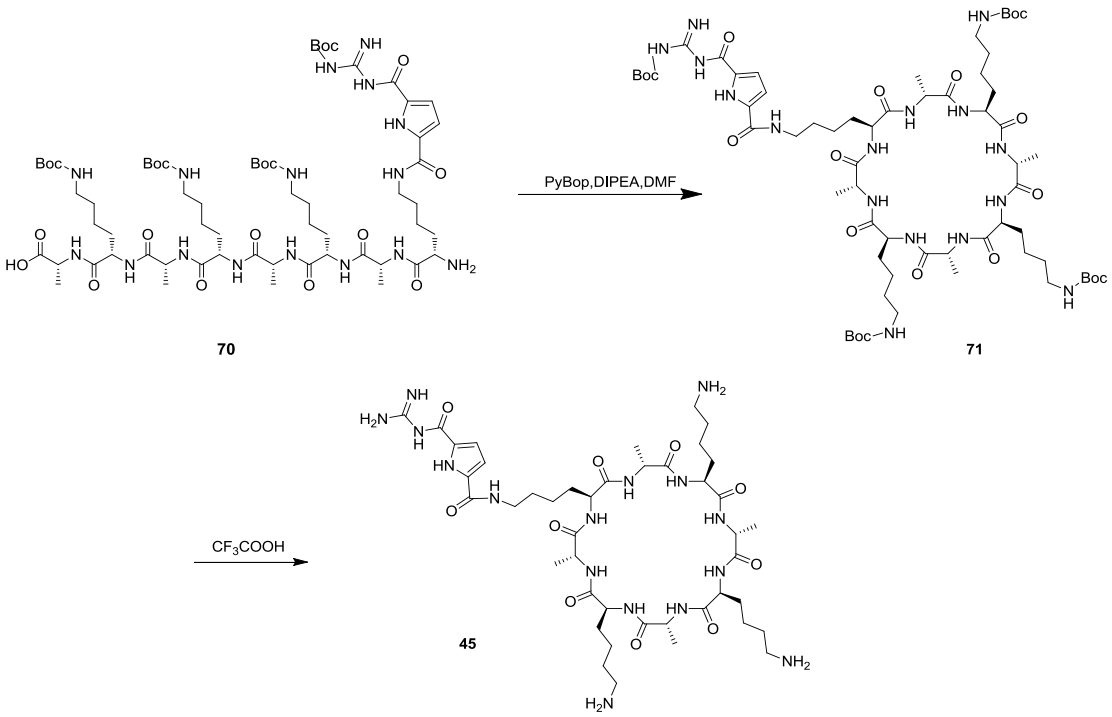

The linear precursor (200mg, 143 μmol) was dissolved in DMF (90 mL). The solution was cooled to 0 °C in an ice bath. PyBop (223 mg, 429 μmol) was dissolved in DMF (30 mL), cooled to 0 ℃, was slowly added to the solution mixture while stirring at 0 ℃. DIPEA (148 μL, 858 μmol) was added slowly to the mixture. The reaction mixture was left to stir for 6 hours at 0 ℃ and then at room temperature for two days. DMF was removed by vacuum distillation at 55 ℃, resulting in a gel-like residue. The crude product was used without further purification.

The cyclized product was dissolved in 10mL of 95% v/v TFA, 2.5% v/v TIS and 2.5% v/v H_2O. The mixture was left to stir for two hours at room temperature. The deprotected product was then precipitated using cold ether (100 mL). The mixture was centrifuged, and ether was then decanted. This step was repeated twice, resulting in an off-white precipitate. The product was then dissolved in H_2O (5 mL), and lyophilized giving an off-white fluffy solid. The crude product was purified by MPLC on C18 reversed-phase silica gel (15% to 55% methanol/water in 45 min, 0.1 % TFA) to obtain **45** as white solid (5 mg, 5%) with 91% purity by analytical RP-HPLC.

^{1}H-NMR (500 MHz, d^{6}-DMSO): δ [ppm] = 1.14-1.23 (m, 21H, Lys-CH_2, Ala-CH_3), 1.26-1.59 (m, 15H, Lys-CH_2), 2.73-2.74 (s, 6H, Lys-CH_2), 3.18 (s, 2H, Lys-CH_2), 4.21-4.40(m, 8H, Ala-CH, Lys-CH), 6.84 (s, 1H, pyrrole-CH), 7.10 (s, 1H, pyrrole-CH), 7.68-7.71 (s, 9H, amine-NH3+), 8.09-8.19 (m, 8H, amide-NH), 8.41 (br.s, 4H, guanidine-NH).

^{13}C-NMR (125 MHz, d^{6}-DMSO): δ [ppm] = 19.0 (Ala-CH_3), 22.0-22.6 (Lys-CH_2), 26.5 (Lys-CH_2), 26.6 (Lys-CH_2), 28.4 (Lys-CH_2), 38.5 (Lys-CH_2), 47.8-47.9 (Ala-CH), 51.8-51.9 (Lys-CH), 112.3 (pyrrole-CH), 155.0 (GCP-carbonyl), 157.7 (GCP-carbonyl), 170.7-170.9 (Ala-carbonyl), 171.7-171.8 (Lys-carbonyl).

MALDI-TOF-MS (pos.) m/z calculated for $C_{43}H_{75}N_{16}O_{10}$ $[M + H]^+$ 975.58, found 975.85

Synthesis of linear precursor (72):

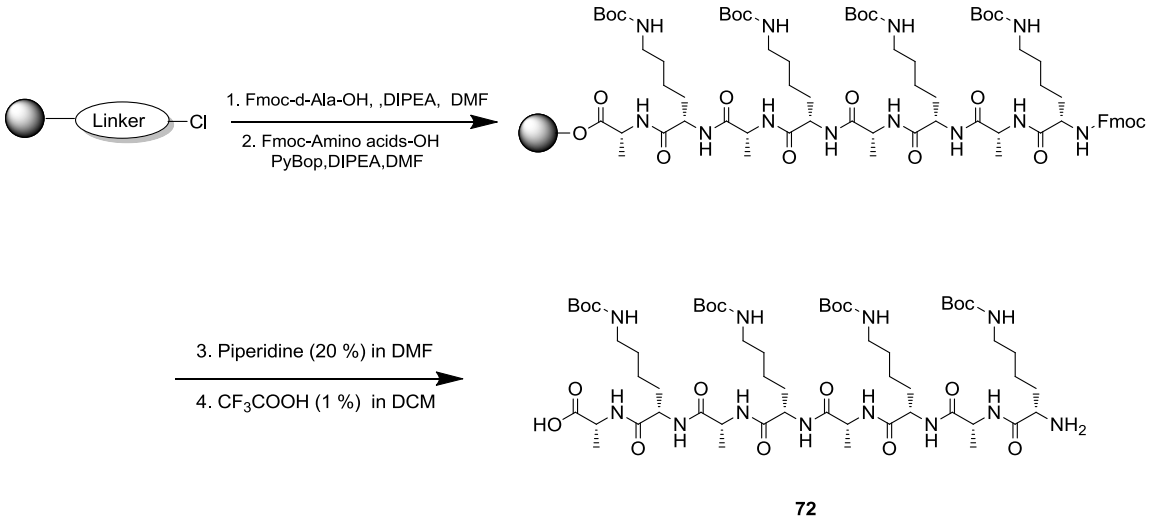

72

2-chlorotrityl chloride resin was swollen in DMF (5 ml) for 2 h. The first residue Fmoc-D-Ala-OH (3 eq.) was attached to the resin at room temperature under argon atmosphere with DIPEA (6 eq.) in DMF (5 ml) for 2h and consequent washing with DMF (3 × 5 ml). Coupling and washing steps were repeated. Methanol was then added to block remaining chloride residues. The resin was filtered and washed with DMF, DCM and methanol, and left to dry under vacuum. The Fmoc protecting group was then removed by stirring the resin in 20% piperidine in DMF solution for 20 mins. After Fmoc deprotection the remaining solid was washed intensively with DMF. A solution of PyBop (3eq.) and Fmoc-L-Lys-(Boc)-OH (3eq.) in DMF was added to the loaded resin, followed by the addition of DIPEA (6eq.). The mixture was left to stir in 2h and consequent washed with DMF. The reaction was repeated with fresh reagents. The resin was filtered and washed with DMF, DCM and methanol, and left to dry under vacuum. The Fmoc protecting group was then removed as described above, and the same procedure was done for the next six amino acids. After final Fmoc removal the resin was washed with DCM (3 × 5 ml), methanol (3 × 5 ml), and DCM (3 × 5 ml) and dried under reduced pressure for one hour.

To cleave the linear precursor, the resin was shaken under argon atmosphere in a mixture containing 1% TFA, 2.5 % water, and 2.5 % TIS in DCM for 20 minutes and washed twice with DCM. The filtrates were combined and concentrated in high vacuum at room temperature. Diethyl ether (20 ml) was added and the resulting suspension was centrifuged. The supernatant solvent was decanted and the solid was washed with diethyl ether and

centrifuged again. After decanting, the raw product was dissolved in little methanol, water (30 ml) was added, and the mixture was freeze-dried in vacuum. The resulting white solid (210 mg, 70%) was used to next step without further purification.

Synthesis of cyclic peptide (65):

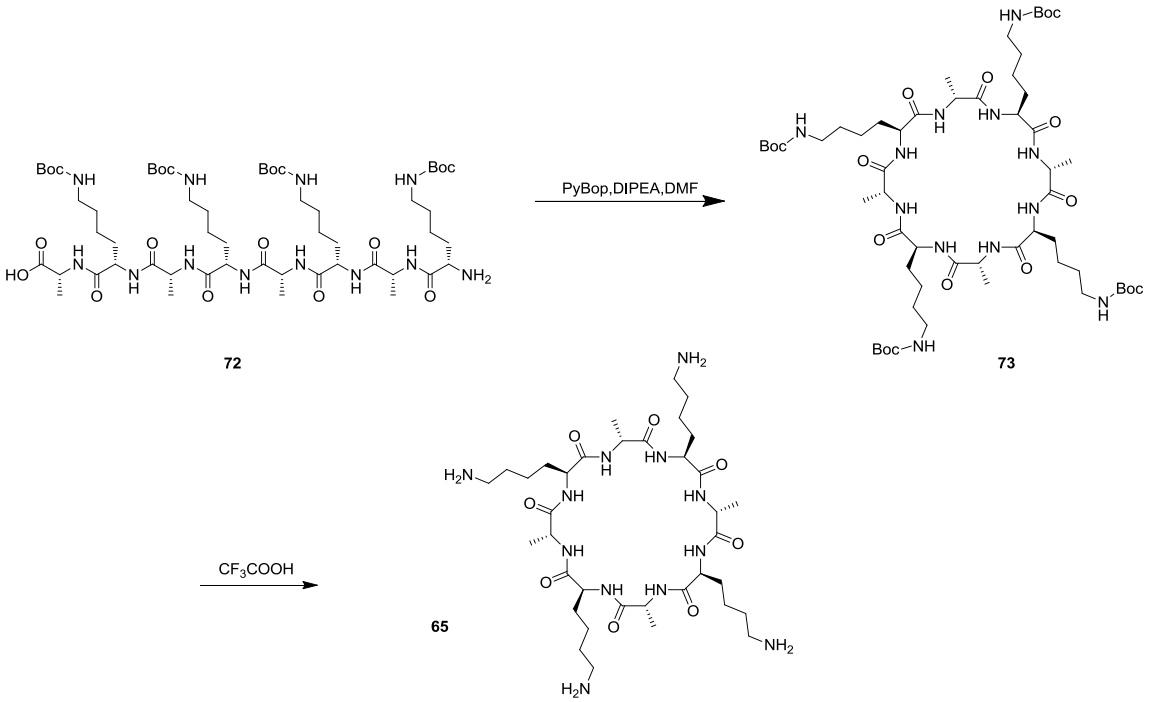

The linear precursor (210mg, 173 µmol)) of cyclic peptide 2 was dissolved in DMF (90 mL). The solution was cooled to 0 °C in an ice bath. PyBop (270 mg, 519 µmol) was dissolved in DMF (30 mL), cooled to 0 ℃, was slowly added to the solution mixture while stirring at 0 ℃. DIPEA (179 µL, 1.04 mmol) was added slowly to the mixture. The reaction mixture was left to stir for 6 hours at 0 ℃ and then at room temperature for two days. DMF was removed by vacuum distillation at 55 ℃, resulting in a gel-like residue. The crude product was used without further purification.

The cyclized product was dissolved in 10mL of 95% TFA, 2.5% TIS and 2.5% H_2O. The mixture was left to stir for two hours at room temperature. The deprotected product was then precipitated using cold ether (100 mL). The mixture was centrifuged, and ether was then decanted. This step was repeated twice, resulting in an off-white precipitate. The product was then dissolved in H_2O (5 mL), and lyophilized giving an off-white fluffy solid. The crude product was purified by MPLC on C18 reversed-phase silica gel (5 % to 45 % methanol/water in 45 min, 0.1 %TFA) to obtain **65** as white solid (9 mg, 6.5%) with >90% purity by analytical RP-HPLC.

^{1}H-NMR (500 MHz, d^6-DMSO):δ [ppm] = 1.27-1.29 (m, 20H, Lys-CH_2, Ala-CH3), 1.43-1.60 (m, 16H, Lys-CH_2), 2.73-2.75 (s, 8H, Lys-CH_2), 4.17-4.45(m, 8H, Lys-CH,

Ala-CH), 7.72(s, 12H, amine-NH_3+), 8.07-8.09 (d, J= 5Hz, 4H, amide-NH), 8.18-8.20 (d, , J= 5Hz, 4H, amide-NH).

^{13}C-NMR (125 MHz, d^6-DMSO): δ [ppm] = 18.9 (Ala-CH_3), 22.0 (Lys-CH_2), 26.6 (Lys-CH_2), 31.8 (Lys-CH_2), 38.6 (Lys-CH_2), 47.9 (Ala-CH), 51.8 (Lys-CH), 170.8 (Ala-carbonyl), 171.8 (Lys-carbonyl).

MALDI-TOF-MS (pos.) m/z calculated for $C_{36}H_{68}N_{12}O_8Na$ $[M + Na]^+$ 819.53, found 819.88

6.4.4 Synthesis of β-helix mimetic peptide

Synthesis of peptide 46:

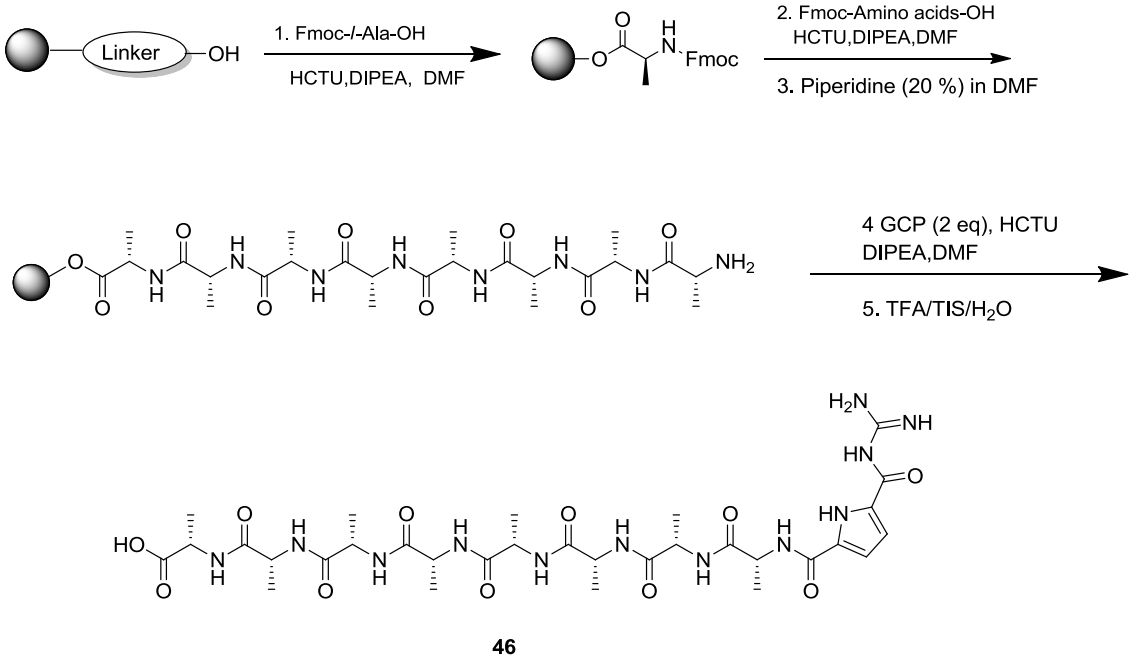

46

Wang resin was swollen in DMF (5 ml) for 2 h. The first residue Fmoc-L-Ala-OH (3 eq.) was attached to the resin at room temperature under argon atmosphere with HCTU (3 eq.), DIPEA (6 eq.) in DMF (5 ml) for 2 h and consequent washing with DMF (3 × 5 ml). Coupling and washing steps were repeated. The resin was filtered and washed with DMF, DCM and methanol, and left to dry under vacuum. The Fmoc protecting group was then removed by stirring the resin in 20% piperidine in DMF solution for 20 mins. After Fmoc deprotection the remaining solid was washed intensively with DMF. A solution of HCTU (3eq.) and Fmoc-D-Ala-OH (3eq.) in DMF was added to the loaded resin, followed by the addition of DIPEA (6eq.). The mixture was shaken for 2h and subse-quently washed with DMF. The reaction was repeated with fresh reagents. The resin was filtered and washed with DMF, and left to dry under vacuum. The Fmoc protecting group was then removed as described above and the same procedure was done for the rest amino acids. After Fmoc removal, the GCP group (2 eq.) were attached to the resin under argon atmosphere with HCTU (3 eq.), DIPEA (6 eq) in DMF (5 ml) for 8h and subsequently washing with DMF (3 × 5 ml). The coupling process was repeated until Kaiser Test showed negative result. Afterwards

the resin was washed with DCM (3 × 5 ml), methanol (3 × 5 ml), and DCM (3 × 5 ml) and dried under reduced pressure for one hour. To cleave the peptide, the resin was shaken under argon atmosphere in a mixture containing 10mL of 95% v/v TFA, 2.5% v/v TIS and 2.5% v/v H_2O for 3h and washed with TFA. The filtrates were combined and concentrated in high vacuum at room temperature. The product was then precipitated using cold ether (50 mL). The mixture was centrifuged, and ether was then decanted. This step was repeated twice, resulting in an off-white precipitate. The product was then dissolved in H_2O (5 mL), and lyophilized giving a white fluffy solid. The crude product was purified by MPLC on C18 reversed-phase silica gel (20 % to 50 % methanol/water in 45 min, 0.1 % TFA) to obtain **46** as white solid (10 mg, 10 %) with 97 % purity by analytical RP-HPLC.

^{1}H-NMR (500 MHz, D_2O): δ [ppm] = 1.22-1.23 (d, 3H, J = 5 Hz, Ala-CH_3), 1.34-1.40 (m, 18H, Ala-CH_3), 1.48-1.49 (d, 3H, J = 5 Hz, Ala-CH_3), 4.20-4.33 (m, 7H, Ala-CH), 4.49-4.52 (q, 1H, J = 5 Hz, Ala-CH), 6.93-6.94 (d, 1H, J = 5 Hz, pyrrole-CH), 7.12-7.13 (d, 1H, J = 5 Hz, pyrrole-CH).

^{13}C-NMR (500 MHz, D_2O): δ [ppm] = 16.1-16.6 (m, Ala-CH_3), 49.0-50.2 (m, Ala-CH), 113.1 (pyrrole-CH), 115.6 (pyrrole-CH), 155.2 (guanidine-CH), 160.7 (guanidine-carbonyl), 161.6 (Ala-carbonyl), 174.4-175.2 (m, Ala-carbonyl), 176.8 (Ala-carboxylate).

ESI-MS (pos.) m/z calculated for $C_{31}H_{49}N_{12}O_{11}$ $[M + H]^+$ 765.36, found 765.41.

Synthesis of peptide 66:

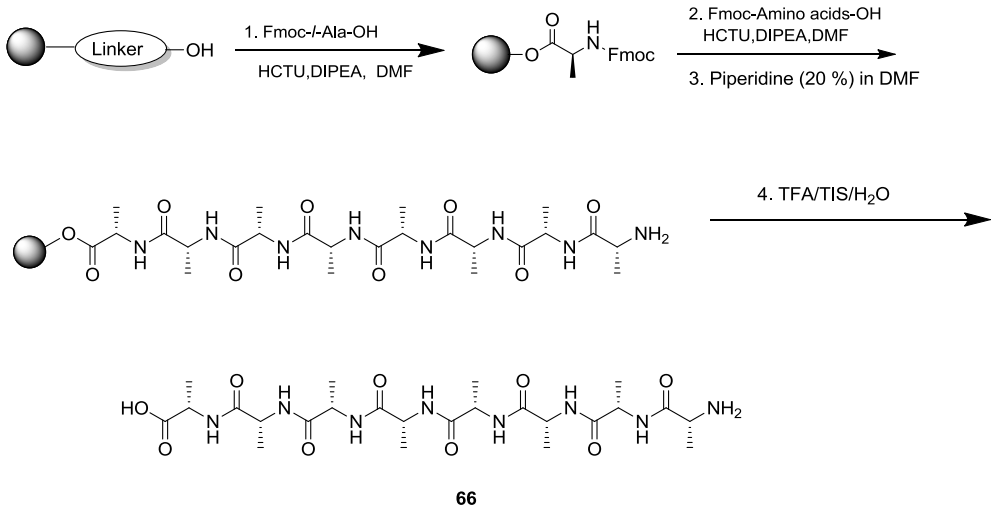

66

Wang resin was swollen in DMF (5 ml) for 2 h. The first residue Fmoc-L-Ala-OH (3 eq.) was attached to the resin at room temperature under argon atmosphere with HCTU (3 eq.), DIPEA (6 eq.) in DMF (5 ml) for 2 h and consequent washing with DMF (3 × 5 ml). Coupling and washing steps were repeated. The resin was filtered and washed with DMF, DCM and methanol, and left to dry under vacuum. The Fmoc protecting group was then removed by stirring the resin in 20% piperidine in DMF solution for 20 mins. After Fmoc deprotection the remaining solid was washed intensively with DMF. A solution of HCTU (3eq.) and Fmoc-D-Ala-OH (3eq.) in DMF was added to the loaded resin, followed by the addition of DIPEA (6eq.). The mixture was shaken for 2h and subsequently washed with DMF. The reaction was repeated with fresh reagents. The resin was filtered and washed with DMF, and left to dry under vacuum. The Fmoc protecting group was then removed as described above and the same procedure was done for the rest amino acids. Afterwards the resin was washed with DCM (3 × 5 ml), methanol (3 × 5 ml), and DCM (3 × 5 ml) and dried under reduced pressure for one hour. To cleave the peptide, the resin was shaken under argon atmosphere in a mixture containing 10mL of 95 % v/v TFA, 2.5 % v/v TIS and 2.5 % v/v H_2O for 3 h and washed with TFA. The filtrates were combined and concentrated in high vacuum at room temperature. The product was then precipitated using cold ether (50 mL). The mixture was centrifuged, and ether was then decanted. This step was repeated twice, resulting in an off-white precipitate. The product was then dissolved in H_2O (5 mL), and lyophilized giving a

white fluffy solid. The crude product was purified by MPLC on C18 reversed-phase silica gel (10 % to 50 % methanol/water in 45 min, 0.1 % TFA) to obtain 1 as white solid (20 mg, 20 %) with 93 % purity determined by analytical RP-HPLC.

^{1}H-NMR (300 MHz, D_2O): δ [ppm] = 1.35-1.39 (m, 21H, Ala-CH_3), 1.50-1.52 (d, 3H, J = 6 Hz, Ala-CH_3), 4.03-4.10 (q, 1H, J = 5 Hz, Ala-CH), 4.21-4.36 (m, 7H, Ala-CH).

^{13}C-NMR (300 MHz, D_2O): δ [ppm] = 16.1-16.6 (m, Ala-CH_3), 49.0-50.2 (m, Ala-CH), 161.6 (Ala-carbonyl), 174.4-175.2 (m, Ala-carbonyl), 176.8 (Ala-carboxylate).

ESI-MS (pos.) m/z calculated for $C_{24}H_{43}N_8O_9$ $[M + H]^+$ 587.31, found 587.46.

6.4.5 Synthesis of Fmoc-dipeptide analogues

Synthesis of peptide (47):

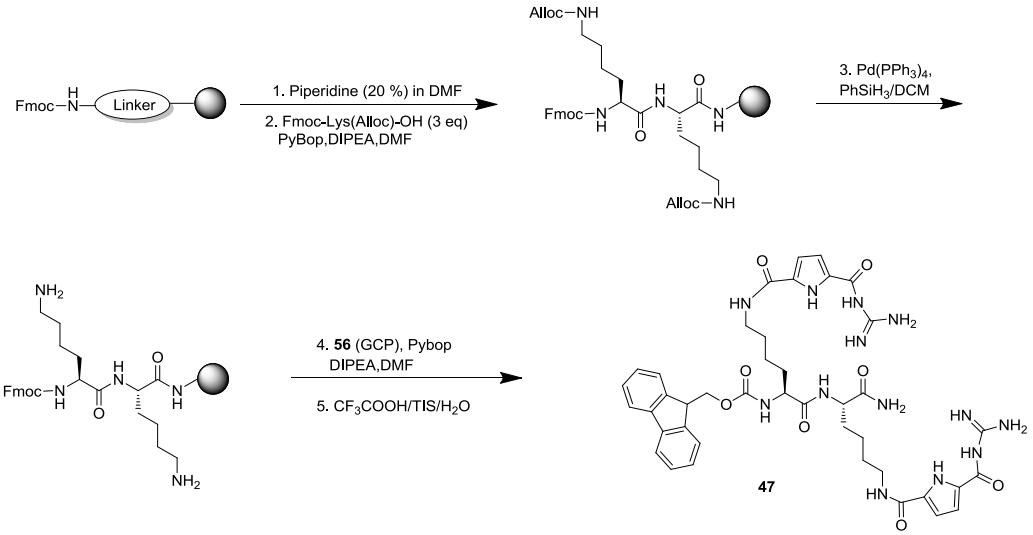

Rink-Amide MBHA resin (200 mg, 0.62mmol/g) was swollen in DCM (5 ml) for 2 h. Fmoc removal was achieved by shaking the resin in 20 % piperidine/DMF (5 ml) for 20 min twice followed by washing with DMF (6 × 5 ml). The first residue Fmoc-Alloc- *l*-Lys-OH (169 mg, 0.37 mmol, 3 eq) was attached to the resin with PyBOP (194 mg, 0.37 mmol, 3 eq), DIPEA (130 µl, 0.74 mmol, 6 eq) in DMF (5 ml) for 8 hours and consequent washing with DMF (3 × 5 ml). Coupling and washing steps were repeated. After Fmoc deprotection, the second residue Fmoc-Alloc-*l*-Lys-OH was attached to the resin as described above, also repeating coupling and washing steps. Alloc removal was achieved by $Pd(PPh_3)_4$ (28 mg, 0.02 mmol, 0.2 eq), $PhSiH_3$ (183 µl, 1.50 mmol, 24 eq) in 7 ml DCM for 30 min at room temperature under argon bubbling and consequent washing with DMF (3 × 5 ml). The deprotection and washing process was repeated. The GCP groups (197 mg, 0.99 mmol, 4 eq) were attached to the resin by microwave irradiation for 20 min at 20 W and a maximum temperature of 60 ° C under argon atmosphere with PyBOP (258 mg, 0.55 mmol, 4 eq), DIPEA (168 µl, 0.99 mmol, 8 eq) in DMF (5 ml) and consequent washing with DMF (3 × 5 ml). The coupling process was repeated until *Kaiser Test* showed negative result. Afterwards, the resin was washed with DCM (3 × 5 ml), methanol (3 × 5 ml), and DCM (3 × 5 ml) and dried under reduced pressure for one hour. To cleave the product, the resin was transferred to a flask equipped with a frit onto a Heidolph Rotamax 120 shaker. There it was shaken under

argon atmosphere in a mixture containing 95 % TFA, 2.5 % water, and 2.5 % TIS for three hours and washed twice with the cleavage mixture. The filtrates were combined and concentrated in high vacuum at room temperature. Diethyl ether (40 ml) was added and the resulting suspension was centrifuged. The supernatant solvent was decanted and the solid was washed with diethyl ether and centrifuged again. After decanting, the raw product was dissolved in little methanol, water (30 ml) was added, and the mixture was freeze-dried in vacuum. The resulting solid was purified by MPLC on C18 reversed-phase silica gel (10 % to 100 % methanol/water in 45 min, 0.1 % TFA) to obtain **47** as white solid (40 mg, 38%) with 93 % purity determined by analytical RP-HPLC.

^{1}H-NMR (500 MHz, d^{6}-DMSO): δ [ppm] = 1.31-1.64 (m, 12H, Lys-CH_2), 3.20 (s, 4H, Lys-CH_2), 3.99-4.36 (m, 5H, Lys-CH, Fmoc-CH_2, Fmoc-CH), 6.85 (s, 2H, pyrrole-CH), 7.01-7.07 (m, 3H, phenyl-CH, pyrrole-CH), 7.27-7.41 (m, 4H, phenyl-CH), 7.51 (s, 1H, amide-NH), 7.67 (m, 2H, pyrrole-NH), 7.81-7.88 (m, 2H, amide-NH), 8.21-8.50 (m, 10H, guanidine-NH), 11.22 (s, 2H, amine-NH_2), 12.30 (s, 2H, amide-NH_2).

^{13}C-NMR (125 MHz, d^{6}-DMSO): δ [ppm] = 22.8 (Lys-CH_2), 22.9 (Lys-CH_2), 28.8 (Lys-CH_2), 31.6 (Lys-CH_2), 31.9 (Lys-CH_2), 38.8 (Lys-CH_2), 45.8 (Lys-CH_2), 46.7 (Fmoc-CH), 52.2 (Lys-CH), 54.8 (Lys-CH), 65.7 (Fmoc-CH_2), 112.7 (pyrrole-CH), 120.1 (pyrrole-CH), 125.4 (phenyl-CH), 127.1 (phenyl-CH), 127.7 (phenyl-CH), 140.8 (Cq), 143.7 (Cq), 143.9 (Cq), 156.0 (Cq), 159.1 (Cq), 171.9 (Cq), 173.6 (Cq).

MALDI-TOF-MS (pos.) m/z calculated for $C_{41}H_{50}N_{13}O_8$ $[M + H]^+$ 852.38, found 852.78

Synthesis of peptide (67):

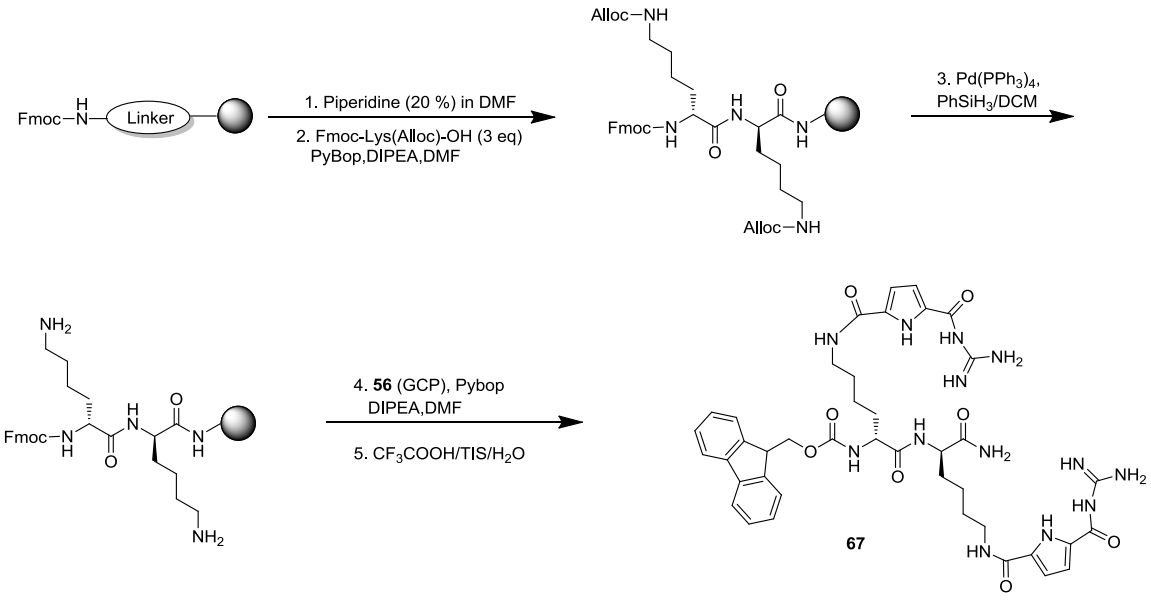

Rink-Amide MBHA resin (200 mg, 0.62mmol/g) was swollen in DCM (5 ml) for 2 h. Fmoc removal was achieved by shaking the resin in 20 % piperidine/DMF (5 ml) for 20 min twice followed by washing with DMF (6 × 5 ml). The first residue Fmoc-Alloc-*d*-Lys-OH (169 mg, 0.37 mmol, 3 eq) was attached to the resin with PyBOP (194 mg, 0.37 mmol, 3 eq), DIPEA (130 µl, 0.74 mmol, 6 eq) in DMF (5 ml) for 8 hours and consequent washing with DMF (3 × 5 ml). Coupling and washing steps were repeated. After Fmoc deprotection the second residue Fmoc-Alloc- *d*-Lys-OH was attached to the resin as described above, also repeating coupling and washing steps. Alloc removal was achieved by $Pd(PPh_3)_4$ (28 mg, 0.02 mmol, 0.2 eq), $PhSiH_3$ (183 µl, 1.50 mmol, 24 eq) in 7 ml DCM for 30 min at room temperature under argon bubbling and consequent washing with DMF (3 × 5 ml). The deprotection and washing process was repeated. The GCP groups (197 mg, 0.99 mmol, 4 eq) were attached to the resin by microwave irradiation for 20 min at 20 W and a maximum temperature of 60 ° C under argon atmosphere with PyBOP (258 mg, 0.55 mmol, 4 eq), DIPEA (168 µl, 0.99 mmol, 8 eq) in DMF (5 ml) and consequent washing with DMF (3 × 5 ml). The coupling process was repeated until *Kaiser Test* showed negative result. Afterwards, the resin was washed with DCM (3 × 5 ml), methanol (3 × 5 ml), and DCM (3 × 5 ml) and dried under reduced pressure for one hour. To cleave the product, the resin was transferred to a flask equipped with a frit onto a Heidolph Rotamax 120 shaker. There it was shaken under

argon atmosphere in a mixture containing 95 % TFA, 2.5 % water, and 2.5 % TIS for three hours and washed twice with the cleavage mixture. The filtrates were combined and concentrated in high vacuum at room temperature. Diethyl ether (40 ml) was added and the resulting suspension was centrifuged. The supernatant solvent was decanted and the solid was washed with diethyl ether and centrifuged again. After decanting, the raw product was dissolved in little methanol, water (30 ml) was added, and the mixture was freeze-dried in vacuum. The resulting solid was purified by MPLC on C18 reversed-phase silica gel (10 % to 100 % methanol/water in 45 min, 0.1 % TFA) to obtain **67** as white solid (20 mg, 19%) with 94 % purity determined by analytical RP-HPLC.

^{1}H-NMR (500 MHz, d^{6}-DMSO): δ [ppm] = 1.31-1.66 (m, 12H, Lys-CH_2), 3.21 (s, 4H, Lys-CH_2), 3.99-4.27 (m, 5H, Lys-CH, Fmoc-CH_2, Fmoc-CH), 6.82 (s, 2H, pyrrole-CH), 7.02-7.29 (m, 3H, phenyl-CH, pyrrole-CH), 7.31-7.41 (m, 5H, phenyl-CH, amide-NH), 7.52 (s, 1H, amide-NH), 7.68 (m, 2H, pyrrole-NH), 7.70-8.40 (m, 11H, guanidine-NH), 12.10 (br.s, 1H, amide-NH_2).

^{13}C-NMR (125 MHz, d^{6}-DMSO): δ [ppm] = 18.4 (Lys-CH_2), 22.7 (Lys-CH_2), 23.0 (Lys-CH_2), 28.8 (Lys-CH_2), 29.0 (Lys-CH_2), 31.6 (Lys-CH_2), 31.9 (Lys-CH_2), 38.7 (Lys-CH_2), 46.6 (Fmoc-CH), 52.1 (Lys-CH), 54.7 (Lys-CH), 65.6 (Fmoc-CH_2), 112.1 (pyrrole-CH), 116.3 (pyrrole-CH), 118.3 (pyrrole-CH), 120.1 (pyrrole-CH), 125.3 (phenyl-CH), 127.1 (phenyl-CH), 127.6 (phenyl-CH), 140.7 (Cq), 143.7 (Cq), 143.9 (Cq), 156.0 (Cq), 157.9 (Cq), 158.1 (Cq), 159.1 (Cq), 171.8 (Cq), 173.5 (Cq).

MALDI-TOF-MS (pos.) m/z calculated for $C_{41}H_{50}N_{13}O_8$ $[M + H]^+$ 852.38, found 853.80

Synthesis of peptide (68):

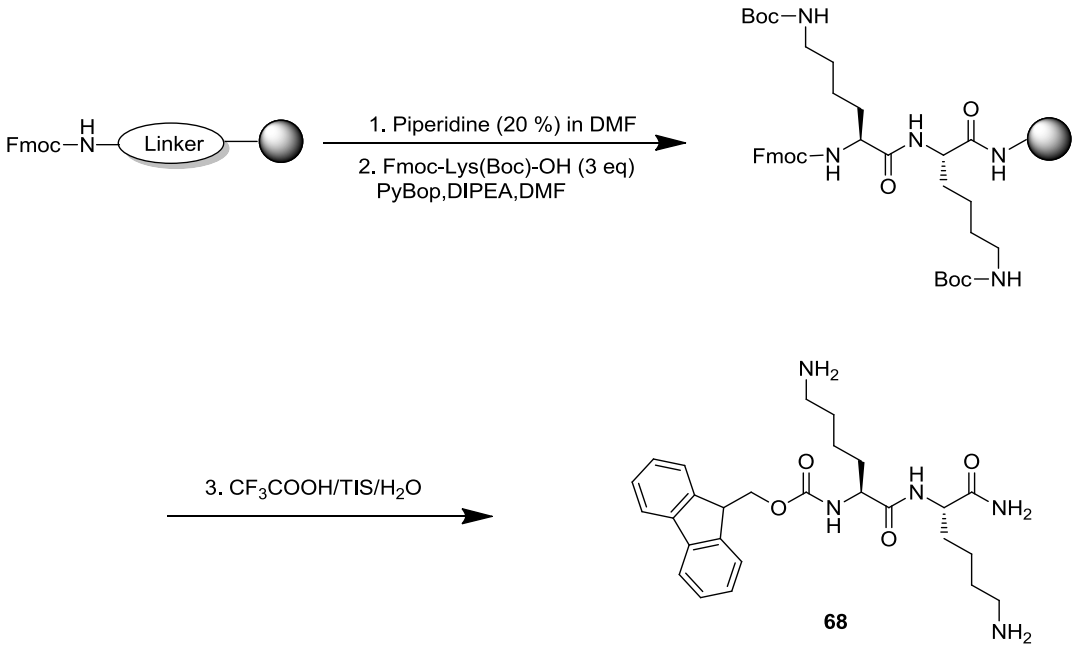

Rink-Amide MBHA resin (200 mg, 0.62mmol/g) was swollen in DCM (5 ml) for 2 h. Fmoc removal was achieved by shaking the resin in 20 % piperidine/DMF (5 ml) for 20 min twice followed by washing with DMF (6 × 5 ml). The first residue Fmoc-Boc-*l*-Lys-OH (169 mg, 0.37 mmol, 3 eq) was attached to the resin with PyBOP (194 mg, 0.37 mmol, 3 eq), DIPEA (130 µl, 0.74 mmol, 6 eq) in DMF (5 ml) for 8 hours and consequent washing with DMF (3 × 5 ml). Coupling and washing steps were repeated. After Fmoc deprotection the second residue Fmoc-Boc-*l*-Lys-OH was attached to the resin as described above, also repeating coupling and washing steps. Afterwards, the resin was washed with DCM (3 × 5 ml), methanol (3 × 5 ml), and DCM (3 × 5 ml) and dried under reduced pressure for one hour. To cleave the product, the resin was shaken under argon atmosphere in a mixture containing 95 % TFA, 2.5 % water, and 2.5 % TIS for three hours and washed twice with the cleavage mixture. The filtrates were combined and concentrated in high vacuum at room temperature. Diethyl ether (40 ml) was added and the resulting suspension was centrifuged. The supernatant solvent was decanted and the solid was washed with diethyl ether and centrifuged again. After decanting, the raw product was dissolved in little methanol, water (30 ml) was added, and the mixture was freeze-dried in vacuum. The resulting solid was purified by MPLC on C18 reversed-phase silica gel (10 % to 100 % methanol/water in 45 min, 0.1 % TFA) to obtain **68** as white solid (20 mg, 19%) with 94 % purity determined by analytical RP-HPLC.

^{1}H-NMR (500 MHz, d^{6}-DMSO): δ [ppm] = 1.35-1.36 (m, 4H, Lys-CH_2), 1.56-1.66 (m, 8H, Lys-CH_2), 2.73 (s, 4H, Lys-CH_2), 4.15-4.25 (m, 5H, Lys-CH, Fmoc-CH_2, Fmoc-CH), 7.05 (s, 1H, amide-NH), 7.31-7.74 (m, 9H, phenyl-CH, amide-NH), 7.88-8.02 (m, 8H, amide-NH_2, amine-NH_3^+),

MALDI-TOF-MS (pos.) m/z calculated for $C_{27}H_{38}N_5O_4$ $[M + H]^+$ 496.28, found 497.13

6.5 Analytical methods

6.5.1. Development of novel cell penetrating peptide

6.5.1.1 Isothermal Titration Calorimetry

All measurements were carried out in sodium cacodylate buffer (0.05 M, pH 7.40 ± 0.01) at 25 °C. All solutions were ultrasonicated and degassed in vacuum prior to the experiments. Aliquots of heparin sulfate (1.0 mM, 5μL) were injected from a 297μl rotating syringe (307 rpm) into the calorimeter reaction cell containing 1.45 ml of corresponding peptide **40**, and **41** solutions (0.05mM). Blank experiments were conducted to determine the heats of dilution of heparin sodium. These were subtracted from the heats measured in the titration experiments. Data was analyzed using Origin 7.0 software according to a single set of sites binding mode.

6.5.1.2 Cellular Uptake Study

Human cervix carcinoma cell lines (HeLa) were seeded in 8-well plates and grown for 24 h. Afterwards, cells were incubated with 5 μM, 10 μM, 15 μM, 20 μM **58** and 10 μM, 20 μM **60**, respectively. After the incubation for 1 h, cells were thoroughly washed with PBS buffer for three times. Fresh DMEM cell culture medium was supplemented and examined under a confocal fluorescence microscope (SP5 LCSM, *Leica*). Images were processed using LAS AF software (*Leica*) and Adobe Photoshop CS2.

6.5.1.3 Cell Co-localization Study

Golgi-apparatus

HeLa cells were seeded in 8-well plates, grown for 24 h and transfected with 2 μg of Golgi marker plasmid-DNA mixed with 1 mM PEI. After an additional incubation of 24 h, cells were incubated with 10 μM **58** for 1 h. Afterwards, DAPI was added to stain nucleus and incubated for 5 minutes. Cells were then thoroughly washed with PBS buffer for three times and examined under a confocal fluorescence microscope (SP5 LCSM, *Leica*). Images were processed using LAS AF software (*Leica*) and Adobe Photoshop CS2.

Endosome and lysosome (immunostaining)

HeLa cells were seeded in 8-well plates, grown for 24 h and incubated with 10 μM **58** for 1 h. Fluorochrome-conjugated antibody targeting endosome and lysosome respectively were added. Afterwards, DAPI was added to stain nucleus and incubated for 5 minutes. Cells were then thoroughly washed with PBS buffer for three times and fixed with fixation examined under a confocal fluorescence microscope (SP5 LCSM, *Leica*). Images were processed using LAS AF software (*Leica*) and Adobe Photoshop CS2.

6.5.1.4 Alamar Blue Cell Viability Assay

HeLa cells were grown and incubated with **58** and PEI as described above. Before incubation, 24 h after incubation, cells were incubated with Alamar Blue dye (*Invitrogen*, 10 % v/v) for 3 h at 37 °C at 5 % CO_2. Fluorescence was measured at 590 nm using a multimode reader (GloMax-Multi+DetectionSystem, *Promega*).

6.5.2. Development of cell penetrating peptide based gene delivery vector

6.5.2.1 EB Displacement Assay

Spectra were recorded at 25 °C in aqueous sodium cacodylate buffer (0.01 M, pH 7.00 ± 0.01) in quartz fluorescence micro-cuvettes (1 cm) equipped with a stopper. To a solution of ethidium bromide (900 μL, 0.75 μM, 1 eq), ctDNA was added and incubated for 15 min. The fluorescence emission was then measured from 560 to 650 nm utilizing an excitation wavelength of 520 nm. To this mixture a stock solution (50 μM) of **42**, **43, 44, 62, 63** or **64** was added in aliquots (1–32 μl). After each addition the cuvette was gently shaken and the mixture was incubated for 1 min to ensure that the equilibria were established (no change was observed with longer incubation time). An excerpt of the fluorescence emission at 600 nm was corrected for ethidium bromide ś own emission and plotted against [EB]/[**42**], [EB]/[**43**], [EB]/[**44**], [EB]/[**62**], [EB]/[**63**] and [EB]/[**64**], respectively. An exponential decay first order function was fitted using Origin 7.0. The reciprocal x-value at half of the maximum fluorescence emission is the IC_{50} value representing the equivalents of **42**, **43, 44, 62, 63** or **64** that are necessary to displace half of the ethidium bromide from the EB/DNA complex.

6.5.2.2 Isothermal Titration Calorimetry

All measurements were carried out in sodium cacodylate buffer (0.05 M, pH 7.00 ± 0.01) at 25 °C. All solutions were ultrasonicated and degassed in vacuum prior to the experiments. Aliquots of ctDNA (0.7 mM, 5μL) were injected from a 297μl rotating syringe (307 rpm) into the calorimeter reaction cell containing 1.45 ml of corresponding peptide **42**, **43, 44, 62, 63** and **64** solutions (0.05mM). Blank experiments were conducted to determine the heats of dilution of heparin sodium. These were subtracted from the heats measured in the titration experiments. Data was analyzed using Origin 7.0 software according to a single set of sites binding mode.

6.5.2.3 DLS Experiments

All measurements were carried out in sodium cacodylate buffer (0.01 M, pH 7.00 ± 0.01) at 25 °C in UV-transparent micro-cuvettes (1 cm) equipped with a stopper. Mixtures of ctDNA (50 μM) and solution (150 μM) of **42**, **43, 44, 62, 63** or **64** were prepared respectively and filtered prior to measuring via 0.20 μm nylon filters. The autocorrelation functions of the backscattered light fluctuations were analyzed with the DTS 6.20 software from Malvern providing the hydrodynamic diameter (Z-average), polydispersity, size distribution (NNLS analysis) and Zeta potential.

6.5.2.4 AFM Measurements

AFM images were obtained in tapping mode using a NanoDrive Controller with an Innova Scanning Probe Microscope (*Veeco Germany,* Mannheim) and N-type silicon cantilever (AC 160TS *OLYMPUS*). The scan rate was about 5 μm/s. Mixtures of ctDNA (50 μM) and solution (150 μM) of **42**, **44,** or **64** were prepared respectively. Samples were spin-coated (66 rps) onto a freshly cleaved mica surface (*Plano GmbH*) for 2 minutes. The AFM data were analyzed using Gwiddion-2.20 software.

6.5.2.5 Spectrophotometric Titrations

UV/Vis Titrations

All measurements were carried out in aqueous sodium cacodylate buffer (0.01 M, pH 7.00 ± 0.01) in quartz UV micro-cuvettes (1 cm) equipped with a stopper at 25℃. The pH was adjusted with aqueous HCl or NaOH solution. To a solution of **42**, **43,** or **64** (800 µL, 2 × 10^{-5} M) a stock solution of ctDNA, $pdAdT_2$, $pdGdC_2$, pApU were added in aliquots (5 – 100 µL).

Fluorimetric Titrations

All measurements were carried out in aqueous sodium cacodylate buffer (0.01 M, pH 7.00 ± 0.01) in quartz fluorescence micro-cuvettes (1 cm) equipped with a stopper at 25℃. The pH was adjusted with aqueous HCl or NaOH solution. To a solution of **42**, **43,** or **64** (800 µL, 2 × 10^{-5} M) a stock solution of ctDNA, $pdAdT_2$, $pdGdC_2$, pApU were added in aliquots (5 – 100 µL).

CD Titrations

All measurements were carried out in aqueous sodium cacodylate buffer (0.01 M, pH 7.00 ± 0.01) in quartz UV micro-cuvettes (1 cm) equipped with a stopper at 25℃. The pH was adjusted with aqueous HCl or NaOH solution. To a solution of **42**, **43,** or **64** (800 µL, 2 × 10^{-5} M) a stock solution of ctDNA, $pdAdT_2$, $pdGdC_2$, pApU were added in aliquots (5 – 100 µL).

6.5.2.6 Transfection and Microscopy

Per well, 1 × 10^4 cells were seeded in 96 well cell culture plates (*Greiner bio-one*) in a total medium volume of 200 µl 24 h before transfection. The cationic transfection reagent polyethylenimine (PEI, pH 6.8, *Sigma-Aldrich*) was used at a concentration of 0.15 mM in PBS (*Invitrogen*) with 2 µg of plasmid DNA per well. Transfection with **42**, **43, 44, 61, 62, 63** or **64** were carried out in a concentration range of 0.05, 0.10, 0.15 and 0.25 mM with 2 µg plasmid DNA in a total volume of 30 µl in PBS buffer. Transfection efficiency was analyzed 24 and 48 h after transfection with an inverted fluorescence microscope (Axiovert 200M, *Carl Zeiss*) with a 10X air objective. Images were processed and analyzed using MetaMorph 6.3r6 (*Molecular Devices*) and Adobe Photoshop CS2 (*Adobe Systems*).

6.5.2.7 Endosomal Escape Assay

Cells were incubated with complete medium containing 25 μM chloroquine and 150 nM bafilomycin 30 min before transfection. Transfection was carried out with 0.15 mM **42**, **43, 44, 61, 62, 63**, **64** or PEI and 2 μg plasmid-DNA.

6.5.2.8 Alamar Blue Cell Viability Assay

HeLa cells were grown and transfected as described above. Before transfection, 24 h and 48 h after transfection cells were incubated with Alamar Blue dye (*Invitrogen*, 10 % v/v) for 3 h at 37 ℃ at 5% CO_2. Fluorescence was measured at 590 nm using a multimode reader (GloMax-Multi+DetectionSystem, *Promega*).

6.5.3 Development of cyclic peptide nanotube based gene delivery vector

6.5.3.1 DLS Experiments

All measurements were carried out in sodium cacodylate buffer (0.01 M, pH 7.40 ± 0.01) at 25 °C in UV-transparent micro-cuvettes (1 cm) equipped with a stopper. Mixtures of ctDNA (0.02 mM) and solution (0.4 mM) of **45** and **65** were prepared respectively and filtered prior to measuring. The autocorrelation functions of the backscattered light fluctuations were analyzed with the DTS 6.20 software from *Malvern* providing the hydrodynamic diameter (Z-average), polydispersity, size distribution (NNLS analysis) and Zeta potential.

6.5.3.2 AFM Experiments

AFM images were obtained in tapping mode using a NanoDrive Controller with an Innova Scanning Probe Microscope (*Veeco Germany*, Mannheim) and N-type silicon cantilever (AC 160TS OLYMPUS). The scan rate was about 5 μm/s. 0.4 mM of **45** and **65** sample solutions in water were prepared and spin-coated (66rps) onto a freshly cleaved mica surface (*Plano GmbH*) for 2 minutes. The AFM data were analyzed using Gwiddion-2.20 software.

6.5.3.3 TEM Experiments

TEM images were obtained using a CM 200 FEG (*Phillips Company*). A drop of a freshly prepared sample solution of **45** and **45**/ctDNA was placed on 400-mesh formvar copper grid coated with carbon. About 2 min after the deposition the grid was tapped with filter paper to remove remaining solvent from the surface. Negative staining was performed by addition of a drop of an ethanolic solution of uranyl formate (0.5 %) onto the copper grid. After 1 min, the liquid on the surface of the grid was removed by tapping it with a filter paper.

6.5.3.4 Transfection Experiments

Per well, 1×10^4 cells were seeded in 96 well cell culture plates (*Greiner bio-one*) in a total medium volume of 200 µl 24 h before transfection. The cationic transfection reagent polyethylenimine (PEI, pH 6.8, *Sigma-Aldrich*) was used at a concentration of 0.15 mM in PBS (*Invitrogen*) with 2 µg of plasmid DNA per well. Transfections with **45** or **65** were carried out in a concentration of 0.4 mM with 2 µg plasmid DNA in a total volume of 30 µl in PBS buffer. Transfection efficiency was analyzed 24 and 48 h after transfection with an inverted fluorescence microscope (Axiovert 200M, *Carl Zeiss*) with a 10X air objective. Images were processed and analyzed using MetaMorph 6.3r6 (*Molecular Devices*) and Adobe Photoshop CS2 (*Adobe Systems*).

6.5.3.5 Plasmid DNA Labeling and Co-localization

Plasmid DNA was labeled with the PromoFluor-500 Nick Translation Labeling Kit (*PromoKine*) according to the manufacturer's instructions. Briefly, following nick translation of the pF143-GFP vector with PromorFluor-500-dUTPs for 2 h at 15℃, cleanup of the mixture was performed using a DNA purification Kit (*Macharey-Nagel*) as advised. Afterwards, 1 µL labeled DNA (1 µg/µL) was added to 10µL of 0.4 mM peptide **45**. The resulting mixture was directly dropped on a glass bottom culture dish and then examined with confocal fluorescence microscopy (SP5 LCSM, *Leica*).

6.5.3.6 Endosomal Escape Assay

Cells were incubated with complete medium containing 25 µM chloroquine and 150 nM

bafilomycin 30 min before transfection. Transfection was carried out with 0.4 mM **45** or PEI and 2 μg plasmid-DNA as described above.

6.5.3.7 Alamar Blue Cell Viability Assay

HeLa cells were grown and transfected as described above. Before transfection and 24 h after transfection, cells were incubated with Alamar Blue dye (*Invitrogen*, 10 % v/v) for 3 h at 37℃ at 5% CO_2. Fluorescence was measured at 590 nm using a multimode reader (GloMax-Multi+DetectionSystem, *Promega*).

6.5.3.8 Molecular Modelling

Virtual molecular studies were carried out by a conformational search using *Macro Model* with the OPLS2005 force-field, GB/SA solvent model for water, 500000 iterations and a convergence threshold of 0.05. The conformational search has been processed with mixed torsional / low-mode sampling with 1000 maximum steps and 100 steps per rotable bond. The collected conformations have been in an energy window of 5kJ/mol and have been of similar shape, so that the shown structure represents all found conformations in that specific energy window. For the illustration of peptide **45**, PyMOL was used with arrow cartoon mode for a better representation.

6.5.4 Development of supramolecular β-helix mimetic peptide

6.5.4.1 Circular dichroism (CD)

Stock solutions of 5 mM peptide **46** and **66** were prepared respectively (dissolved in water). CD spectrum was recorded with *JASCO* J-815 CD Spectrometer at 25℃ in 10 mm quartz cuvette with following parameters: range = 600-210 nm, sensitivity = standard (100 mdeg), scanning speed = 200 nm/min, data pitch = 0.1 nm, bandwidth = 1 nm, response = 1 sec, accumulation = 3. The corresponding samples were freshly prepared and adjusted the pH with HCl or sodium hydroxide. The CD spectrum was recorded first and the samples were left at room temperature for 8 days; after 8 days the same solution was recorded again with the same parameters as last time.

6.5.4.2 UV-Vis spectroscopy

UV spectrum was recorded with *JASCO* V-660 spectrometer at 25℃ in 10 mm quartz cuvette with following parameters: sensitivity = standard, scanning speed = 200nm/min, data pitch = 0.1 nm, bandwidth = 1 nm, response = 1 sec. The according sample was prepared and adjusted the pH with sodium hydroxide solution and left at room temperature for several weeks. The temperature of the sample solution was gradually increased and UV-vis adsorption at 295 nm was recorded under different temperatures. The data was analyzed with Origin 8.0 software.

6.5.4.3 DLS Experiments

All measurements were carried out at 25 ° C in UV-transparent micro-cuvettes (1 cm) equipped with a stopper. 0.1 mM peptide **46** solution in water was prepared and filtered prior to measuring. The pH was adjusted with sodium hydroxide solution accordingly. The aging effect of peptide **46** was followed every hour. The autocorrelation functions of the backscattered light fluctuations were analyzed with the DTS 6.20 software from *Malvern* providing the hydrodynamic diameter (Z-average), polydispersity, size distribution (NNLS analysis).

6.5.4.4 AFM Experiments

AFM images were obtained in tapping mode using a NanoDrive Controller with an Innova Scanning Probe Microscope (*Veeco Germany*, Mannheim) and N-type silicon cantilever (AC 160TS OLYMPUS). The scan rate was about 5 μm/s. Fresh prepared, 5 days and 8 days old 0.1 mM of **45** and **65** sample solutions in water were spin-coated (66rps) onto a freshly cleaved mica surface (*Plano GmbH*) for 2 minutes. The AFM data were analyzed using Gwiddion-2.20 software.

6.5.4.5 TEM Experiments

TEM images were obtained using a CM 200 FEG (*Phillips Company*). A drop of a freshly prepared and 8 days old sample solution of **45** was placed on 400-mesh formvar copper grid coated with carbon. About 2 min after the deposition the grid was tapped with filter paper to

remove remaining solvent from the surface. Negative staining was performed by addition of a drop of an ethanolic solution of uranyl formate (0.5 %) onto the copper grid. After 1 min, the liquid on the surface of the grid was removed by tapping it with a filter paper.

6.5.5 Development of functionalized amphiphilic peptide assembly

6.5.5.1 AFM Experiments

AFM images were obtained in tapping mode using a NanoDrive Controller with an Innova Scanning Probe Microscope (*Veeco Germany*, Mannheim) and N-type silicon cantilever (AC 160TS OLYMPUS). The scan rate was about 5 μm/s. Fresh prepared sample solutions in water were spin-coated (66rps) onto a freshly cleaved mica surface (*Plano GmbH*) for 2 minutes. The AFM data were analyzed using Gwiddion-2.20 software.

6.5.5.2 TEM Experiments

TEM images were obtained using a CM 200 FEG (*Phillips Company*). A drop of a freshly prepared sample solution was placed on 400-mesh formvar copper grid coated with carbon. About 2 min after the deposition the grid was tapped with filter paper to remove remaining solvent from the surface. For negative staining, a drop of an ethanolic solution of uranyl formate (0.5 %) was added onto the copper grid. After 1 min, the liquid on the surface of the grid was removed by tapping it with a filter paper.

6.5.5.3 Circular dichroism (CD)

Stock solutions of 5 mM peptide **47**, **67** and **68** were prepared respectively (dissolved in DMSO). CD spectrum was recorded with *JASCO* J-815 CD Spectrometer at 25℃ in 10 mm quartz cuvette with following parameters: range = 600-210 nm, sensitivity = standard (100 mdeg), scanning speed = 200 nm/min, data pitch = 0.1 nm, bandwidth = 1 nm, response = 1 sec, accumulation = 3. The corresponding samples were freshly prepared and adjusted the pH with HCl or sodium hydroxide.

6.5.5.4 Transfection Experiments

Per well, 1×10^4 cells were seeded in 96 well cell culture plates (*Greiner bio-one*) in a total

medium volume of 200 µl 24 h before transfection. The cationic transfection reagent polyethylenimine (PEI, pH 6.8, *Sigma-Aldrich*) was used at a concentration of 0.15 mM in PBS (*Invitrogen*) with 2 µg of plasmid DNA per well. Transfection with **47** was carried out in a concentration of 0.4 mM with 2 µg plasmid DNA in a total volume of 30 µl in PBS buffer. Transfection efficiency was analyzed 24 and 48 h after transfection with an inverted fluorescence microscope (Axiovert 200M, *Carl Zeiss*) with a 10X air objective. Images were processed and analyzed using MetaMorph 6.3r6 (*Molecular Devices*) and Adobe Photoshop CS2 (*Adobe Systems*)

7. APPENDIX

7.1 Abbreviations

δ	chemical shift
℃	Celsius
λ	wavelength
μ	micro
ε	extinction coefficient
π	pi
ζ	zeta potential
Å	Ångstrom
A	alanine/adenine
AA	amino acid
Aβ	amyloid beta
abs	absolute
Ac	acetyl
AD	adamantane
ADP	adenosine diphosphate
AFM	atomic force microscopy
Ala	alanine
Alloc	allyloxycarbonyl
AMP	adenosine monophosphate
Ar	argon
Arg	arginine
Asp	aspartic acid
ATP	adenosine triphosphate
Au	gold
NPs	nanoparticles
Bn	benzyl

Boc	*tert*-butyloxycarbonyl
*t*Bu	*tert*-butyl
br	broad
c	concentration
C	cytosine
ca.	circa
CD	circular dichroism
$CDCl_3$	deuterated chloroform
Chol	cholesterol
cm	centimeter
CPP	cell penetrating peptide (s)
d	doublet / diameter/ day
dAdT	deoxyadenylic-deoxythymidylic acid
dGdC	deoxyguanylic-deoxycytidylic acid
D	diffusion constant
Da	dalton
DCM	dichloromethane
DIPEA	N,N´-diisopropylethyl amine
DLS	dynamic light scattering
DMF	N,N´-dimethyl formamide
DMSO	dimethyl sulfoxide
d^6-DMSO	deuterated dimethyl sulfoxide
DNA	deoxyribonucleic acid
DOPE	dioleoylphosphatidylethanolamine
ds	double strand
dsDNA	double strand deoxyribonucleic acid
dsRNA	double strand ribonucleic acid
E	glutamic acid
EB	ethidium bromide
e.g.	for example

eq	equivalent
ESI	electrospray ionization
ESI-MS	electrospray ionization mass spectrometry
Et_3N	triethylamine
F	phenylalanine
Fmoc	9-fluorenylmethyloxycarbonyl
FT-IR	fourier transform infrared spectroscopy
g	gram
G	glycine/guanine
GFP	green fluorescence protein
Gln	glutamine
Glu	glutamic acid
Gly	glycine
GCP	guanidiniocarbonyl pyrrole
GSH	glutathione
h	hour (s)
HCTU	1-H-Benzotriazolium 1-[bis(dimethylamino)methylene] -5chloro-,hexafluorophosphate (1-),3-oxide
H-donor	hydrogen bond donor
His	histidine
HIV	human immunodeficiency virus
HOBt	1-hydroxybenzotriazole
H_2O	water
HPLC	high performance liquid chromatography
HRMS	high resolution mass spectrometry
Hz	Hertz
IC_{50}	half maximal displacement concentration
ICD	induced circular dichroism
Ile	isoleucine
ITC	isothermal titration calorimetry

K	lysine/kelvin
kJ	kilo Joule
Kd	dissociation constant
L	liter/ leucine
Leu	leucine
Lys	lysine
m	milli / multiplett / meter
M	mol/L
m/z	mass per charge
max	maximum
MBHA	p-methylbenzhydrylamine
Me	methyl
MeOH	methanol
MHz	megahertz
min	minute (s)
μM	micromolar
mM	millimolar
MPLC	medium performance liquid chromatography
MS	mass spectrometry
n	nano
nm	nanometer
nM	nanomolar
NMM	N-methylmorpholin
NMR	nuclear magnetic resonance
NPs	nanoparticles
p	para
PAMAM	polyamidoamine dendrimer
Pbf	2,2,4,6,7-pentamethyldihydrobenzofuran-5-sulfonyl
PEG	polyethylenglycol
PEI	polyethylenimine

PLL	polylysine
Pd	palladium
Pd/C	palladium on charcoal
$Pd(PPh_3)_4$	Tetrakis(triphenylphosphine)palladium(0)
PDI	polydispersity index
pH	pondus hydrogenii
Phe	phenylalanine
$PhSiH_3$	phenylsilane
pKa	logarithmic acid dissociation constant
PNA	peptide nucleic acid
ppm	parts per million
Pro	proline
PyBOP	benzotriazol-1-yl-N-oxy-tris(pyrrolidino)phosphonium hexafluorophosphate
q	quadruplet
QSAR	quantitative structure–activity relationship
r	radius
R	arginine
RNA	ribonucleic acid
RP	reversed phase
rt	room temperature
s	singulett / second(s)
Ser	serine
siRNA	small interfering ribonucleic acid
SPPS	solid phase peptide synthesis
t	time
T	temperature/thymine
Tat	Trans-Activator of Transcription
TEM	transmission electron microscopy
TFA	trifluoroacetic acid

THF	tetrahydrofuran
TIS	triisopropylsilane
Trt	trityl
Trp	tryptophan
Tyr	tyrosine
U	uracil
UV	ultraviolet
UV/Vis	ultraviolet/ visible
V	volume / valine
Val	valine
W	tryptophan

7.2 Supplementary Experiment Data

7.2.1 HPLC data

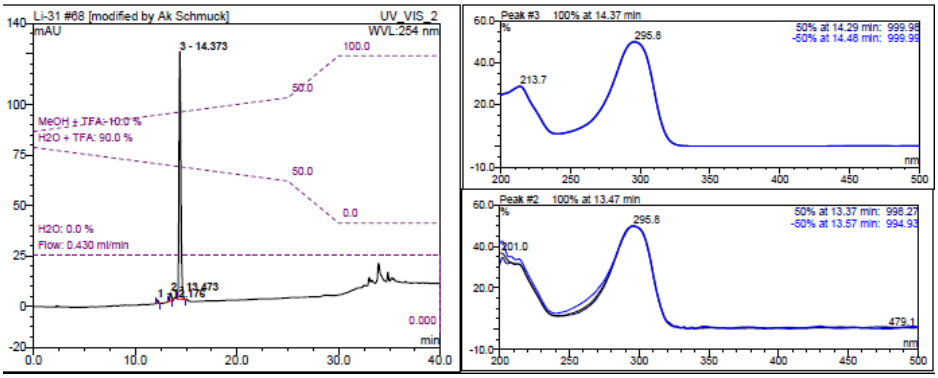

Figure 7.1 Analytical HPLC run of peptide **40** with 96% purity, solvent: 10% to 50% MeOH/H_2O (0.05 % TFA) in 30 min, flow rate: 0.43 ml/min, retention time t_R= 14.4 min; the peak integration is based on detection at 254 nm.

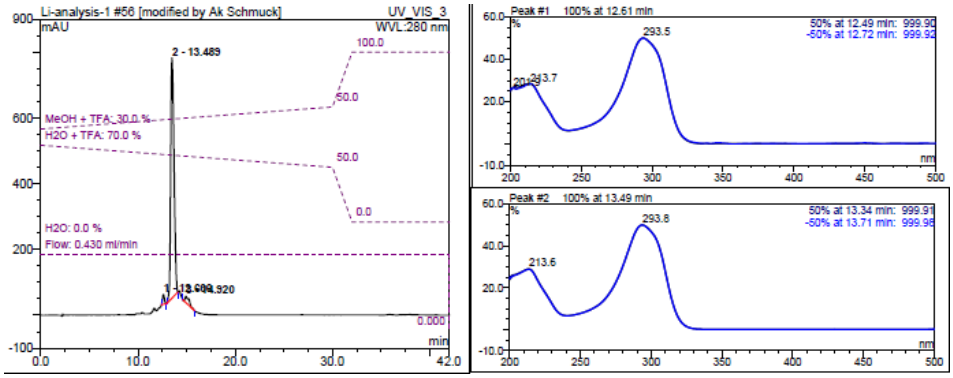

Figure 7.2 Analytical HPLC run of peptide **42** with 93% purity, solvent: 30% to 50% MeOH/H_2O (0.05 % TFA) in 30 min, flow rate: 0.43 ml/min, retention time t_R= 13.4 min; the peak integration is based on detection at 280 nm.

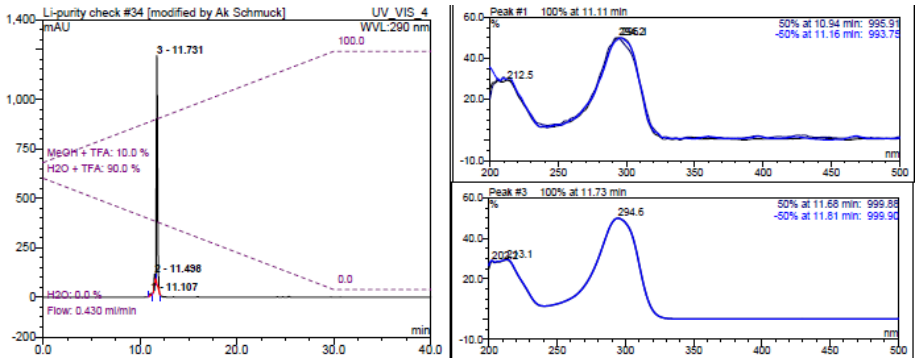

Figure 7.3 Analytical HPLC run of peptide **62** with 95% purity, solvent: 10% to 100% MeOH/H_2O (0.05 % TFA) in 30 min, flow rate: 0.43 ml/min, retention time t_R= 11.7 min; the peak integration is based on detection at 290 nm.

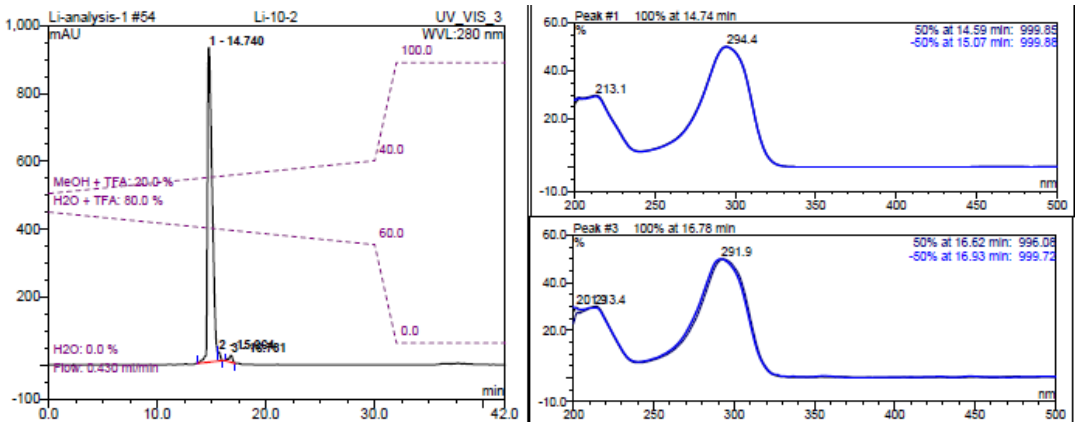

Figure 7.4 Analytical HPLC run of peptide **61** with 95% purity, solvent: 20% to 40% MeOH/H_2O (0.05 % TFA) in 30 min, flow rate: 0.43 ml/min, retention time t_R= 14.7 min; the peak integration is based on detection at 280 nm.

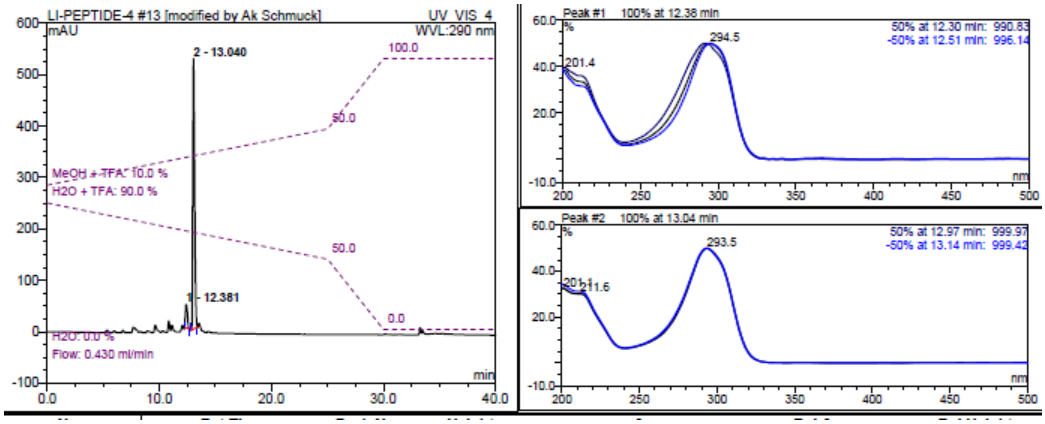

Figure 7.5 Analytical HPLC run of peptide **63** with 91% purity, solvent: 10% to 60% MeOH/H_2O (0.05 % TFA) in 30 min, flow rate: 0.43 ml/min, retention time t_R= 13.0 min; the peak integration is based on detection at 290 nm.

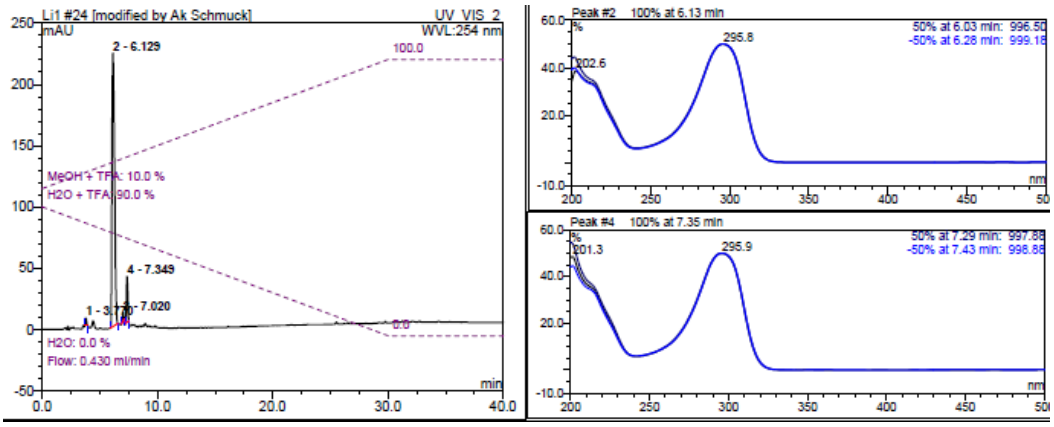

Figure 7.6 Analytical HPLC run of peptide **64** with 89% purity, solvent: 10% to 100% MeOH/H_2O (0.05 % TFA) in 30 min, flow rate: 0.43 ml/min, retention time t_R= 6.1 min; the peak integration is based on detection at 254 nm.

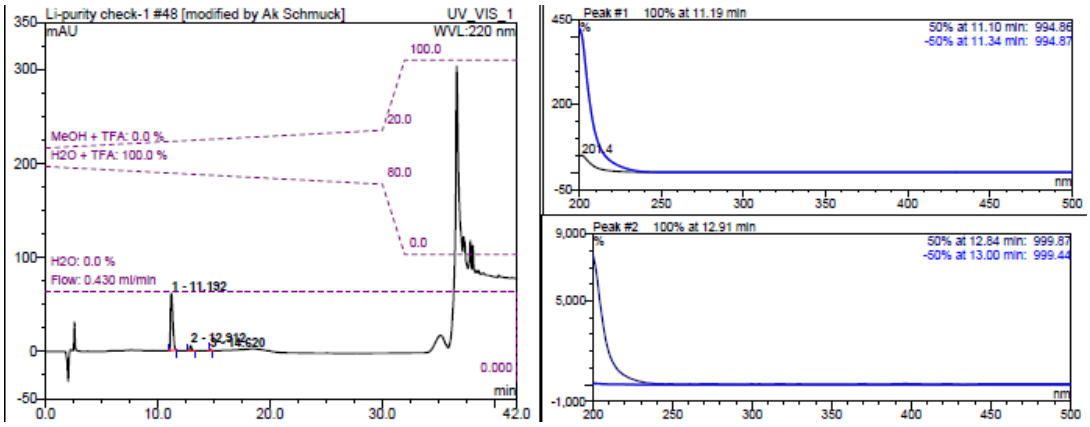

Figure 7.7 Analytical HPLC run of peptide **43** with 92% purity, solvent: 0% to 20% MeOH/H_2O (0.05 % TFA) in 30 min, flow rate: 0.43 ml/min, retention time t_R= 11.1 min; the peak integration is based on detection at 220 nm.

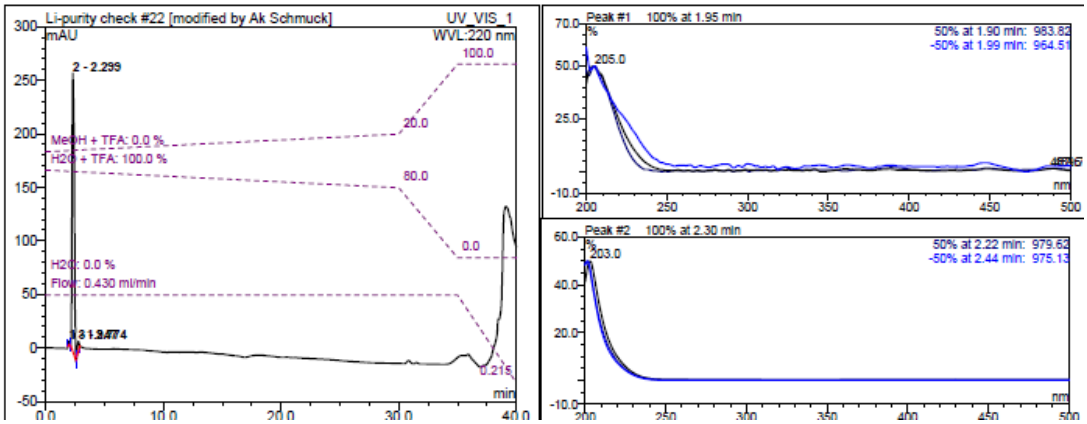

Figure 7.8 Analytical HPLC run of peptide **44** with 97% purity, solvent: 0% to 20% MeOH/H_2O (0.05 % TFA) in 30 min, flow rate: 0.43 ml/min, retention time t_R= 2.3 min; the peak integration is based on detection at 220 nm.

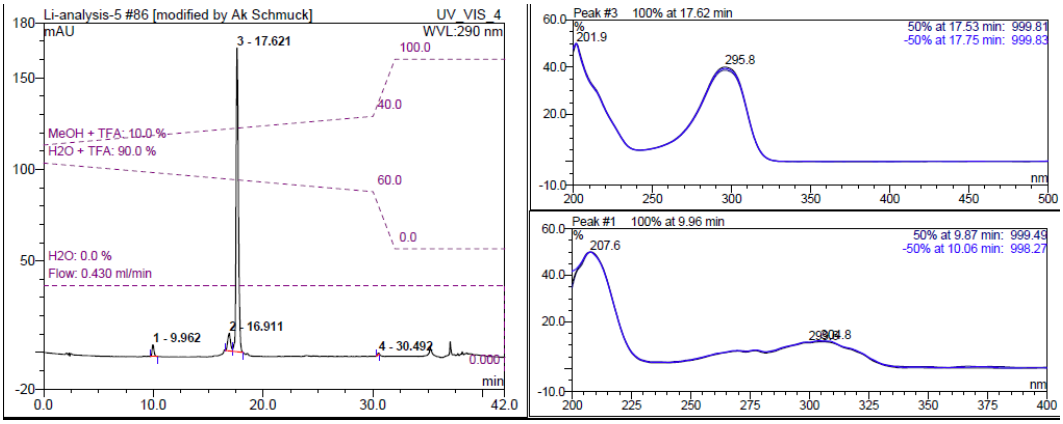

Figure 7.9 Analytical HPLC run of peptide **45** with 90% purity, solvent: 10% to 40% MeOH/H_2O (0.05 % TFA) in 30 min, flow rate: 0.43 ml/min, retention time t_R= 17.6 min; the peak integration is based on detection at 290 nm.

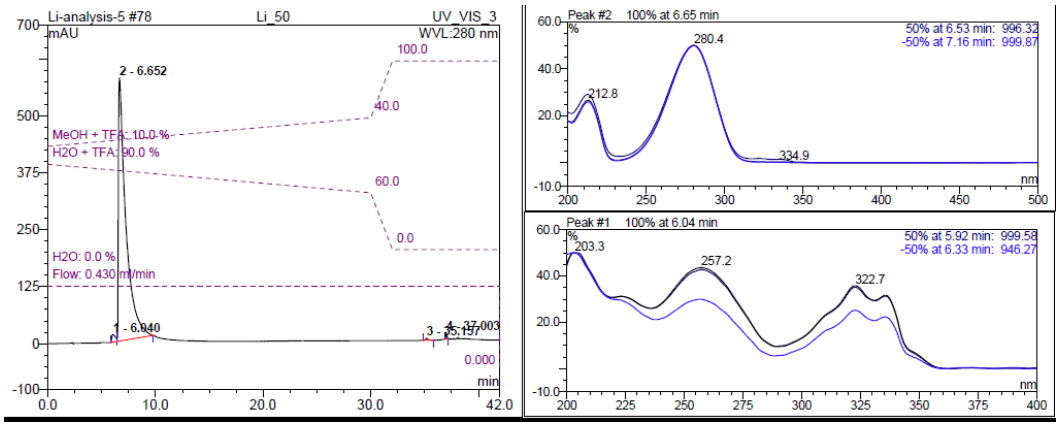

Figure 7.10 Analytical HPLC run of peptide **65** with 98% purity, solvent: 10% to 40% MeOH/H_2O (0.05 % TFA) in 30 min, flow rate: 0.43 ml/min, retention time t_R= 6.6 min; the peak integration is based on detection at 280 nm.

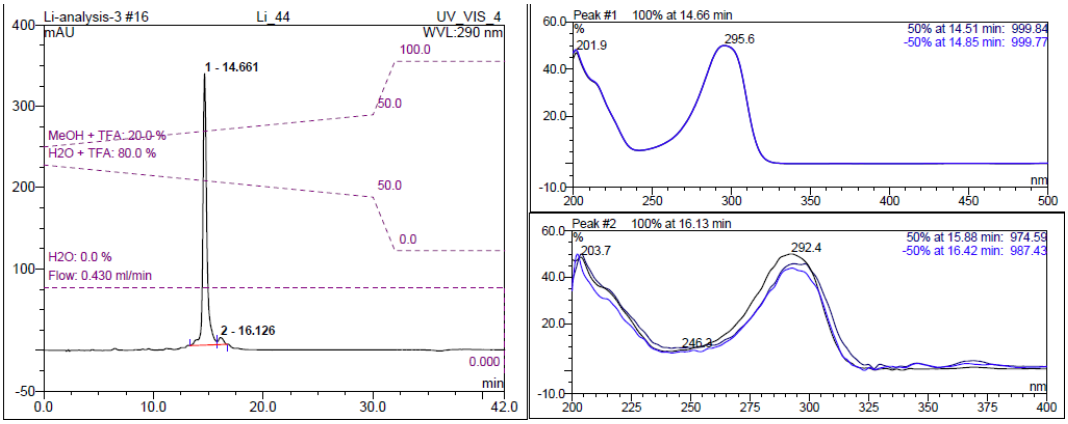

Figure 7.11 Analytical HPLC run of peptide **46** with 97% purity, solvent: 20% to 50% MeOH/H_2O (0.05 % TFA) in 30 min, flow rate: 0.43 ml/min, retention time t_R= 14.6 min; the peak integration is based on detection at 290 nm.

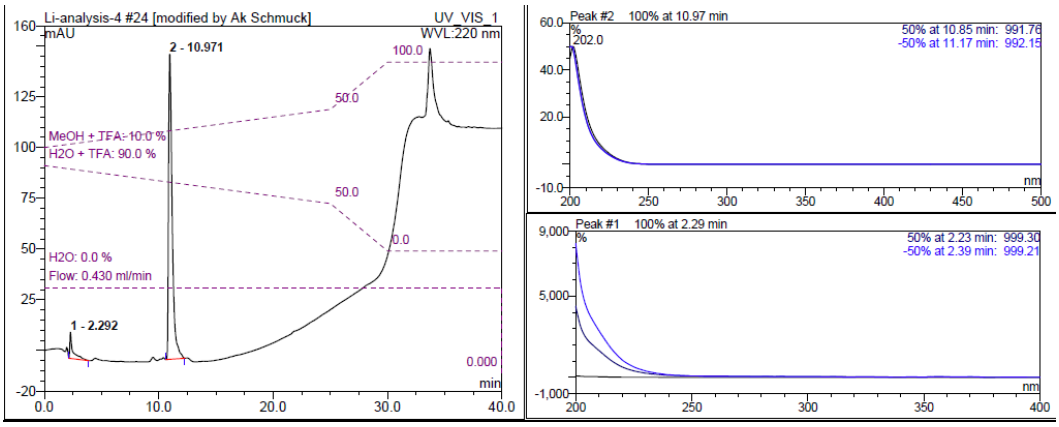

Figure 7.12 Analytical HPLC run of peptide **66** with 93% purity, solvent: 10% to 50% MeOH/H_2O (0.05 % TFA) in 30 min, flow rate: 0.43 ml/min, retention time t_R= 10.9 min; the peak integration is based on detection at 220 nm.

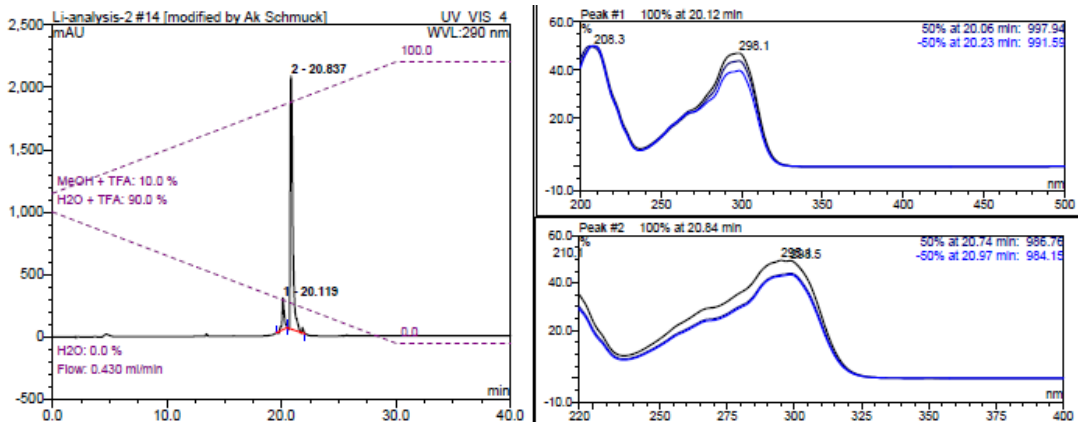

Figure 7.13 Analytical HPLC run of peptide **47** with 91% purity, solvent: 10% to 100% MeOH/H_2O (0.05 % TFA) in 30 min, flow rate: 0.43 ml/min, retention time t_R= 20.8 min; the peak integration is based on detection at 254 nm.

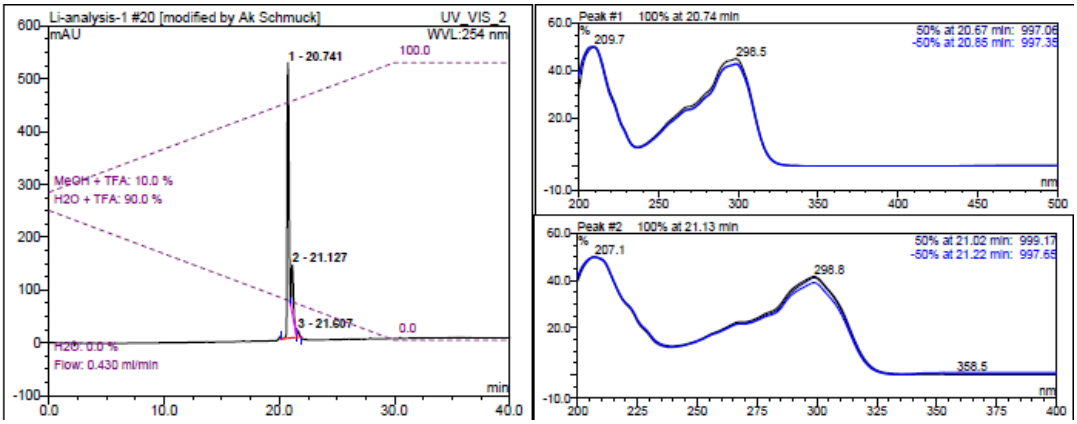

Figure 7.14 Analytical HPLC run of peptide **67** with 85% purity, solvent: 10% to 100% MeOH/H_2O (0.05 % TFA) in 30 min, flow rate: 0.43 ml/min, retention time t_R= 20.8 min; the peak integration is based on detection at 254 nm.

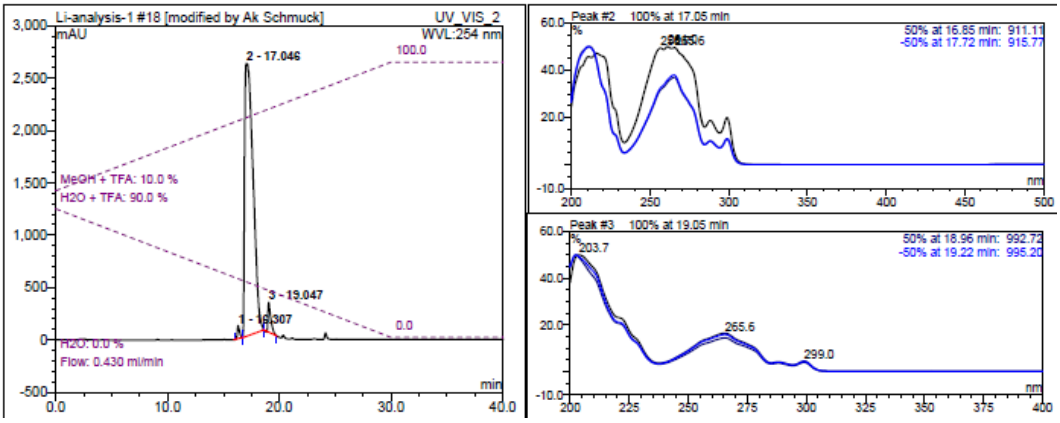

Figure 7.15 Analytical HPLC run of peptide **68** with 91% purity, solvent: 10% to 100% MeOH/H_2O (0.05 % TFA) in 30 min, flow rate: 0.43 ml/min, retention time t_R= 17.0 min; the peak integration is based on detection at 254 nm.

7.2.2 ITC data

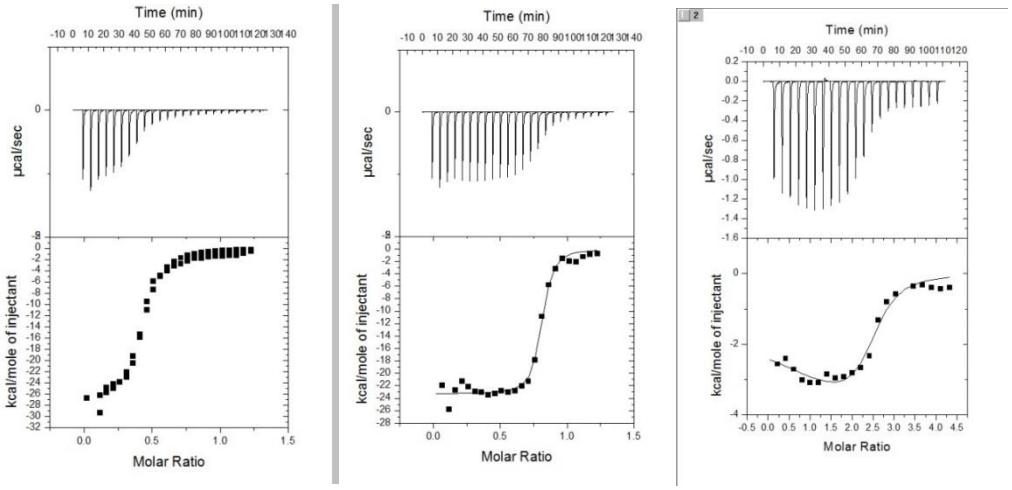

Figure 7.16 Top: ITC experiments were carried out in sodium cacodylate buffer (0.01 M) at neutral pH by titrating aliquots of 5 µL of ctDNA (0.7 mM) to **42**, **62** or **63** (c = 0.05 mM). Bottom: the titrations were corrected for dilution and fitted with a one-site model. The titrations with **42**, **62** or **63** are corrected for the first data point.

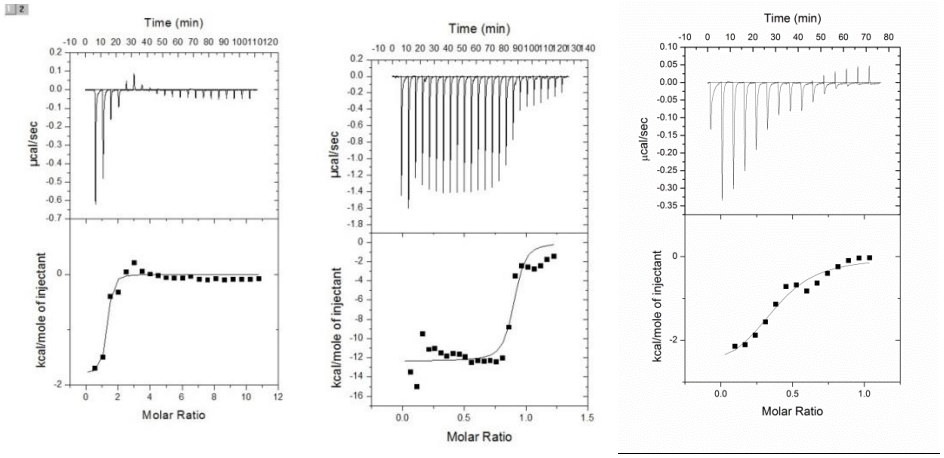

Figure 7.17 Top: ITC experiments were carried out in sodium cacodylate buffer (0.01 M) at neutral pH by titrating aliquots of 5 µL of ctDNA (0.7 mM) to **64**, **43** or **44** (c = 0.05 mM). Bottom: the titrations were corrected for dilution and fitted with a one-site model. The titrations with **64**, **43** or **44** are corrected for the first data point.

7.2.3 Molecular modeling data

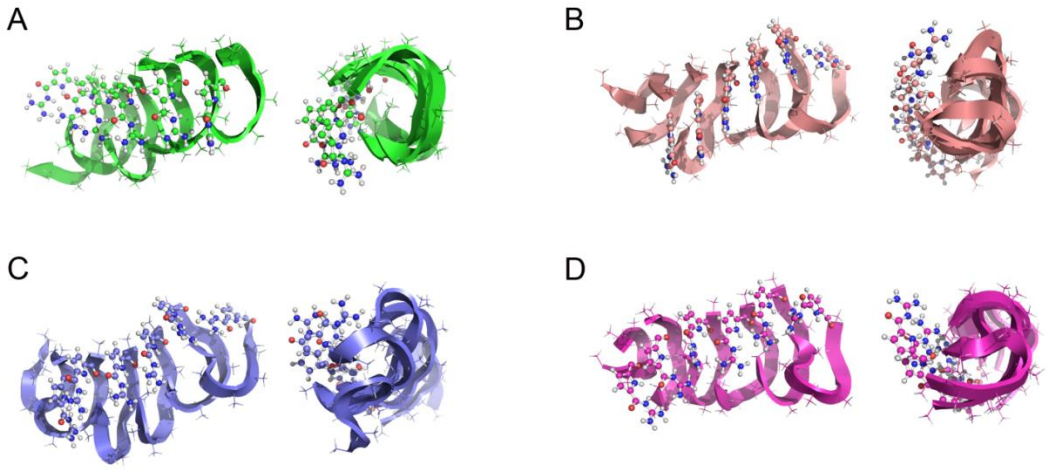

Figure 7.18 Additional images (side view and top view) of molecular modeling results of peptide **46**

7.3 Curriculum viate

The biography is not included in the online version for reasons of data protection.

7.4 List of Publications

Journal (Peer-Reviewed)

1. M. Li, M. R. Stojković, M. Ehlers, E. Zellermann, I. Piantanida, C. Schmuck; Supramolecular beta-helix mimic self-assembled into pH responsive helical peptide fiber; *Submitted*
2. M. Li, S. Schlesiger, S. K. Knauer, C. Schmuck; Enhanced affinity with cell surface glycosaminoglycan resulted in the smallest cell penetrating dipeptide analogue; *Submitted*
3. M. Li, E. Zellermann, M. R. Stojković, Christian Schlütting, I. Piantanida, C. Schmuck; A multifunctional self-assembled peptide template for the fabrication of metal-organic nanowire; *In Preparation.*.
4. M. Li, C. Schmuck; A straightforward approach to shift the thermodynamic profile of peptide/DNA binding; *In Preparation.*
5. M. Li, M. Ehlers, S. Schlesiger, E. Zellermann, S. K. Knauer, C. Schmuck; Incorporation of a non-natural arginine analogue into a cyclic peptide leads to formation of positively charged nanotubes capable of gene transfection; *Angew. Chem. Int. Edit.* **2016**, 55, 598-601.
6. M. Li, S. Schlesiger, S. K. Knauer, C. Schmuck; A Tailor-Made Specific Anion-Binding Motif in the Side Chain Transforms a Tetra peptide into an Efficient Vector for Gene Delivery; *Angew. Chem. Int. Edit.* **2015**, 54, 2941-2944.

Activities

1. 3rd German Symposium in Supramolecular Chemistry, SupraChem 2015 (Germany), *Poster presentation*
2. 1st CRC1093 International Symposium Supramolecular Chemistry on Proteins (Germany), 2015, *Participant*
3. Mini-symposium on Supramolecular Polymers (Germany), 2014, *Participant*
4. 7th National Conference on Chemical Biology (China), 2011, *Poster presentation*
5. 3rd Technology and Application Conference of small Nucleic Acid (China), 2011, *Participant*
6. 2nd Roundtable on Chemical Biology of Nucleic Acid and Carbohydrates in China, 2009, *Participant*

8. BIBLIOGRAPHY

(1) Naldini, L. *Nature* **2015**, *526*, 351.

(2) Castanotto, D.; Rossi, J. J. *Nature* **2009**, *457*, 426.

(3) Phalon, C.; Rao, D. D.; Nemunaitis, J. *Expert Rev. Mol. Med.* **2010**, *12*.

(4) Aagaard, L.; Rossi, J. J. *Adv. Drug Deliv. Rev.*. **2007**, *59*, 75.

(5) Marlin, F.; Simon, P.; Saison-Behmoaras, T.; Gioyannangeli, C. *Chembiochem* **2010**, *11*, 1493.

(6) Brown, M. D.; Schatzlein, A. G.; Uchegbu, I. F. *Int. J. Pharm.* **2001**, *229*, 1.

(7) Mintzer, M. A.; Simanek, E. E. *Chem. Rev.* **2009**, *109*, 259.

(8) Juliano, R.; Alam, M. R.; Dixit, V.; Kang, H. *Nucleic Acids Res.* **2008**, *36*, 4158.

(9) Aied, A.; Greiser, U.; Pandit, A.; Wang, W. X. *Drug Discov. Today* **2013**, *18*, 1090.

(10) Ishikawa, K.; Tilemann, L.; Ladage, D.; Aguero, J.; Leonardson, L.; Fish, K.; Kawase, Y. *Gene Ther.* **2012**, *19*, 670.

(11) Shu, S. A.; Wang, J. J.; Tao, M. H.; Leung, P. S. C. *Clin. Rev. Allerg. Immu.* **2015**, *49*, 163.

(12) Gao, K.; Huang, L. *Mol. Pharmaceut.* **2009**, *6*, 651.

(13) Meade, B. R.; Dowdy, S. F.*Adv. Drug Deliv. Rev.* **2007**, *59*, 134.

(14) Futaki, S.; Suzuki, T.; Ohashi, W.; Yagami, T.; Tanaka, S.; Ueda, K.; Sugiura, Y. *J. Biol. Chem.* **2001**, *276*, 5836.

(15) Tunnemann, G.; Ter-Avetisyan, G.; Martin, R. M.; Stockl, M.; Herrmann, A.; Cardoso, M. C. *J. Pept. Sci.* **2008**, *14*, 469.

(16) Futaki, S.; Ohashi, W.; Suzuki, T.; Niwa, M.; Tanaka, S.; Ueda, K.; Harashima, H.; Sugiura, Y. *Bioconjugate Chem.* **2001**, *12*, 1005.

(17) Lehto, T.; Abes, R.; Oskolkov, N.; Suhorutsenko, J.; Copolovici, D. M.; Mager, I.; Viola, J. R.; Simonson, O. E.; Ezzat, K.; Guterstam, P.; Eriste, E.; Smith, C. I.; Lebleu, B.; Samir El, A.; Langel, U. *J. Control. Release* **2010**, *141*, 42.

(18) Naik, R. J.; Chandra, P.; Mann, A.; Ganguli, M. *J. Biol. Chem.* **2011**, *286*, 18982.

(19) Matson, J. B.; Stupp, S. I. *Chem. Commun.* **2012**, *48*, 26.

(20) Cui, H. G.; Webber, M. J.; Stupp, S. I. *Biopolymers* **2010**, *94*, 1.

(21) Rawat, A.; Nagaraj, R. *Cur.r Top. Med. Chem.* **2014**, *14*, 740.

(22) Hamley, I. W. *Angew. Chem. Int. Edit.* **2014**, *53*, 6866.

(23) Hosseinkhani, H.; Hong, P. D.; Yu, D. S. *Chem. Rev.* **2013**, *113*, 4837.

(24) Zhao, X. B.; Pan, F.; Xu, H.; Yaseen, M.; Shan, H. H.; Hauser, C. A. E.; Zhang, S. G.; Lu, J. R. *Chem. Soc. Rev.* **2010**, *39*, 3480.

(25) Zhang, S. G.; Marini, D. M.; Hwang, W.; Santoso, S. *Curr. Opin. Chem. Biol.* **2002**, *6*, 865.

(26) Gale, P. A.; Busschaert, N.; Haynes, C. J. E.; Karagiannidis, L. E.; Kirby, I. L. *Chem. Soc. Rev.* **2014**, *43*, 205.

(27) Wenzel, M.; Hiscock, J. R.; Gale, P. A. *Chem. Soc. Rev.* **2012**, *41*, 480.

(28) Gale, P. A. *Acc. Chem. Res.* **2006**, *39*, 465.

(29) Gunnlaugsson, T.; Glynn, M.; Tocci, G. M.; Kruger, P. E.; Pfeffer, F. M. *Coord. Chem. Rev.* **2006**, *250*, 3094.

(30) Piatek, A. M.; Gray, M.; Anslyn, E. V. *J. Am. Chem. Soc.* **2004**, *126*, 9878.

(31) Meot-Ner, M. *Chem. Rev.* **2005**, *105*, 213.

(32) Schmuck, C.; Lex, J. *Org. Lett.* **1999**, *1*, 1779.

(33) Schmuck, C. *Coord. Chem. Rev.* **2006**, *250*, 3053.

(34) Schmuck, C.; Rehm, T.; Klein, K.; Grohn, F. *Angew. Chem. Int. Ed.* **2007**, *46*, 1693.

(35) Schmuck, C.; Geiger, L. *J. Am. Chem. Soc.* **2005**, *127*, 10486.

(36) Zepik, H. H.; Benner, S. A. *J. Org. Chem.* **1999**, *64*, 8080.

(37) Schmidtchen, F. P.; Berger, M. *Chem. Rev.* **1997**, *97*, 1609.

(38) Heys, L.; Moore, C. G.; Murphy, P. J. *Chem. Soc. Rev.* **2000**, *29*, 57.

(39) Zarate, S. G.; Santana, A. G.; Bastida, A.; Revuelta, J. *Curr. Org. Chem.* **2014**, *18*, 2711.

(40) Schmuck, C. *Chem. Commun*. **1999**, 843.

(41) Schmuck, C. *Chem. Eur. J*. **2000**, *6*, 709.

(42) Schmuck, C.; Machon, U. *Chem. Eur. J.* **2005**, *11*, 1109.

(43) Schmuck, C.; Bickert, V. *Org. Lett.* **2003**, *5*, 4579.

(44) Schmuck, C.; Geiger, L. *J. Am. Chem. Soc.* **2004**, *126*, 8898.

(45) Schmuck, C.; Hernandez-Folgado, L. *Org. Biomol. Chem.* **2007**, *5*, 2390.

(46) Schmuck, C.; Rupprecht, D.; Wienand, W. *Chem. Eur. J.* **2006**, *12*, 9186.

(47) Schmuck, C.; Heil, M. *Chembiochem* **2003**, *4*, 1232.

(48) Schmuck, C.; Heil, M. *Org. Biomol. Chem.* **2003**, *1*, 633.

(49) Schmuck, C.; Frey, P.; Heil, M. *Chembiochem* **2005**, *6*, 628.

(50) Schmuck, C.; Heil, M.; Scheiber, J.; Baumann, K. *Angew. Chem. Int. Edit.* **2005**, *44*, 7208.

(51) Schmuck, C.; Heil, M. *Chem. Eur. J.* **2006**, *12*, 1339.

(52) Hernandez-Folgado, L.; Schmuck, C.; Tomic, S.; Piantanida, I. *Bioorg. Med. Chem. Lett.* **2008**, *18*, 2977.

(53) Stojkovic, M. R.; Piotrowski, P.; Schmuck, C.; Piantanida, I. *Org. Biomol. Chem.* **2015**, *13*, 1629.

(54) Groger, K.; Baretic, D.; Piantanida, I.; Marjanovic, M.; Kralj, M.; Grabar, M.; Tomic, S.; Schmuck, C. *Org. Biomol. Chem.* **2011**, *9*, 198.

(55) Hernandez-Folgado, L.; Baretic, D.; Piantanida, I.; Marjanovic, M.; Kraij, M.; Rehm, T.; Schmuck, C. *Chem. Eur. J.* **2010**, *16*, 3036.

(56) Klemm, K.; Stojkovic, M. R.; Horvat, G.; Tomisic, V.; Piantanida, I.; Schmuck, C. *Chem. Eur. J.* **2012**, *18*, 1352.

(57) Kuchelmeister, H. Y.; Schmuck, C. *Chem. Eur. J.* **2011**, *17*, 5311.

(58) Kuchelmeister, H. Y.; Gutschmidt, A.; Tillmann, S.; Knauer, S.; Schmuck, C. *Chem. Sci.* **2012**, *3*, 996.

(59) Kuchelmeister, H. Y.; Karczewski, S.; Gutschmidt, A.; Knauer, S.; Schmuck, C. *Angew. Chem. Int. Ed.* **2013**, *52*, 14016.

(60) Fire, A.; Xu, S. Q.; Montgomery, M. K.; Kostas, S. A.; Driver, S. E.; Mello, C. C. *Nature* **1998**, *391*, 806.

(61) Rosenberg, S. A.; Aebersold, P.; Cornetta, K.; Kasid, A.; Morgan, R. A.; Moen, R.; Karson, E. M.; Lotze, M. T.; Yang, J. C.; Topalian, S. L.; Merino, M. J.; Culver, K.; Miller, A. D.; Blaese, R. M.; Anderson, W. F. *New Engl. J. Med.* **1990**, *323*, 570.

(62) Ginn, S. L.; Alexander, I. E.; Edelstein, M. L.; Abedi, M. R.; Wixon, J. *J. Gene. Med.* **2013**, *15*, 65.

(63) Schaffer, D. V.; Zhou, W. C. *Adv. Biochem. Eng. Biot.* **2005**, *99*, 1.

(64) Little, S. R.; Langer, R. *Adv. Biochem. Eng. Biot.* **2005**, *99*, 93.

(65) Zhi, D.; Zhang, S.; Cui, S.; Zhao, Y.; Wang, Y.; Zhao, D. *Bioconjugate Chem.* **2013**, *24*, 487.

(66) Zhi, D. F.; Zhang, S. B.; Wang, B.; Zhao, Y. N.; Yang, B. L.; Yu, S. J. *Bioconjug. Chem.* **2010**, *21*, 563.

(67) Ouyang, D.; Zhang, H.; Parekh, H. S.; Smith, S. C. *Biophys. Chem.* **2011**, *158*, 126.

(68) Pullmannova, P.; Bastos, M.; Bai, G. Y.; Funari, S. S.; Lacko, I.; Devinsky, F.; Teixeira, J.; Uhrikova, D. *Biophys. Chem.* **2012**, *160*, 35.

(69) Felgner, J. H.; Kumar, R.; Sridhar, C. N.; Wheeler, C. J.; Tsai, Y. J.; Border, R.; Ramsey, P.; Martin, M.; Felgner, P. L. *J. Biol. Chem.* **1994**, *269*, 2550.

(70) Khalil, I. A.; Kogure, K.; Akita, H.; Harashima, H. *Pharmacol. Rev.* **2006**, *58*, 32.

(71) Bareford, L. A.; Swaan, P. W. *Adv. Drug Deliv. Rev.* **2007**, *59*, 748.

(72) Larocca, D.; Baird, A. *Drug Discov. Today* **2001**, *6*, 793.

(73) Shete, H. K.; Prabhu, R. H.; Patravale, V. B. *J. Nanosci. Nanotechno.* **2014**, *14*, 460.

(74) Grabe, M.; Oster, G. *J. Gen. Physiol.* **2001**, *117*, 329.

(75) Mehier-Humbert, S.; Guy, R. H. *Adv. Drug Deliv. Rev.* **2005**, *57*, 733.

(76) Wells, D. J. *Gene Ther.* **2004**, *11*, 1363.

(77) Giacca, M.; Zacchigna, S. *J. Control. Release* **2012**, *161*, 377.

(78) Yue, Y. N.; Wu, C. *Biomater Sci-Uk* **2013**, *1*, 152.

(79) Duncan, R. *Anti-Cancer Drug* **1992**, *3*, 175.

(80) Chang, C.; Weiskopf, M.; Li, H. J. *Biochemistry* **1973**, *12*, 3028.

(81) Laemmli, U. K. *Proc. Natl. Acad. Sci. USA* **1975**, *72*, 4288.

(82) Zhou, X. H.; Klibanov, A. L.; Huang, L. *BBA* **1991**, *1065*, 8.

(83) Gottschalk, S.; Sparrow, J. T.; Hauer, J.; Mims, M. P.; Leland, F. E.; Woo, S. L. C.; Smith, L. C. *Gene Ther.* **1996**, *3*, 448.

(84) Zauner, W.; Ogris, M.; Wagner, E. *Adv. Drug Deliv. Rev.*. **1998**, *30*, 97.

(85) Wong, S. Y.; Pelet, J. M.; Putnam, D. *Prog. Polym. Sci.* **2007**, *32*, 799.

(86) Fischer, D.; von Harpe, A.; Kunath, K.; Petersen, H.; Li, Y. X.; Kissel, T. *Bioconjugate Chem.* **2002**, *13*, 1124.

(87) Dunlap, D. D.; Maggi, A.; Soria, M. R.; Monaco, L. *Nucleic Acids Res.* **1997**, *25*, 3095.

(88) Yue, Y. A.; Jin, F.; Deng, R.; Cai, J. G.; Chen, Y. C.; Lin, M. C. M.; Kung, H. F.; Wu, C. *J. Control. Release* **2011**, *155*, 67.

(89) Funhoff, A. M.; van Nostrum, C. F.; Koning, G. A.; Schuurmans-Nieuwenbroek, N. M. E.; Crommelin, D. J. A.; Hennink, W. E. *Biomacromolecules* **2004**, *5*, 32.

(90) Kichler, A.; Chillon, M.; Leborgne, C.; Danos, O.; Frisch, B. *J. Control. Release* **2002**, *81*, 379.

(91) Tang, G. P.; Zeng, J. M.; Gao, S. J.; Ma, Y. X.; Shi, L.; Li, Y.; Too, H. P.; Wang, S. *Biomaterials* **2003**, *24*, 2351.

(92) Neu, M.; Fischer, D.; Kissel, T. *J. Gene Med.* **2005**, *7*, 992.

(93) Petersen, H.; Merdan, T.; Kunath, F.; Fischer, D.; Kissel, T. *Bioconjug. Chem.* **2002**, *13*, 812.

(94) Taranejoo, S.; Liu, J.; Verma, P.; Hourigan, K. *J. Appl. Polym. Sci.* **2015**, *132*.

(95) Peng, Q.; Zhong, Z. L.; Zhuo, R. X. *Bioconjugate Chem.* **2008**, *19*, 499.

(96) Matsumoto, S.; Christie, R. J.; Nishiyama, N.; Miyata, K.; Ishii, A.; Oba, M.; Koyama, H.; Yamasaki, Y.; Kataoka, K. *Biomacromolecules* **2009**, *10*, 119.

(97) Cortez, M. A.; Godbey, W. T.; Fang, Y. L.; Payne, M. E.; Cafferty, B. J.; Kosakowska, K. A.; Grayson, S. M. *J. Am. Chem. Soc.* **2015**, *137*, 6541.

(98) Reineke, T. M.; Davis, M. E. *Bioconjugate Chem.* **2003**, *14*, 247.

(99) Tang, M. X.; Redemann, C. T.; Szoka, F. C. *Bioconjugate Chem.* **1996**, *7*, 703.

(100) Dufes, C.; Uchegbu, I. F.; Schatzlein, A. G. *Adv. Drug Deliv. Rev.*. **2005**, *57*, 2177.

(101) Gonzalez, H.; Hwang, S. J.; Davis, M. E. *Bioconjugate Chem.* **1999**, *10*, 1068.

(102) Davis, M. E. *Mol. Pharmaceut* **2009**, *6*, 659.

(103) Bhattacharya, S.; Bajaj, A. *Chem. Commun.* **2009**, 4632.

(104) Wong, T. K.; Nicolau, C.; Hofschneider, P. H. *Gene* **1980**, *10*, 87.

(105) Felgner, P. L.; Gadek, T. R.; Holm, M.; Roman, R.; Chan, H. W.; Wenz, M.; Northrop, J. P.; Ringold, G. M.; Danielsen, M. *Proc. Natl. Acad. Sci. USA* **1987**, *84*, 7413.

(106) Sakurai, F.; Nishioka, T.; Yamashita, F.; Takakura, Y.; Hashida, M. *Eur. J. Pharm. Biopharm.* **2001**, *52*, 165.

(107) Zhou, X. H.; Huang, L. *Bba-Biomembranes* **1994**, *1189*, 195.

(108) Hui, S. W.; Langner, M.; Zhao, Y. L.; Ross, P.; Hurley, E.; Chan, K. *Biophys. J.* **1996**, *71*, 590.

(109) Mochizuki, S.; Kanegae, N.; Nishina, K.; Kamikawa, Y.; Koiwai, K.; Masunaga, H.; Sakurai, K. *Bba-Biomembranes* **2013**, *1828*, 412.

(110) Du, Z. X.; Munye, M. M.; Tagalakis, A. D.; Manunta, M. D. I.; Hart, S. L. *Sci. Rep.* **2014**, *4*.

(111)Zuhorn, I. S.; Oberle, V.; Visser, W. H.; Engberts, J. B. F. N.; Bakowsky, U.; Polushkin, E.; Hoekstra, D. *Biophys. J.* **2002**, *83*, 2096.

(112) Niculescu-Duvaz, D.; Heyes, J.; Springer, C. J. *Curr. Med. Chem.* **2003**, *10*, 1233.

(113) Bennett, M. J.; Aberle, A. M.; Balasubramaniam, R. P.; Malone, J. G.; Malone, R. W.; Nantz, M. H. *J. Med. Chem.* **1997**, *40*, 4069.

(114) Banerjee, R.; Das, P. K.; Srilakshmi, G. V.; Chaudhuri, A.; Rao, N. M. *J. Med. Chem.* **1999**, *42*, 4292.

(115) Banerjee, R.; Mahidhar, Y. V.; Chaudhuri, A.; Gopal, V.; Rao, N. M. *J. Med. Chem.* **2001**, *44*, 4176.

(116) Rosenzweig, H. S.; Rakhmanova, V. A.; MacDonald, R. C. *Bioconjugate Chem.* **2001**, *12*, 258.

(117) Bhattacharya, S.; Samanta, S. K. *J. Phys. Chem. Lett.* **2011**, *2*, 914.

(118) Lewis, J. D.; Song, Y.; de Jong, M. E.; Bagha, S. M.; Ausio, J. *Chromosoma* **2003**, *111*, 473.

(119) Queralt, R.; Adroer, R.; Oliva, R.; Winkfein, R. J.; Retief, J. D.; Dixon, G. H. *J. Mol. Evol.* **1995**, *40*, 601.

(120) Karmali, P. P.; Chaudhuri, A. *Med. Res. Rev.* **2007**, *27*, 696.

(121) Herscovici, J.; Egron, M. J.; Quenot, A.; Leclercq, F.; Leforestier, N.; Mignet, N.; Wetzer, B.; Scherman, D. *Org. Lett.* **2001**, *3*, 1893.

(122) Sen, J.; Chaudhuri, A. *J. Med. Chem.* **2005**, *48*, 812.

(123) Vigneron, J. P.; Oudrhiri, N.; Fauquet, M.; Vergely, L.; Bradley, J. C.; Basseville, M.; Lehn, P.; Lehn, J. M. *Proc. Natl. Acad. Sci. USA* **1996**, *93*, 9682.

(124) Aissaoui, A.; Martin, B.; Kan, E.; Oudrhiri, N.; Hauchecorne, M.; Vigneron, J. P.; Lehn, J. M.; Lehn, P. *J. Med. Chem.* **2004**, *47*, 5210.

(125) Gehin, C.; Montenegro, J.; Bang, E. K.; Cajaraville, A.; Takayama, S.; Hirose, H.; Futaki, S.; Matile, S.; Riezman, H. *J. Am. Chem. Soc.* **2013**, *135*, 9295.

(126) Meekel, A. A. P.; Wagenaar, A.; Smisterova, J.; Kroeze, J. E.; Haadsma, P.; Bosgraaf, B.; Stuart, M. C. A.; Brisson, A.; Ruiters, M. H. J.; Hoekstra, D.; Engberts, J. B. F. N. *Eur. J. Org. Chem.* **2000**, 665.

(127) Roosjen, A.; Smisterova, J.; Driessen, C.; Anders, J. T.; Wagenaar, A.; Hoekstra, D.; Hulst, R.; Engberts, J. B. F. N. *Eur. J. Org. Chem.* **2002**, 1271.

(128) Dal-Maso, A. D.; Dellacasagrande, J.; Legendre, F.; Tiraby, G.; Blonski, C.; Hoffmann, P. *Eur. J. Med. Chem.* **2008**, *43*, 1758.

(129) Budker, V.; Gurevich, V.; Hagstrom, J. E.; Bortzov, F.; Wolff, J. A. *Nat. Biotechnol.* **1996**, *14*, 760.

(130) Mevel, M.; Neveu, C.; Goncalves, C.; Yaouanc, J. J.; Pichon, C.; Jaffres, P. A.; Midoux, P. *Chem. Commun.* **2008**, 3124.

(131) Gao, X.; Huang, L. *Biochem. Biophys. Res. Commun.* **1991**, *179*, 280.

(132) Green, M.; Loewenstein, P. M. *Cell* **1988**, *55*, 1179.

(133) Vives, E.; Brodin, P.; Lebleu, B. *J. Biol. Chem.* **1997**, *272*, 16010.

(134) Joliot, A.; Pernelle, C.; Deagostinibazin, H.; Prochiantz, A. *Proc. Natl. Acad. Sci. USA* **1991**, *88*, 1864.

(135) Derossi, D.; Joliot, A. H.; Chassaing, G.; Prochiantz, A. *J. Biol. Chem.* **1994**, *269*, 10444.

(136) Pooga, M.; Hallbrink, M.; Zorko, M.; Langel, U. *FASEB J.* **1998**, *12*, 67.

(137) Goldfarb, D. S.; Gariepy, J.; Schoolnik, G.; Kornberg, R. D. *Nature* **1986**, *322*, 641.

(138) Mitchell, D. J.; Kim, D. T.; Steinman, L.; Fathman, C. G.; Rothbard, J. B. *J. Pept. Res.* **2000**, *56*, 318.

(139) Astriab-Fisher, A.; Sergueev, D. S.; Fisher, M.; Shaw, B. R.; Juliano, R. L. *Biochem. Pharmacol.* **2000**, *60*, 83.

(140) Eguchi, A.; Akuta, T.; Okuyama, H.; Senda, T.; Yokoi, H.; Inokuchi, H.; Fujita, S.; Hayakawa, T.; Takeda, K.; Hasegawa, M.; Nakanishi, M. *J. Biol. Chem.* **2001**, *276*, 26204.

(141) Rudolph, C.; Plank, C.; Lausier, J.; Schillinger, U.; Muller, R. H.; Rosenecker, J. *J. Biol. Chem.* **2003**, *278*, 11411.

(142) Torchilin, V. P.; Rammohan, R.; Weissig, V.; Levchenko, T. S. *Proc. Natl. Acad. Sci. USA* **2001**, *98*, 8786.

(143) Torchilin, V. P.; Levchenko, T. S.; Rammohan, R.; Volodina, N.; Papahadjopoulos-Sternberg, B.; D'Souza, G. G. M. *Proc. Natl. Acad. Sci. USA* **2003**, *100*, 1972.

(144) Lo, S. L.; Wang, S. *Biomaterials* **2008**, *29*, 2408.

(145) Jin, E.; Zhang, B.; Sun, X.; Zhou, Z.; Ma, X.; Sun, Q.; Tang, J.; Shen, Y.; Van Kirk, E.; Murdoch, W. J.; Radosz, M. *J. Am. Chem. Soc.* **2013**, *135*, 933.

(146) Yamano, S.; Dai, J.; Hanatani, S.; Haku, K.; Yamanaka, T.; Ishioka, M.; Takayama, T.; Yuvienco, C.; Khapli, S.; Moursi, A. M.; Montclare, J. K. *Biomaterials* **2014**, *35*, 1705.

(147) Tonges, L.; Lingor, P.; Egle, R.; Dietz, G. P.; Fahr, A.; Bahr, M. *RNA* **2006**, *12*, 1431.

(148) Moriguchi, R.; Kogure, K.; Akita, H.; Futaki, S.; Miyagishi, M.; Taira, K.; Harashima, H. *Int. J. Pharm.* **2005**, *301*, 277.

(149) Nakamura, Y.; Kogure, K.; Futaki, S.; Harashima, H. *J. Control. Release* **2007**, *119*, 360.

(150) Kim, W. J.; Christensen, L. V.; Jo, S.; Yockman, J. W.; Jeong, J. H.; Kim, Y. H.; Kim, S. W. *Mol. Ther.* **2006**, *14*, 343.

(151) Kumar, P.; Wu, H.; McBride, J. L.; Jung, K. E.; Kim, M. H.; Davidson, B. L.; Lee, S. K.; Shankar, P.; Manjunath, N. *Nature* **2007**, *448*, 39.

(152) Allinquant, B.; Hantraye, P.; Mailleux, P.; Moya, K.; Bouillot, C.; Prochiantz, A. *J. Cell Biol.* **1995**, *128*, 919.

(153) Astriab-Fisher, A.; Sergueev, D.; Fisher, M.; Shaw, B. R.; Juliano, R. L. *Pharm. Res.* **2002**, *19*, 744.

(154) Simmons, C. G.; Pitts, A. E.; Mayfield, L. D.; Shay, J. W.; Corey, D. R. *Bioorg. Med. Chem. Lett.* **1997**, *7*, 3001.

(155) Ou, J. S.; Geiger, T.; Ou, Z.; Ackerman, A. W.; Oldham, K. T.; Pritchard, K. A. *Biochem. Biophys. Res. Commun.* **2003**, *305*, 605.

(156) Amand, H. L.; Fant, K.; Norden, B.; Esbjorner, E. K. *Biochem. Biophys. Res. Commun.* **2008**, *371*, 621.

(157) Wyman, T. B.; Nicol, F.; Zelphati, O.; Scaria, P. V.; Plank, C.; Szoka, F. C. *Biochemistry***1997**, *36*, 3008.

(158) Fominaya, J.; Gasset, M.; Garcia, R.; Roncal, F.; Albar, J. P.; Bernad, A. *J. Gene. Med.* **2000**, *2*,

455.

(159) Ghosh, P.; Han, G.; De, M.; Kim, C. K.; Rotello, V. M. *Adv. Drug Deliv. Rev.* **2008**, *60*, 1307.

(160) Slowing, I. I.; Vivero-Escoto, J. L.; Wu, C. W.; Lin, V. S. Y. *Adv. Drug Deliv. Rev.*. **2008**, *60*, 1278.

(161) Xie, J.; Lee, S.; Chen, X. Y. *Adv. Drug Deliv. Rev.*. **2010**, *62*, 1064.

(162) Arsianti, M.; Lim, M.; Marquis, C. P.; Amal, R. *Langmuir* **2010**, *26*, 7314.

(163) Vigderman, L.; Zubarev, E. R. *Adv. Drug Deliv. Rev.*. **2013**, *65*, 663.

(164) Trewyn, B. G.; Giri, S.; Slowing, I. I.; Lin, V. S. Y. *Chem. Commun.* **2007**, 3236.

(165) Scherer, F.; Anton, M.; Schillinger, U.; Henkel, J.; Bergemann, C.; Kruger, A.; Gansbacher, B.; Plank, C. *Gene Ther.* **2002**, *9*, 102.

(166) Kami, D.; Takeda, S.; Makino, H.; Toyoda, M.; Itakura, Y.; Gojo, S.; Kyo, S.; Umezawa, A.; Watanabe, M. *J. Artif. Organs.* **2011**, *14*, 215.

(167) Plank, C.; Zelphati, O.; Mykhaylyk, O. *Adv. Drug Deliv. Rev.*. **2011**, *63*, 1300.

(168) Arsianti, M.; Lim, M.; Marquis, C. P.; Amal, R. *Biomacromolecules* **2010**, *11*, 2521.

(169) Yiu, H. H. P.; McBain, S. C.; El Haj, A. J.; Dobson, J. *Nanotechnology* **2007**, *18*.

(170) Gonzalez, B.; Ruiz-Hernandez, E.; Feito, M. J.; de Laorden, C. L.; Arcos, D.; Ramirez-Santillan, C.; Matesanz, C.; Portoles, M. T.; Vallet-Regi, M. *J. Mater. Chem.* **2011**, *21*, 4598.

(171) Liu, W. M.; Xue, Y. N.; Peng, N.; He, W. T.; Zhuo, R. X.; Huang, S. W. *J. Mater. Chem.* **2011**, *21*, 13306.

(172) Thomas, M.; Klibanov, A. M. *Proc. Natl. Acad. Sci. USA* **2003**, *100*, 9138.

(173) Sharma, A.; Tandon, A.; Tovey, J. C. K.; Gupta, R.; Robertson, J. D.; Fortune, J. A.; Klibanov, A. M.; Cowden, J. W.; Rieger, F. G.; Mohan, R. R. *Nanomed. Nanotechnol.* **2011**, *7*, 505.

(174) Hu, C.; Peng, Q.; Chen, F. J.; Zhong, Z. L.; Zhuo, R. X. *Bioconjugate Chem.* **2010**, *21*, 836.

(175) He, W. T.; Xue, Y. N.; Peng, N.; Liu, W. M.; Zhuo, R. X.; Huang, S. W. *J. Mater. Chem.* **2011**, *21*, 10496.

(176) Li, J.; Chen, Y. C.; Tseng, Y. C.; Mozumdar, S.; Huang, L. *J. Control. Release* **2010**, *142*, 416.

(177) Li, D.; Li, G. P.; Li, P. C.; Zhang, L. X.; Liu, Z. J.; Wang, J.; Wang, E. K. *Biomaterials* **2010**, *31*, 1850.

(178) Liu, J. W.; Jiang, X. M.; Ashley, C.; Brinker, C. J. *J. Am. Chem. Soc.* **2009**, *131*, 7567.

(179) Liu, J. W.; Stace-Naughton, A.; Jiang, X. M.; Brinker, C. J. *J. Am. Chem. Soc.* **2009**, *131*, 1354.

(180) Ashley, C. E.; Carnes, E. C.; Phillips, G. K.; Padilla, D.; Durfee, P. N.; Brown, P. A.; Hanna, T. N.; Liu, J. W.; Phillips, B.; Carter, M. B.; Carroll, N. J.; Jiang, X. M.; Dunphy, D. R.; Willman, C. L.; Petsev, D. N.; Evans, D. G.; Parikh, A. N.; Chackerian, B.; Wharton, W.; Peabody, D. S.; Brinker, C. J. *Nat. Mater.* **2011**, *10*, 476.

(181) Mishra, D.; Hubenak, J. R.; Mathur, A. B. *J. Biomed. Mater. Res. A* **2013**, *101*, 3646.

(182) Laurent, S.; Forge, D.; Port, M.; Roch, A.; Robic, C.; Elst, L. V.; Muller, R. N. *Chem. Rev.* **2008**, *108*, 2064.

(183) Lewin, M.; Carlesso, N.; Tung, C. H.; Tang, X. W.; Cory, D.; Scadden, D. T.; Weissleder, R. *Nat. Biotechnol.* **2000**, *18*, 410.

(184) Josephson, L.; Tung, C. H.; Moore, A.; Weissleder, R. *Bioconjugate Chem.* **1999**, *10*, 186.

(185) Song, H. P.; Yang, J. Y.; Lo, S. L.; Wang, Y.; Fan, W. M.; Tang, X. S.; Xue, J. M.; Wang, S. *Biomaterials* **2010**, *31*, 769.

(186) Baoum, A. A.; Berkland, C. *J. Pharm. Sci.* **2011**, *100*, 1637.

(187) Zhang, X.; Sun, C.; Fang, N. *J. Nanopart. Res.* **2004**, *6*, 125.

(188) Dvir, T.; Timko, B. P.; Kohane, D. S.; Langer, R. *Nat. Nanotechnol.* **2011**, *6*, 13.

(189) Farokhzad, O. C.; Langer, R. *Adv. Drug Deliv. Rev.*. **2006**, *58*, 1456.

(190) Gazit, E. *Chem. Soc. Rev.* **2007**, *36*, 1263.

(191) Lowik, D. W. P. M.; van Hest, J. C. M. *Chem. Soc. Rev.* **2004**, *33*, 234.

(192) Ramanathan, M.; Shrestha, L. K.; Mori, T.; Ji, Q. M.; Hill, J. P.; Ariga, K. *PCCP* **2013**, *15*, 10580.

(193) Thota, B. N. S.; Urner, L. H.; Haag, R. *Chem. Rev.* **2016**, *116*, 2079.

(194) Israelachvili, J. N.; Mitchell, D. J.; Ninham, B. W. *J. Chem. Soc. Farad. T.* **1976**, *72*, 1525.

(195) Hartgerink, J. D.; Beniash, E.; Stupp, S. I. *Science* **2001**, *294*, 1684.

(196) Guler, M. O.; Soukasene, S.; Hulvat, J. F.; Stupp, S. I. *Nano Lett* **2005**, *5*, 249.

(197) Hartgerink, J. D.; Beniash, E.; Stupp, S. I. *Proc. Natl. Acad. Sci.USA* **2002**, *99*, 5133.

(198) Claussen, R. C.; Rabatic, B. M.; Stupp, S. I. *J. Am. Chem. Soc.* **2003**, *125*, 12680.

(199) Paramonov, S. E.; Jun, H. W.; Hartgerink, J. D. *J. Am. Chem. Soc.* **2006**, *128*, 7291.

(200) Ortony, J. H.; Newcomb, C. J.; Matson, J. B.; Palmer, L. C.; Doan, P. E.; Hoffman, B. M.; Stupp, S. I. *Nat. Mater.* **2014**, *13*, 812.

(201) Silva, G. A.; Czeisler, C.; Niece, K. L.; Beniash, E.; Harrington, D. A.; Kessler, J. A.; Stupp, S. I. *Science* **2004**, *303*, 1352.

(202) Beniash, E.; Hartgerink, J. D.; Storrie, H.; Stendahl, J. C.; Stupp, S. I. *Acta. Biomater.* **2005**, *1*, 387.

(203) Arnold, M. S.; Guler, M. O.; Hersam, M. C.; Stupp, S. I. *Langmuir* **2005**, *21*, 4705.

(204) Rajangam, K.; Behanna, H. A.; Hui, M. J.; Han, X. Q.; Hulvat, J. F.; Lomasney, J. W.; Stupp, S. I. *Nano Lett.* **2006**, *6*, 2086.

(205) Hsu, L.; Cvetanovich, G. L.; Stupp, S. I. *J. Am. Chem. Soc.* **2008**, *130*, 3892.

(206) Guler, M. O.; Claussen, R. C.; Stupp, S. I. *J. Mater. Chem.* **2005**, *15*, 4507.

(207) Bull, S. R.; Guler, M. O.; Bras, R. E.; Meade, T. J.; Stupp, S. I. *Nano Lett.* **2005**, *5*, 1.

(208) Li, L. S.; Stupp, S. I. *Angew. Chem. Int. Ed.* **2005**, *44*, 1833.

(209) Niece, K. L.; Czeisler, C.; Sahni, V.; Tysseling-Mattiace, V.; Pashuck, E. T.; Kessler, J. A.; Stupp, S. I. *Biomaterials* **2008**, *29*, 4501.

(210) Zhang, S. M.; Greenfield, M. A.; Mata, A.; Palmer, L. C.; Bitton, R.; Mantei, J. R.; Aparicio, C.; de la Cruz, M. O.; Stupp, S. I. *Nat. Mater.* **2010**, *9*, 594.

(211) Ryan, D. M.; Nilsson, B. L. *Poly. Chem.* **2012**, *3*, 18.

(212) Gortner, R. A.; Hoffman, W. F. *J. Am. Chem. Soc.* **1921**, *43*, 2199.

(213) Menger, F. M.; Yamasaki, Y.; Catlin, K. K.; Nishimi, T. *Angew. Chem. Int. Ed.* **1995**, *34*, 585.

(214) Menger, F. M.; Caran, K. L. *J. Am. Chem. Soc.* **2000**, *122*, 11679.

(215) Reches, M.; Gazit, E. *Science* **2003**, *300*, 625.

(216) Jayawarna, V.; Ali, M.; Jowitt, T. A.; Miller, A. E.; Saiani, A.; Gough, J. E.; Ulijn, R. V. *Adv. Mater.* **2006**, *18*, 611.

(217) Mahler, A.; Reches, M.; Rechter, M.; Cohen, S.; Gazit, E. *Adv. Mater.* **2006**, *18*, 1365.

(218) Smith, A. M.; Williams, R. J.; Tang, C.; Coppo, P.; Collins, R. F.; Turner, M. L.; Saiani, A.; Ulijn, R. V. *Adv. Mater.* **2008**, *20*, 37.

(219) Tang, C.; Smith, A. M.; Collins, R. F.; Ulijn, R. V.; Saiani, A. *Langmuir* **2009**, *25*, 9447.

(220) Toledano, S.; Williams, R. J.; Jayawarna, V.; Ulijn, R. V. *J. Am. Chem. Soc.* **2006**, *128*, 1070.

(221) Yang, Z. M.; Gu, H. W.; Fu, D. G.; Gao, P.; Lam, J. K.; Xu, B. *Adv. Mater.* **2004**, *16*, 1440.

(222) Yang, Z. M.; Xu, B. *Chem. Commun.* **2004**, 2424.

(223) Gao, J.; Wang, H. M.; Wang, L.; Wang, J. Y.; Kong, D. L.; Yang, Z. M. *J. Am. Chem. Soc.* **2009**, *131*, 11286.

(224) Sadownik, J. W.; Leckie, J.; Ulijn, R. V. *Chem. Commun.* **2011**, *47*, 728.

(225) Yang, Z. M.; Liang, G. L.; Wang, L.; Xu, B. *J. Am. Chem. Soc.* **2006**, *128*, 3038.

(226) Yang, Z. M.; Liang, G. L.; Ma, M. L.; Gao, Y.; Xu, B. *J. Mater. Chem.* **2007**, *17*, 850.

(227) Yang, Z. M.; Liang, G. L.; Ma, M. L.; Abbah, A. S.; Lu, W. W.; Xu, B. *Chem. Commun.* **2007**, 843.

(228) Li, X. M.; Kuang, Y.; Shi, J. F.; Gao, Y.; Lin, H. C.; Xu, B. *J. Am. Chem. Soc.* **2011**, *133*, 17513.

(229) Vauthey, S.; Santoso, S.; Gong, H. Y.; Watson, N.; Zhang, S. G. *Proc. Natl. Acad. Sci.USA* **2002**, *99*, 5355.

(230) Khoe, U.; Yang, Y. L.; Zhang, S. G. *Langmuir* **2009**, *25*, 4111.

(231) Zhao, X. J.; Nagai, Y.; Reeves, P. J.; Kiley, P.; Khorana, H. G.; Zhang, S. G. *Proc. Natl. Acad. Sci.USA* **2006**, *103*, 17707.

(232) Wang, X. Q.; Corin, K.; Baaske, P.; Wienken, C. J.; Jerabek-Willemsen, M.; Duhr, S.; Braun, D.; Zhang, S. G. *Proc. Natl. Acad. Sci.USA* **2011**, *108*, 9049.

(233) Tasis, D.; Tagmatarchis, N.; Bianco, A.; Prato, M. *Chem. Rev.* **2006**, *106*, 1105.

(234) Tenne, R.; Margulis, L.; Genut, M.; Hodes, G. *Nature* **1992**, *360*, 444.

(235) Remskar, M. *Adv. Mater.* **2004**, *16*, 1497.

(236) Tenne, R. *Angew. Chem. Int. Ed.* **2003**, *42*, 5124.

(237) Goldberger, J.; Fan, R.; Yang, P. D. *Accounts Chem. Res.* **2006**, *39*, 239.

(238) Ghadiri, M. R.; Granja, J. R.; Milligan, R. A.; Mcree, D. E.; Khazanovich, N. *Nature* **1994**, *372*, 709.

(239) Brea, R. J.; Reiriz, C.; Granja, J. R. *Chem. Soc. Rev.* **2010**, *39*, 1448.

(240) Amorin, M.; Castedo, L.; Granja, J. R. *J. Am. Chem. Soc.* **2003**, *125*, 2844.

(241) Amorin, M.; Castedo, L.; Granja, J. R. *Chem. Eur. J.* **2005**, *11*, 6543.

(242) Amorin, M.; Brea, R. J.; Castedo, L.; Granja, J. R. *Org. Lett.* **2005**, *7*, 4681.

(243) De Greef, T. F. A.; Smulders, M. M. J.; Wolffs, M.; Schenning, A. P. H. J.; Sijbesma, R. P.; Meijer, E. W. *Chem. Rev.* **2009**, *109*, 5687.

(244) Kobayashi, K.; Granja, J. R.; Ghadiri, M. R. *Angew. Chem. Int. Ed.* **1995**, *34*, 95.

(245) Clark, T. D.; Buriak, J. M.; Kobayashi, K.; Isler, M. P.; McRee, D. E.; Ghadiri, M. R. *J. Am. Chem. Soc.* **1998**, *120*, 8949.

(246) Hartgerink, J. D.; Granja, J. R.; Milligan, R. A.; Ghadiri, M. R. *J. Am. Chem. Soc.* **1996**, *118*, 43.

(247) Suga, T.; Osada, S.; Kodama, H. *Bioorg. Med. Chem.* **2012**, *20*, 42.

(248) Granja, J. R.; Ghadiri, M. R. *J. Am. Chem. Soc.* **1994**, *116*, 10785.

(249) Sanchez-Quesada, J.; Kim, H. S.; Ghadiri, M. R. *Angew. Chem. Int. Ed.* **2001**, *40*, 2503.

(250) Khazanovich, N.; Granja, J. R.; Mcree, D. E.; Milligan, R. A.; Ghadiri, M. R. *J. Am. Chem. Soc.* **1994**, *116*, 6011.

(251) Hourani, R.; Zhang, C.; van der Weegen, R.; Ruiz, L.; Li, C. Y.; Keten, S.; Helms, B. A.; Xu, T. *J. Am. Chem. Soc.* **2011**, *133*, 15296.

(252) Danial, M.; Tran, C. M. N.; Young, P. G.; Perrier, S.; Jolliffe, K. A. *Nat. Comm.* **2013**, *4*.

(253) Chapman, R.; Koh, M. L.; Warr, G. G.; Jolliffe, K. A.; Perrier, S. *Chem. Sci.* **2013**, *4*, 2581.

(254) Ashkenasy, N.; Horne, W. S.; Ghadiri, M. R. *Small* **2006**, *2*, 99.

(255) Reiriz, C.; Brea, R. J.; Arranz, R.; Carrascosa, J. L.; Garibotti, A.; Manning, B.; Valpuesta, J. M.; Eritja, R.; Castedo, L.; Granja, J. R. *J. Am. Chem. Soc.* **2009**, *131*, 11335.

(256) Montenegro, J.; Vazquez-Vazquez, C.; Kalinin, A.; Geckeler, K. E.; Granja, J. R. *J. Am. Chem. Soc.* **2014**, *136*, 2484.

(257) Chapman, R.; Danial, M.; Koh, M. L.; Jolliffe, K. A.; Perrier, S. *Chem. Soc. Rev.* **2012**, *41*, 6023.

(258) Horne, W. S.; Wiethoff, C. M.; Cui, C. L.; Wilcoxen, K. M.; Amorin, M.; Ghadiri, M. R.; Nemerow, G. R. *Bioorg. Med. Chem.* **2005**, *13*, 5145.

(259) Vollmer, M. S.; Clark, T. D.; Steinem, C.; Ghadiri, M. R. *Angew. Chem. Int. Ed.* **1999**, *38*, 1598.

(260) Steinem, C.; Janshoff, A.; Vollmer, M. S.; Ghadiri, M. R. *Langmuir* **1999**, *15*, 3956.

(261) Ghadiri, M. R.; Granja, J. R.; Buehler, L. K. *Nature* **1994**, *369*, 301.

(262) Fernandez-Lopez, S.; Kim, H. S.; Choi, E. C.; Delgado, M.; Granja, J. R.; Khasanov, A.; Kraehenbuehl, K.; Long, G.; Weinberger, D. A.; Wilcoxen, K. M.; Ghadiri, M. R. *Nature* **2001**, *414*, 329.

(263) Fletcher, J. T.; Finlay, J. A.; Callow, M. E.; Callow, J. A.; Ghadiri, M. R. *Chem. Eur. J.* **2007**, *13*, 4008.

(264) Motiei, L.; Rahimipour, S.; Thayer, D. A.; Wong, C. H.; Ghadiri, M. R. *Chem. Commun.* **2009**, 3693.

(265) He, H. Y.; Williamson, R. T.; Shen, B.; Graziani, E. I.; Yang, H. Y.; Sakya, S. M.; Petersen, P. J.; Carter, G. T. *J. Am. Chem. Soc.* **2002**, *124*, 9729.

(266) Fletcher, J. M.; Harniman, R. L.; Barnes, F. R.; Boyle, A. L.; Collins, A.; Mantell, J.; Sharp, T. H.; Antognozzi, M.; Booth, P. J.; Linden, N.; Miles, M. J.; Sessions, R. B.; Verkade, P.; Woolfson, D. N. *Science* **2013**, *340*, 595.

(267) Schneider, J. P.; Pochan, D. J.; Ozbas, B.; Rajagopal, K.; Pakstis, L.; Kretsinger, J. *J. Am. Chem. Soc.* **2002**, *124*, 15030.

(268) Pochan, D. J.; Schneider, J. P.; Kretsinger, J.; Ozbas, B.; Rajagopal, K.; Haines, L. *J. Am. Chem. Soc.* **2003**, *125*, 11802.

(269) Aggeli, A.; Bell, M.; Boden, N.; Keen, J. N.; Knowles, P. F.; McLeish, T. C. B.; Pitkeathly, M.; Radford, S. E. *Nature* **1997**, *386*, 259.

(270) Aggeli, A.; Nyrkova, I. A.; Bell, M.; Harding, R.; Carrick, L.; McLeish, T. C. B.; Semenov, A. N.; Boden, N. *Proc. Natl. Acad. Sci. USA* **2001**, *98*, 11857.

(271) Zou, R. F.; Wang, Q.; Wu, J. C.; Wu, J. X.; Schmuck, C.; Tian, H. *Chem. Soc. Rev.* **2015**, *44*, 5200.

(272) Gilmartin, B. P.; Ohr, K.; McLaughlin, R. L.; Koerner, R.; Williams, M. E. *J. Am. Chem. Soc.* **2005**, *127*, 9546.

(273) Sawada, T.; Matsumoto, A.; Fujita, M. *Angew. Chem. Int. Ed.* **2014**, *53*, 7228.

(274) Fujimura, F.; Kimura, S. *Org. Lett.* **2007**, *9*, 793.

(275) Ikemi, M.; Kikuchi, T.; Matsumura, S.; Shiba, K.; Sato, S.; Fujita, M. *Chem. Sci.* **2010**, *1*, 68.

(276) Pires, M. M.; Lee, J.; Ernenwein, D.; Chmielewski, J. *Langmuir* **2012**, *28*, 1993.

(277) Hamley, I. W. *Angew. Chem. Int. Ed.* **2007**, *46*, 8128.

(278) Hamley, I. W. *Chem. Rev.* **2012**, *112*, 5147.

(279) Cinar, G.; Ceylan, H.; Urel, M.; Erkal, T. S.; Tekin, E. D.; Tekinay, A. B.; Dana, A.; Guler, M. O. *Biomacromolecules* **2012**, *13*, 3377.

(280) Teoh, C. L.; Su, D. D.; Sahu, S.; Yun, S. W.; Drummond, E.; Prelli, F.; Lim, S.; Cho, S.; Ham, S.; Wisniewski, T.; Chang, Y. T. *J. Am. Chem. Soc.* **2015**, *137*, 13503.

(281) Li, D.; Jones, E. M.; Sawaya, M. R.; Furukawa, H.; Luo, F.; Ivanova, M.; Sievers, S. A.; Wang, W. Y.; Yaghi, O. M.; Liu, C.; Eisenberg, D. S. *J. Am. Chem. Soc.* **2014**, *136*, 18044.

(282) Mehta, A. K.; Lu, K.; Childers, W. S.; Liang, Y.; Dublin, S. N.; Dong, J. J.; Snyder, J. P.; Pingali, S. V.; Thiyagarajan, P.; Lynn, D. G. *J. Am. Chem. Soc.* **2008**, *130*, 9829.

(283) Pham, J. D.; Chim, N.; Goulding, C. W.; Nowick, J. S. *J. Am. Chem. Soc.* **2013**, *135*, 12460.

(284) Pham, J. D.; Spencer, R. K.; Chen, K. H.; Nowick, J. S. *J. Am. Chem. Soc.* **2014**, *136*, 12682.

(285) Morgan, D. M.; Dong, J. J.; Jacob, J.; Lu, K.; Apkarian, R. P.; Thiyagarajan, P.; Lynn, D. G. *J.*

Am. Chem. Soc. **2002**, *124*, 12644.

(286) Kotch, F. W.; Raines, R. T. *Proc. Natl. Acad. Sci. USA* **2006**, *103*, 3028.

(287) O'Leary, L. E. R.; Fallas, J. A.; Bakota, E. L.; Kang, M. K.; Hartgerink, J. D. *Nat. Chem.* **2011**, *3*, 821.

(288) Cejas, M. A.; Kinney, W. A.; Chen, C. L.; Leo, G. C.; Brett, T.; Vinter, J. G.; Joshi, P. P.; Maryanoff, B. E. *Abstr. Pap. Am. Chem. S.* **2007**, *233*.

(289) Jin, H. E.; Jang, J.; Chung, J.; Lee, H. J.; Wang, E.; Lee, S. W.; Chung, W. J. *Nano Lett.* **2015**, *15*, 7138.

(290) Pires, M. M.; Przybyla, D. E.; Chmielewski, J. *Angew. Chem. Int. Ed.* **2009**, *48*, 7813.

(291) Cejas, M. A.; Kinney, W. A.; Chen, C. L.; Vinter, J. G.; Almond, H. R.; Balss, K. M.; Maryanoff, C. A.; Schmidt, U.; Breslav, M.; Mahan, A.; Lacy, E.; Maryanoff, B. E. *Abstr. Pap. Am. Chem. S.* **2008**, *236*.

(292) Gore, T.; Dori, Y.; Talmon, Y.; Tirrell, M.; Bianco-Peled, H. *Langmuir* **2001**, *17*, 5352.

(293) Reimer, A. E.; Feher, K. M.; Hernandez, D.; Slowinska, K. *J. Mater. Chem.* **2012**, *22*, 7701.

(294) Yolamanova, M.; Meier, C.; Shaytan, A. K.; Vas, V.; Bertoncini, C. W.; Arnold, F.; Zirafi, O.; Usmani, S. M.; Muller, J. A.; Sauter, D.; Goffinet, C.; Palesch, D.; Walther, P.; Roan, N. R.; Geiger, H.; Lunov, O.; Simmet, T.; Bohne, J.; Schrezenmeier, H.; Schwarz, K.; Standker, L.; Forssmann, W. G.; Salvatella, X.; Khalatur, P. G.; Khokhlov, A. R.; Knowles, T. P. J.; Weil, T.; Kirchhoff, F.; Munch, J. *Nat. Nanotechnol.* **2013**, *8*, 130.

(295) Yan, X. H.; He, Q.; Wang, K. W.; Duan, L.; Cui, Y.; Li, J. B. *Angew. Chem. Int. Ed.* **2007**, *46*, 2431.

(296) Liu, L.; Guo, Q. X. *Chem. Rev.* **2001**, *101*, 673.

(297) Kuchelmeister, H. Y.; Gutschmidt, A.; Tillmann, S.; Knauer, S.; Schmuck, C. *Chem. Sci.* **2012**, *3*, 996.

(298) Larson, M. R.; Rajashankar, K. R.; Patel, M. H.; Robinette, R. A.; Crowley, P. J.; Michalek, S.; Brady, L. J.; Deivanayagam, C. *Proc. Natl. Acad. Sci.USA* **2010**, *107*, 5983.

(299) Liu, G.; Prabhakar, A.; Aucoin, D.; Simon, M.; Sparks, S.; Robbins, K. J.; Sheen, A.; Petty, S. A.; Lazo, N. D. *J. Am. Chem. Soc.* **2010**, *132*, 18223.

(300) Banwell, E. F.; Abelardo, E. S.; Adams, D. J.; Birchall, M. A.; Corrigan, A.; Donald, A. M.; Kirkland, M.; Serpell, L. C.; Butler, M. F.; Woolfson, D. N. *Nat. Mater.* **2009**, *8*, 596.

(301) Kelkar, D. A.; Chattopadhyay, A. *Bba-Biomembranes* **2007**, *1768*, 2011.

(302) Wallace, B. A. *J. Struct. Biol.* **1998**, *121*, 123.

(303) Bano, M. C.; Braco, L.; Abad, C. *Biochemistry* **1991**, *30*, 886.

(304) Killian, J. A.; Prasad, K. U.; Hains, D.; Urry, D. W. *Biochemistry* **1988**, *27*, 4848.

(305) Jenkins, J.; Pickersgill, R. *Prog. Biophys. Mol. Bio.* **2001**, *77*, 111.

(306) Mitraki, A.; Miller, S.; van Raaij, M. J. *J. Struct. Biol.* **2002**, *137*, 236.

(307) Chakrabartty, A.; Kortemme, T.; Baldwin, R. L. *Protein Sci.* **1994**, *3*, 843.

(308) Wallace, B. A.; Veatch, W. R.; Blout, E. R. *Biochemistry***1981**, *20*, 5754.

(309) Graether, S. P.; Kuiper, M. J.; Gagne, S. M.; Walker, V. K.; Jia, Z. C.; Sykes, B. D.; Davies, P. L. *Nature* **2000**, *406*, 325.